Dgat1 is a lipid metabolism oncoprotein that enables cancer cells to accumulate fatty acid while avoiding lipotoxicity

A thesis submitted to The University of Manchester for the degree of Doctor of Philosophy in the Faculty of Biology, Medicine and Health

2020

Daniel J. Wilcock

School of Medical Sciences, Division of Cancer Sciences

Table of contents

Word count 44,366

List of Figures

List of Tables

Common Abbreviations

4EBP	eIF4E-Binding protein
4HNE	4-Hydroxynonenal
AcCa	Acyl carnitine
ACLY	ATP-citrate lyase
AMPK	AMP-activated protein kinase
ATP	Adenosine triphosphate
CDK1	Cyclin-dependent kinase 1
CE	Cholesteryl esters
CPT	Carnitine palmitoyltransferase
DAGs	Diacylglycerols
DGAT	Diacylglycerol O-acyltransferase
ECM	Extracellular matrix
EdU	5-Ethynyl-2´-deoxyuridine
eEF2	Eukaryotic elongation factor 2
EGFP	Enhanced Green Fluorescence Protein
eIF4E	Eukaryotic translation initiation factor
EMT	Epithelial to Mesenchymal transition
ER	Endoplasmic reticulum
ERK	Extracellular signal-related kinase
FA	Fatty acid
FABP	Fatty acid binding protein
FAO	Fatty acid oxidation
FASN	Fatty acid synthase
FATP	Fatty acid transport protein
Ferro-1	Ferrostatin-1
FFA	Free fatty acid
FGF	Fibroblast growth factor

GAP	GTPase-activating protein
GEM	Genetically engineered mouse
GPCR	G protein-coupled receptor
GTP	Guanosine-5'triphosphate
IFNγ	Interferon gamma
KEAP1	Kelch-like ECH-associated protein 1
LCFA	Long chain fatty acids
LD	Lipid droplets
LoF	Loss of function
LPC	Lysophosphatidylcholines
LPE	Lysophosphaidylethanolamine
LPL	Lipoprotein lipase
LPL	Lipoprotein lipase
MAPK	Mitogen-activated protein kinase
MEK	Mitogen-activated protein kinase kinase
MITF	Microphthalmia-associated transcription factor
MMPs	Matrix metalloproteinase
mTOR	Mammalian target of rapamycin
mTORC	Mammalian target of rapamycin complex
NAC	N-acetyl cysteine
NHM	Normal human melanocytes
NRF2	Nuclear factor erythroid 2-related factor 2
OS	Overall survival
OXPHOS	Oxidative phosphorylation
PA	Phosphatidic acid
PFS	Progression free survival
PTEN	Phosphatase and tensin homolog
PUFA	Poly-unsaturated fatty acids
REDOX	Reduction-oxidation

RGP	Radial Growth Phase
ROS	Reactive oxygen species
RTK	Receptor tyrosine kinase
RTqPCR	Real Time quantitative polymerase chain reaction
S6K	S6 kinase
SCD	Stearoyl-CoA desaturase
SESN2	Sestrin 2
SFA	Saturated fatty acids
shRNA	Short hairpin RNA
SILAC	Stable Isotope Labelling with Amino Acids in Cell Culture
siRNA	Small interfering RNA
SOD	Superoxide dismutase
TAG	Triacylglycerol
TCA	Tricarboxylic acid
TME	Tumour microenvironment
TNFα	Tumour necrosis factor alpha
UHPLC-MS	Ultra-High-Performance Liquid Chromatography-Mass Spectrometry
UV	Ultraviolet
VEGF	Vascular endothelial growth factor
VGP	Vertical growth phase

Abstract

Metabolic reprogramming is one of eight hallmarks of cancer; altered lipid metabolism such as enhanced fatty acid (FA) synthesis and uptake support the membrane biogenesis and ATP requirements for melanoma cell growth and division. As yet, few druggable oncoproteins directly responsible for altered metabolism in cancer cells have been identified. To thrive, however, cancer cells must avoid the reduction in cell growth signalling and generation of toxic lipid peroxides that ordinarily accompany excess free FA. Here, we have uncovered the frequent up-regulation and amplification in melanoma of the enzyme Diacylglycerol O-acyltransferase 1 (DGAT1). DGAT1 catalyses triacylglyceride synthesis, the final step in lipid droplet formation, which allow cancer cells to tolerate excess FA. Using zebrafish transgenesis, we found forced Dgat1 expression in melanocytes accelerated melanoma development driven by oncogenic BRAF or NRAS. Strikingly, in p53 mutant zebrafish melanocytes forced Dgat1 expression alone induced melanoma formation. Utilising both *in vitro* and *in vivo* models we found that the pro-oncogenic activity of DGAT1 was mediated through the stimulation of mTOR-S6K, signalling melanoma cell growth and protecting melanoma cells from cell death induced by oxidative stress and lipotoxicity. Inhibition of DGAT1 leads to a decrease in mTOR signalling through S6K and increased production of toxic metabolites leading to a loss of mitochondrial membrane potential and an increase in reactive oxygen species, ultimately leading to melanoma cell death. Together, our data identifies *DGAT1* as a *bona fide* oncogene that stimulates cell growth and suppresses oxidative stress while enabling fatty acid accumulation and thus, a putative therapeutic target in melanoma.

Declaration

I hereby declare that no portion of the work referred to in the thesis has been submitted in support of an application for another degree or qualification of this or any other university or other institute of learning, unless otherwise stated.

The materials and methods section has been previously published as a preprint, in which I am first author, available on bioRxiv.

(https://www.biorxiv.org/content/10.1101/2020.06.23.166603v1.full).

Contributions to the work

The majority of the work presented in this thesis is my own work. Some complete experiments were performed by fellow colleagues in the lab and some experiments were performed with assistance, which are outlined below.

The sectioning and staining of zebrafish tumours in figure 3.C were carried out by Andrew Badrock. The minicoopR experiment in the transgenic mitfa:BRAFV600E; tp53 mutant; nacre genetic background was carried out by our collaborators in the lab of Craig Ceol at the University of Massachusetts Medical School.

Trimming and aligning of the raw RNA-sequencing reads from zebrafish tumours in chapter 3 was carried out by Sam Ogden.

The Mass spectrometry in both chapter 4 and chapter 6 was carried out in collaboration with the Francavilla lab at the University of Manchester. I was involved in all stages of sample collection and preparation and analysis, but assistance was provided by Paul Fullwood and Jo Watson.

The following experiments in chapters four and five were carried out by Rhys Owens and appear in his master's dissertation:.4.4D DGAT2 inhibition in MM485 and SKMEL28 melanoma cells, 4.7A DGAT1 siRNA knockdown in MM485 melanoma cells, BODIPY and LIPIDTOX staining in Figure 5B-D.

The samples for lipidomic analysis in chapter 5 were generated by me, but the UHPLC and data processing was carried out by our collaborators at the Phenome centre at the University of Birmingham.

Copyright Statement

Acknowledgements

Firstly, I would like to thank both my PhD supervisors Claudia Wellbrock and Adam Hurlstone. Thank you to Claudia for initially taking me on to do my PhD and for providing a great lab environment in which to start my PhD. Thank you to Adam for taking me in when Claudia left and giving me the freedom to grow and learn while working on this project whilst providing support and guidance along the way. I have loved working in your lab and enjoyed working with you.

I would also like to thank the members of both the Wellbrock and Hurlstone Labs that have helped me through my PhD and making it an enjoyable four years. Jen, Emily and Zso you were there from the beginning, we had some great laughs and you helped me get started and continued to support me throughout my four years. In particular I want thank Andy for his guidance and help with the zebrafish work and friendship over the past four years. A special thanks to Michael who not only is a great friend but guided and supported me from the very beginning and played a huge role in making my PhD enjoyable and making me the scientist I am today.

I would also like to thank our collaborators in the Ceol Lab in Boston, the Francavilla lab in Manchester and the Phenome centre in Birmingham for their assistance and advice in carrying out zebrafish work, mass spectrometry and lipidomics.

A big thank you to all of the technical staff at the University of Manchester in the BSF, the mass spectrometry, flow cytometry and bioimaging facilities for their guidance and help.

Lastly a huge thank you to my wife Jess for all of the support you have provided over the past four years, putting up with late evenings and weekends in the lab and constant chat about DGAT. I will never be able to thank you enough and can only hope to support you in the same way as you finish your PhD and as we go through life side by side.

Chapter 1 Introduction

Melanoma is the deadliest form of skin cancer, predominantly due to its highly metastatic nature. The rate of incidence of melanoma is increasing, more than doubling in the UK since the early nineties, with incidence predicted to carry on rising. In the UK alone there were 16,000 new cases every year between 2014 and 2016, making it the fifth most common cancer. When detected at an early stage, melanoma can be cured through surgery alone, with 90% of those diagnosed surviving for ten years or more. However, despite huge advances in both targeted and immune therapies, if melanoma is diagnosed in the latest stage of the disease only 1 in 2 survive for more than one year, thus highlighting the need to further the understanding of melanoma biology and elucidate pathways critical for the development of the disease and harness their therapeutic potential.

Statistics from Cancer Research UK[1]

1.1 The Phases of Melanoma Development

Melanoma is a disease that arises from melanocytes within the basal layer of the epidermis, through an interplay of genetic susceptibility and environmental risk factors and progresses in stages to metastatic disease. The highly differentiated melanocytes main role is the production of the pigment molecule melanin[2], a molecule that plays multiple beneficial roles including the protection of DNA from harmful UV[3,4] light and protection from reactive oxygen species (ROS) as a result of UV irradiation[5]. Melanocytes are derived from neural crest cells, a population of highly migratory and multipotent cells[6]. The neural crest cells undergo stepwise differentiation firstly undergoing epithelial to mesenchymal transition (EMT), differentiating into melanoblasts which then migrate into the correct location. A number of key transcriptional programmes are then critical for terminal differentiation into melanocytes such as the SOX10, Wnt, MITF, PAX3 and Endothelin signalling pathways[7,8].

The main environmental risk factor for melanoma development is exposure to UV radiation, with increased risk linked directly to the level of UV in the UV-B spectrum[9]. Several studies have now demonstrated that intermittent sun exposure and a history of sunburn leads to the highest increased risk of melanoma [10,11].Additionally, UV-A from artificial sources such as sun beds has also been shown to increase the risk of melanoma, with UV from sun beds now formally classed as a human carcinogen[12].

In addition to environmental risks a number of host factors have also been linked with increased susceptibility to the development of melanoma. A small number of cases of truly heritable melanoma are found, with mutations in the cell cycle regulator cyclin-dependent kinase inhibitor 2A the most common genetic abnormality; found in 25-40% of melanoma prone families[13,14]. A few rare cases have also been found with mutations in cyclin-dependent kinase 4[13,14] or MITF[15]. Phenotypic characteristics such as light skin, red hair and low pigmentation are often due to polymorphisms in melanocortin receptor 1 (MCR1); a receptor found on melanocytes which plays a vital role in stimulating the production of melanin, which causes increased sensitivity to UV and therefore an increased risk of developing melanoma[16]. Another host risk factor is the number of melanocytic nevi, benign accumulations of melanocytes which can be congenital or acquired. One recent meta-analysis demonstrated that patients with more than 100 nevi have a 7-fold increased risk of melanoma development[17,18]. Not only is it the number of nevi that is associated with increased melanoma risk but also the size and type of nevi[19].

In the Clark model of melanoma[20] (Figure 1.1) it is these benign nevi that are thought to be the first step in the progression from normal melanocytes to melanoma. The nevi are transformed but structurally normal melanocytes that have undergone clonal expansion, however most of these nevi will stop dividing and enter cellular senescence, with only small percentage forming dysplastic nevi[21]. Genetically, these nevi are usually characterised by an activating mutation in BRAF (70-80%)[22,23] or NRAS (5-15%)[23,24], and the induction of cellular senescence is thought to be due to

an increase in the cell cycle regulator p16[25,26]. Not all cases of melanoma come from pre-existing nevi, it can occur *de novo* through the direct transformation of melanocytes[27]. The next stage of melanoma development is the radial growth phase (RGP) in which dysplastic nevi can spread laterally within the epidermis. In order for the nevi to exit senescence and proliferate in an uncontrolled manner these cells must acquire further genetic changes in genes involved in both cell cycle progression and survival such as cyclin D1[28], p16[29,30], PTEN[31,32] and MITF[33]. RGP melanoma cells then transition into the vertical growth phase (VGP) in which the cells acquire the ability to invade into the dermis and subcutaneous tissue, a process which again requires genetic changes in the melanoma cells. In transitioning from RGP to VGP the genetic changes acquired in the melanoma cells include changes in the levels of cadherins[34,35] , changes in AKT signalling[36] and increased expression of matrix metalloproteinases[37]. These crucial gene expression changes endow the melanoma cells with metastatic potential, the final step in melanoma development. The melanoma cells reach the blood vessels and can spread into other tissue and organ sites the most common of which being the brain, lung and bone, forming metastatic lesions[38].

The understanding of the molecular drivers of melanoma development and progression is key to the development of novel therapies, as such the key oncogenic mutations and epigenetic changes in melanoma are discussed below.

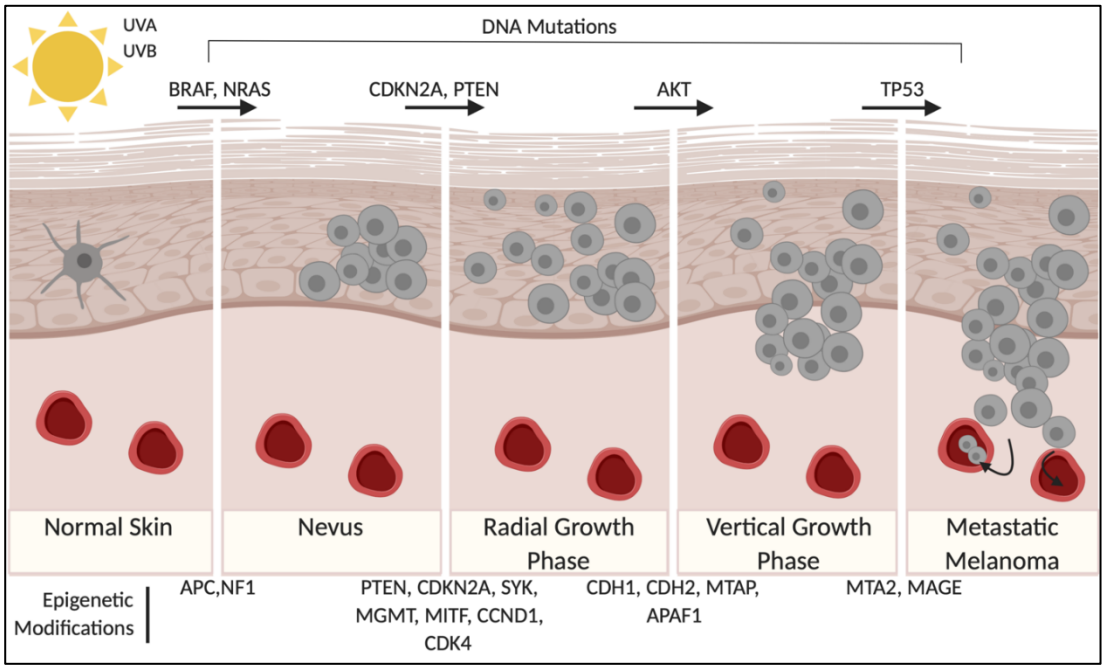

Figure 1.1 Melanoma development

Melanoma arises from benign nevi, which are structurally normal melanocytes that have undergone clonal expansion. Which through a series of both DNA mutations and epigenetic modification under a stepwise progression from dysplastic nevi through to the radial growth phase and finally to metastatic melanoma.

1.2 Oncogenes in Melanoma

Tissue homeostasis is maintained through the tightly regulated co-ordination of cell division, differentiation, senescence and apoptosis. Cancer is the abnormal growth of cells, in which homeostasis has been deregulated; this occurs through a combination of both genetic and epigenetic alterations within cancer cells [39]. The specific genes implicated in driving the transformation of normal cells into malignant cancer cells and furthering tumour progression are dubbed oncogenes.

The first evidence of oncogenes came from studies in the 1970s on oncogenic retroviruses, which started with the identification of viral RNA as the constituent of Rous sarcoma virus (RSV) responsible for transforming chick embryo fibroblasts in culture[40]. Arguably the seminal moment in the discovery of oncogenes occurred in

1976 when, in the lab of Harold Varmus and Mike Bishop, it was revealed that the RSV gene behind the viruses oncogenic ability (v-src) was in fact a transduced version of an avian cellular gene (c-src)[41]. This finding stimulated a wave of research into the key drivers in the transforming properties of other viruses. Two studies in avian acute leukaemia viruses led to the identified of a further two novel oncogenes , which were later shown to be derived from cellular oncogenes MYC and ERBB/EGFR[42–44]. Further key oncogenes were discovered in murine sarcoma retroviruses, identifying the key oncogenic proteins in both Harvey sarcoma virus (Hras) and Kirsten sarcoma virus (Kras)[45–47]. Further experiments then linked the ras oncogenes directly to human cancer, whereby the transfer of DNA from human cancer cells was found to transform recipient mouse cells[48], coupled with the finding that this transforming DNA was homologous to ras[49,50]. This was quickly followed by the identification of the third ras isoform (Nras) through further DNA transfer experiments[51]. These initial discoveries provided the foundation for demonstrating the genetic basis of cancer through oncogenes leading to present day situation where next generation sequencing and the development of cancer bioinformatics pipelines has accelerated the discovery of novel oncogenes[52].

Genes whic are frequently altered in cancer can be divided into two groups based on whether they are gain of function oncogenes, or loss of function tumour-suppressor genes. The activation of proto-oncogenes into oncogenes can be through point mutation, amplification or a translocation of a single allele leading to a dominant activity over the normal wild type allele. Inactivation of tumour suppressor genes occurs mainly through the deletion of one allele, followed by a point mutation of the second allele, leading to loss of function[53] .In the majority of cases point mutations are found to activate proto-oncogenes leading to enhanced and uncontrolled activity, as seen with mutant RAS[54] and RAF[55] oncogenes. Genetic translocations can lead to a proto-oncogene being placed under the control of a constitutively active promotor, leading to its continuous expression. This is seen in Burkitt lymphoma where the MYC gene is controlled by the active immunoglobulin heavy chain cluster promotor[56] and in prostate cancer where the TMPRSS2-ERG fusion puts ERG under

the control of an androgen sensitive promotor[57]. Translocations can also lead to the production of fusion proteins which cause the constitutive activation of proliferative signalling pathways such as the EML4-ALK in non-small cell lung carcinoma (NSCLC) which leads to activation of ERK and AKT signalling[58].

All of these oncogenic mechanisms are found in melanoma. However, when discussing oncogenic drivers in melanoma it is important to note that out of all human cancers melanomas carry the highest mutation burden, with more than 10 mutations per mega base (Mb) on average[59]. This makes the identification of key drivers over passenger genetic changes challenging, however, through the identification of a number of driver alterations, the key role of both the MAPK pathway and the PI3K pathway has become apparent. Specifically, a hyper activation of ERK signalling is seen in ~90% of melanoma[60]. The importance of these signalling pathways, and both well-known oncogenes and newer oncogene candidates in melanoma will be discussed below.

1.3 MAPK Pathway

The RAS/RAF/MEK/ERK (MAPK) pathway regulates diverse biological functions such as cell growth, survival, and differentiation downstream of multiple Receptor Tyrosine Kinases (RTKs) , G-protein coupled receptors (GPCRs) , cytokine receptors and adhesion proteins[61,62] (Figure 1.2). The pathway is activated by several growth factors in melanocytes such as stem-cell factor (SCF), fibroblast growth factor (FGF) and hepatocyte growth factor (HGF) [62]. Activation of these RTKs, stimulated by growth factors, leads to the activation of RAS through several adaptor proteins and exchange factors. Activation of RTKs allows the phosphorylated Src Homology 2 (SH2) domain of the Growth factor receptor-bound protein 2 (GRB2) adaptor protein to bring Son of Sevenless (SOS) into close proximity with RAS which, in its inactive GDP-bound form, is localised to the membrane [63]. SOS is a guanine nucleotide exchange factor (GEF), and through binding RAS exchanging the GDP for GTP leads to RAS

activation[63]. In humans there are four members of the RAS GTPase family HRAS, NRAS, KRASA, KRASB[64]. Activated RAS is now able to bind and recruit RAF kinases to the plasma membrane, binding to the RAF protein in a highly conserved ras binding domain (RBD) in the N-terminus (CR1). There are three RAF isoforms in humans ARAF, BRAF and CRAF all of which are structurally similar and contain highly conserved regions (CR1, CR2 and CR3 domains), but functionally play non-redundant roles. RAF kinase activation is tightly regulated, involving membrane localisation, phosphorylation, hetero or homo-dimerization conformational changes and scaffold protein binding, with each isoform requiring different activation steps[62]. All of these steps increase the kinase activity of RAF proteins, which are then able to phosphorylate the next mitogen activated protein kinase in the pathway, MEK1 and 2. MEK is phosphorylated at two sites in its activation loop[65]. Activated MEK then activates the third protein kinase in the pathway ERK 1 and 2, through phosphorylation. Activated ERK has a number of targets including transcription factors and cytoskeletal proteins, involved in the control of wide range of processes, such as proliferation, survival, cell motility and differentiation[66] (Figure 1.2).

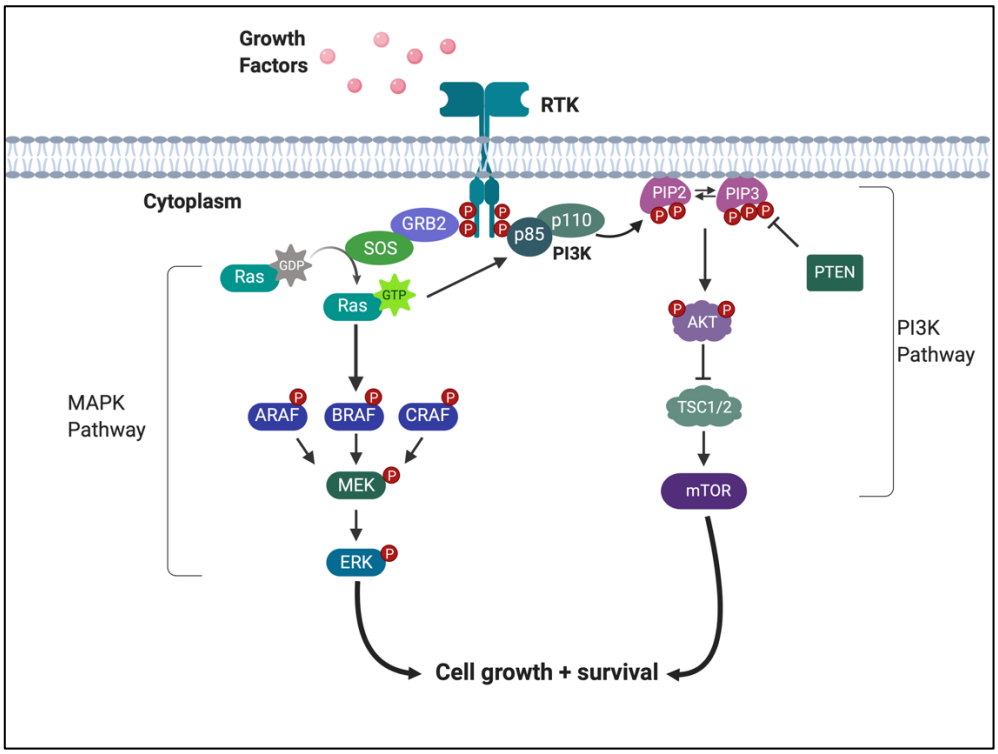

Figure 1.2 MAPK & PI3K Signalling pathways.
The MAPK and PI3K pathways are both activated by growth factor, cytokine or hormone binding to receptor tyrosine which leads to the recruitment and activation of signalling protein which activate signalling cascades regulating diverse cellular functions including growth, proliferation and survival.

1.4 PI3K Pathway

Just like the MAPK pathway, the PI3K pathway is another major pathway regulating a diverse range of cellular functions like cell growth and proliferation, angiogenesis and survival[67]. Again, like the MAPK pathway, activation occurs through growth factor, cytokine or hormone binding to an RTK, this binding leads to the autophosphorylation of tyrosine residues on the RTK. This autophosphorylation recruits PI3K to the membrane through the SH2 domains in the adaptor unit, resulting in allosteric activation of the catalytic subunit of PI3K[68]. Now activated, PI3K catalyses the production of the secondary messenger molecule phosphatidylinositol (3,4,5)-trisphosphate (PIP_3) from phosphatidylinositol (4,5)-bisphosphate (PIP_2),

through phosphorylation of the inositol ring of lipids in the plasma membrane[69] . Negative regulation of the signalling pathway can occur at this point, PIP_3 is the main lipid substrate of PTEN deleted on chromosome 10 (PTEN). PTEN dephosphorylates PIP_3 into PIP_2[70]. PIP_3 is able to recruit a subset of signalling proteins with pleckstrin homology (PH) domains, including AKT. PIP_3 binds to the PH domain of AKT in its inactive form, leading to recruitment to the plasma membrane whereby, through a phosphorylation event, AKT becomes activated. Activated AKT phosphorylates a plethora of proteins regulating cell growth and survival[71]. The phosphorylation of one of these proteins, TSC2, leads to its inhibition and results in activation of mammalian target of rapamycin (mTOR)[68]. mTOR is a key signalling hub integrating multiple upstream signalling events and controls protein translation, cell growth and survival through multiple downstream effectors such as S6 kinase (S6K) , SGK1, 4EBP and ULK1[72] (Figure 2).

1.5 Established Melanoma Oncogenes

NRAS

As mentioned above, the RAS genes were first identified as the proteins mediating the transforming activity of murine sarcoma retroviruses [45–47], and were linked directly to human cancer through DNA transfer experiments[48–51]. NRAS was the first melanoma oncogene discovered when, in 1984, a group screened 30 melanoma cell lines for genes with transforming properties, identified activating mutations in NRAS in 4 samples[73].

The RAS genes have now been shown to be the most frequently mutated oncogenes in human cancers, with >20% of all tumours harbouring mutations in one of the RAS genes[74]. Although KRAS mutations dominate RAS mutations in human cancer, accounting for over 85% of RAS mutations, it is NRAS mutations which are found predominantly in melanoma. NRAS mutations are found in 15-20% of tumours ,

whilst KRAS and HRAS are found in only 2% and 1% of melanomas respectively[75]. The RAS oncogenes are activated through point mutation at three main hotspots at codons 12, 13 and 61. In melanoma over 80% of NRAS mutations occur in codon 61[75]. The most common NRAS mutations at codon 61 Q61R (CAA/CGA) and Q61K (CAA/AAA) lead to substitutions from glutamine to arginine or to lysine respectively. The Q61 residue plays an essential role in GTP hydrolysis, forming a hydrogen bond with a specific residue of a GAP protein, allowing the nucleophilic attack of a water molecule critical for GTP hydrolysis. Thus, mutations in this residue impair the GTPase activity, leading to constitutively active GTP-bound NRAS[76]. NRAS mutations are detected in multiple phases of melanoma from the radial growth phase right through to metastasis [77,78]. Thus, confirming that NRAS mutations are somatic mutations and critical in the early development of melanoma.

Mutant NRAS has been shown to be a potent oncogene in multiple models of melanoma, driving melanoma progression by promoting growth, survival and invasion through potent activation of both MAPK signalling and PI3K signalling[79] (Figure 1.2). Some of the earliest evidence came in the 1980s from DNA transfer experiments, in which it was demonstrated that NRAS-transformed NIH/3T3 cells were able to form tumours in nude mice[73,80]. Over 30 years on we now have multiple genetically engineered mouse (GEM) models of melanoma in which melanocyte specific expression of mutant NRAS has been shown to cause hyperpigmentation and tumour development[81]. Further GEM models have demonstrated that other key regulators of cell cycle progression cooperate with mutant NRAS; with loss of p16Ink4a accelerating tumour formation and progression[81–83]. The critical importance of NRAS was highlighted in a tetracycline inducible GEM model wherein removal of tetracycline and thus removal of mutant NRAS expression resulted in rapid and complete tumour regression[83]. Transgenic zebrafish have also been used to prove the oncogenicity of mutant NRAS, in which melanocyte specific expression of $NRAS^{Q61K}$ led to hyperpigmentation and, in the background of p53-/-, led to melanoma development[84].

The exact reason as to why NRAS is so prevalent in melanoma, when KRAS is the most frequently mutated human oncogene is not yet completely understood. However, it is thought that NRAS may be overexpressed in melanocytes compared to other RAS isoforms. Additionally, it is also known that the RAS isoforms activate different signalling pathways. This is supported by evidence in ink4a/Arf-deficient mouse melanocytes, in which mutant NRAS both increased cellular proliferation and greatly increased tumorigenicity when compared to mutant KRAS[85]. It also appears that there may be a role for UV in the predominance of $NRAS^{Q61}$ mutations, as clinical evidence demonstrates that the highest frequencies of $NRAS^{Q61}$ are found in primary tumours from chronically sun exposed sites[86]. Experimental evidence both *in vitro*[87,88] and *in vivo* has demonstrated that NRAS Q61 is a UV mutation hotspot and UV induced mouse melanoma models preferentially harbour NRAS mutations[89,90]. Additionally, further studies using mouse melanoma models have clearly demonstrated the increased oncogenicity of NRAS Q61R when compared to NRAS G12D[82]. All of these findings provide reasons as to why the NRAS Q61 mutation is prevalent in melanoma, however the clear mechanistic basis for its enhanced oncogenic activity in melanoma still remains to be elucidated.

BRAF

Raf was first discovered as an oncogene in a murine leukaemia virus, the encoded protein was called v-Raf and was able to transform NIH 3T3 cells and the recovered virus able to elicit tumours in mice[91]. The cellular homologue c-Raf was found in both humans and mice. Coinciding with this discovery, the Bister group discovered another oncogene in the avian retrovirus Mill-Hill No.2 (MH2), which was named v-mil[92]. It was later discovered that these two oncogenes encoded homologues of the same protein kinase in mice and chickens[93] and two related genes A-Raf and B-Raf found in vertebrates[94].

However, it wasn't until 2002 that the role of BRAF as an oncogene in human cancer was fully appreciated and its importance as more than just a key player downstream of oncogenic RAS discovered (Figure 2). BRAF mutations were found in approximately 7% of human cancers and as stated previously, 50% of melanomas[22,75], making it the most frequently mutated melanoma oncogene. Over 40 different missense BRAF mutations were found, however most of these mutations are very rare accounting for only 0.1-2 % of cases [22]. One mutation, V600E, accounts for 90% of all BRAF mutations found in melanoma[22]. This mutation was one of the most active mutants discovered, leading to *in vitro* kinase activity 500-fold greater than that of BRAF wild-type ($BRAF^{WT}$) [95]. The $BRAF^{V600E}$ mutant has been shown to be a potent oncogene inducing constitutive (growth-factor independent) ERK signalling (Figure 1.2) and increased growth in mouse melanocytes, whilst also increasing tumorgenicity in nude mice[96]. This effect was also observed in transgenic zebrafish models of melanoma, in which $BRAF^{V600E}$, under the control of a melanocyte specific promoter, again increased ERK signalling and induced formation of melanocytic nevi[97]. Additionally, p53-deficient zebrafish potently induced melanocytic lesions and invasive melanoma[97]. In line with this interesting finding in zebrafish models, $BRAF^{V600E}$ mutations are found in 70-80% of melanocytic nevi[23,98], suggesting that BRAF mutations occur early in tumorigenesis and may be a founder event, yet it is not sufficient to induce cancer without further oncogenic alternations within the cells. This is further corroborated in GEM models, in which BRAF has been shown to co-operate with a number of other tumour drivers to promote melanoma formation and development. Mutant BRAF alone leads to melanocytic hyperplasia and nevi formation but also leads to cellular senescence; for melanoma to develop, a secondary driver genetic alteration is required such as loss of PTEN[99], loss or mutation of P53[100,101], loss of ink4a[102] and loss of CDKN2A[100] to bypass senescence.

Solving the crystal structure of BRAF provided the answer as to why $BRAF^{V600E}$ mutations are oncogenic and stimulate constitutive ERK signalling. The V600E mutation occurs in the activation segment, usually held in the inactive conformation by a hydrophobic interaction with the glycine rich loop[95]. The V600E mutation

disrupts this interaction, destabilising the inactive conformation, leaving BRAF constitutively active[95]. The crystal structure of BRAF also provided clues as to why BRAF is found mutated in human cancers but ARAF and CRAF mutations are very rare. In the N region of A, B and C-RAF there must be a negative charge for full activation of the kinase domain. When comparing BRAF to CRAF, the critical amino acid is already negatively charged (CRAF:Y341, BRAF:D448), and a further key phosphorylation site in CRAF (S338) is constitutively phosphorylated in BRAF (S445). The result is that BRAF has both the strongest basal kinase activity, and is poised ready for activation, requiring only RAS-mediated membrane recruitment for activation. Thus, unlike ARAF or CRAF, BRAF only requires a single point mutation to become activated, explaining why it is BRAF mutations that are prevalent in cancer.

NF1

The *NF1* gene was first identified as the mutated gene causing the familial cancer syndrome neurofibromatosis type I. An inherited genetic syndrome which causes a predisposition to the development of multiple tumours, commonly derived from the neural crest[103]. The importance of *NF1* in melanoma was identified in a recent study assessing the genomic landscape of melanoma, which established four subtypes of melanoma based on the pattern of the most prevalent, significantly mutated genes. This study identified a mutant NF1 subtype of melanoma, with *NF1* being the third most frequently mutated gene behind BRAF and NRAS[75]. However, unlike BRAF or NRAS which are proto-oncogenes, NF1 is a tumour suppressor, with mutations in NF1 leading to loss of function (LoF) [75,104].

The *NF1* encodes for a protein critical to the regulation of RAS activity. NF1 is a RAS GTPase- activating protein (GAP), which negatively regulates RAS by catalysing the hydrolysis of RAS-GTP to RAS-GDP[105]. As such, although NF1 LoF mutations do co-occur with both BRAF and NRAS mutations, the highest percentage of mutations are found in wild-type NRAS and BRAF melanoma, with NF1 LoF mutations acting as an

alternative method of MAPK activation. Accordingly, RAS signalling and it's downstream pathways are activated in NF1 mutant melanoma[106]. The most frequent co-occurring mutations with NF1 are found in genes involved in RASopathys such as RASA2 and SOS1; again highlighting the key role of RAS signalling in NF1 mutant melanoma[104]. In GEM models of melanoma loss of NF1 has been shown to co-operate with both mutant BRAF and RAC1 and loss of p53 to promote tumorigenesis[107,108].

c-KIT

The fourth melanoma subtype identified, in a recent study assessing the genomic landscape of melanoma, is Triple WT melanoma. These melanoma do not contain mutations in NRAS, BRAF or NF1, the more frequent mutations were found in c-KIT[75]. KIT is a receptor tyrosine kinase, which upon binding of its ligand, dimerises, resulting in autophosphorylation of the intracellular RTK domain, leading to activation of the MAPK and PI3K signalling pathways (Figure 2).

Unlike NRAS or BRAF which contain single hotspot mutations , driver KIT mutations are found in four hotspots L576, K642, W557-V560, and D816-A829, with these hotspots making up 70% of KIT mutations found in melanoma[109]. These mutations have been shown to be oncogenic in melanocytes[109,110]. Additionally, amplification of KIT is found in approximately 6-8% of cutaneous melanoma patients [111–113], although both mutation and amplification of KIT are far more common in both mucosal and acral melanoma[111]. Oncogenic amplification or mutation of KIT is found to be mutually exclusive to mutation of either mutant NRAS or BRAF, the predominant mutations in cutaneous melanoma[113]. Interestingly, in both BRAF and NRAS mutant melanoma, KIT is often found to have decreased expression, due to increased promoter hypermethylation[114]. This may be favourable in order to avoid hyper-stimulation of MAPK signalling that would cause cell cycle arrest and senescence, as observed when both mutant NRAS and BRAF are co-expressed in melanoma cells[115]. These observations are supported by a zebrafish model of

melanoma in which loss of functional KIT was demonstrated to accelerate tumorigenesis in a BRAF mutant model of melanoma[116].

1.6 Putative and Secondary Drivers

In addition to the classical melanoma oncogenes and primary drivers discussed above defining the four melanoma subtypes, there are a number of other key oncogenic genetic alterations found in melanoma that often are found co-occurring with other driver mutations, or in some rare cases are found as the primary driver.

The PI3K pathway is critical to melanoma development and growth[117](Figure 1.2). As such, genetic alteration of key members of this pathway is found in melanoma. The second most common alteration behind mutation of NRAS is loss of PTEN, a negative regulator of P13K signalling (Figure 2). PTEN is a tumour suppressor gene and the loss of function is achieved through either chromosomal deletion, mutation or epigenetic silencing. Genetic deletion or mutation of PTEN is found in 12-17% of melanoma tumours[113,118], with the highest incidence found in metastatic melanoma tumours. Additional studies have demonstrated that PTEN expression in melanoma is also lost through epigenetic mechanisms[119], further highlighting the importance of PTEN as an important tumour suppressor in melanoma. Moreover, in other tumour types including breast, glioblastoma and bladder post-translation modifications of PTEN including s-nitrosylation[120], phosphosphorylation[121], oxidation[122] and ubiquitination[123] also contribute towards loss of PTEN function[124,125]. Loss of PTEN is most commonly found alongside BRAF mutations[113,126], but is generally mutually exclusive to NRAS mutations[127], possibly due to mutant NRAS already being a potent driver of PI3K signalling[79] . Melanoma *in vivo* models have demonstrated that LoF PTEN co-operates with oncogenic $BRAF^{V600E}$ in both mouse[99] and zebrafish[97] and CDKN2A deletion in mice[128] to drive melanoma formation and progression. Oncogenic genetic alterations in other members of the PI3K pathway are rare, however in metastatic melanomas 3% contain an activating mutation in P13K[129].

Melanoma development and growth is not only dependent on hyper-activation of key growth pathways but also the bypassing of cell cycle control checkpoints to allow uncontrolled cellular proliferation. As such, it appears that it is the G1/S checkpoint that appears crucial in melanoma, with genetic alterations in key regulators of this checkpoint found playing a critical role in melanoma development and growth. The mostly frequently altered cell cycle regulator is the CDKN2A locus encoding the p16INK4A protein, which controls G1/S transition through binding to CDK4/6 to negatively regulate cell cycle progression[130]. Deletion or missense mutations in the CDKN2A locus, and thus LoF of the tumour suppressor p16INK4A, occurs in almost 50% of primary melanomas[113,131]. Loss of p16INK4A correlates in patients with increased proliferation rate and using *in vivo* melanoma models, co-operates with BRAF, NRAS and PTEN to promote melanoma development and growth[81,102,128]. Additionally, loss of p16INK4A alone has been shown to increase susceptibility to carcinogen-induced and spontaneous melanoma[132]. Another gene involved in the control of the G1/S checkpoint, CCND1, has also been implicated in melanoma formation and growth. CCND1 encodes for Cyclin D1, which binds to CDK4/6 prompting the transition from G1 to S phase of the cell cycle. It is found amplified or with increased expression in melanoma samples, although the degree to which it is amplified is unclear, with studies demonstrating amplification ranging between 4%-83% of patients in different studies[133–136]. Nonetheless, *in vivo* evidence for the importance of CCND1 in melanoma demonstrated that knockdown of CCND1 in melanoma xenografts resulted in tumour shrinkage[134].

Microphthalmia-associated transcription factor (MITF) acts as a master regulator of melanocyte development and cell type specific functions in melanocytic cells. The relevance of MITF in melanocyte biology is maintained in melanoma, and has been dubbed a 'lineage survival oncogene'[137] Specifically it is the M-MITF isoform which is expressed exclusively in melanocytes and carries out essential roles in regulating differentiation, cell cycle progression and survival in these cells[138]. The diversity of the pathways modulated by MITF highlight the complexity of its role in melanocytes and melanomas, as such both low and high MITF levels have been observed in

melanomas and play key roles in tumour initiation and progression[138,139]. In order to link the melanoma phenotypes observed with MITF levels, the rheostat model was developed; with low MITF linked to a stem-like and invasive phenotype and high levels linked to high levels of proliferation[140,141]. MITF is found to be amplified in 10-20% of tumours[113,137,142]. It is thought that the oncogenic nature of this amplification and increased levels of MITF are due to increased cell cycle progression through induction of both CDK2 and CDK4[143,144] , increased survival through regulation of BCL2[145] and the regulation of oxidative metabolism[146]. Further highlighting the importance of MITF, several studies demonstrated that knockdown of MITF reduces xenograft growth[147,148], and induces a G1 arrest in both MITF low and MITF high expressing cells[140,143]. However, the complex nature of the role of MITF in melanocytes and melanoma biology means there is still much to be elucidated about the oncogenic role of MITF.

A series of studies using high throughput sequencing technologies has further identified potential novel oncogenic drivers in melanoma. These include mutation in genes involved directly in MAPK signalling such as MAPK2K1,MAP2K[149] and MAP3K9[150], mutation of Ras subfamily members like RAC1[104] as well as the RAC1 activator PREX2[151], mutations in RTKs such as ERRB4[152], LoF mutation of ARID2 a member of the chromatin remodelling complex[113], alternations DNA damage response pathways such as MDM2 amplification or TP53 mutation[75] and mutation of the TERT promoter a critical gene involved in the telomerase complex[75]. However, the exact role of these alterations is still to be fully understood and further *in vivo* modelling is required to provide more definitive evidence for the oncogenic nature of these alterations and to determine whether these alterations co-operate with established oncogenes.

The identification of these oncogenic genetic alterations in melanoma and the critical signalling pathways involved in melanoma growth and survival has dramatically altered the treatment of melanoma. The standard of care shifting from

chemotherapeutic agents to targeted therapy with small molecule inhibitors affecting the mutated proteins and key pathways.

1.7 Therapeutic Challenges in Melanoma

Targeted Therapy

Prior to 2011 the standard of care for late stage melanoma was treatment with the alkylating chemotherapeutic agent Dacarbazine, yet the response rate was low at between 5-10%[153,154] and 5-year survival only 2-6%[155]. In 2011 the first selective BRAF inhibitor, Vemurafenib, was approved as a therapy for patients with advanced stage melanoma. Vemurafenib is an ATP competitive inhibitor inhibiting the kinase activity of BRAF, and demonstrated selectivity over other kinases and wildtype BRAF. In clinical trials, treatment with Vemurafenib led to increased progression free survival (PFS) , increased overall survival (OS) and a response rate of 90% in patients with a BRAF V600E mutation[156]. This success was followed by the approval of two other selective BRAF inhibitors Dabrafenib in 2014 and Encorafenib in 2018, both of which demonstrated better clinical activity[157,158]. However, there are two major problems associated with single agent BRAF inhibition (BRAFi). Firstly, although BRAF inhibitors are effective in blocking MAPK signalling in BRAF mutant cells, they paradoxically activate MAPK in RAS mutant and RAF WT cells through a drug bound, wild type BRAF-CRAF dimer leading to MAPK activation[159,160]. Secondly, despite the initial observed clinical benefit, resistance to BRAFi monotherapy with either vemurafenib or dabrafenib occurs after approximately 6-8 months in 50% of patients, through reactivation of MAPK signalling[156,161–163].

In parallel to the development of selective inhibitors of BRAF, inhibitors of the downstream kinase MEK (Figure 2) were also developed. The first to receive approval for use in $BRAF^{mut}$ melanoma patients was Trametinib in 2013, with trials demonstrating increased progression free survival in advanced stage melanoma

patients, but was not as effective as vemurafenib or dabrafenib as a single agent[164]. This has led to the use of MEK inhibitors in combination with BRAF inhibitors in advanced stage $BRAF^{mut}$ melanoma patients to improve patient survival and combat resistance to BRAFi monotherapy. There are currently three approved BRAFi + MEKi combination therapies approved in melanoma; vemurafenib plus cobimetinib, dabrafenib plus trametinib, and encorafenib plus binimetinib, with all three combinations improving both progression free survival and overall survival in patients when compared with BRAFi plus placebo[158,165,166]. However, delayed therapy resistance still occurs and remains a major problem in the treatment of advanced stage melanoma patients.

Multiple resistance mechanisms have been identified both within the melanoma cells themselves and through signalling from the microenvironment. Resistance mechanisms in the tumour cells themselves leading to reactivation of ERK signalling includes: upregulation of signalling by RTKs such as EGFR, AXL or PDGFR[167–169]; mutations leading to increased MAPK signalling in NRAS, MEK1,MEK2 and MLK[170–173]; alterations in BRAF itself such as amplification and aberrant splicing[174,175]; loss of the RAS suppressor NF1[176]; alteration in PI3K signalling such as mutation of AKT or loss of PTEN[177,178] and amplification of MITF or BCL2A increasing cell survival[179–181]. Both fibroblast and tumour associated macrophages (TAMs) are implicated in conferring MAPK resistance, with fibroblast secreted hepatocyte growth factor (HGF) and extra cellular matrix (ECM) remodelling leading to reactivation of MAPK signalling[182]. TAMs can also secrete growth factors such as VEGF leading to reactivation of MAPK signalling[183] and also secrete tumour necrosis factor alpha (TNFα) leading to increase survival through MITF [184].

Immunotherapy

The success seen with targeted therapies for the treatment of advanced stage $BRAF^{mut}$ melanoma has been mirrored by huge advances in immune based therapies. In 2011 the antibody Ipilimumab, a first in class immune checkpoint blockade therapy, targeting the inhibitory CTLA-4 receptor on T-lymphocytes[185] was approved for use in metastatic melanoma patients. In clinical trials, treatment with ipilimumab lead to increased overall patient survival when compared to the melanoma peptide vaccine gp100 or Dacarbazine[186–188]. The long term survival of patients after treatment with Ipilimumab is impressive with ~20% of patients surviving for at least 10 years[189].

The success of ipilimumab was quickly followed by the approval of two new immune checkpoint blockage therapies Nivolumab and Pembrolizumab. Both of these monoclonal antibodies bind the PD1 receptor, predominantly expressed on activated T lymphocytes, causing exhaustion and negatively regulating their anti-tumour activity. However, the PD1 receptor is also found on other activated lymphocyte subsets like NK or B cells[185]. In initial clinical trials the response rate to nivolumab was 30%[190], with subsequent trials going on to demonstrate increased overall response rates and progression free survival with both agents as a second line treatment in patients previously treated with ipilimumab, when compared to chemotherapy[191,192]. Nivolumab also demonstrated increased overall survival when used as the front line therapy in $BRAF^{wt}$ advanced melanoma patients when compared to chemotherapy[193]. Clinical trials have also demonstrated that both nivolumab and pembrolizumab provided increased response rates, progression free survival and overall survival benefit compared with ipilimumab as a front line therapy in advanced melanoma patients[194,195]. However, as with targeted therapy, it is combination therapy that has demonstrated the largest clinical benefit; a combination of nivolumab and ipilimumab demonstrated substantially improved response rate and

progression free survival in advance melanoma patients compared with either nivolumab or ipilimumab alone[194]. Further clinical trials have gone on to demonstrate improved overall survival with the combination of nivolumab and ipilimumab when compared to ipilimumab alone[196]. In 2015, the combination of nivolumab and ipilimumab was approved as the first line therapy for advanced melanoma patients with wild type BRAF.

Despite the successes observed with immune checkpoint blockade therapies in improving clinical outcomes for advanced stage melanoma patients, there are still issues to overcome. Firstly, there are a number of immune related adverse events which include rashes, epidermal necrolysis, colitis, , severe and persistent diarrhoea, hepatitis, pancreatitis, iridocyclitis, lymphadenopathy and neuropathies[190,197]. Secondly, as is observed with targeted therapies, a significant number of patients acquire resistance to immune checkpoint blockade or already are resistant to immune checkpoint blockade. There have been a number of mechanisms identified in playing a key role in immune checkpoint blockade resistance: upregulation of SK1 leading to potent Treg accumulation[198]; loss of function (LOF) mutations or downregulation of components of the antigen processing machinery and MHC class I antigen presentation pathways[199–201]; loss of PTEN[202,203]; increased beta catenin signalling[203,204], and loss of sensitivity of interferon gamma signalling[201,205].

Current melanoma therapies focus on only a few of the recognised cancer hallmarks, targeting the key mutations in MAPK signalling pathways which promote sustained proliferation and evasion of growth suppression and death, and through inhibiting negative regulators of immune destruction and inflammation. Another, perhaps underappreciated and therapeutically untapped cancer hallmark, is the alteration of cellular metabolism, providing tumour cells with the nutrients required for sustained growth and proliferation. A further understanding of the metabolic dependencies of cancer cells could provide new therapeutic targets for the treatment of melanoma.

1.8 Melanoma Metabolism

The study of cancer metabolism is one of the oldest areas of cancer biology research, predating the discovery of proto-oncogenes and tumour suppressors. For any cell it is essential to have the proper metabolic resources before attempting to proliferate; doing so in the absence of these resources could lead to cell death. This becomes even more critical in cancer cells due to their highly proliferative nature. Thus, tumorigenesis is highly dependent on the reprogramming of cellular metabolism to meet the bioenergetic and biosynthetic needs of malignant cells. These alterations which allow uncontrolled proliferation include: increased metabolite uptake such as glucose, amino acids or fatty acids; preferentially channelling nutrients through pro-tumorigenic metabolic pathways; influencing metabolite driven gene regulation and thus cellular fate, and metabolic interactions in the tumour microenvironment[206]. The alterations in tumour cell metabolism are now considered as hallmarks of cancer, playing a significant role in the initiation, maintenance and progression of cancer[39]. Tumour cells, and more specifically melanoma cells, are characterised by remarkable metabolic flexibility, robustness and versatility and are able to use a variety of fuels to meet both the bioenergetic and biosynthetic demands of melanoma initiation and progression. Melanoma cells are able to use both cytosolic and mitochondrial metabolic pathways to produce the key cellular energy currency, adenosine triphosphate (ATP), and synthesise key biosynthetic building blocks during cancer progression[207].

Glycolysis

In 1920 Otto Warburg made the striking discovery that even in the presence of sufficient levels of oxygen, cancer cells increase their uptake of glucose and preferentially metabolise glucose through glycolysis rather than oxidative phosphorylation (OXPHOS), leading to the production of lactate[208,209]. This is seemingly paradoxical given that the process of glycolysis is only able to produce two ATP, from a single glucose molecule, whereas complete OXPHOS through the TCA

cycle is able to produce thirty six[210]. Warburg hypothesised that this metabolic reprogramming was due to dysfunctional mitochondria, and that this event was the primary cause of cancer[211]. This particular hypothesis has since been disproven and the importance of OXPHOS and functional mitochondria has been demonstrated in melanoma[212,213]. This phenotype of upregulated glycolysis has now been termed the Warburg effect.

The predominant metabolic phenotype within melanoma, as with many other tumour types, is upregulated glycolysis leading to lactate production regardless of oxygen levels[212,214–216]. Reasons for this shift towards glycolysis in melanoma are still not yet fully understood and is multifaceted. Oncogenic activation of the MAPK pathway, through the predominant mutation in melanoma $BRAF^{V600E}$, not only promotes uncontrolled proliferation but is also, in part, responsible for metabolic reprogramming. Constitutive ERK1/2 signalling promotes glycolysis through induction of the transcriptional regulators of glycolysis[215,217], alteration of signalling through pyruvate dehydrogenase kinase 1 (PDK1) inhibiting OXPHOS[218], and inhibition of both Peroxisome proliferator-activated receptor-γ coactivator 1α (PGC-1α) and MITF, again key modulators of OXPHOS[146] . The PI3K pathway also plays a key role in this metabolic switch; loss of the tumour suppressor PTEN mediates HIF1a expression, a key activator of glycolytic metabolism[219]. Increases in HIF1α have been demonstrated to increase GLUT1 expression, a key glucose uptake transporter[220,221].

In normal tissue, glycolysis is the physiological response to hypoxia, thus this shift towards a glycolytic phenotype in tumours may just be a response to the hypoxic conditions in a tumour[222,223]. In tumours, O_2 levels are variable but in some cases have been shown to be often close to 0 mm Hg[222,223]. Exposure of melanoma cells to hypoxic conditions further increases the flux of glucose through glycolytic pathways[212]. However, there are a number of additional factors which may also explain this glycolytic shift. Although, the number of ATPs produced from one molecule of glucose is much lower when comparing glycolysis to the TCA cycle[210], the

rate at which glycolysis occurs when compared to the TCA cycle (occurring 10-100 times faster) means that, over the same period of time, comparable amounts of ATP can be produced[224]. This higher rate of glucose metabolism may give the tumour cells an advantage when competing with other cells types in the tumour microenvironment for limited energy resources[225,226]. Produced as the final product of glycolysis, lactate is secreted, altering the tumour microenvironment (TME), facilitating angiogenesis, supressing the immune response and promoting metastasis[227]. Lactate is taken up by the endothelial cells in the microenvironment leading to upregulation of VEGF[228] and the release of intracellular protons from lactic acid dissociation into the TME, lowering the pH[229], which promotes metastasis.

Furthermore, this high rate of glycolysis not only provides ATP for the bioenergetic needs of the cells, but also satisfies the biosynthetic needs by generating metabolic intermediates for multiple biosynthetic pathways. The first pathway branch point in glycolysis is into the pentose phosphate pathway (PPP), a pathway essential for nucleotide biosynthesis that is frequently elevated in tumorigenesis [230,231]. Glucose-6-phosphate is channelled out of glycolysis and oxidised to generate ribose-5-phosphate and NADPH. The next metabolic intermediate utilised from glycolysis is fructose-6-phosphate, which is used as a substrate in hexosamine biosynthesis. The hexosamine provides substrates for cellular glycosylation reactions which is essential for regulation and stability of proteins[232,233]. Perhaps the most important utilisation of glycolysis intermediates is the use of 3-phosphoglycerate as a precursor for serine and glycine biosynthesis. Serine is the major substrate of the one carbon cycle which contributes a number of metabolites used for cellular biosynthetic and regulatory purposes, including substrates for the biosynthesis of purines, thymidine[234]. The key enzyme Phosphoglycerate dehydrogenase (PHGDH), which catalyses the initial step of the serine/glycine synthesis pathway, is amplified in 40% of melanomas[235], highlighting the importance of this pathway.

TCA Cycle

Although a large percentage of melanomas are characterised by the highly glycolytic Warburg phenotype, a subset of melanomas rely on OXPHOS through the TCA cycle for the supply of ATP[146,236]. The high OXPHOS phenotype is driven by the upregulation of peroxisome proliferator-activated receptor γ 1-α (PGC1α), through mTOR mediated MITF nuclear translocation and subsequent PGC1α transcription[146,236]. PGC1α is highly expressed in this melanoma subset along with a number of other critical OXPHOS genes such as nuclear respiratory factors and mitochondrial factors involved in fission/fusion and mitochondrial transcription[237].

The TCA also plays a critical role in melanomas characterised by the Warburg phenotype. Although only a small amount of pyruvate enters the TCA cycle, OXPHOS still contributes a significant portion of cellular ATP, due to large quantities of ATP being produced from only a few molecules of pyruvate[210,212]. As with glycolysis, the TCA cycle also provides several metabolic precursors involved in key biosynthetic pathways in cancer cells, such as amino acid biosynthesis and fatty acid synthesis. Precursors for the non-essential amino acids aspartate and asparagine are produced through the TCA cycle, with the production of both having been shown to be important for melanoma cell growth and dependent on the ability of the cell to carry out OXPHOS[238,239]. Citrate from the TCA cycle can be exported into the cytosol which, when broken down by ATP citrate lyase (ACL) into acetyl-CoA and oxaloacetate, increases the pool of cytosolic acetyl-CoA which can then enter the fatty acid synthesis pathway[240]. Fatty acid synthesis is key for melanoma cell growth and survival and will be discussed further below.

In order to keep up with the demand for metabolic intermediates for biosynthetic pathways melanoma cells carry out a process called anaplerosis to replenish these TCA cycle intermediates. In melanoma cells the main carbon source for entry into the TCA cycle and the production of these critical biosynthetic precursors is glutamine[212].

This process, called glutaminolysis, involves the conversion of glutamine to glutamate through cytosolic glutaminase which, once converted to α-ketoglutarate, can enter the TCA cycle and maintain OXPHOS[239,241]. Glutaminolysis through the TCA cycle not only provides a source of energy for the proliferating cells but also, through a reverse in TCA cycle flow, provides citrate for fatty acid synthesis , through the carboxylation of α-ketoglutarate[212,242]. The importance of glutamine is appreciated in a number of cell types, this is also the case in melanoma where reduction of glutamine availability to melanoma cells or inhibiting its flux in the TCA cycle reduces melanoma cell viability[239,242,243].

1.9 Lipid Metabolism

Alterations in lipid metabolism comprise another key aspect of pro tumorigenic reprogramming of cellular metabolism. Fatty acids (FA) are essential for transformed cells, providing the building blocks for synthesis of a diverse range of lipids to maintain membrane biosynthesis during proliferation, provide an energy source in metabolically stressful conditions and act as secondary messengers in signal transduction pathways. As such, alterations in fatty acid synthesis, uptake, catabolism and storage are all hallmarks of this altered lipid metabolic phenotype observed in transformed cells[244–246]. Enrichment of a 5 gene signature, including genes involved in both fatty acid uptake and fatty acid oxidation, has been shown to predict a significantly worse prognosis for melanoma patients[247], highlighting the importance of these alterations in lipid metabolism in melanoma.

Fatty Acid Synthesis

De novo synthesis of fatty acids in mammalian cells is usually restricted to certain cell lineages such as adipocytes and hepatocytes, located in the liver, adipose and lactating breast tissue. The majority of mammalian cells preferentially use the uptake of free fatty acids (FFA) and lipoproteins to meet their lipid requirements. However,

melanoma cells reactivate *de novo* lipid biosynthesis, even in the presence of exogenous sources of lipid.

The main substrate for fatty acid biosynthesis is cytosolic acetyl CoA and is derived from citrate produced in the TCA cycle from either glucose or glutamine, through oxidation or carboxylation respectively. Citrate is converted into cytosolic acetyl CoA by ATP–citrate lyase (ACLY), acetyl CoA is then irreversibly carboxylated into malonyl-CoA by acetyl-CoA carboxylase (ACC). The next step is catalysed by fatty acid synthase (FASN) and involves condensing 7 malonyl-CoA molecules and one acetyl-CoA producing the saturated 16-carbon FA palmitate (FA16:0). Palmitic acid is then elongated and desaturated by a myriad of enzymes such as stearoyl-CoA desaturase SCD, ELOVL (fatty acid elongase) COX1/2, 1-acylglycerol-3-phosphate O-acyltransferase (AGPAT) and SPHK (sphingosine-1-kinase) to produce a highly diverse range of lipid species.

The expression of enzymes involved in FA synthesis are controlled by a master transcriptional regulator Sterol regulatory element-binding proteins 1 (SREBPs), part of a family of ER bound transcription factors[248]. It is the SREBPC1c splice variant which controls the expression of the genes involved in FA synthesis; in normal cells its activity is controlled by insulin, progesterone and estrogen[249,250]. In cancer cells, including melanoma, the activity of SREBPC1c is constitutively driven by the hyperactivated MAPK and PI3K pathways, which causes an upregulation in the levels of FASN[251,252]. FASN catalyses the rate limiting step in FA synthesis, and as such, drives a lipogenic phenotype, meeting the FA needs of highly proliferative cells, to produce cellular and organelle membranes[250]. Increased FASN levels are observed in metastatic melanoma and are associated with increased tumour invasion and a worse outcome in melanoma patients[253–255]. Inhibition of FASN has been shown to lead to melanoma cell death and reduce metastasis in a mouse model of melanoma[256–258].Increased expression of members of the FA synthesis pathway, such as FASN and ACLY, have also been linked to resistance to MAPK inhibition in

melanoma models both *in vitro* and *in vivo*[251,259]. However the use of inhibitors of FASN in a clinical setting have been limited due to side effects and poor pharmacological properties[260].

Fatty Acid Uptake

In order to meet the high demands for FA, cancer cells not only increase lipid synthesis, but also scavenge exogenous free fatty acids (FFA) from either the blood supply or close contacts with adipocytes. In order to uptake exogenous FFA, specialised transporters are required to facilitate efficient uptake across the plasma membrane, these include CD36, also known as fatty acid translocase (FAT), fatty acid transport protein family (FATPs), and plasma membrane fatty acid-binding proteins (FABP), all of which display increased expression across multiple tumour types.

In melanoma, overexpression of two members of the FABP family, FABP3 and FABP7, have been shown to be upregulated when compared to benign nevi, with FABP7 enhancing melanoma cell proliferation and invasion[261–264]. CD36 has been shown to be linked with enhanced fatty acid scavenging in metastasis initiating cells in melanoma[265]. Among the members of the FATP family, FATP1 is significantly overexpressed in melanoma. FATP1 has been shown to be critical for uptake of lipids from adipocytes, with inhibition of FATP1 leading to a decrease in melanoma cell lipid uptake, invasion and proliferation[266]. Additionally, in both a transgenic zebrafish model and mouse xenograft model of melanoma, overexpression of FATP1 cooperated with $BRAF^{V600E}$ to accelerate melanoma development[266]. Further highlighting the importance of FFA uptake in melanoma, transcriptomics of mutant RAS driven zebrafish melanoma highlighted an enrichment of genes involved in FA scavenging, including LPL, FABP7 and FATP2[267]. Lipoprotein lipase (LPL) is secreted by cells and acts as a hydrolase breaking down triglycerides into fatty acids for transport into the cell by CD36 or the FATP proteins. LPL was found to be expressed in human melanoma cells and knock down of LPL in cell lines with low FASN expression, and thus lower levels of lipid synthesis, lead to inhibition of melanoma cell growth[267]. Co-inhibition of both FASN and LPL in FASN-high melanoma cell lines

synergised to reduce melanoma cell growth. Additionally, overexpression of LPL co-operated with oncogenic RAS to accelerate melanoma development and growth in a transgenic zebrafish model of melanoma[267].

Fatty Acid Beta Oxidation

Despite the seeming contradiction with the increase in fatty acid synthesis in cancer cells, the breakdown of FA through mitochondrial beta oxidation (FAO) has also been shown to play a key role in cancer development and progression. FAO has the capacity to fuel cancer cells under conditions of metabolic stress, acting as a source of both ATP and NADH thus meeting both the energetic and REDOX needs of cancer cells[268,269].

FAO is a multi-step catabolic process in which the mitochondria convert long-chain FA into acetyl-CoA for use in the TCA cycle and the electron transport chain, to meet the bioenergetic demands and redox homeostasis in a cell. Before entering the mitochondria, fatty acyl CoA synthase activates fatty acids into fatty acyl CoA, then, on the outer mitochondrial membrane, Carnitine palmitoyltransferase I CPT1 coverts fatty acyl CoA into fatty acyl carnitine. Fatty acyl carnitine is then transported into the mitochondria by the carnitine/acylcarnitine translocase (CACT), where it is then reconverted into acyl CoA by Carnitine palmitoyltransferase II CPT2, acyl CoA is then cleaved into acetyl CoA in a 4-step catalytic cycle. Acetyl-CoA can then enter the TCA cycle and be used to produce ATP, or used to produce NADPH to support biosynthesis and redox homeostasis[270].

FAO has been shown to play an important role in cell growth, metastasis, cancer stem cells and drug resistance across a number of tumour types[268,269]. In melanoma, only a little is known about the role of FAO in driving progression. The key enzyme translocating fatty acids into the mitochondria, CPT2, is highly upregulated in melanoma compared to benign nevi[261], suggesting melanoma do rely on FAO.

Additionally, two different studies have highlighted a role for FAO in melanoma metastasis; the first demonstrated that derived metastatic melanoma cells were much more reliant on FAO for their bioenergetic needs, relative to non-metastatic controls[271]. A second study has shown cross talk between adipocytes and melanoma cells, the adipocytes secrete exomes that increased FAO in the melanoma cells and promotes migration and invasion[272].

Fatty Acid Storage- Lipid Droplets

In order to avoid lipid overload, due to both increased FA synthesis and uptake, which can lead to aberrant FAO and consequently ROS, lipid peroxidation and protein and DNA damage, cells maintain FA homeostasis through the storage of lipids in cytoplasmic organelles termed lipid droplets (LDs). LDs originate from the endoplasmic reticulum (ER) and are characterised by a monolayer of phospholipid embedded with a diverse content of proteins covering a hydrophobic neutral lipid core containing mainly triacylglycerol (TAGs) and cholesteryl esters (CEs). The storage of lipids and thus the maintenance of FA homeostasis is perhaps more critical in cancer cells in which the biosynthetic and bioenergetic demands are increased. The first evidence for LDs in human tumours came in the 1960s in mammary carcinomas[273] and lymphomas[274]. In spite of this, it has not been until the last 10-15 years that the role of LDs in promoting numerous cancer hallmarks has been uncovered[275].

LD biogenesis and breakdown is highly dynamic and controlled by cellular and environmental cues such as nutrient levels, oxidative stress, mitochondrial dysfunction, hypoxia and autophagy. LD biogenesis occurs in the ER, where, between two leaflets of the ER membrane, both TGs and CEs are synthesised, with the final steps catalysed by Diacylglycerol acyltransferases 1 and 2 (DGAT1/2) and acyl-CoA cholesterol acyltransferases 1 and 2 (ACAT1/2 respectively)[276–279]. This forms a lipid lens within the ER bilayer which, once sufficient lipids have accumulated, is able to

bud off to form a nascent lipid droplet, which maintains contact with the ER, enabling bidirectional transfer of cargo, or can form contact with other cellular components such as the mitochondria, autophagosome and proteasome[279–281]. In addition to neutral lipids, LDs also contain a subset of proteins, most of which are involved in lipid metabolism, such as sterol biosynthetic enzymes or lipases. Using these lipases is one of the ways lipid droplets are broken down through lipolysis to provide a regulated release of FA for use in FAO, membrane synthesis, ER homeostasis and the synthesis of lipid signalling molecules. Lipolysis is carried out by three lipases, adipose triglyceride lipase (ATGL), hormone-sensitive lipase (HSL) and monoacylglycerol lipase (MAGL)[282]. The second mechanism by which FA can be released from lipid droplets is through lipophagy, in which LDs are delivered to lysosomes through macroautphagy and acid lipases act to liberate FA[283].

Despite the dearth of evidence for the role of lipid droplets specifically in melanoma, the tumour promoting roles of lipid droplets have been highlighted in other cancer types, and further evidence can be found in exploring lipid droplet function in various cell types. Lipid droplets have been shown to impact upon several hallmarks of cancer including, reprogrammed metabolism, increased proliferation , alterations in cell signalling, immune modulation and resisting cell death[275]. Perhaps the primary role of LDs is to act as a lipid reservoir, balancing FA homeostasis through sequestering FFAs, DAGs, CEs and ceramides into inert neutral lipids to prevent lipotoxicity leading to cell death[284,285]. LDs and FAO are intrinsically linked; excess FA can only be removed through storage in the form of LDs, or are broken down during FAO. Channelling of excess FA in LDs has been shown to protect various cell types from lipotoxicity, as a result of lipid overload, due to diet induced obesity, cardiomyopathy and incubation with exogenous FA[284,286–288]. Although the roles of different FA species in supporting LD accumulation in cancer is still not yet fully understood, LD biogenesis in breast cancer models has been shown to prevent lipotoxicity upon challenge with exogenous FA, with unsaturated FA being preferentially incorporated in TAGs[289–293] .

In addition to lipotoxic stress, LDs have also been shown to be highly important for both normal and cancer cells in dealing with other stressors such as nutrient and oxidative stress and hypoxia. Somewhat surprisingly, in both normal and cancer cells, including fibroblasts, glioblastoma and ovarian cancer cells, starvation has been shown to increase lipid droplet biogenesis[294–296], a paradox considering that TAG synthesis is an ATP-consuming process. LDs must therefore be critical for cell survival under these conditions and have been shown to be necessary for both preventing lipotoxicity due to release of FA through autophagy[295] and highly efficient transfer of FA through lipolysis into the mitochondria for ATP production through FAO[297,298]. Hypoxia has also been shown to lead to an increase in LD formation in cancer cells[299–302]; this maybe a consequence of a metabolic switch in these cells that renders them dependent on fatty acid uptake to meet the demand for unsaturated FA[300,303]. Under oxygen deprivation, the pro-tumorigenic impact of increased LD is three-fold; firstly through preventing ROS accumulation and managing redox homeostasis[300]; secondly through preventing the toxic build-up of saturated lipid species[304] and finally providing temporary storage of FA which, upon reoxygenation, can be released into the mitochondria for FAO to enable cell growth[301]. Additionally, oxidative stress can also occur due to an accumulation of oxidised poly-unsaturated fatty acids (PUFA), which are highly vulnerable to lipid peroxidation due to ROS and further amplify ROS production[305,306]. In an aggressive breast cancer cell line model, PUFA were found to be concentrated in LD, shielding them from peroxidation[290].

LD have also been linked to two further cancer hallmarks: sustaining proliferative signalling and evasion of immune destruction. A study recently demonstrated that LD number and localisation were linked with cell cycle progression in untransformed cells, with higher numbers of LDs observed during S phase and polarisation during mitosis[307]. In clear-cell renal carcinoma cells LDs contribute to the bypassing of a lipid mediated G1 checkpoint under lipid deprivation conditions[308], whilst in colon cancer, increased LD density led to loss of the cell cycle inhibitor p27kip1 in a FOXO3 dependent manner[309]. Additionally, several signalling proteins with well-established roles in oncogenic transformation and progression have been found localised in LD,

further highlighting the role of LD as a proliferative hub[310,311]. LDs also act as specialised sites for the synthesis of signalling lipids such as eicosanoids, which play key roles in both cellular proliferation and suppressing immune surveillance[312]. In both colon cancer and melanoma models, the eicosanoid PGE_2 has been shown to promote cellular proliferation[313,314], and in melanoma to play a key role in immune evasion through inducing immunosuppression[315]. In addition to their roles with tumour cells themselves, LD are also found within immune cell types such as macrophages, dendritic cells and myeloid derived suppressor cells; although the roles of LD within these cells isn't yet fully understood, LD have been shown to play key roles in the immunometabolic phenotype of these cells[316–319]. This provides a further mechanism in which LD are able to modulate an immunosuppressive microenvironment to promote tumour survival.

The evidence for lipid droplets and thus their importance in melanoma is limited. Two studies used staining for a protein that coats lipid droplets, adipophilin, as a marker of lipid droplets, demonstrating that an increase in adipophilin expression was increased from stage I/II through to stage III/IV melanoma and that high adipophilin was associated with both a higher proliferation rate and a decrease in both overall survival and metastasis survival[320,321]. LD accumulation has also been linked with dedifferentiated stem-like melanoma cells; Oil Red O staining in melanoma melanosphere stem models correlated with expression of the stemness marker CD133 and lipid storage PPAR/SREBP transcriptional programmes[322]. A more recent study demonstrated that co-culture of melanoma cells with adipocytes led to an increase in the number of lipid droplets in the melanoma cells and increased proliferation and invasion[266]. The increase in lipid droplets upon culture with adipocytes was also confirmed in an *in vivo* zebrafish xenograft model of melanoma[266].

Further understanding of the role of lipid metabolism in cancer and the maintenance of FA homeostasis through synthesis, catabolism and storage and the enzymes

involved has provided new therapeutic opportunities for the treatment of melanoma. Specifically, the role of LD in lipid metabolism in cancer, promoting multiple hallmarks of cancer and the enzymes involved in the biogenesis and breakdown of LD may also provide therapeutic targets.

Diacyclglycerol acyltransferase 1 (DGAT1)

The final and committing step in TAG synthesis is catalysed by the Diacylglycerol acyltransferases 1 and 2. These ER-localised transmembrane proteins perform an esterification reaction of diacylglycerol (DAG) and fatty acyl-CoA to form TAGs, which can be assembled to form lipid droplets[323]. Although able to carry out the same esterification reaction, DGAT1 and DGAT2 are encoded by two distinct genes, on chromosome 8 and chromosome 11 respectively, which share very little homology and are part of two separate gene families[276,277]. Both DGAT1 and DGAT2 are expressed almost ubiquitously and are most highly expressed in tissues that synthesise the largest amounts of triglycerides, such as the intestine, adipose tissue and the liver, although their expression patterns do differ[276,277]. Animal models suggest that DGAT1 and DGAT2 have non-redundant roles, however their specific cellular functions are still yet to be fully understood[323–325]. Whereas DGAT1 has only been shown to localise in the ER, DGAT2 has been found as part of a complex in both the mitochondrial associated membrane and in LD themselves, shedding some light on the possible different functions of DGAT2[326,327]. In mice, knockout of DGAT2 (*Dgat2*$^{-/-}$) is incompatible with life, with mice only surviving for a few hours after birth[328], whereas DGAT1 (*Dgat1*$^{-/-}$) knockout mice are viable and have altered lipid and glucose metabolism[323]. Therefore, there has been a focus on DGAT1 as a possible therapeutic target in both obesity and diabetes in humans.

The understanding of the physiological role of DGAT1 has predominantly come from studies in genetically modified mice, and has demonstrated that beyond its biochemical function, DGAT1 modulates complex physiological processes with

implications for disease. DGAT1 knockout (*Dgat1*$^{-/-}$) mice have a lean phenotype, due to an approximately 50% reduction in adipose mass than wild-type mice on a standard chow diet[329]. The knockout of DGAT1 (*Dgat1*$^{-/-}$) also leads to resistance to diet induced obesity, maintaining a lean phenotype even on a high fat chow diet, due to both a decrease in the rate of TAG absorption from the gut and increased energy expenditure through an increase in thermogenesis[329–332]. This genetic evidence is now supported by studies using small molecule inhibitors of DGAT1, in which inhibition of DGAT1 protects mice from diet induced obesity[333,334]. *Dgat1*$^{-/-}$ mice also do not develop obesity linked hepatic steatosis when fed a high fat diet[332], again this is supported by evidence demonstrating similar protection using a small molecule inhibitor of DGAT1[334]. Further highlighting the critical importance of DGAT1 in the observed phenotype, enterocyte specific overexpression of *Dgat1* causes the *Dgat1*$^{-/-}$ mice to no longer have resistance to diet induced obesity[335]. Alterations in glucose metabolism are also observed in *Dgat1*$^{-/-}$ mice, correlating with the decrease adiposity. This is evidenced by improved glucose tolerance and increased glucose infusion rate after challenge with either an intraperitoneal glucose load or an insulin injection in the *Dgat1*$^{-/-}$ mice[330,336]. Hyperinsulinemia-euglycemic clamp experiments confirm increased insulin sensitivity, showing *Dgat1*$^{-/-}$ mice require ~20% higher glucose infusion rate when compared to WT mice to maintain normal blood glucose levels[330,336]. The precise cellular mechanisms that mediate the alterations in glucose metabolism are unknown, however alterations in the expression levels of key proteins regulating insulin signalling such as PI3K, protein kinase B, protein kinase Cλ and insulin receptor substrate-1 are observed in *Dgat1*$^{-/-}$ mice[336,337]. DGAT1 also has a role in mediating lipotoxicity at both the tissue and cellular level, through its critical role in mediating TAG storage in LD. In mice, the overexpression of *Dgat1* in white adipose tissue (WAT) leads to increased TAG deposition in WAT but decreased deposition in non-adipose tissues, when fed a high fat diet, thus protecting non-adipose tissues from lipotoxicity[338]. This observation has been replicated in cardiac tissue in which overexpression of *Dgat1* in cardiac tissue decreases lipotoxicity and knockout leads to a build-up of toxic lipid species[287,339]. This is also supported by evidence in cell line models such as mouse embryonic fibroblasts, where, under nutrient stress, knockdown of DGAT1 leads to increased

oxidative stress and lipotoxicity, due to an overloading of the mitochondria with acyl carnitines[295], mechanistically tying in with the known roles played by LD. Similar effects are also observed in cell line adipocyte models, in which DGAT1 plays a crucial role in preventing a toxic build-up of FA in the ER leading to lipotoxicity[288].

Very little is known about the role of DGAT1 in cancer, with studies examining DGAT1 in prostate cancer. The expression of DGAT1 was found to be increased in prostate cancer cell lines (PCa) when compared to normal prostate epithelial cells, and small molecule inhibition of DGAT1 over a period of 36 hours decreased PCa proliferation, migration and invasion and also a reduction in the number and density of LD in these cells[340]. Similar results were obtained using siRNA to knockdown DGAT1 in LNCaP prostate cancer cells, with both a reduction in LD and proliferation observed[341]. The suppression of PCa growth was also observed *in vivo*; pre-treatment of PC3 prostate cancer cells with a DGAT1 inhibitor prior to implantation under the kidney capsule of SCID mice decreased tumour growth when compared to a vehicle treated control[340], corroborating with the *in vitro* data the DGAT1 inhibitor treated cells had a both a reduced proliferative capacity and a reduction in the number of lipid droplets[340]. This highlights a role for DGAT1 and LD promoting PCa growth and survival. Given the numerous cancer hallmarks modulated by LD and critical role of DGAT1 in LD biogenesis it is possible to suggest DGAT1 may play a tumour promoting role in a wider array of cancer types.

Major Thesis Aims

The major aims of this thesis can therefore be explained in three key points:

- To identify novel metabolic oncogenes in melanoma using a cross-species oncogenomic approach using zebrafish models of melanoma and the TGCA patient dataset, we hypothesise that this cross-species approach will enable the identification of bone fide oncogenes.
- Elucidate the oncogenic potential of the identified metabolic oncoproteins in an *in vivo* model of melanoma, utilising the miniCoopR system in Tg(mitfa:BRAFV600E;p53-/-;mitfa-/-), Tg(mitfa:NRASG12D;p53-/-;mitfa-/-) and (tp53M214K/M214k; mitfa-/-) transgenic zebrafish. we hypothesise that the identified putative oncogenes co-operate with known melanoma oncogenes to accelerate tumour development.
- Identify the oncogenic mechanisms of the identified metabolic oncoproteins using both *in vivo* and *in vitro* models of melanoma utilising both omics approaches and *in vitro* techniques assessing cellular signaling, growth and metabolism.

Chapter 2 Materials and Methods

2.1 Experimental Models

Regulated procedures involving zebrafish were ethically approved by The University of Manchester Animal Welfare and Ethical Review Body (AWERB), or by the UMMS Institution Animal Care and Use Committee (A-2016, A-2171), and carried out under a licence issued by the appropriate national regulatory authority. Zebrafish were housed at ~28 °C under a 14 h light/10 h dark cycle. Transgenic zebrafish expressing *BRAF*^{V600E} or *NRAS*^{G12D} have been previously described[342,343] and were crossed onto a *mitfa*$^{w2/w2}$ (*mitfa*$^{-/-}$) background to suppress melanocyte development and further onto a *tp53*$^{M214K/M214K}$ background to promote tumorigenesis. Melanocyte restoration and simultaneous over-expression of Dgat1a, Dgat2 or EGFP was then achieved by injection of embryos with a mitfa-minigene containing plasmid as previously described. Briefly, zebrafish *dgat1a* and *dgat2* were amplified from cDNA of wild-type 48 h post-fertilisation zebrafish embryos, and subcloned into the pDONR221 vector (see Key Resource Table for oligonucleotide sequences). The pDest-mitfa:dgat1a-pA and pDest-mitfa:dgat2-pA destination vectors were created using an LR clonase reaction consisting of p5E-mitfap, pME-dgat1a or pME-dgat2, p3E-pA and an empty destination vector. Expression plasmid was injected into zebrafish zygotes along with Tol2 mRNA. pCS2-TP plasmid for Tol2 mRNA generation was a kind gift from Dr Koichi Kawakami (National Institute of Genetics). Sufficient embryos for all experimental arms were generated simultaneously, pooled and then randomly assigned to a construct, although formal randomization techniques were not used. Zebrafish were group-housed according to the construct. Only zebrafish embryos with near complete melanocyte rescue at 5 days were retained for further analysis. Analysis of tumor formation was not performed blinded to the construct identity. Sample sizes were not predetermined based on statistical power calculations but were based on our experience with these assays. To assess the statistical significance of differences in overall survival, we used Mantel–Cox's log-rank tests.

2.2 Methods Details

2.2.1 Cell Lines

Human melanoma cell lines were cultured in High Glucose DMEM with 10 % FBS, and penicillin–streptomycin (Sigma) at 37 °C and 5 % CO_2. Normal human melanocytes were purchased from Cascade Biologics and cultured according to manufacturer´s guidelines. Lenti-X cells were cultured in High Glucose DMEM with 10 %v/v FBS, and penicillin–streptomycin (Sigma) at 37 °C and 5 % CO_2. All cells tested negative for mycoplasma and cell lines were authenticated using STR profiling.

Cell line	**Genetic drivers**	**DGAT1 status**
888MEL	$BRAF^{V600E}$	DGAT1 low
SKMEL28	$BRAF^{V600E}$	DGAT1 medium
SKMEL2	$NRAS^{Q61R}$	DGAT1 over expressed
MM485	$NRAS^{Q61R}$	DGAT1 over expressed
A375	$BRAF^{V600E}$	DGAT1 over expressed
SKMEL105	$BRAF^{V600E}$	DGAT1 over expressed
LOXIMVI	$BRAF^{V600E}$	DGAT1 amplified
SKMEL5	$BRAF^{V600E}$	DGAT1 amplified

Table 1. Cell Lines

2.2.2 Compounds and Antibodies

Compounds were used at the following concentrations unless otherwise noted 50 µM AZD3988 (Tocris), 30 µM A922500 (Stratech) 50 µM AZD7687, 70 µM T863 (Sigma), 1 µM Oligomycin (Sigma), 0.5 µM FCCP (Sigma), 1 µM Antimycin-A (Sigma), 1 µM Rotenone (Sigma), 50 µM PF-06424439 (Sigma), 5 µM Ebselen (Tocris), 1 mM Tempol, 200 µM Paraquat (Sigma), Menadione (Sigma), 100 µM Etomoxir (Sigma), 1 µM LY2584702 (Stratech), 10 µM PF-4708671 (Generon), 5/10 µM Compound C (Sigma), 2 µM Ferrostatin-1 (Sigma).

Antibodies against DGAT1 (ab54037), phospho-PDE1a (ab92696) and 4-Hydroxynonenal (ab46545) were purchased from abcam. Antibodies against Vinculin (66305-1-Ig), Beta-Tubulin (10094-1-AP), PINK1 (23274-1-AP), Parkin (14060-1-AP), SOD1 (10269-1-AP), SOD2 (24127-1-AP), Sestrin 2 (10795-1-AP), GAPDH (60004-1-Ig), and PDK4 (12949-1-AP) were purchased from Proteintech. Antibodies against phospho-S6 (2215), phospo-eEF2 (2331), phospho-AMPK (50081), phospho-RAPTOR (2083), Caspase-3 (9662), phospho-P70 S6 kinase (9206), P70 S6 Kinase (2708), S6 (2317) and GFP (2956) were purchased from Cell Signalling. The Antibody against HA (901533) was purchased from Biolegend. The Antibody against gamma-tubulin (T5326) was purchased from Sigma.

2.2.3 Plasmids & siRNA

All plasmids were transfected using Lipofectamine (Invitrogen) following standard protocols. The plasmids used were purchased from Addgene: pRK7-HA-S6K1-WT (8984); pRK7-HA-S6K1-F5A-E389-deltaCT (8990); pcDNA3.1-mMaroon1 (83840). The GFP and WPRE elements were excised from pCDH-MCS-T2A-copGFP (a kind gift from Andrew Gilmore, The University of Manchester) using BspEI and KpnI. mApple (BspEI and XhoI adapters) and WPRE (XhoI-KpnI adapters) were PCR amplified, digested and subcloned to create the pCDH-MCS-T2A-mApple vector (see Key Resource Table for

oligonucleotide sequences). DGAT1 was further subcloned into the both the pCDNA3.1 vector and pCDH-MCS-T2A-mApple using the MCS.

All siRNA was transfected using Lipofectamine RNAi Max (Invitrogen) following standard protocols. The following siRNA were ordered from Dharmacon: DGAT1 007 5' UCAAGGACAUGGACUACUC 3'; DGAT1 008 5' GCUGUGGUCUUACUGGUUG 3'; DGAT1 smart pool #J-009333-00-0005; DGAT2 01 5' GAACACACCCAAGAAAGGU 3'; DGAT2 02 5'GGAGGUAUCUGCCCUGUCA3'; DGAT2 03 5' UCAUGGAGCUGACCUGGUU 3'; DGAT2 04 5'GAAUGCCUGUGUUGAGGGA 3'; DGAT2 smart pool #J-009333-08; SESN2 19 5'GGAGGGAGUAUUAGAUUAU3'; SESN2 20 5'GCAGGGACCCGUUGAACAA3'. The scrambled control siRNA (SIC002) was ordered from Sigma.

2.2.4 Viral transduction

Briefly, Lenti-X cells were transfected with pMDLg/pRRE, pMD2.G, pRSV-Rev plasmids (all kind gifts from Angeliki Malliri, Cancer Research UK Manchester Institute) and pCDH-EF1α-DGAT1-T2A-mApple viral vectors using Fugene (Promega) following standard protocols. The viral containing supernatant was filtered using a 0.45 μm filter and frozen at –80 °C prior to transduction of target cells. The supernatant containing the viral particles was added to target cells along with 10 ng/ml Polybrene (Millipore) for 24 h. Target cells were then grown and selected from single cell colonies.

2.2.5 Protein lysate preparation and Western Blotting

Cells were washed with PBS and lysed with sample buffer (62.5 mM TRIS pH 6.8, 2 %w/v Sodium dodecyl sulfate (SDS), 10 %v/v glycerol, 0.01%w/v bromophenol blue, 3 %v/v 2-mercaptoethanol). Lysates were then sonicated and heated to 95°C for 10 minutes prior to being evenly loaded onto SDS-polyacrylamide gels using the Mini Trans-Bot electrophoresis system (Biorad), followed by transfer to PVDF using standard western blotting procedures.

2.2.6 Lipid droplet staining and image analysis

Bodipy 493/503

Indicated cells were stained with 2 µM Bodipy 493/503 (ThermoFisher Scientific) and 5 ng/ml Hoecsht 3342 (Cell Signalling) for 30 minutes prior to fixing in 4 %w/v paraformaldehyde and imaging using a Leica microscope system. Images were processing using Fiji.

Lipidtox

Indicated cells were fixed in 4 %w/v paraformaldehyde and stained with LipidTox Green (ThermoFisher Scientific) according to manufacturer's instructions, and 5ng/ml Hoecsht 3342 (Cell Signalling) for 15 minutes prior to imaging using a Leica microscope system. Images were processing using Fiji.

2.2.7 RNA Isolation and real-time PCR analysis

RNA from cell lines was isolated with TRIZOL® (Invitrogen). After chloroform extraction and centrifugation, 5 µg RNA was DNase treated using RNase-Free DNase Set (Qiagen). 1 µg of DNase treated RNA was then taken for cDNA synthesis using the Protoscript I first strand cDNA synthesis kit (New England Biolabs). Selected genes were amplified by quantitative real time PCR (RT-qPCR) using Sygreen (PCR Biosystems). Relative expression was calculated using the delta-delta CT methodology and beta-actin was used as reference housekeeping gene. Sequences for primers used can be found in the key resource table.

2.2.8 Incucyte cell-proliferation assay and apoptosis assay

Indicated cell lines were seeded into 24-well plates at a density of 15,000–20,000 cells per well, depending on growth rate and the design of the experiment. After 24 h drugs or siRNA were added, and cells were imaged every hour using the Incucyte ZOOM (Essen Bioscience) Phase-contrast images were analysed to detect cell proliferation based on cell confluence. For cell apoptosis, caspase-3 and caspase-7 green apoptosis-assay reagent (Life Technologies) was added to the culture medium following manufacturer's instructions. Cell apoptosis was analysed based on green fluorescent staining of apoptotic cells.

2.2.9 Flow cytometry

Mitochondrial Membrane potential

Indicated cell lines were trypzinized and pelleted by centrifugation at 500 g for 5 min, washed with PBS. For mitochondrial membrane potential cells were stained with 2 µM JC-1 (Life Technologies) for 30 minutes at 37 °C. For positive control samples 0.5µM FCCP was added simultaneously with JC-1. Data was acquired by the BD BIOsciences Foretessa and quantified using the Flowjo software. A minimum of 10,000 cells were analysed per condition.

Lipid peroxidation

Indicated cell lines were trypzinized and pelleted by centrifugation at 500 g for 5 min, followed by a PBS wash. For lipid peroxidation cells were stained with either 5 µM BODIPY™ 581/591 C11 (ThermoFisher Scientific) or MitoPerOx (Abcam) for 30 minutes at 37 °C. Data was acquired by the BD BIOsciences Foretessa and quantified using the Flowjo software. A minimum of 10,000 cells were analysed per condition.

Mitochondrial ROS

Indicated cell lines were trypzinized and pelleted by centrifugation at 500 g for 5 min, followed by a PBS wash. For mitochondrial specific ROS detection, cells were stained with 2.5 µM Mitosox (ThermoFisher Scientific) for 30 minutes at 37 °C. Data was acquired by the BD BIOsciences Foretessa and quantified using the Flowjo software. A minimum of 10,000 cells were analysed per condition.

2.2.10 Proliferation Assays

Crystal Violet

Indicated cells were stained and fixed with 0.5 %w/v crystal violet (Sigma) in 4 %w/v paraformaldehyde/PBS for 30 minutes. Fixed cells were then solubilised in 2 %w/v SDS/PBS and absorbance measured at 595 nm using Synergy H1 microplate reader (BioTek).

EdU Incorporation

Indicated cells were labelled with 20 µM 5-ethynyl-2'-deoxyuridine (EdU) for 4 h and processed following the manufacturer's protocol (Click-iT® EdU Alexa Fluor® 488 Imaging Kit, Thermo Fisher). Prior to imaging cells were then stained with 5ng/ml Hoecsht 3342 for 15 minutes. Stained cells were analysed using a using a Leica microscope system. Images were processing using Fiji.

2.2.11 Dihydroethidium Assay

Cells were stained with 5 µM Dihydroethidium for 20 minutes in the dark at 37 °C. Fluorescence was measured at excitation 480nm emission 570 nm using Synergy H1 micro plate reader (BioTek). Fluorescence values were normalised to cell number by staining the cells with crystal violet after fluorescence read.

2.2.12 Cancer bioinformatics

We evaluated both point mutations and CNV in the TCGA SKCM firehose legacy, TCGA pan-cancer and Cancer Cell Line Encyclopedia datasets using the cBioPortal platform[344]. The GISTIC2.0 algorithm was used to identify focal amplifications[345]. Gene Ontology analysis was carried out using both enrichR[346] and metascape software[347]. Association between mRNA expression in TCGA datasets and survival was evaluated using OncoLnc[348]. mRNA levels determined by microarray were accessed through the Oncomine platform[349].

2.2.13 RNA-seq and Gene Ontology Analysis

Zebrafish tumors were excised and the RNA isolated using RNeasy RNA extraction kit (Qiagen) after homogenisation. RNA-seq libraries were prepared using a TruSeq stranded mRNA sample prep kit and run on a HiSeq 4000 (Illumina) platform. Adapters were trimmed from raw sequencing reads using Trimmomatics v0.32[350]. Trimmed reads were aligned to the zebrafish genome (Ensembl, GRCz11) using STAR v2.5.3[351]. and the Ensembl GRCz11 annotation file. Reads that mapped to chromosomes 1-25 were retained. Gene counts were determined using featureCounts v1.6.2[352] and differential expression analysis was performed using DESeq2 v1.14.1[353], using a adjusted p-value cut off of <0.05. DESeq2 was used to generate log2-normalised variance stabilising transformed (VST) counts. Heatmaps were produced using morpheus (https://software.broadinstitute.org/morpheus). Hierarchical clustering was performed using the one minus Pearson correlation method. Prior to Gene Ontology analysis, zebrafish genes were converted to their human orthologue (bioDBnet), the analysis was carried out using enrichR[346] and metascape[347].

2.2.14 Proteomics

SILAC labelling

For quantitative mass spectrometry, A375 cells were labelled in SILAC DMEM supplemented with 10 %v/v dialyzed fetal bovine serum (Sigma), 2 mM glutamine, 100 U/ml penicillin and 100 µg/ml streptomycin for 15 days to ensure complete incorporation of amino acids (data not shown). Two cell populations were obtained: one labelled with natural variants of the amino acids (light label; Lys0, Arg0) and a second one with heavy variants of the amino acids (L-[13C6,15N4]Arg (+10) and L-[13C6,15N2]Lys (+8)) (Lys8,Arg10). The light amino acids were from Sigma, while their heavy variants were from Cambridge Isotope Labs.

Sample Preparation for Mass Spectrometry Analysis

Cells from the two SILAC conditions treated as indicated were lysed at 4°C in ice cold modified RIPA buffer (50 mM Tris, pH 7.5, 150 mM NaCl, 1 %v/v NP-40, 0.1 %w/v sodium deoxycholate, 1 mM EDTA, 5 mM β-glycerolphosphate, 5 mM sodium fluoride, 1 mM sodium orthovanadate, 1 complete inhibitor cocktail Tablet per 50 ml). Proteins were precipitated for two hours at -20°C in four-fold excess of ice-cold acetone. The acetone-precipitated proteins were solubilized in denaturation buffer (10 mM HEPES, pH 8.0, 6 M urea, 2 M thiourea) and the SILAC-labelled lysates were mixed 1:1 based on protein concentrations. Proteins were reduced with 1 mM dithiothreitol (DTT) for 60 min, alkylated with 5.5 mM chloroacetamide (CAA) for 60 min and digested first with endoproteinase Lys-C (Wako, Osaka, Japan) and then, after a five-fold dilution with 50 mM ammonium bicarbonate (ABC), with trypsin (modified sequencing grade, Sigma). The peptide mixture was desalted and concentrated on a C18-SepPak cartridge (Waters, USA) and eluted with 50 %v/v acetonitrile. Phosphorylated peptides were enriched using TiO2beads (5 µm, GL Sciences Inc., Tokyo, Japan), as previously described[354]. Equal amounts of SILAC lysates were then mixed 1:1, reduced with DTT, and alkylated with CAA before being

resolved on SDS-PAGE (8-12 %w/v, Invitrogen). Separated proteins were fixed in the gel and visualized with colloidal Coomassie staining (Invitrogen). Each gel lane was excised and separated into eight segments that were sliced, destained with 50 %v/v EtOH in 25 mM ABC, and dehydrated with 100 %v/v EtOH. Proteins were digested with sequence-grade trypsin (Sigma) overnight. Trypsin activity was quenched by acidification with trifluoroacetic acid (TFA) and peptides were extracted from the gel sections with increasing concentrations of acetonitrile. Organic solvent was evaporated in a vacuum centrifuge, as described[355].

Mass Spectrometry Analysis

Both enriched phosphorylated peptides and in-gel digested peptides were desalted and concentrated on STAGE-tips with two C18 filters and eluted using 40 %v/v acetonitrile, dried and reconstituted in 5 %v/v acetonitrile in 0.1 %v/v formic acid prior to analysis by LC-MS/MS using an UltiMate 3000 Rapid Separation LC (RSLC,Dionex Corporation, Sunnyvale, CA) coupled to a QE HF (Thermo Fisher Scientific, Waltham, MA) mass spectrometer. Mobile phase A was 0.1 %v/v formic acid in water and mobile phase B was 0.1 %v/v formic acid in acetonitrile and the analytical column utilized was a 75 mm x 250 µm inner diameter 1.7 µm CSH C18 (Waters). Samples were transferred to a 5 µl loop before loading on to the column at a flow of 300 nl/min for 5 minutes at 5 %v/v B. The loop was subsequently taken out of line and the peptides separated using a gradient that went from 5 %v/v to 7 %v/v B and from 300 nl/min to 200 nl/min in 1 min followed by a shallow gradient from 7 %v/v to 18 %v/v B in 64 min, then from 18 %v/v to 27 %v/v B in 8 min and finally from 27 %v/v B to 60 %v/v B in 1 min. The column was washed at 60 %v/v B for 3 min before re-equilibration to 5 %v/v B in 1 min. At 85 min, the flow was increased to 300 nl/min until the end of the run at 90 min. Mass spectrometry data was acquired in a data dependent manner for 90 min in positive mode. Peptides were selected for fragmentation automatically by data dependent analysis on a basis of the top 8 (phospho-proteome) or top 12 (proteome) peptides with m/z between 300 to 1750 Th and a charge state of 2, 3 or 4 with a dynamic exclusion set at 15 sec. The MS

Resolution was set at 120,000 with an AGC target of 3e6 and a maximum fill time set at 20 ms. The MS2 Resolution was set to 30,000, with an AGC target of 2e5, a maximum fill time of 45 ms, isolation window of 1.3 Th and a collision energy of 28.

Data Analysis of quantitative MS data

Raw data were analyzed with the MaxQuant software suite, version 1.5.6.5, with the integrated Andromeda search engine[356]. Proteins were identified by searching the HCD-MS/MS peak lists against a target/decoy version of the human Uniprot database, which consisted of the complete proteome sets and isoforms (2016 release) supplemented with commonly observed contaminants such as porcine trypsin and bovine serum proteins. Tandem mass spectra were initially matched with a mass tolerance of 7 ppm on precursor masses and 0.02 Da or 20 ppm for fragment ions. Cysteine carbamidomethylation was searched as a fixed modification. Protein N-acetylation, oxidized methionine and either deamidation of asparagine and glutamine (proteome analysis) or phosphorylation of serine, threonine, and tyrosine (phosphoproteome analysis) were searched as variable modifications. Labelled lysine and arginine were specified as fixed or variable modification, depending on prior knowledge about the parent ion (MaxQuant SILAC identification). False discovery rate was set to 0.01 for peptides, proteins and modification sites. Minimal peptide length was six amino acids. Only peptides with Andromeda score >40 were included. To pinpoint the actual phosphorylated amino acid residue(s) within all identified phospho-peptide sequences, MaxQuant calculated the localization probabilities of all putative phosphorylation sites using the PTM score algorithm as described[357]. Potential contaminants, reverse sequenced peptides and phosphorylation sites with a localisation probability of less than 0.75 (class I)[357] were filtered from the dataset. The remaining data were filtered to remove sites or peptides without quantification in at least two of the three replicates for each time point. The median of the replicates was taken. Sites or peptides with a SILAC ratio of greater than 1.5 were considered up-regulated whilst those with a ratio less than 0.75 were considered down-regulated. Correlation was based on Pearson coefficient and visualized in R.

The Phosphopeptide enrichment score was calculated using Webgestalt[358]. Gene network visualization was performed using enrichR[346]. For the proteome analysis a minimum of three to seven peptide identifications with at least two being uniquely assigned to the particular protein were required. Sequence coverage of the identified proteins was at least 5%. Gene Ontology analysis was carried out using enrichR[346] and metascape[347].

2.2.15 Lipidomics

Sample preparation

Cells were seeded in 6 well plates at a density of 150,000 cells per well and treated with/without A922500 for 24-72 h. Cells were then washed in PBS and snap frozen on dry ice. All data was normalised to cell number calculated by crystal violet staining in wells that had undergone the exact same experimental conditions. Ice-cold 3:1 propan-2-ol: water (both LC-MS grade, VWR) was added to each well containing washed, frozen cells. The amount of solvent added was normalised to the cell density (ranges from 0.9-1.8 mL). Working quickly on wet ice, cells were scraped into the solvent solution using cell scrapers (Corning). Cell and solvent suspension mix was removed to a 2 mL microfuge tube and freeze thawed twice and vortexed (30 s) to lyse cells, precipitate proteins and solubilise lipids. Samples were centrifuged (20,000 g, 4 °C, 20 min) and the total supernatant was taken and dried in a SpeedVac concentrator (Thermo Fisher). An extract blank sample was created by carrying out the above procedure in the absence of cells. For zebrafish tumors, tissue was dissected and snap frozen in liquid nitrogen and stored frozen until lipid extraction. Frozen samples were weighed (mass ranges 6-18 mg) and then homogenised in 45.7 µL/mg wet tissue mass 75:25 propan-2-ol/water (both LC-MS grade, VWR) using a Precellys24 homogeniser and CK14 homogenisation tubes (both Stretton Scientific, UK). Samples were centrifuged (20,000 g, 4 °C, 20 min) and the 250 µL of the supernatant was taken (equivalent to extraction from a 5.5 mg piece of tissue) and dried in a SpeedVac concentrator (Thermo Fisher). An extract blank sample was

created by carrying out the above procedure in the absence of tissue. Prior to UHPLC-MS analysis, samples were re-suspended in ice-cold 3:1 propan-2-ol: water (i) for cell extracts this was normalised to cell density readings (added solvent ranges between 100-200 µL); (ii) for tissue extracts a fixed volume of 100 µL was added. Samples were vortexed (30 s) and centrifuged (20,000-g, 4 °C, 20 min). A fixed volume of supernatant (25 µL) was taken from each sample and mixed by vortexing (30 s) to create a pooled QC. The remainder of the supernatant from each sample was removed into HPLC vials. The pooled QC was divided into multiple HPLC vials. All samples were set on the autosampler at 4 °C for immediate UHPLC-MS analysis.

UHPLC-MS lipidomics

The samples were maintained at 4 °C and analysed applying two Ultra-High-Performance Liquid Chromatography-Mass Spectrometry (UHPLC-MS) methods using a Dionex UltiMate 3000 Rapid Separation LC system (Thermo Fisher Scientific, MA, USA) coupled with a heated electrospray Q Exactive Focus mass spectrometer (Thermo Fisher Scientific, MA, USA). Lipid extracts were analysed on a Hypersil GOLD column (100 x 2.1mm, 1.9 µm; Thermo Fisher Scientific, MA, USA). Mobile phase A consisted of 10 mM ammonium formate and 0.1 %v/v formic acid in 60 %v/v acetonitrile/water and mobile phase B consisted of 10 mM ammonium formate and 0.1 %v/v formic acid in 90 %v/v propan-2-ol/water. Flow rate was set for 0.40 mL.min-1 with the following gradient: t=0.0, 20 %v/v B; t=0.5, 20 %v/v B, t=8.5, 100 %v/v B; t=9.5, 100 %v/v B; t=11.5, 20 %v/v B; t=14.0, 20 %v/v B, all changes were linear with curve = 5. The column temperature was set to 55 °C and the injection volume was 2 µL. Data were acquired in positive and negative ionisation mode separately within the mass range of 150 – 2000 m/z at resolution 70,000 (FWHM at m/z 200). Ion source parameters were set as follows: Sheath gas = 48 arbitrary units, Aux gas = 15 arbitrary units, Sweep gas = 0 arbitrary units, Spray Voltage = 3.2 kV (positive ion) / 2.7 kV (negative ion), Capillary temp. = 380 °C, Aux gas heater temp. = 450 °C. Data dependent MS2 in 'Discovery mode' was used for the MS/MS spectra acquisition using following settings: resolution = 17,500 (FWHM at m/z 200);

Isolation width = 3.0 m/z; stepped collision energies (stepped CE) = 20, 40, 100 [positive ion mode] / 40, 60, 130 [negative ion mode]. Spectra were acquired in five different mass ranges: 150 – 510 m/z; 500 – 710 m/z; 700 – 860 m/z; 850 – 1010 m/z; 1000 – 2000 m/z. A Thermo ExactiveTune 2.8 SP1 build 2806 was used as instrument control software in both cases and data were acquired in profile mode. Quality control (QC) samples were analysed as the first ten injections and then every seventh injection with two QC samples at the end of the analytical batch. Two blank samples were analysed, the first as the sixth injection and then the second at the end of each batch.

Mass spectrometry raw metabolomics data processing

Raw data acquired in each analytical batch were converted from the instrument-specific format to the mzML file format applying the open access ProteoWizard (version 3.0.11417) msconvert tool[359]. During this procedure, peak picking and centroiding, were achieved using vendor algorithms. Isotopologue Parameter Optimization (IPO - version 1.0.0, using XCMS - version 1.46.0)[360] was used to perform automatic optimization of XCMS[361] peak picking parameters. For centWave peak picking algorithm following parameters and ranges were used: min_peakwidth (from 2 to 10); max_peakwidth (from 20 to 60); ppm (from 5 to 15); mzdiff (-0.001 to 0.01); snthresh (10); noise (10000); prefilter (3); value_of_prefilter (100); mzCenterFun (wMean); integrate (1); fitgauss (FALSE); verbose.columns (FALSE). Optimised XCMS parameters for raw data files deconvolution were: min_peakwidth (6); max_peakwidth (30); ppm (14); mzdiff (0.001); snthresh (10); noise (100); prefilter (3); value_of_prefilter (100); mzCenterFun (wMean); integrate (1); fitgauss (FALSE); verbose.columns (FALSE). For feature grouping method *density* was used with following: minfrac (0.5); minsamp (1); bw (0.25); mzwid (0.01); max (50); sleep (0). A data matrix of metabolite features (*m/z*-retention time pairs) versus samples was constructed with peak areas provided where the metabolite feature was detected for each sample.

Peak matrix processing

The data for pooled QC samples were applied to perform QC filtering. The first five QCs for each batch were used to equilibrate the analytical system and therefore subsequently removed from the data before the data was processed and analysed. The data from the pooled QC samples were used to apply QC filtering. For each metabolite feature detected QC samples 1-8 were removed (i.e. leaving a blank and 2 QCs at the start of each batch) and the relative standard deviation and percentage detection rate were calculated using the remaining QC samples. Blank samples at the start and end of a run were used to remove features from non-biological origins. Any feature with an average QC intensity less than 20 times the average intensity of the blanks was removed. Any samples with >50% missing values were excluded from further analysis. Metabolite features with a RSD > 30 % and present in less than 90 % of the QC samples were deleted from the dataset. Features with a <50% detection rate over all samples were also removed. Prior to statistical analysis, the data was normalised using probabilistic quotient normalisation (PQN)Dieterle 2006 . For multivariate analysis missing values were replaced by applying *k* nearest neighbour (kNN) missing value imputation (k = 5) followed by log transformation[362].

Lipid annotation

LipidSearch (version 4.2, Thermo Fisher Scientific) was used to annotate peaks based on their MS/MS fragmentation patterns. For lipid annotation, all experimental LC-MS/MS spectra data were searched against a MS/MS lipid library in the LipidSearch software database using the following potential ion forms: positive ion = $[M+H]^+$, $[M+NH_4]^+$, $[M+Na]^+$, $[M+K]^+$, $[M+2H]^{2+}$; negative ion = $[M-H]^-$, $[M+HCOO]^-$, $[M+CH_3COO]^-$, $[M+Cl]^-$, $[M-2H]^{2-}$. The quality of the annotation was graded as A-D. This is defined as: Grade A = all fatty acyl chains and class were completely identified; Grade B = some fatty acyl chains and the class were identified; Grade C = either the lipid class or some fatty acyls were identified; Grade D = identification of less specific fragment ions. Only peaks with an MS/MS identification were discussed in this

manuscript. All lipid annotations are reported at a confidence of level 3 according to the Metabolomics Standards Initiative[363].

Univariate Statistics

For univariate statistics the normalised data was used to avoid including imputed values in the calculations. Fold changes were computed between all pairs of groups. For 2-group comparisons a t-test was applied to determine features showing a significant different between groups. For comparisons exploring two factors a 2-way ANOVA with an interaction term was applied to determine features showing a significant difference between factor levels. For features found to be significant, Tukey's Honest Significant Difference (HSD) was applied to determine between which levels the difference was significant ($p<0.05$). A False Discovery Rate (FDR) correction (Benjamini-Hochburg) was applied to adjust for multiple testing and control the number of false positives ($q < 0.05$) for both t-test and ANOVA.

Software

All peak matrix processing, univariate and multivariate analyses were performed in the R environment using STRUCT (STatistics in R Using Class Templates) and STRUCTToolbox packages, which make use of PMP and SBCMS packages. These packages are maintained by Phenome Centre Birmingham and available on GitHub (https://github.com/computational-metabolomics).

2.2.16 Quantification and Statistical Analysis

Unless otherwise detailed above, the data obtained was tested for normality using the Shapiro-Wilk test. Data was considered to be normally distributed if $p>0.05$. Differences in the number of lipid droplets per cell, relative cell number and percentage EdU incorporation between DMSO and drug treated cells were assessed

using an unpaired two-sided *t*-test, or Mann-Whitney test if data were not normally distributed. In comparing the differences in these same characteristics between cells transfected with either non-target or one of several siRNA oligonucleotides, a one-way ANOVA with Tukey's multiple comparisons test (or Friedman with Dunn's multiple comparisons test if data were not normally distributed) was used to measure significance. Differences were considered significant if $p<0.05$. All data obtained was analysed using Graphpad Prism 8.1.

2.2.17 Data and Code Availability

The zebrafish tumor RNA-seq data has been deposited with the Gene Expression Omnibus (GEO) with the accession code GSE144555 and all RNA-seq analysis can be found in supplementary tables in the Mendeley data portal. The mass spectrometry proteomics data have been deposited with the ProteomeXchange Consortium via the PRIDE partner repository with the dataset identifier PXD017487. Extended Lipidomics Data for zebrafish tumors and human melanoma cell lines can be found in supplementary tables in Mendeley data portal. Supplementary images for BODIDPY analysis can be found in the Mendeley data portal. Code for proteomic and transcriptomic analysis can be found on the Mendeley data portal. Mendeley data portal access will be provided to examiners.

2.3 Key Resources Table

Reagent or Resource	Source	Product Code
Antibodies		
Rabbit monoclonal anti-DGAT1	Abcam	ab181180
Mouse monoclonal anti-Vinculin	Proteintech	66305-1-Ig
Rabbit monoclonal anti- GFP (D5.1) XP	Cell Signaling	#2956
Rabbit polyclonal anti-Beta Tubulin	Proteintech	10094-1-AP
Rabbit polyclonal anti-Phospho-S6 Ribosomal Protein (Ser240/244)	Cell Signaling	#2215
Rabbit polyclonal anti-Phospho-eEF2 (Thr56)	Cell Signalling	#2331
Mouse monoclonal anti- HA.11 Epitope Tag	Biolegend	# 901533
Rabbit polyclonal anti-Phospho-AMPKα (Thr172)	Cell Signaling	#50081
Rabbit polyclonal anti-Phospho-Raptor (Ser792)	Cell Signaling	#2083
Rabbit polyclonal anti-PINK1	Proteintech	23274-1-AP
Rabbit polyclonal anti-Parkin	Proteintech	14060-1-AP
Rabbit polyclonal anti-Caspase-3	Cell Signaling	#9662
Rabbit polyclonal anti-SOD1	Proteintech	10269-1-AP
Rabbit polyclonal anti-SOD2	Proteintech	24127-1-AP
Rabbit polyclonal anti-Sestrinf 2	Proteintech	10795-1-AP
Rabbit polyclonal anti-PDK4	Proteintech	12949-1-AP
Rabbit polyclonal anti-Phospho-PDHE1A (S232)	Sigma-Aldrich	SAB1305601
Mouse monoclonal anti- Phospho-p70 S6 Kinase (Thr389)	Cell Signaling	#9206
Mouse monoclonal anti-GAPDH	Proteintech	60004-1-Ig
Rabbit monoclonal anti-Phospho-Akt (Ser473)	Cell Signaling	#4060
Mouse monoclonal anti-ERK 1/2	Santa Cruz Biotechnology	sc-135900
Mouse monoclonal anti- S6 Ribosomal Protein	Cell Signaling	#2317
Rabbit monoclonal anti-p70 S6 Kinase	Cell Signaling	#2708
Rabbit polyclonal anti-4 Hydroxynonenal	Abcam	ab46545
Mouse monoclonal anti-γ-Tubulin	Sigma-Aldrich	T5326
Chemicals, Peptides, and Recombinant Proteins		

Trypsin porcine pancreas (proteomics grade)	Sigma-Aldrich	T6567
Lysyl Endopeptidase	FUJIFILM Wako Chemicals	129-02541
TiO beads “Titanspheres”	GL Sciences	5020-75000
Pre-cast gradient gel: Nu-PAGE 4-12% Bis-Tris Gel 1.0mm 10 well	Invitrogen	NP0321BOX
Sep-Pak Classic C18 cartridges	Waters	WAT051910
Solid Phase Extraction Disk “Empore” C18 (Octadecyl) 3M	Agilent Technologies	2215
Solid Phase Extraction Disk “Empore” C8 (Octyl) 3M	Agilent Technologies	2214
L-ARGININE:HCL	Cambridge Isotope Laboratories	CLM-2265-H-0.25
L-ARGININE:HCL	Cambridge Isotope Laboratories	CNLM-539-H-0.5
L-ARGININE:HCL	Sigma-Aldrich	A6969
L-LYSINE:2HCL	Cambridge Isotope Laboratories	DLM-2640-0.5
L-LYSINE:2HCL	Cambridge Isotope Laboratories	CNLM-291-H-0.5
L-LYSINE:2HCL	Sigma-Aldrich	L8662
2,5-Dihydroxybenzoic acid	Sigma-Aldrich	85707
RPMI 1640 Medium for SILAC	ThermoFisher Scientific	88365
TRIzol™ Reagent	ThermoFisher Scientific	Cat. No. 15596026
T863- DGAT1 Inhibitor	Sigma-Aldrich	SML0539-5MG
A922500- DGAT1 Inhibitor	Stratech Scientific Ltd	A4382-APE-50mg
AZD3988- DGAT1 Inhibitor	Tocris Bioscience	Cat. No. 4837
AZD7687- DGAT1 Inhibitor	Stratech Scientific Ltd	A3215-APE-5mg
LY2584702 Tosylate- S6K inhibitor	Stratech Scientific Ltd	S7704-SEL
PF 4708671	Generon	A11755-25
Polybrene Transfection Reagent	Millipore UK Limited	R-1003-G
PARAQUAT DICHLORIDE X-HYDRATE PESTANAL	Sigma-Aldrich	36541-100MG
Menadione	Fluorochem Limited	049845-25G
Oligomycin A	Sigma-Aldrich	75351
FCCP	Cambridge Bioscience Limited	2398-5

Oligomycin Complex	Stratech Scientific Ltd	C3007-APE-5mg
Rotenone, PESTANAL, analytical standard	Scientific Laboratory Supplies Ltd	45656-250MG
Antimycin A from Streptomyces sp.	Sigma-Aldrich	A8674
PF-06424439- DGAT2 Inhibitor	Sigma-Aldrich	PZ0233
Ebselen	Sigma-Aldrich	E3520-25MG
Tempol	Stratech Scientific Ltd	S2910-SEL-100mg
Etomoxir	Stratech Scientific Ltd	A3404-APE-10mg
Ferrostain-1	Sigma-Aldrich	SML0583
Compound C	Sigma-Aldrich	171260
BODIPY 581/591 C11 (Lipid Peroxidation Sensor)	ThermoFisher Scientific	D3861
MitoPerOx, fluorescent mitochondria-targeted lipid peroxidation probe	Abcam	ab146820
BODIPY™ 493/503 (4,4-Difluoro-1,3,5,7,8-Pentamethyl-4-Bora-3a,4a-Diaza-s-Indacene)	Life Technologies	D3922
HCS LipidTOX™ Green Neutral Lipid Stain	ThermoFisher Scientific	H34475
Molecular Probes MitoSOX Red Mitochondrial Superoxide Indicator	ThermoFisher Scientific	11579096
DIHYDROETHIDIUM	Cambridge Bioscience	12013-5mg-CAY
H2DCFDA	Tocris Bioscience	5935/100
Hoechst 33342	New England Biolabs	4082S
Lipofectamine RNAiMAX Transfection Reagent	ThermoFisher Scientific	10601435
Lipofectamine Transfection Reagent	Life Technologies	18324020
FuGENE HD Transfection Reagent	Promega UK	E2311
Seahorse XFe96 FluxPak mini	Agilent Technologies	102601-100
Seahorse XF DMEM medium, pH 7.4, 500 mL.	Agilent Technologies	103575-100
qPCRBIO SyGreen Mix Separate-ROX	PCR Biosystems	PB20.14
Crystal violet solution	Sigma-Aldrich	V5265-250ML
Commercial Assays		
Click-iT EdU Alexa Fluor 488 Imaging Kit-1 kit	Life Technologies	C10337
MitoProbe JC-1 Assay Kit	Life Technologies	M34152

CellEvent Caspase-3/7 Green Detection Reagent	Life Technologies	C10423
ProtoScript; II First Strand cDNA Synthesis Kit	New England Biolabs	E6560L
RNeasy RNA Extraction Kit	Qiagen	74136
Deposited Data		
Phospho-proteome and total proteome data	ProteomeXchange Consortium PRIDE	PXD017487
RNA-seq data	Gene Expression Omnibus	GSE144555
Experimental Models: Cell Lines		
888MEL	Gift from Claudia Wellbrock	CVCL 4632
888MEL Clone 1-3 DGAT Overexpression	This study	N/A
SKMEL28	ATCC	HTB-72
SKMEL105	Memorial Sloan Kettering Cancer Center	N/A
A375	ATCC	CRL- 1619
MM485	Gift from Claudia Wellbrock	CVCL_2610
WM266-4	Gift from Claudia Wellbrock	CVCL_2765
LOX-IMVI	Sigma-Aldrich	SCC201
SKMEL5	ATCC	HTB-70
Experimental Models: Organisms/Strains		
tp53m214K/m214k; mitfa-/-	Leonard Zon	N/A
tp53m214K/m214k; mitfa-/-; braf V600E	Craig Ceol	N/A
tp53m214K/m214k; mitfa-/-; nras G12D	This study	N/A
Oligonucleotides		
SIRNA UNIV NEGATIVE CONTROL #2	Sigma-Aldrich	SIC002
hSCD_F; TCCAGAGGAGGTACTACAAACCT	This study	N/A
hSCD_R; GCACCACAGCATATCGCAAG	This study	N/A
hACOX2_F; GCACCCCGACATAGAGAGC	This study	N/A
hACOX2_R; CTGCGGAGTGCAGTGTTCT	This study	N/A

hIREB1_F;	AACCCATTCGCACACCTTG	This study	N/A
hIREB1_R;	ATGGTAAGCGCCCATATCTTG	This study	N/A
hTOMM40L_F;	GACATGGCAGTTTGATGGCG	This study	N/A
hTOMM40L_R;	GATCACCGACTCCCCAATCAG	This study	N/A
hACOT2_F;	CGTCCCGGCTGTACCAATG	This study	N/A
hACOT2_R;	GGAACCCTAATGATCTGACCAAC	This study	N/A
hCPT1C_F;	TTTGCCTCGTGTTTGTGGG	This study	N/A
hCPT1C_R;	CAGCCGTGGTAGGACAGAA	This study	N/A
hHMOX1_F;	AGGGAATTCTCTTGGCTGGC	This study	N/A
hHMOX1_R;	GCTGCCACATTAGGGTGTCT	This study	N/A
hLONP2_F;	CAGGCAACGTACGACAGGAT	This study	N/A
hLONP2_R;	GGGACATCTTGCATACCCCTA	This study	N/A
hGYG1_F;	CAAACGATGCCTACGCCAAA	This study	N/A
hGYG1_R;	TCGCCACTGTCCAAGACATC	This study	N/A
hSESN2_F;	CCCGCTACATGACCTGACTC	This study	N/A
hSESN2_R;	CTGCACATCACACACAAGCC	This study	N/A
hFDFT1_F;	GAAGCACCTACTCCACAGGTC	This study	N/A
hFDRT1_R;	GCGAGTCCTGGTCCATCTTG	This study	N/A
hTIMM8B_F;	GAAGCCGATGAAGCGGAGT	This study	N/A
hTIMM8B_R;	GCGAGAGTCTAGGCGATTCC	This study	N/A
hSLMO2_F;	CAGGTGTAGCCTCTGTGCC	This study	N/A
hSLMO2_R;	CTGTGGCTGTGCAACTTTCC	This study	N/A
hTIMM17A_F;	CCCATGGCGAATTGTGGATG	This study	N/A
hTIMM17A_R;	TATGGCTCCCGTTAAGGCAC	This study	N/A
hECH1_F;	CTACTGACCCGGCGACTGA	This study	N/A
hECH1_R;	TGACAAGGTCCACACCTCCG	This study	N/A
hACADM_F;	CGTTTTCATTGGAGATCACAGC	This study	N/A
hACADM_R;	CCAAGACCTCCACAGTTCTCT	This study	N/A
hHADHA_F;	GCCGACATGGTGATTGAAGC	This study	N/A
hHADHA_R;	CCAGCTTCTTCGGGTCAACT	This study	N/A
hGCDH_F;	CCCCCGAGATGGTTTCTCTG	This study	N/A
hGCDH_R;	AGGATCAGGGCGTGAATGTC	This study	N/A
hABCD1_F;	GCCTATGGAGCCCACAAAGT	This study	N/A

hABCD1_R;	CAGGTAACGGATGGCACTGT	This study	N/A
hETFA_F;	AAGCTCCAATTTTCCAAGTGGC	This study	N/A
hETRA_R;	GGCTGGTGGAGACAATCATGT	This study	N/A
hCRAT_F;	GACACAGTCAGCAACTTCAGC	This study	N/A
hCRAT_R;	GCTGCACAAAGATCTGATCCG	This study	N/A
hCPT2_F;	CTGTAGCACTGCCGCATTCA	This study	N/A
hCPT2_R;	AGAGCAAACAAGTGTCGGTCAA	This study	N/A
hIREB2_F;	CCATCCTGCTTGTCCGACAG	This study	N/A
hIREB2_R;	CACAAGATCCTCGGCAGGTAG	This study	N/A
hACOX1_F;	TTGTGGGCGCATACATGAAG	This study	N/A
hACOX1_R;	ATCCGACATGCTTCAATGCC	This study	N/A
hPEX2_F;	TAACCTGCAGTGTCTCTGAGC	This study	N/A
hPEX2_R;	CGAGCTAACAGCCCAGGTTT	This study	N/A
hNFE2L2_F;	TCAGCGACGGAAAGAGTATGA	This study	N/A
hNRE2L2_R;	CCACTGGTTTCTGACTGGATGT	This study	N/A
hNQO1_F;	GAAGAGCACTGATCGTACTGGC	This study	N/A
hNQO1_R;	GGATACTGAAAGTTCGCAGGG	This study	N/A
hGSTM1_F;	TCTGCCCTACTTGATTGATGGG	This study	N/A
hGSTM1_R;	TCCACACGAATCTTCTCCTCT	This study	N/A
zDgat1a_qF1;	GGAGAGGACACATTCAGCTG	This study	N/A
zDgat1a_qR1;	ATAAGGTTCTCCAGCACGAG	This study	N/A
Dr_gpd1b_1_SG QuantiTect Primer Assay		Qiagen	QT02087449
Dr_slc2a11b_1_SG QuantiTect Primer Assay		Qiagen	QT02176580
Dr_pparab_1_SG QuantiTect Primer Assay		Qiagen	QT02106748
Dr_scdb_1_SG QuantiTect Primer Assay		Qiagen	QT02096913
Dr_aldoab_1_SG QuantiTect Primer Assay		Qiagen	QT02103941
Dr_rpn1_1_SG QuantiTect Primer Assay		Qiagen	QT02145157
Dr_pltp_1_SG QuantiTect Primer Assay		Qiagen	QT02065567
Dr_pdia3_1_SG QuantiTect Primer Assay		Qiagen	QT02491034
Dr_atp2a2b_1_SG QuantiTect Primer Assay		Qiagen	QT02094743
Dr_dnajc10_1_SG QuantiTect Primer Assay		Qiagen	QT02071699
Dr_hsp90aa1.1_1_SG QuantiTect Primer Assay		Qiagen	QT02224012
mApple_BspEI_F; GACAGATCCGGAGTGAGCAAG		This study	N/A

mApple_XhoI_R; GACAGACTCGAGTCACTTGTACAGCTCGTC	This study	N/A
WPRE_X XhoI _F; GACAGACTCGAGAGCTGAATCTAAGTCGAC	This study	N/A
WPRE_KpnI_R; GACAGAGGTACCAGGCGGGGAGGCGGCCCAAAGGGAGATC	This study	N/A
hDGAT1_EcoRI_F; GACAGAGAATTCGCCACCATGGGCGACCGCGGCAGCTC	This study	N/A
hDGAT1_NotI_nosR; GACAGAGCGGCCGCGGCCTCTGCAGAGGCC	This study	N/A
hDGAT1_XbaI_R; GACAGATCTAGATCAGGCCTCTG	This study	N/A
zDgat1_EcoRI_F; GACAGAGAATTCGCCACCATGGGCGACAGAAACGAGAAG	This study	N/A
zDgat1_SpeI_R; GACAGAACTAGTTCACGGCGCTGCGGCCTCAGAC	This study	N/A
dgat2_EcoRI_F; GACAGAGAATTCGCCACCATGAAGACCATACTTGCTGC	This study	N/A
dgat2_SpeI_R; GACAGAACTAGTTCAGTGAATGATAAGGGTATCG	This study	N/A
Recombinant DNA		
pMDLg/pRRE	Gift from Angeliki Malliri	Addgene #12251
pRSV-Rev	Gift from Angeliki Malliri	Addgene #12253
pMD2.G	Gift from Angeliki Malliri	Addgene #12259
pCDH-EF1α-MCS*-T2A-GFP	Gift from Andrew Gilmore	Systems Bioscience CD526A-1
pCDH-EF1α-MCS*-T2A-mApple	This study	N/A
pCDH-EF1α-DGAT1-T2A-mApple	This study	N/A
pDONR221	ThermoFisher Scientific	12536017
pDest-mitfa:dgat1a-pA	This study	N/A
pDest-mitfa:dgat2-pA	This study	N/A

pCS2-TP	Gift from Koichi Kawakami	N/A
pRK7-HA-S6K1-WT	Addgene	#8984
pRK7-HA-S6K1- F5A-E389-deltaCT	Addgene	#8990
pcDNA3.1-mMaroon1	Addgene	# 83840
pcDNA3.1-DGAT1	This study	N/A
Software and Algorithms		
Fiji- Image J	Schindelin, J et al. (2012)	https://imagej.net/Fiji
GraphPad Prism version 8.0.0	GraphPad Software	www.graphpad.com
Enrichr	Chen EY et al. (2013)	https://amp.pharm.mssm.edu/Enrichr/
WebGestalt	Liao, Y et al. (2019)	http://www.webgestalt.org/#
Metascape	Zhou et al. (2019)	https://metascape.org/gp/index.html#/main/step1
MaxQuant	Cox, J et al. (2008)	https://www.maxquant.org
Trimmomatics v0.32	Bolger, AM et al. (2014)	N/A
STAR v2.5.3	Dobin, A et al. (2013)	N/A
featureCounts v1.6.2	Liao, Y et al. (2014)	N/A
DESeq2 v1.14.1	Love, MI et al. (2014)	N/A
Morpheus	Broad Institute	(https://software.broadinstitute.org/morpheus)
FlowJo	www.flowjo.com	N/A

Table 2 Key resources

Chapter 3 – DGAT1 is amplified and up-regulated in melanoma and a bone fide melanoma oncogene

3.1 Introduction

We are now in a post genomic cancer era in which the majority of human cancers have now been sequenced, with the major challenge now of deciphering which genetic alterations are consequential and which aren't. Although this has aided and accelerated the discovery of new driver genes, the number of genes with genetic alterations with an unclear functional importance is vast and far outweighs the number of major driver genes identified. This problem becomes more acute in melanoma when considering the high mutational burden of melanoma at more than 10 per Mb and 70,000 point mutations[59,151]. Mouse models have been the cornerstone of *in vivo* cancer research, confirming the functional importance of genetic alterations in driving tumourigenesis. Transgenic cancer and xenograft mouse models have provided key insights into a number of major driver genes. However, over the past 10-15 years, the zebrafish has come to the fore as an appropriate organism for modelling cancer and probing oncogene function.

The small, tropical fish, *Danio rerio*, commonly known as zebrafish has fast become a powerful *in vivo* model for oncogene discovery. There are a number of key advantages of zebrafish for research, including its high fecundity year round, the generation of optically clear embryos that develop external to the mother and its rapid generation time[364]. The external development of zebrafish embryos make them highly amenable to genetic manipulation through the micro-injection of embryos at the one-cell stage. There is also a high degree of conservation with 84 % of genes related to human disease having a zebrafish counterpart and more comparable telomere biology to humans than mice[365,366]. The first zebrafish tumour models involved the use of mutagens such as dimethylnitramine, ethylnitrosourea

(ENU) and N-methyl-nitrosoguanadine (MNNG) which gave rise to various spontaneous malignant neoplasms[367–369]. In 2003 the field took a huge jump forward which, off the back of the development of rapid transgenic technology, led to the development of the first transgenic zebrafish model of cancer[370]. A model of T-cell leukaemia was developed in transgenic zebrafish expressing the mouse oncogene Myc under the zebrafish recombination activating gene 2 (rag2) promoter, which restricts Myc expression to lymphoid cells[370]. This initial discovery led to the development of other tumour models in zebrafish such as melanoma, pancreatic neuroendocrine and malignant nerve sheath tumours[97,371,372]. Additionally, the development of CRISPR- Cas9 in zebrafish has further increased the potential for new cancer models, facilitating investigations into tumour suppressor genes through knockout, in combination with proto-oncogene overexpression[373–375]. Further work has also demonstrated that both embryonic and adult zebrafish can also be harnessed for use as a donor in both allograft and xenograft cancer models; providing a high-throughput model of tumour growth and metastasis allowing for detailed analysis of even single cells, due to the development of transparent zebrafish strains[84,376–380].

Transgenic Zebrafish Models of Melanoma

The first transgenic zebrafish model of melanoma placed the most common human melanoma oncogene $BRAF^{V600E}$ downstream of the melanocyte specific *mitfa* promoter, which drives overexpression of mutant BRAF in zebrafish melanocytes[97]. As is observed in human melanoma, the expression of $BRAF^{V600E}$ in zebrafish melanocytes leads to the development of benign pigmented nevi, which was not observed with the over expression of WT BRAF[97]. Furthermore, injection of the $BRAF^{V600E}$ construct into zebrafish with mutations in the tumour suppressor gene p53 ,which in human melanoma is mutated in approximately 15% of patients, led to the development of melanomas that were similar to human melanomas in biological behaviour and histopathologically[97]. The mitfa:$BRAF^{V600E}$;$tp53^{-/-}$ zebrafish melanoma model has since been used to provide further insight into melanoma genetics,

providing insight into new modulators relevant to human melanoma[343,381,382]. In 2009 a further transgenic zebrafish model of melanoma was created through the melanocyte specific expression of $NRAS^{Q61K}$, the second most frequent driver mutation found in human melanoma; like the BRAF model, the background of a LoF p53 led to the development of melanoma[84]. The NRAS mutant zebrafish melanoma model was found to be strikingly similar to human NRAS mutant melanoma both pathologically and at a gene expression level[84]. Rarer melanoma driver mutations and subtypes have also been modelled in zebrafish utilising mutant HRAS, GNAQ and MITF[382–384].

The MiniCoopR System

In order to investigate novel modifiers of melanoma development and progression, a melanocyte rescue and lineage restricted expression system was developed using an engineered vector named the miniCoopR vector and utilities *Tol2*-mediated transgenesis[343]. The development of the assay initially involved introducing a *mitfa* loss of function mutation into the Tg(mitfa:$BRAF^{V600E}$); p53(lf) line, which prevented melanocyte development and thus melanoma formation[343]. The miniCoopR vector encodes the wild-type *mitfa* minigene under control of the mitfa promoter, and injection of this vector into Tg(mitfa:BRAFV600E);p53-/-;mitfa-/- embryos rescues melanocytes and leads to development of melanoma[343]. Also encoded in the miniCoopR vector is a gateway recombination cassette, again under the control of the mitfa promoter, into which candidate melanoma driver genes can be recombined[343]. Thus allowing the melanocyte specific expression of candidate oncogene in rescued melanocytes . The miniCoopR system has been used to identify and establish novel melanoma modifiers and oncogenes such as the histone methyltransferase *SETDB1*[343], growth differentiation factor 6 (GDF6) involved in BMP signalling[381], the neural crest transcription factor SOX10[385] and two genes important for FA uptake FATP1[266] and LPL[267].

Together, the above discoveries and developments highlight the power of zebrafish to model melanoma that bear striking resemblance to the human disease. Thus zebrafish models of melanoma can be used to identify novel genetic alterations, providing new insights into melanoma development and progression.

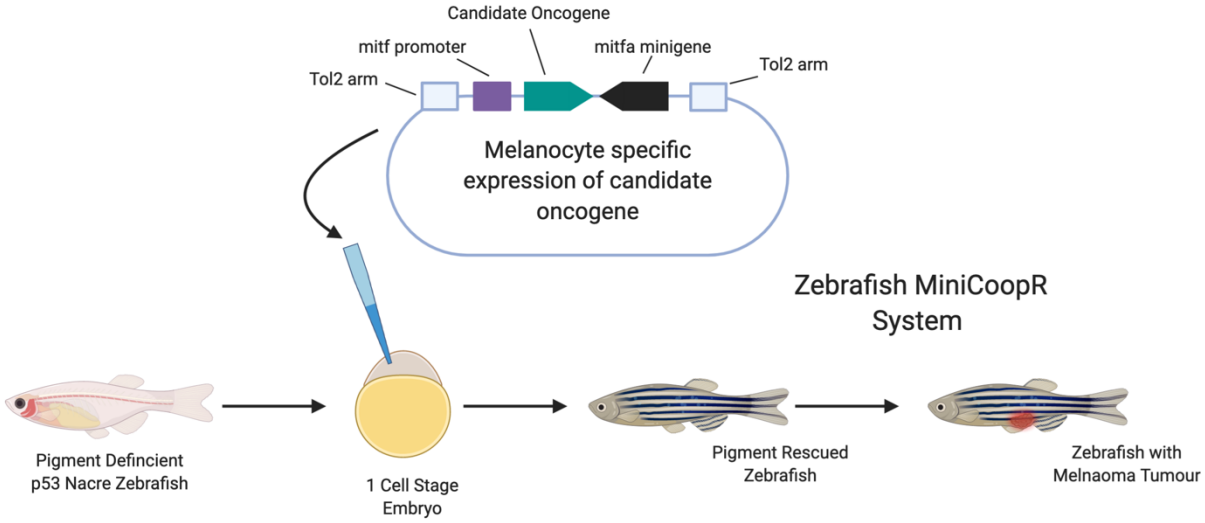

Figure 3.1 Zebrafish MiniCoopR system

An overview of the experimental strategy of the melanocyte rescue and lineage restricted MiniCoopR expression system.

3.2 Aims

- To identify novel metabolic oncogenes in melanoma using a cross-species oncogenomic approach using zebrafish models of melanoma and the TGCA patient dataset.
- Elucidate the oncogenic potential of the identified metabolic oncoproteins using the miniCoopR system in Tg(mitfa:BRAFV^{600E};p53$^{-/-}$;mitfa$^{-/-}$), Tg(mitfa:NRAS^{G12D};p53$^{-/-}$;mitfa$^{-/-}$) and (tp53$^{M214K/M214k}$; mitfa$^{-/-}$) transgenic zebrafish.
- Use RNA-seq analysis and a cross-species comparative approach to identify the oncogenic mechanisms of the identified metabolic oncoproteins.

3.3 Results

There is a clear need to further the understanding of melanoma development and progression in order to aid in the discovery of new oncoproteins that can be targeted for therapeutic intervention. Given the dearth of metabolic oncogenes to pursue as therapeutic targets and the clear importance of lipid metabolism in melanoma development and progression we further interrogated the lipid metabolism signature we observed in an aggressive RAS driven zebrafish model of melanoma[267]. Previously, the Hurlstone lab generated transgenic zebrafish which developed melanomas replicating the stages of melanoma development from benign nevi through to VGP[267] (Figure 1.1). Using the *mitfa* promotor to drive melanocyte specific expression of human $BRAF^{V600E}$ leads to the development of benign melanocyte hyperplasia, whereas driving expression of human $HRAS^{G12V}$ gives rise initially to RGP melanoma prior to infiltrating the subcutaneous tissue and developing into VGP melanoma[267]. When interrogating the lipid metabolism signature found to be unique to VGP phase RAS driven melanoma we found dgat1a to be an outlier as the highest up-regulated gene product when considering only genes with highly significant ($P<0.0001$) differential expression, demonstrating an approximately 40-fold up-regulation[267] (Figure 3.2A).

We further interrogated this gene set by looking at the association between the expression of the human homologues and melanoma patient survival. Using the SKCM TGCA cohort we separated out patients by mRNA abundance (25% top vs 75% bottom), and found 3 genes that were significantly ($P<0.0001$) associated with survival of melanoma patients DGAT1, TAMM41 and SULT1A1 (Figure 3.2A). The enzyme DGAT1, which catalyses the committing step in TAG synthesis and thus critical for LD biosynthesis, stood out as being both highly-upregulated in aggressive RAS driven zebrafish melanoma and being predictive of a significantly worse patient outcome (Figure 3.2A,B). Interestingly, *dgat2/DGAT2* which is able to catalyse the exact same diglyceride acyltransferase reaction but is structurally different to DGAT1, was found to be only modestly up-regulated in RAS driven zebrafish melanoma and

no association with patient survival, indicating a possible unique function of DGAT1 in melanoma (Figure 3.2A,B).

Furthermore, we investigated *DGAT1* and *DGAT2* expression in human melanoma first using two mRNA expression datasets comparing normal skin, benign melanocytic nevi and melanoma samples. *DGAT1* expression was elevated in melanoma samples relative to both skin and benign nevi, indicating that up-regulation of *DGAT1/dgat1a* is conserved across both human and zebrafish melanoma (Figure 3.2C). No up-regulation of *DGAT2* was observed in human melanoma when compared to skin or benign nevi samples, again further highlighting a unique role of DGAT1 in human melanoma (Figure 3.2C). Additionally, in a panel of melanoma cell lines, western blotting demonstrated that when compared to normal human melanocytes (NHM) almost all of the melanoma cell lines had elevated DGAT1 protein levels, irrespective of their NRAS or BRAF mutational status (Figure 3.2D).

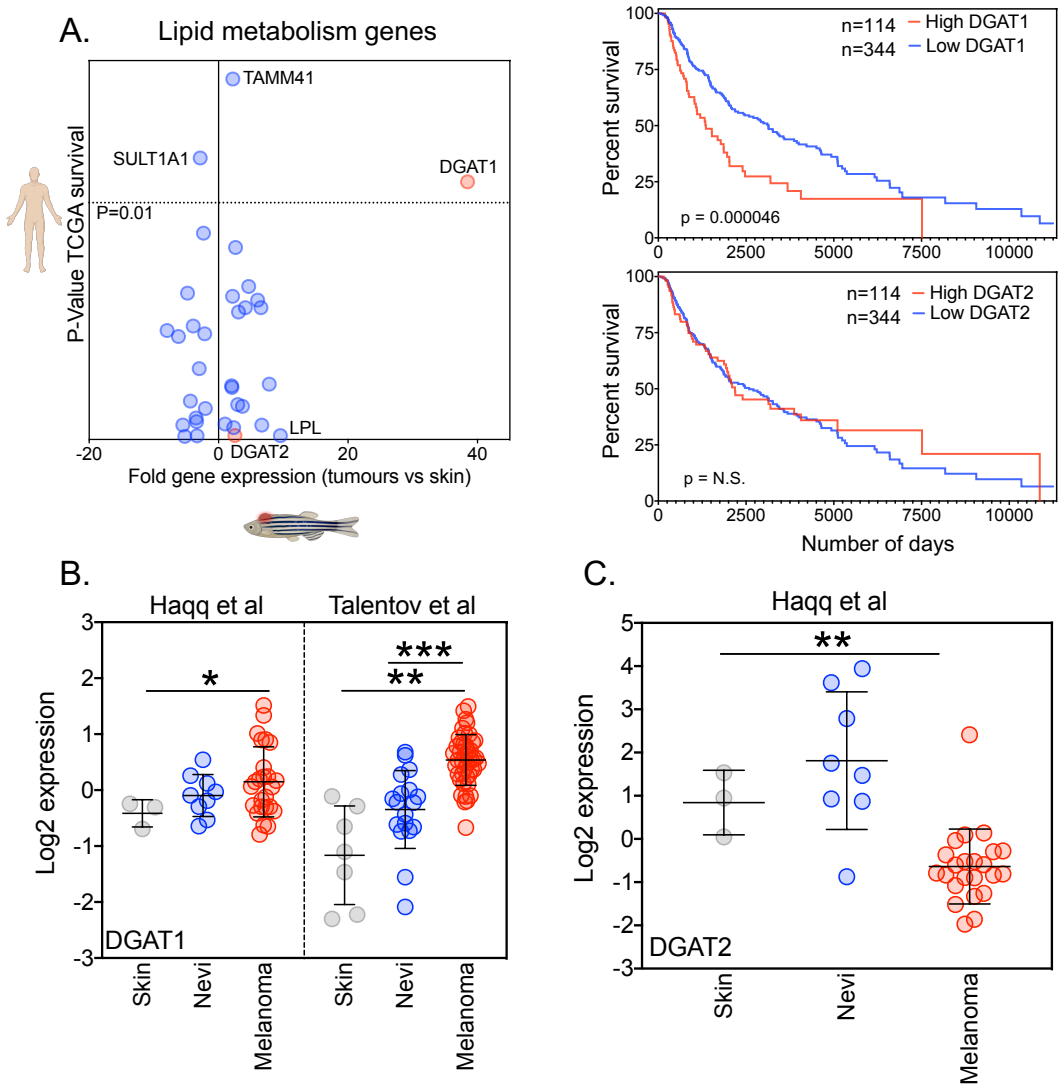
A.
Lipid metabolism genes
TAMM41
SULT1A1
DGAT1
P=0.01
LPL
P-Value TCGA survival
-20
0
DGAT2
20
40
Fold gene expression (tumours vs skin)
n=114 High DGAT1
n=344 Low DGAT1
Percent survival
p = 0.000046
n=114 High DGAT2
n=344 Low DGAT2
p = N.S.
Number of days
B.
Haqq et al
Talentov et al
Log2 expression
DGAT1
Skin
Nevi
Melanoma
C.
Haqq et al
DGAT2
D.
RASmutant
BRAFmutant
NHM
WM1361
MELJUSO
MV3
D10
D04
MM485
SKMEL2
MM415
MNT1
RPMI7951
A375
A2058
UACC62
DGAT1
Vinculin
BRAFmutant
NHM
WM852
WM793
WM266-4
SKMEL190
888MEL
SKMEL39
SKMEL28
WM164
WM98
SKMEL105
WM9
501MEL
WM35
DGAT1
Vinculin

Figure 3.2 DGAT1 is amplified and up-regulated in melanoma and is associated with worse patient survival

(A) Patient survival from TCGA melanoma cohort (25% top vs 75% bottom by mRNA abundance, Y-axis) versus fold-change in mRNA expression of lipid metabolism genes in zebrafish tumours (X-axis) (left). Kaplan-Meier survival plot comparing melanoma patients based on expression of DGAT1 or DGAT2 (top 25% vs bottom 75%, TCGA data set) (right)(Logrank p-value). (B) Relative gene expression of DGAT1 in skin, nevi and melanoma tumours from the Haqq and Talentov studies (Mean ± SD, n>3). (C) Relative gene expression of DGAT2 in skin, nevi and melanoma tumours from the Haqq study (Mean ± SD, n>3)(Two-way Anova). (D) Protein expression of DGAT1 and Vinculin (loading control) in indicated melanoma cell lines (NHM- Normal Human Melanocytes).

Next, we considered the mechanism by which DGAT1 expression is up regulated in melanoma. Using cBioPortal we visualised the genetic alterations of the *DGAT1* gene in the TGCA SKCM dataset of 287 patients, which revealed a significant focal amplification (as determined by the GISTIC 2.0 algorithm) in 7% of melanoma cases with available copy number variation (CNV) data but revealed no mutations or genetic deletions (Figure 3.3A). As observed in the melanoma cell line panel, the focal amplification of DGAT1 was not dependent on either NRAS or BRAF mutational status (Figure 3.2D & Figure 3.3A). Additionally, the frequency of the focal amplification of DGAT1 was comparable with other well-established melanoma oncogenes such as CDK4, CCND1, cKIT, MITF (Figure 3.3A). In order to more robustly explore the genetic evidence for DGAT1 as metabolic oncogene, we visualised the genetic alterations of the *DGAT1* gene along with other putative metabolic oncogenes such as *FASN, CD36, FATP1 MAGL, IDH1* and *IDH2* in the TGCA Pan Cancer Atlas dataset, which encompasses 32 different cancer types across 10,953 patients. CD36, FATP1 and LPL that increase FA uptake in cancer cells, were rarely activated by point mutation or activation, similarly the lipase MAGL and key FA synthesis enzyme FASN were also rarely found amplified or with an activating point mutation (Figure 3.3B). Only IDH1, which catalyses the decarboxylation of isocitrate to yield α-ketoglutarate (α-KG) as part of the TCA cycle, was found to be activated at a significant frequency with 5% of patient samples containing a genetic alteration in IDH1, with activating point mutations occurring at the highest frequency (Figure 3.3B). Visualisation of genetic alterations in DGAT1 revealed focal amplification in almost 6% in patients across the TGCA Pan Cancer Atlas dataset, matched only by activation of IDH1 which has been confirm as an oncogenic driver. A similar pattern emerged when visualising genetic alterations of this same gene set in established cancer cell lines. Interrogation of the cancer cell line encyclopaedia dataset again revealed *DGAT1* as the most frequently activated putative metabolic oncogene, with almost 15% of cancer cell lines containing a focal amplification of the *DGAT1* gene (Figure 3.3B). Interestingly, along with an increase in the frequency of DGAT1 alterations when comparing the cancer cell lines to primary tumours, increased focal amplification of *CD36* was also observed, suggesting that the process used to derive cancer cell lines may select for cells with a higher capacity for FA uptake (Figure 3.3B). Although, CD36 may also

regulate other cancer-specific phenotypes through its multiple roles acting not only as receptor for fatty acid but also collagen, thrombospondin, specific oxidised phospholipids impacting upon immune recognition, apoptosis, adhesion and proliferation[386–388].

A more in-depth examination of the focal amplification of DGAT1 in the TGCA Pan Cancer Atlas dataset revealed the breadth of cancer types and distinct cell lineages in which DGAT1 is amplified (Figure 3.3C). The highest frequency of focal amplification of DGAT1 was found in ovarian cancer (25%), followed by invasive breast cancer (12%) and uterine cancers (11%) (Figure 3.3C). Strikingly, across the TGCA Pan Cancer Atlas dataset, amplification of *DGAT1* was associated with significantly worse progression free survival (PFS) across the multiple cancer types, adding further weight to the cancer genomics evidence for DGAT1 as an oncogene (Figure 3.3D).

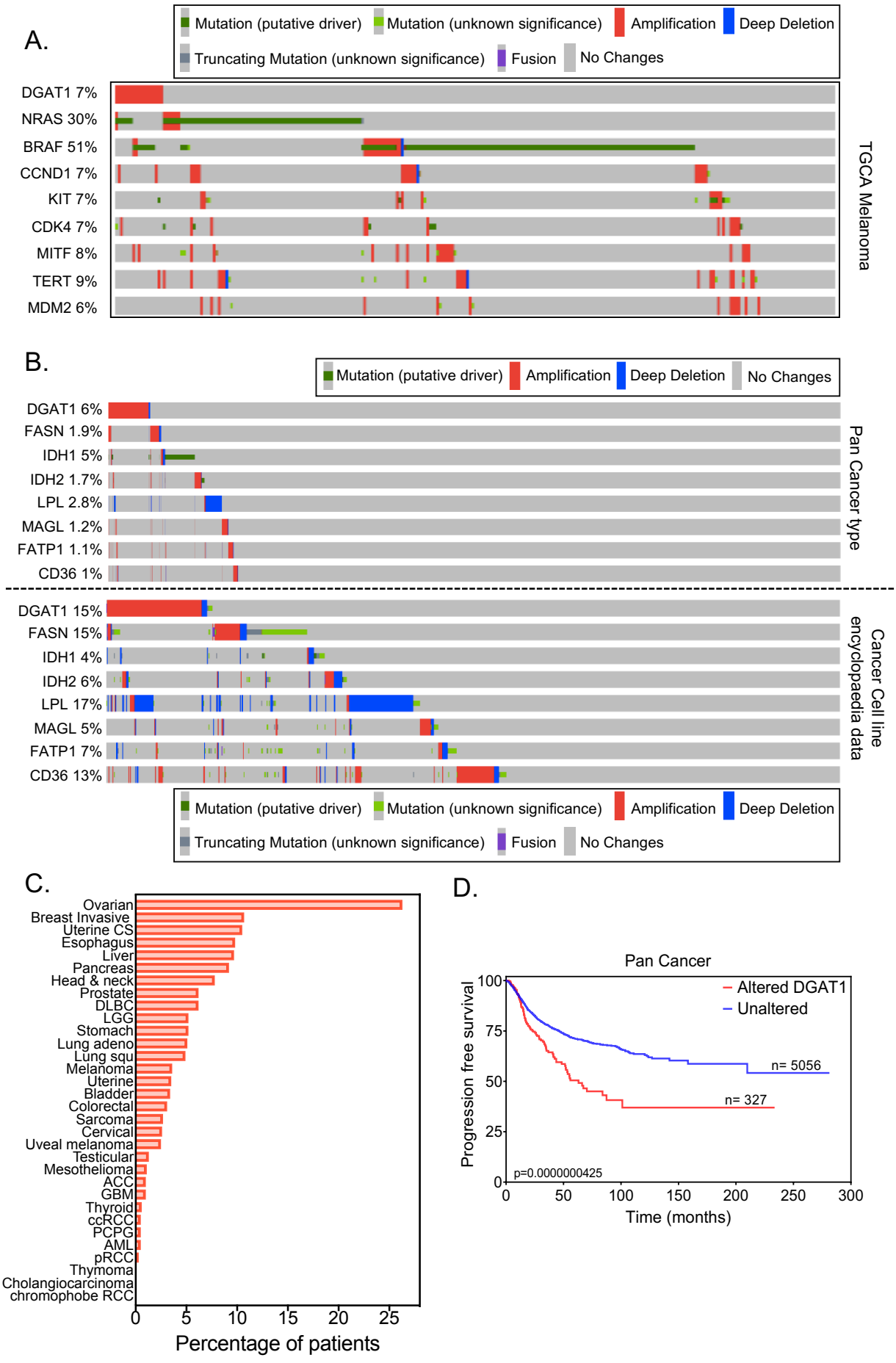
A.
Mutation (putative driver)
Mutation (unknown significance)
Amplification
Deep Deletion
Truncating Mutation (unknown significance)
Fusion
No Changes
DGAT1 7%
NRAS 30%
BRAF 51%
CCND1 7%
KIT 7%
CDK4 7%
MITF 8%
TERT 9%
MDM2 6%
TGCA Melanoma
B.
Mutation (putative driver)
Amplification
Deep Deletion
No Changes
DGAT1 6%
FASN 1.9%
IDH1 5%
IDH2 1.7%
LPL 2.8%
MAGL 1.2%
FATP1 1.1%
CD36 1%
Pan Cancer type
DGAT1 15%
FASN 15%
IDH1 4%
IDH2 6%
LPL 17%
MAGL 5%
FATP1 7%
CD36 13%
Cancer Cell line encyclopaedia data
Mutation (putative driver)
Mutation (unknown significance)
Amplification
Deep Deletion
Truncating Mutation (unknown significance)
Fusion
No Changes
C.
Ovarian
Breast Invasive
Uterine CS
Esophagus
Liver
Pancreas
Head & neck
Prostate
DLBC
LGG
Stomach
Lung adeno
Lung squ
Melanoma
Uterine
Bladder
Colorectal
Sarcoma
Cervical
Uveal melanoma
Testicular
Mesothelioma
ACC
GBM
Thyroid
ccRCC
PCPG
AML
pRCC
Thymoma
Cholangiocarcinoma
chromophobe RCC
0
5
10
15
20
25
Percentage of patients
D.
Pan Cancer
Altered DGAT1
Unaltered
n= 5056
n= 327
p=0.0000000425
Progression free survival
100
75
50
25
0
0
50
100
150
200
250
300
Time (months)

Figure 3.3 *DGAT1* is amplified in multiple cancer types and is associated with worse progression free survival

(A) Alterations for the indicated genes in the TCGA firehose legacy melanoma data set (287 patients, counting only samples with CNV data) obtained from cBioPortal. (B) Cancer cell line encyclopaedia and TGCA data set accessed via cBioPortal quantifying alterations in indicated genes (961 samples). (C) TGCA pan-cancer data set quantifying amplification of DGAT1 accessed via cBioPortal (10,953 patients). (D) Kaplan-Meier progression free survival plot comparing patients across multiple cancer types based on DGAT1 amplification (Logrank p-value).

The *DGAT1* locus residues on the long arm of chromosome 8 (8q); an extra copy of 8q has been observed in approximately 30% of melanomas[389](Figure 3.4A). Interestingly, putative melanoma oncogenes *ASAP1, MYC and GDF6* are also contained on the long arm of chromosome 8. Consistently *DGAT1, MYC, ASAP1* and GDF6 are co-amplified in melanoma and in other cancers, although there are cases where each alone is amplified (Figure 3.4B). However, of these 4 putative oncogenes, high *DGAT1* mRNA expression displayed the strongest association with reduced patient survival when stratifying patients by mRNA abundance (25% top vs 75% bottom) (Figure 3.4C and Figure 3.2A).

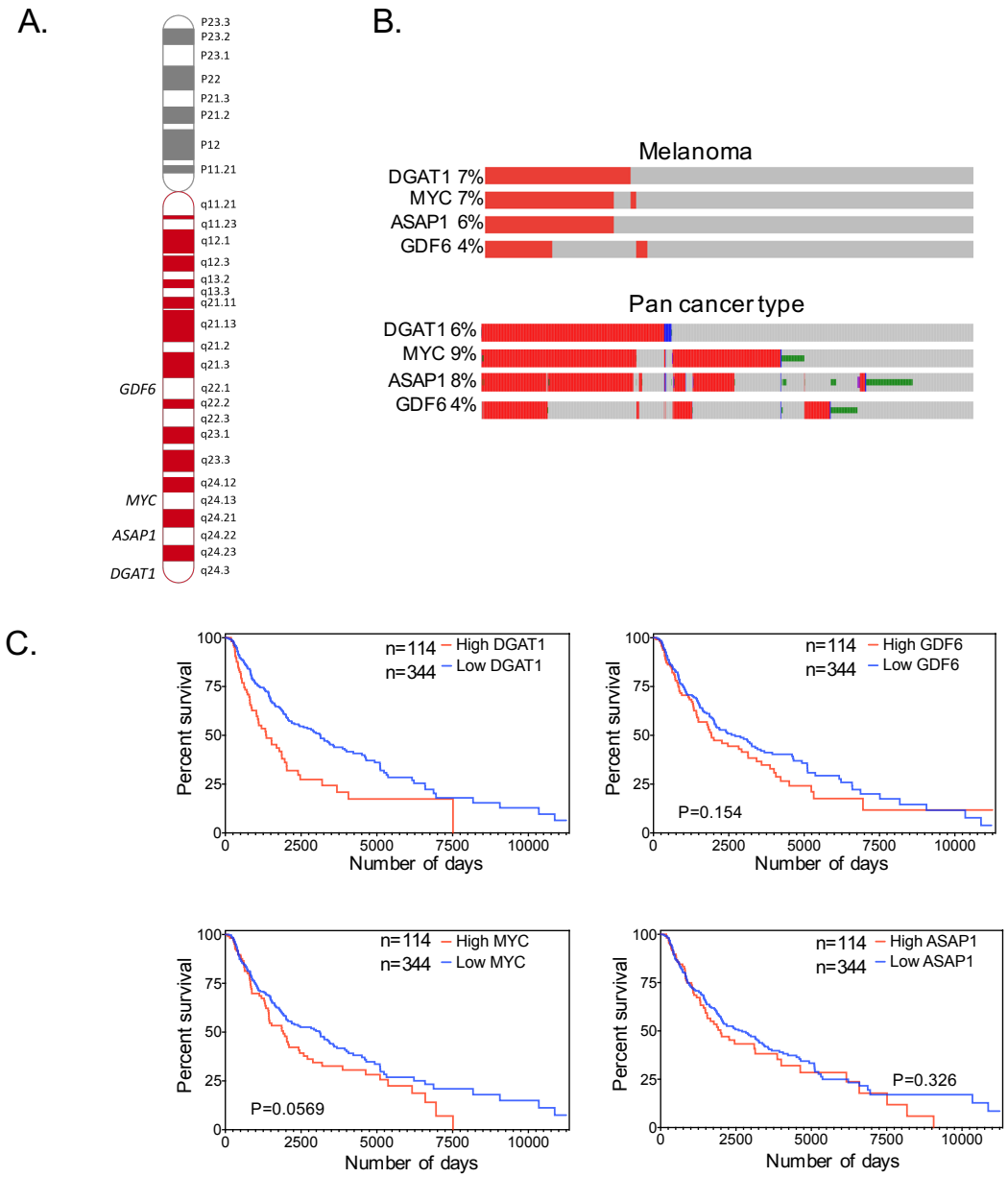

Figure 3.4 *DGAT1* is co-amplified with other putative oncogenes on human chromosome 8

(A) Schematic depicting human chromosome 8 and the locations of GDF6, MYC, ASAP1 and DGAT1 (B) Alterations for the indicated genes in the TCGA firehose legacy melanoma data set (counting only samples with CNV data) obtained from cBioPortal. (C) Kaplan-Meier survival plots for co-amplified genes found on chromosome 8 in melanoma (top 25% vs bottom 75%, TCGA database) (Logrank p-value).

Further evidence for the significance of the amplification of *DGAT1* in melanoma development is found in previous oncogenomic analysis of an oncogenic- BRAF driven zebrafish melanoma model[390]. Using the mitfa promotor to drive expression of human BRAFV600E specifically in the melanocytic lineage with a p53 loss-of-function mutation leads to the development of melanomas in every animal[390]. Array comparative genomic hybridization was carried out on the melanomas that arose autochthonously to generate copy number variation profiles and these values analysed using the JISTIC algorithm, which identifies those regions of the genome that are aberrant more often than would be expected by chance and is able to detect multiple significant sub-regions within large aberrant regions, calculating a statistical J-score representing the strength of aberantion[390]. Using this JISTIC data we investigated the amplification of the zebrafish orthologs of the four putative melanoma oncogenes co-amplified on the long arm of chromosome 8 *DGAT1, ASPAP1, GDF6* and *MYC.* The previous study identified the zebrafish orthologue of *GDF6, gdf6b* to be amplified in oncogenic BRAF driven zebrafish melanoma due to amplification of chromosome 19 (Figure 3.5A). We further interrogated this amplification of chromosome 19 in the oncogenic BRAF driven zebrafish melanoma model and found the *DGAT1* ortholog *dgat1a* to be present on chromosome 19 and co-amplified along with *gdf6b* (Figure 3.5A). Human genes often have 2 zebrafish orthologs because of a partial genome duplication in the teleost lineage. Both the second zebrafish ortholog of human *GDF6*, gdf6a, and *DGAT1*, *dgat1b* found on chromosome 16 were not recurrently amplified (Figure 3.5A). In contrast, neither zebrafish ortholog of both *MYC* and *ASAP1*, found on chromosome 2 and 24, were amplified or up-regulated in the oncogenic BRAF driven zebrafish melanoma model (Figure 3.5B). Taken together this cross-species comparative approach has highlighted the amplification of DGAT1 and both zebrafish and human melanoma, not only this but high DGAT1 mRNA expression is associated with worse patient outcomes in melanoma, thus from a cancer genomics perspective DGAT1 exhibits the hallmarks of a melanoma oncogene.

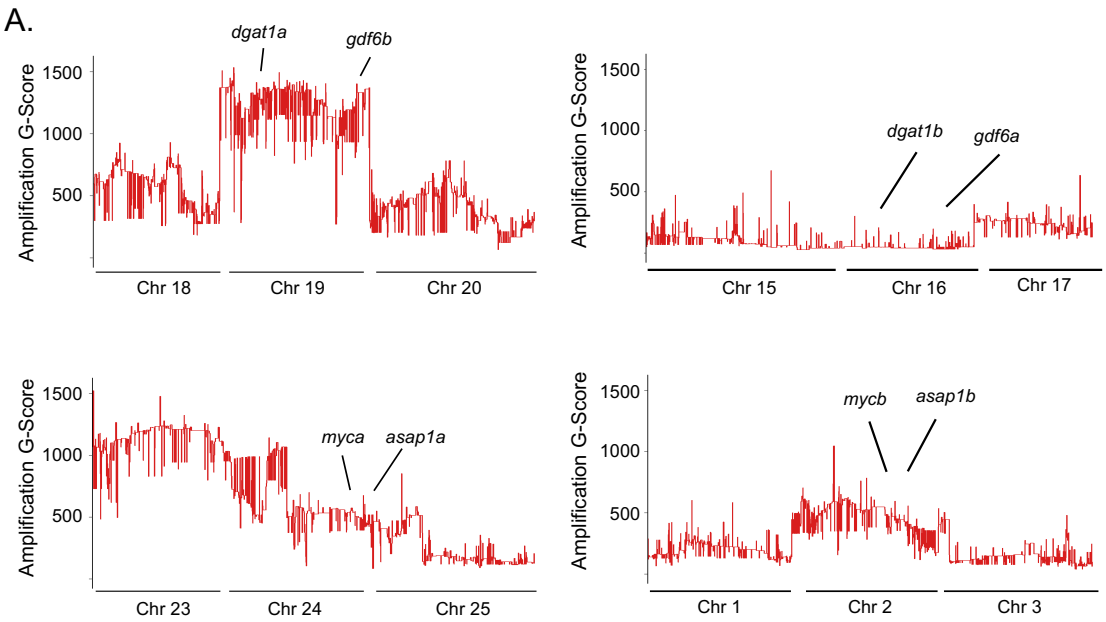

Figure 3.5 *dgat1a* is amplified in BRAF^{V600E} driven zebrafish melanoma

(A) G-Score of amplified regions of zebrafish chromosomes found in BRAF^{V600E} P53 driven tumours, zebrafish paralogues of *DGAT1 and GDF6* locations identified. (B) G-Score of amplified regions of zebrafish chromosomes found in BRAF^{V600E} P53 driven tumours, zebrafish paralogues of *MYC and ASAP1* locations identified.

Next we wanted to further elucidate the oncogenic potential of DGAT1. To address whether DGAT1 may play a role in the initiation and progression of melanoma we utilised a melanocyte rescue and lineage restricted expression system previously used in the lab and developed in the Zon laboratory[343] (Figure 3.1). In human melanoma, *DGAT1* amplification was observed to co-occur with both oncogenic BRAF and NRAS, but also, more rarely, independently of both (Figure 3.6A). In order to replicate this observation we utilised NACRE zebrafish models lacking in functional melanocytes expressing either mutant BRAF ($tp53^{M214K/M214k}$; $mitfa^{-/-}$; $BRAF^{V600E}$), or mutant NRAS ($tp53^{M214K/M214k}$; $mitfa^{-/-}$; $NRAS^{G12D}$) in the background of p53 loss-of-function (LoF) mutation or in animals with just a p53 LoF mutation ($tp53^{M214K/M214k}$; $mitfa^{-/-}$).

cDNA of *dgat1a, dgat2* and *EGFP* were cloned first into a middle entry vector and then into MiniCoopR, prior to injection into single cell zebrafish embryos. The embryos were screened at day 5 for rescued pigment, due to the presence of the wild-type mitf in the construct, and then placed into the nursery. After four weeks post fertilisation (wpf) fish were examined weekly for the development of tumour nodules. Over-expression of Dgat1a in zebrafish melanocytes co-operated with both oncogenic NRAS and BRAF to significantly accelerate the development of nodular melanoma tumours (Figure 3.6B-D), a slight delay in nodular tumour formation was observed in the oncogenic BRAF mutant animals when compared to the oncogenic NRAS mutant animals. Perhaps most strikingly, we found that Dgat1a overexpression in zebrafish melanocytes lacking functional p53 was sufficient to induce melanoma (Figure 3.6D), an outcome that we have only previously observed using the potent well-established oncogenes RAS and BRAF. In order to investigate the specificity of the Dgat1a-mediated acceleration of nodular tumour development, we also overexpressed Dgat2 in zebrafish melanocytes, in the background of both mutant NRAS and LoF p53. Thus, Dgat1 behaves as a melanoma oncoprotein in zebrafish. Significantly, Dgat2 over-expression was indistinguishable from the non-oncogenic EGFP control (Figure 3.6E), indicating that Dgat1-mediated tumorigenesis is specific and cannot be replicated by the functionally related Dgat2.

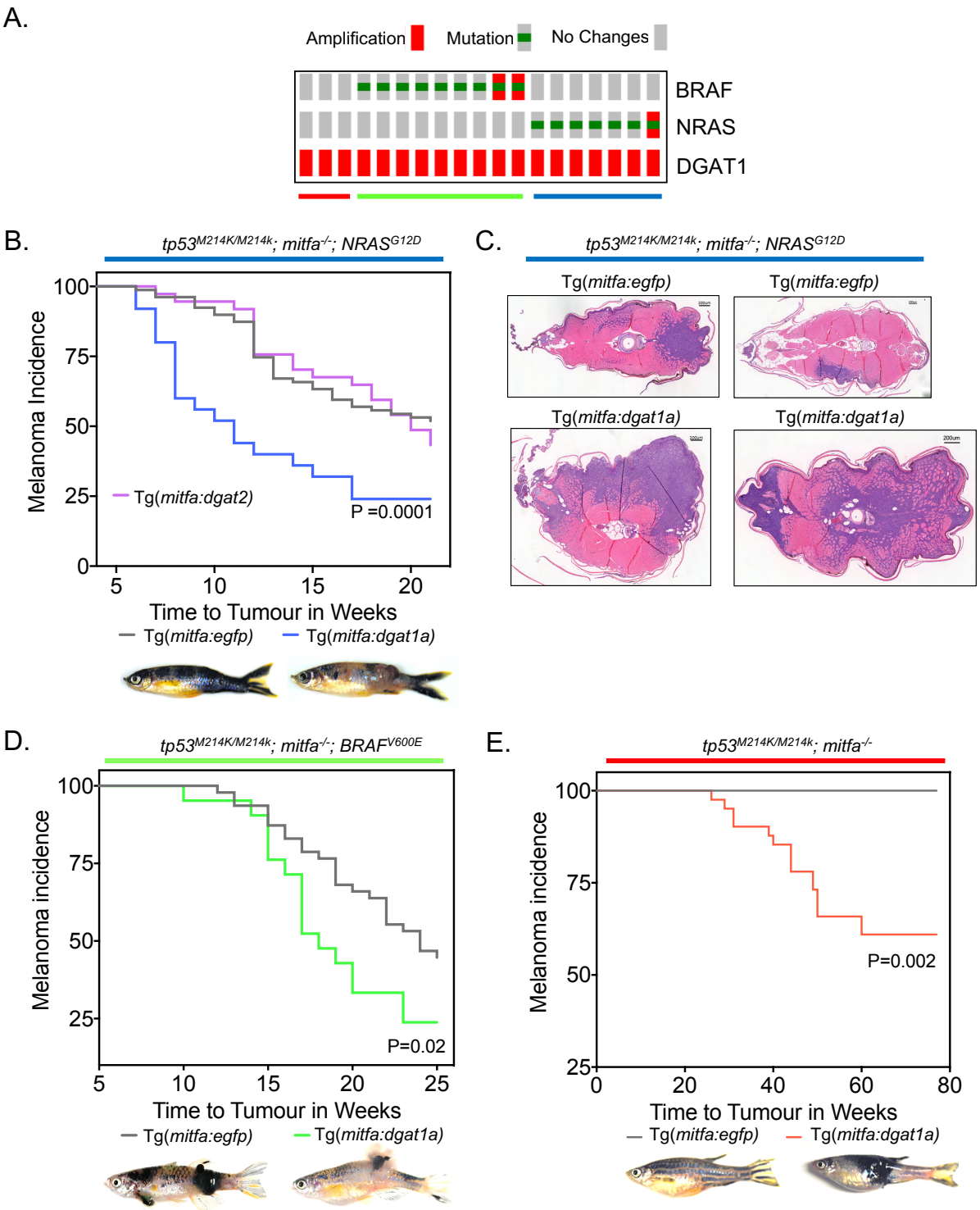
A.
Amplification
Mutation
No Changes
BRAF
NRAS
DGAT1
B.
tp53M214K/M214k; mitfa-/-; NRASG12D
Melanoma Incidence
100
75
50
25
0
5
10
15
20
Time to Tumour in Weeks
Tg(mitfa:dgat2)
P =0.0001
Tg(mitfa:egfp)
Tg(mitfa:dgat1a)
C.
tp53M214K/M214k; mitfa-/-; NRASG12D
Tg(mitfa:egfp)
Tg(mitfa:egfp)
Tg(mitfa:dgat1a)
Tg(mitfa:dgat1a)
D.
tp53M214K/M214k; mitfa-/-; BRAFV600E
Melanoma incidence
100
75
50
25
5
10
15
20
25
Time to Tumour in Weeks
P=0.02
Tg(mitfa:egfp)
Tg(mitfa:dgat1a)
E.
tp53M214K/M214k; mitfa-/-
Melanoma incidence
100
75
50
25
0
20
40
60
80
Time to Tumour in Weeks
P=0.002
Tg(mitfa:egfp)
Tg(mitfa:dgat1a)

Figure 3.6 Dgat1 functions as an oncoprotein in zebrafish

(A) DGAT1 amplification in NRAS- and BRAF-mutant melanoma as well as melanoma wild-type for NRAS and BRAF. (B) Kaplan-Meier plot of melanoma tumour nodule incidence in GFP control , Dgat1a over-expressing or Dgat2 over-expressing animals on the transgenic mitfa:NRASG12D; tp53 mutant; nacre genetic background (all n=25). Representative images are shown at 12 weeks post fertilisation. (C) Hematoxylin and eosin stained transverse sections of GFP expressing or Dgat1a over-expressing melanoma on the transgenic mitfa:NRASG12D; tp53 mutant; nacre genetic background. (D) Kaplan-Meier plot of melanoma tumour nodule incidence in GFP control and Dgat1a over-expressing animals on the transgenic mitfa:BRAFV600E; tp53 mutant; nacre genetic background. Representative images are shown at 12 weeks post fertilisation. (E) as for (D) but in the transgenic tp53 mutant; nacre genetic background. Representative images shown for GFP and DGAT1 positive animals at 54 and 76 weeks post fertilisation respectively. (Mantel–Cox's log- rank tests).

In order to develop a hypothesis describing how *DGAT1* acts as a potent oncogene in melanoma we carried out mRNA expression profiling of melanoma tumours overexpressing Dgat1a, utilizing RNA sequencing (RNA-seq). In order to do this we took age matched tumours that had developed in the oncogenic NRAS mutant animals ($tp53^{M214K/M214k}$; $mitfa^{-/-}$; $NRAS^{G12D}$) overexpressing either Dgat1a or the control EGFP, which had been carefully dissected to avoid skin contamination prior to RNA extraction. Following RNA-sequencing, the raw counts were normalised and differential gene expression analysis carried out using the DSeq2 software package in R studio. Differential gene expression analysis revealed 823 significantly differentially expressed genes and an average 5.5 fold increase in dgat1a expression when comparing Dgat1a over-expressing tumour to the control EGFP overexpressing tumours (Figure 3.7A). Hierarchical clustering using a one-minus Pearson correlation and principle component analysis, revealed patterns of gene expression that clearly distinguished Dgat1a overexpressing tumour from the EGFP controls (Figure 3.7B-C). Additionally, in order to validate the differential gene expression observed in the RNA-seq between the Dgat1a overexpressing tumours and the EGFP control, we carried out RT-qPCR on a selection of the genes found to be upregulated in the Dgat1a overexpressing tumours (Figure 3.7A&D). These genes included those involved in protein folding (hsp90aa1.1,pdia3,rpn1), cellular metabolism and REDOX (dnajc10, atp2a2, gpd1b, aldoab) and genes specifically involved in lipid metabolic processes (pltp, pparab, scdb). RT-qPCR analysis confirmed increased gene expression of our panel, validating what we had observed in our RNA-Seq data (Figure 3.7A&D). Some discrepancies were observed, but this is due to the fold expression calculated from the RNA-seq dataset being an average across the samples so this is entirely expected (Figure 3.7D).

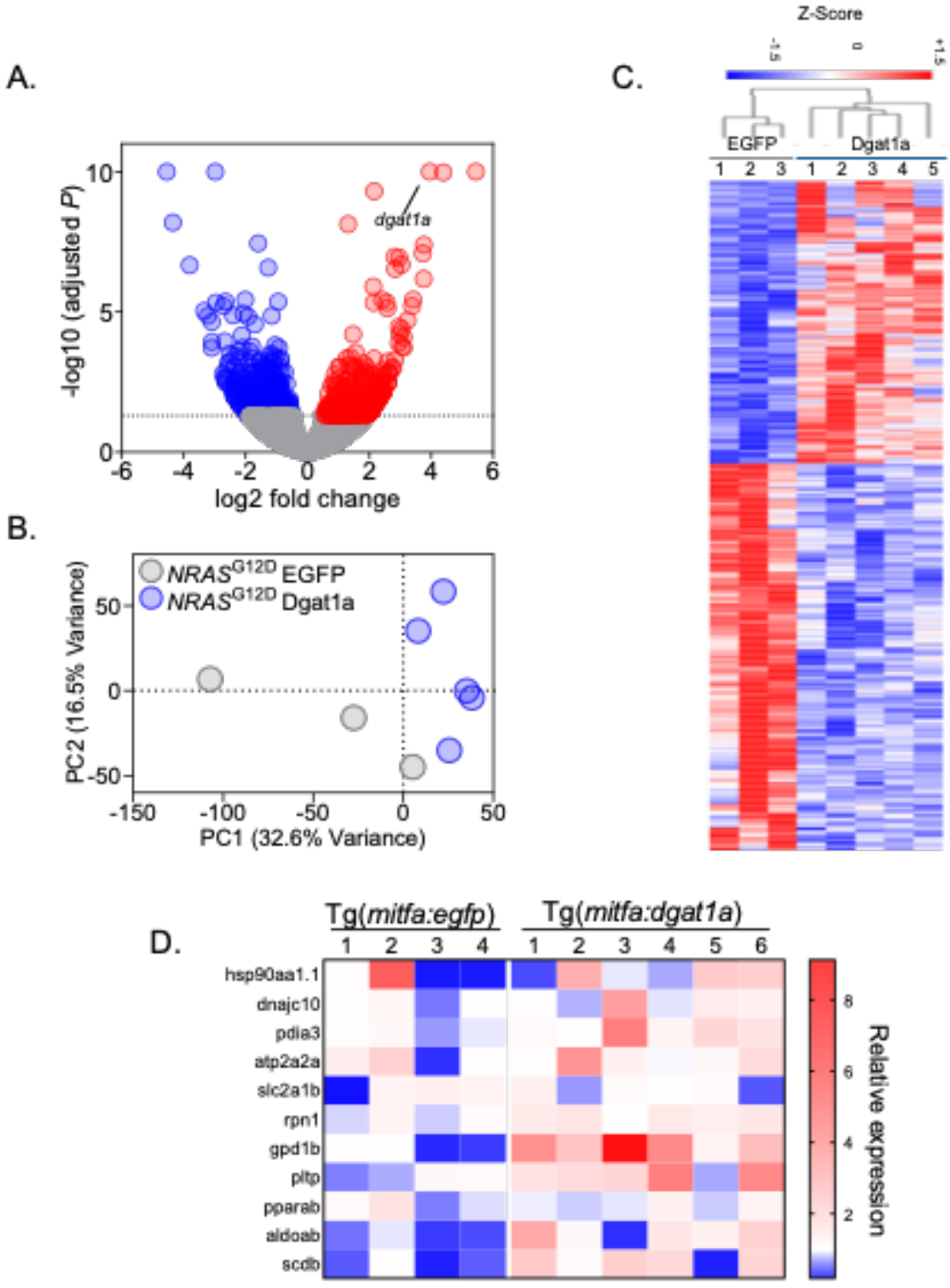
A.
-log10 (adjusted P)
log2 fold change
dgat1a
B.
NRASG12D EGFP
NRASG12D Dgat1a
PC2 (16.5% Variance)
PC1 (32.6% Variance)
C.
Z-Score
EGFP
Dgat1a
D.
Tg(mitfa:egfp)
Tg(mitfa:dgat1a)
hsp90aa1.1
dnajc10
pdia3
atp2a2a
slc2a1b
rpn1
gpd1b
pltp
pparab
aldoab
scdb
Relative expression

Figure 3.7 Over-expression of Dgat1 in zebrafish NRASG12D driven melanoma causes significant gene expression changes

(A) Volcano plot of all genes from RNA-seq data from $NRAS^{G12D}$-positive GFP-expressing (n=3) and Dgat1a over-expressing (n=5) tumours. Fold-change calculated comparing Dgat1a over-expressing tumours to GFP-expressing control tumours. Adjusted p-value cut-off <0.05 (DSEQ2, Benjamini-Hochberg) (B) Principal component analysis (PCA) of RNA-seq data from NRASG12D-positive GFP-expressing (n=3) and Dgat1a over-expressing (n=5) tumours. Principal component 1 explains 32.6 % of the variance observed in the data while Principal component 2 explains 16.5% of the variance observed in the data. (C) One minus pearson correlation heatmap of RNA-seq data NRASG12D-positive GFP-expressing (n=3) and NRASG12D-positive Dgat1a over-expressing (n=5) tumours (morpheus). (D) RT-qPCR analysis of indicated genes in both $NRAS^{G12D}$-positive GFP-expressing and Dgat1a over-expressing tumours. Relative expression calculated using a house keeping control gene (Mean).

To pinpoint the biological processes providing the context for selection of DGAT1 up-regulation and highlighting processes potentially driven by DGAT1 up-regulation, we hypothesised that as with the cancer genomic evidence a cross-species comparative approach would aid in the identification of relevant signalling pathways in understanding the oncogenic role of DGAT1. We again took the TGCA SKCM dataset and first filtered the patients selecting only those with mutant NRAS, best reflecting the genetic background of our zebrafish RNA-seq dataset. We then split the mutant NRAS patients into two groups based on *DGAT1* mRNA expression levels, top 15% v the rest of the cohort as using cbioportal 15% or SKCM patients are determined to have higher than average DGAT1 mRNA levels (Figure 3.8A). We took the normalised RNA-seq data for these patients and carried out differential gene expression analysis using DSeq2, comparing the *DGAT1* high samples to the rest of the cohort, this revealed 1874 significantly differentially expressed genes (Figure 3.8B-C). In order to compare both the human and the zebrafish RNA-seq datasets, the significantly

differentially expressed genes from the zebrafish dataset were converted to their human orthologs. The overlap in enriched genes was modest at 2.2% (Figure 3.8C). However, this was not altogether unexpected given that the genes whose expression most strongly correlated with DGAT1 expression in human tumours consistently mapped to chromosome 8q (data not shown) and were therefore likely co-amplified with DGAT1, whilst dgat1a up-regulation in the zebrafish was driven by randomly integrated transgene combined with expression of endogenous dgat1a on a linkage group distinct from human 8q. To reveal the biological processes and cellular signalling modulated by DGAT1, we carried out Gene set enrichment analysis on the significantly differentially expressed genes in the human and zebrafish RNA-seq datasets respectively, using 13 different gene set databases across both the enrichr and metascape web portals (Figure 3.8D). The GSEA analysis uncovered 893 and 870 significantly enriched gene sets in the Dgat1a overexpression zebrafish tumours and the *DGAT1* high melanoma patients respectively (Figure 3.8D). Although the overlap of enrich gene sets was modest (92, 5.5%), we considered that the conserved gene sets (Supplementary Table 2) would be the most relevant to understanding the oncogenic role of DGAT1. Intriguingly, a number of these conserved gene sets indicated enhanced activation of mTOR signalling and protein translation, as well as alterations in metabolic signalling such as increased glycolysis and lipogenesis (Figure 3.8E). Modulation of mTOR signalling is known to play a key role in both cellular metabolic reprogramming and protein translation and is able to drive a number of pro-tumorigenic processes and as such it may play a key role in modulating the effects potentially driven by DGAT1 up-regulation.

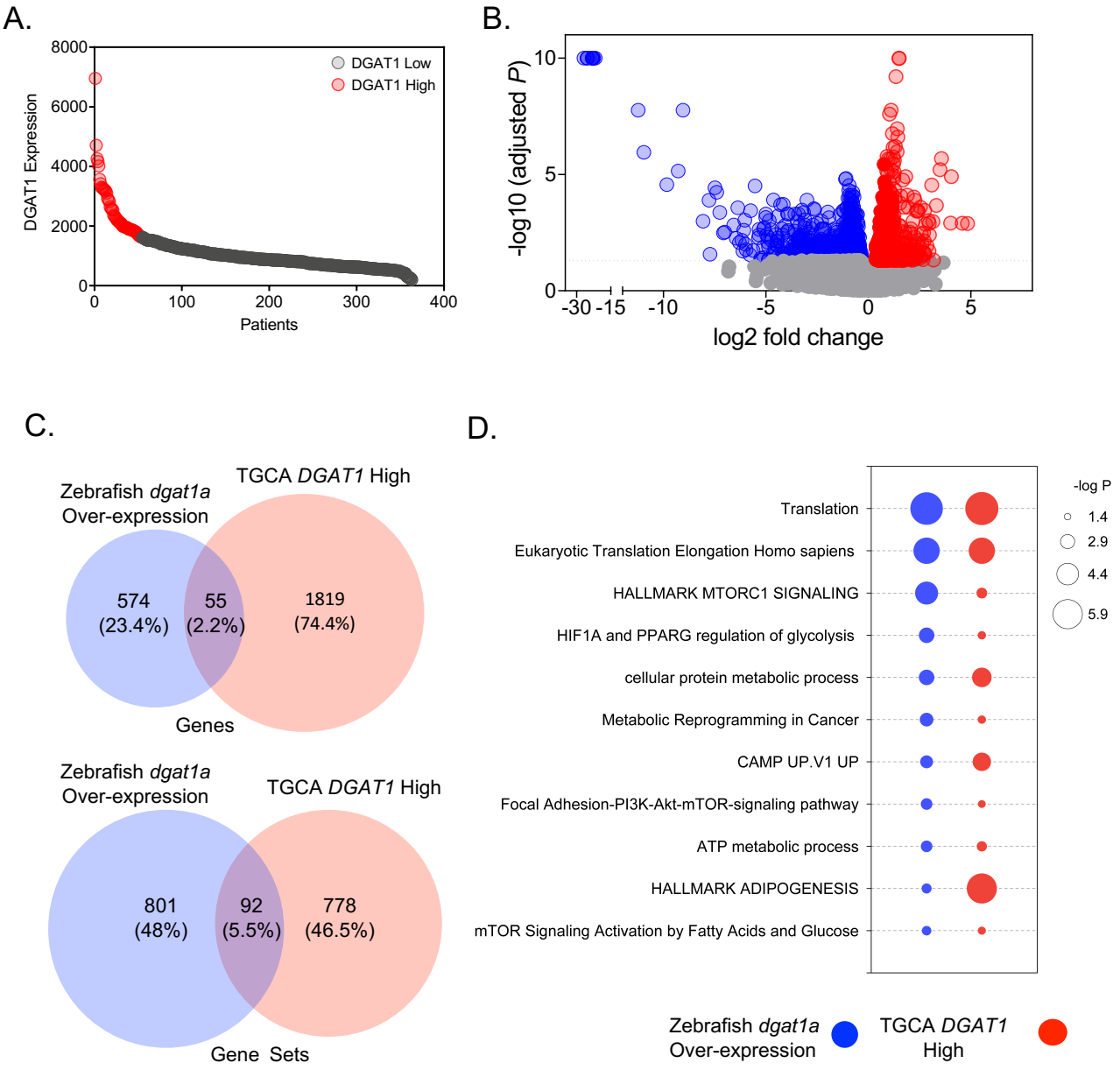
A.
DGAT1 Low
DGAT1 High
DGAT1 Expression
Patients
B.
-log10 (adjusted P)
log2 fold change
C.
Zebrafish dgat1a Over-expression
TGCA DGAT1 High
574 (23.4%)
55 (2.2%)
1819 (74.4%)
Genes
Zebrafish dgat1a Over-expression
TGCA DGAT1 High
801 (48%)
92 (5.5%)
778 (46.5%)
Gene Sets
D.
Translation
Eukaryotic Translation Elongation Homo sapiens
HALLMARK MTORC1 SIGNALING
HIF1A and PPARG regulation of glycolysis
cellular protein metabolic process
Metabolic Reprogramming in Cancer
CAMP UP.V1 UP
Focal Adhesion-PI3K-Akt-mTOR-signaling pathway
ATP metabolic process
HALLMARK ADIPOGENESIS
mTOR Signaling Activation by Fatty Acids and Glucose
-log P
1.4
2.9
4.4
5.9
Zebrafish dgat1a Over-expression
TGCA DGAT1 High

Figure 3.8 Cross-species transcriptomic analysis demonstrates high DGAT1 levels impacts upon multiple hallmarks of cancer

(A) DGAT1 expression in TGCA pan cancer atlas RNA-seq data set filtered for NRASmut melanoma patients. (B) TGCA pan cancer atlas RNA-seq data set filtered for NRASmut melanoma patients. Volcano plot where fold-change was calculated comparing DGAT1 mRNA high tumors (12/72) to the rest of the NRASmut data set (60/72). Adjusted p-value cut-off <0.05 (DSEQ2, Benjamini-Hochberg). (C) Venn diagram of significantly regulated genes (upper) and significantly enriched gene sets after GSEA of significantly regulated genes (lower) comparing either NRASG12D-positive EGFP-expressing (n=3) and NRASG12D- positive Dgat1a over-expressing (n=5) tumors or comparing DGAT1 mRNA high tumors (12/72) to the rest of the NRASmut TGCA dataset (60/72). (D) Selection of 11 pathways from the Venn diagram intersect is shown in the dot-plot. Dot size represents the P value.

3.4 Discussion

Previously, using zebrafish melanoma, work in the Hurlstone lab had found an enrichment of lipid metabolism genes that was unique to aggressive mutant RAS driven VGP melanoma, in which 20% of differentially expressed metabolic genes were related to lipid metabolism. Here, we further interrogated the mRNA expression levels of the individual genes within this RAS driven lipid metabolism subset and identified *DGAT1* as the most significantly up-regulated lipid metabolic enzyme. Thus, highlighting *DGAT1* as a likely key enzyme in driving the observed up-regulated lipid metabolism signature associated with RAS driven melanoma progression in zebrafish. Further promoting a role for the DGAT1 in altered lipid metabolism in melanoma, was the observed association of *DGAT1* mRNA levels and melanoma patient survival, with high levels of *DGAT1* expression significantly associating with a worse patient outcome. Using a cross-species oncogenomic approach we utilized further melanoma patient mRNA expression datasets and a panel of melanoma cell line models, which in agreement with the zebrafish dataset,

demonstrated that DGAT1 mRNA and protein levels are up-regulated in melanoma when compared to skin or benign nevi. This increase in DGAT1 protein and mRNA expression in malignant cells has also been demonstrated in prostate cancer cell lines and glioblastoma cell lines and patient samples, demonstrating that the observed increase in DGAT1 is not melanoma specific[340,391]. Histological staining of benign nevi and melanoma tissue samples from human patients, assessing DGAT1 protein levels would aid in addressing any concerns that increased mRNA does not necessarily lead to increased protein expression due to post-transcriptional regulation[392]. The staining would also confirm the increased levels of DGAT1 protein observed in the melanoma cell line panel.

Copy number analysis of human melanoma samples revealed that DGAT1 up-regulation may be due to focal amplification of the long arm of chromosome 8; a hotspot of other putative melanoma oncogenes. Thus, amplification of DGAT1 may be a bystander effect of the amplification of other key oncoproteins. One of these putative melanoma oncoproteins, c-Myc has been shown to play numerous roles in melanoma; depletion of c-Myc in both $BRAF^{mut}$ and $NRAS^{mut}$ melanoma cell lines leads to the induction of a senescence phenotype, whereas overexpression of c-Myc was able to overcome oncogene induced senescence driven by both $BRAF^{mut}$ and $NRAS^{mut}$ in melanocytes[393]. Further, studies have demonstrated the importance of c-Myc in *NRAS*^{Q61K} *INK4a*$^{-/-}$ models in tumour initiation and metastasis[394]. The other putative melanoma oncogenes found on chromosome 8 ,GDF6 and ASPAP1 have also been implicated in melanoma, with *GDF6* found to be up-regulated at the mRNA level in melanoma and drive neural crest gene signature in melanoma promoting tumour growth[381], research into the role of ASAP1 in melanoma is limited but ASAP1 expression has been shown to promote metastasis in prostate, colorectal and ovarian cancer[395–397]. However, when stratifying melanoma patients into high and low expressing groups based on mRNA expression, of these four genes only high *DGAT1* expression was predictive of a worse patient outcome. Additionally, there are cases in melanoma and other distinct tumour types in which only DGAT1 is amplified. Using cross-species oncogenomics we also find that, of these four, only

DGAT1/dgat1a and *GDF6/gdf6b* are amplified in $BRAF^{mut}$ driven zebrafish melanoma. Several studies have now used this comparative oncogenomics approach , comparing a zebrafish tumours to their human counterparts, in order to find the most functionally important, and perhaps "driver" genetic events in that given cancer type[398]. Examples included identification of GDF6 and SETB1 in melanoma[343,381], and novel oncogenic events in both rhabdomyosarcoma and T-cell acute lymphoblastic leukemia[399,400].

Not all melanoma patients with high *DGAT1* expression have a *DGAT1* amplification (cBioPortal, TGCA SKCM), indicating that transcriptional mechanisms must also lead to the increased level of *DGAT1* expression we observe in human melanoma. Although the transcription factors that control *DGAT1* expression are not yet fully understood, as DGAT1 is up-regulated during adipogenesis it is thought that C/EBPα or PPARγ transcription factors play role[276,401]; as such, a PPAR site occurs in the DGAT1 promoter[402]. Thus, DGAT1 up-regulation may be a consequence of and play a key role in maintaining the observed alterations in lipid metabolism in melanoma[247,253,258,266,267,271].

The evidence we have gathered in our study suggests that DGAT1 up-regulation in melanoma is not just a passenger event due to the focal amplification of the long arm of chromosome 8 in human tumours, and may play a role as a proto-oncogene in its own right. The amplification, up-regulation and the association of high *DGAT1* with a worse patient outcome across multiple tumour types only adds further weight to this hypothesis. Additionally, the amplification of DGAT1 is observed at a similar frequency to other known melanoma oncogenes, and much greater than other putative metabolic oncogenes, again providing evidence for a key role for DGAT1 as a putative metabolic oncogene from an oncogenomic perspective.

The use of the miniCoopR system in order to over-express DGAT1/dgat1a in a lineage restricted manner allowed us to assess the oncogenic potential of DGAT1 in its own right. Indeed, overexpression of DGAT1/dgat1a in zebrafish melanocytes co-operated with both oncogenic BRAF and NRAS to significantly accelerate melanoma development (Figure 3.3B & D). Other studies have also demonstrated the ability of other metabolic drivers of melanoma using the minicoopR system, overexpression of FATP1 accelerated the development of mutant BRAF driven melanoma[266], whereas overexpression of LPL accelerated the development of mutant RAS driven melanoma[267]. The most striking result and possibly the most persuasive in arguing that DGAT1 is a bona fide melanoma oncogene, is the observation that in a background of LoF p53 and without any other known oncogenic melanoma driver, over-expression of DGAT1 led to the development of melanoma. We have only previously observed the development of melanoma in these animals when over-expressing mutant RAS or BRAF, well established potent melanoma oncogenes. To our knowledge we are only the second study to assess the oncogenic potential of a gene in three different transgenic zebrafish melanoma models[375], and the first to demonstrate the oncogenicity of a gene in three different transgenic zebrafish melanoma models in a single study. Future studies, could investigate further the importance of DGAT1 in both oncogenic BRAF and NRAS driven zebrafish melanoma, utilising the CRISPR miniCoopR vector[375]. The CRISPR miniCoopR vector expressing Cas9 and the *mitfa* minigene under the control of the mitfa promoter, and gRNA targeting DGAT1 under the U6 promoter, would enable melanocyte specific knockout of DGAT1. Injection of this construct into both oncogenic BRAF and NRAS transgenic animals would allow for additional assessment of the importance of DGAT1 in melanoma development and progression, and provide additional evidence for the role of DGAT1 as an proto-oncogene.

It should be noted that there are some limitations with our use of zebrafish to model melanoma. Firstly the models we have used are based on the transgenic expression of human oncogenes rather than zebrafish orthologs and thus my not fully replicate physiological function and expression levels. Secondly, zebrafish have a genome

duplication where there are genes with more than one copy (paralogs), therefore some genes may be redundant in function or their function may be shared, which complicates genetic studies in zebrafish[403]. Additionally, in the miniCoopR system the *mitfa* minigene is encoded in the vector, thus driving *mitfa* expression in order to rescue melanocyte expression. The expression levels of MITF have been shown to play a key role in both zebrafish and human melanoma development and progression[139,141,142,382,404], and as such the role of MITF in the development of melanoma using the miniCoopR system needs to be considered. Heterogeneity in MITF expression is observed both inter and intra-tumourally, with low MITF expression levels observed in a subset of individual melanoma cells and in some tumours[405,406], and this heterogeneity is not modelled using the miniCoopR system.

Some of these drawbacks could be addressed through complimentary experiments using human melanocytes. Human melanocytes could be genetically engineered to reflect our three zebrafish melanoma models, expressing either the human melanoma oncogenes $BRAF^{V600E}$ or $NRAS^{Q61R}$. This could be achieved using either lentiviral overexpression vectors to drive exogenous over-expression, or through using CRISPR Cas9 to introduce activating point mutations endogenous proteins; a CRISPR Cas9 approach could also be used to introduce a LoF mutation in p53[393,407,408]. The expression of the oncogenes in human melanocytes leads to the induction of oncogene induced senescence[25,100,393]. Use of a lentiviral expression vector in order to over-express DGAT1 in these engineered human melanocytes would allow us to assess whether DGAT1 was able to overcome the senescence and transform the melanocytes. Assessment of these melanocytes could be carried out using markers of proliferation such as B-galactosidase or Ki67 staining, and gene expression analysis carried out looking at markers of senescence. Furthermore, the impact of DGAT1 over-expression alone could also be investigated in normal human melanocytes, in order to assess the transforming capability of DGAT1 in the absence of other known oncogenes. GEM models could also be used to further assess DGAT1 as an oncoprotein; GEM models have previously been used to demonstrate co-operation between $BRAF^{V600E}$ and PTEN[409] or INK4A[102] and $NRAS^{Q61R}$ and INK4A[410]. If the over-

expression of DGAT1 in both human and mouse melanoma models was able to overcome senescence and accelerate melanoma formation, this would provide additional evidence that DGAT1 is a melanoma oncoprotein.

Using RNA-seq analysis, we were able to identify differentially expressed genes and thus, significantly altered gene sets due to DGAT1/Dgat1a overexpression, in the mutant NRAS driven zebrafish melanoma model, compared to an EGFP control. As with the initial oncogenomic analysis of DGAT1 genetic alterations, we hypothesised that a cross-species oncogenomic approach would allow us to identify the most relevant signalling changes driving the oncogenic role of DGAT1. Differential gene expression analysis and subsequent GSEA was carried out comparing $NRAS^{mut}$ DGAT1 high melanoma patients and $NRAS^{mut}$ DGAT1 low melanoma patients. When assessing the overlapping enriched gene sets in DGAT1 overexpressing zebrafish melanoma and DGAT1 high melanoma patients, we observed significant enrichment of gene sets indicative of altered lipid metabolism and altered mTOR signalling. The alterations in cellular metabolism and changes in mTOR signalling are linked as mTOR is a key signalling hub integrating cellular metabolic signals and cell growth, and has been shown to play a role in lipid metabolism[411–413]. Alterations in cellular metabolism and growth signalling are biochemical hallmarks of cancer and provide biological context for the selection of DGAT1 up-regulation in cancer[39]. The focus of the subsequent chapters in this study will be investigate the importance of oncogenic pathways highlighted in this RNA-seq analysis and delve further into the molecular mechanism behind the oncogenic nature of DGAT1.

The intriguing observations that neither mRNA up-regulation or association with patient survival was observed for *DGAT2*, and that overexpression of *dgat2* did not accelerate mutant NRAS driven zebrafish, identifies a specific role for DGAT1. Although, able to catalyse the same reaction in Triacyl glyceride synthesis, there are distinct difference between DGAT1 and DGAT2; DGAT1 is also able to function as a acyl-CoA retinol acyltransferase maintaining retinoid homeostasis[414], unlike DGAT2

it is not essential for survival[323,328] and it is only found at the ER membrane, whereas DGAT2 has been found in complex with LD[327]. Further investigations will have to be carried out to elucidate further the molecular mechanisms behind why DGAT1 but not DGAT2 is an oncogene in melanoma.

Altogether, this data leads us to the hypothesis that DGAT1 up-regulation modulates several biochemical hallmarks of cancer conserved in both human and zebrafish melanoma, and as such, is able act as a melanoma oncoprotein driving melanoma initiation and progression.

Chapter 4 - DGAT1 enzymatic activity facilitates ribosomal protein S6-kinase (S6K)-stimulated growth

4. 1 Introduction

We have identified DGAT1/Dgat1a as a novel melanoma oncogene using zebrafish models, accelerating melanoma initiation in the background of oncogenic NRAS or BRAF and driving melanoma initiation in the background of LoF P53. RNA-seq analysis highlighted alterations in cellular metabolic processes and mTOR signalling in DGAT1/Dgat1a overexpressing tumours. We hypothesised that the changes in mTOR signalling and cellular metabolism drive the oncogenic nature of DGAT1 and that the further investigation into the role of these pathways downstream of DGAT1 would highlight the specific role of DGAT1.

mTOR is a highly conserved protein kinase which, through the formation of two distinct multi-protein complexes (mTORC1 & mTORC2), acts as a key signalling hub regulating growth, proliferation, metabolism, survival, autophagy and survival[72,415]. mTOR co-ordinates multiple cellular processes predominantly through the balancing of anabolic and catabolic processes. Studies have suggested mTORC1 predominantly regulates cell growth and metabolism through a number of well-established down-stream effectors, whereas although mTORC2 is involved in controlling proliferation and survival, the downstream effectors are lesser known[72,415,416]. In cancer, constitutive activation of mTORC1 has been shown to stimulate anabolic processes thus driving tumour growth and proliferation[416,417].

The mTORC1 complex consists of the two core components, common across mTORC1 and mTORC2; DEP domain-containing mTOR-interacting protein (DEPTOR)[418] and mammalian lethal with sec-13 protein 8 (mLST8)[419], as well as the mTORC1 specific

components regulatory-associated protein of mTOR (RAPTOR)[420] and proline-rich Akt substrate of 40 kDa (PRAS40)[421]. mTORC1 activity is regulated by both extracellular and intracellular cues such as growth factors, amino acids , glucose and cellular energy levels. The regulation of mTOR by growth factors is through the two well characterised signalling pathways, the PI3K pathway and the MAPK pathway (Figure 1.2). Activation of these signalling cascades through growth factor stimulation leads to phosphorylation of TSC2 ,a negative regulator of mTORC1[422,423] . This phosphorylation leads to the dissociation of TSC2 from the lysosome[424] and prevents its activity as a GTPase-activating protein (GAP) inhibiting the Rheb GTPase, thus leaving GTP Rheb to activate mTORC1[425] (Figure 4.1). Additionally, activated Akt can phosphorylate the mTORC1 repressor PRAS40, leading to its dissociation from mTORC1 and subsequent activation of mTORC1 signalling[426] (Figure 4.1). Amino acid regulation of mTORC1 signalling is predominantly regulated by the Rag GTPases (Rag) and Ragulator complex, which through interaction with RAPTOR mediate amino acid signalling to mTORC1 through lysosomal localisation of mTORC1[427,428]. This allows subsequent activation of mTORC1 signalling by Rheb[427,428]. Sensing and direct binding of amino acids is carried out by several cytosolic and lysosomal amino acid sensors such as SLC38A9[429], Sestrin 2 (SESN2)[430], cellular arginine sensor for mTORC1 protein (CASTOR1/2)[431] and S-adenosylmethionine sensor upstream of mTORC1 (SAMTOR)[432], each of which interact with the GAPs and GEFs which act upon the Rag proteins regulating mTORC1 activation (Figure 4.1). For example SESN2, a leucine sensor, is found bound to the GATOR2 complex under leucine starvation , when leucine is present it binds to SESN2 an disrupts the SESN2-GATOR2 interactor, leaving GATOR2 to bind and inhibit GATOR1, leading to the activation of Rag proteins and thus mTORC1[430]. Inhibition of mTORC1 signalling under conditions of energy stress, due to nutrient deprivation or hypoxia, is mediated by AMP-activated protein kinase (AMPK). In periods of energetic stress, AMP binds directly to AMPK and leads to its activation by three mechanisms, 1) promoting phosphorylation of Thr172, by its major upstream kinase LKB1, 2) preventing dephosphorylation of Thr172, 3) allosteric activation of AMPK already phosphorylated on Thr172[433,434]. Activated AMPK regulates mTORC1 through two mechanisms, firstly through an activating phosphorylation of TSC2 thus inhibiting Rheb activation of mTOR[435], and secondly

through a inhibiting phosphorylation of RAPTOR which induces 14-3-3 binding and inhibition of mTORC1[436] (Figure 4.1).

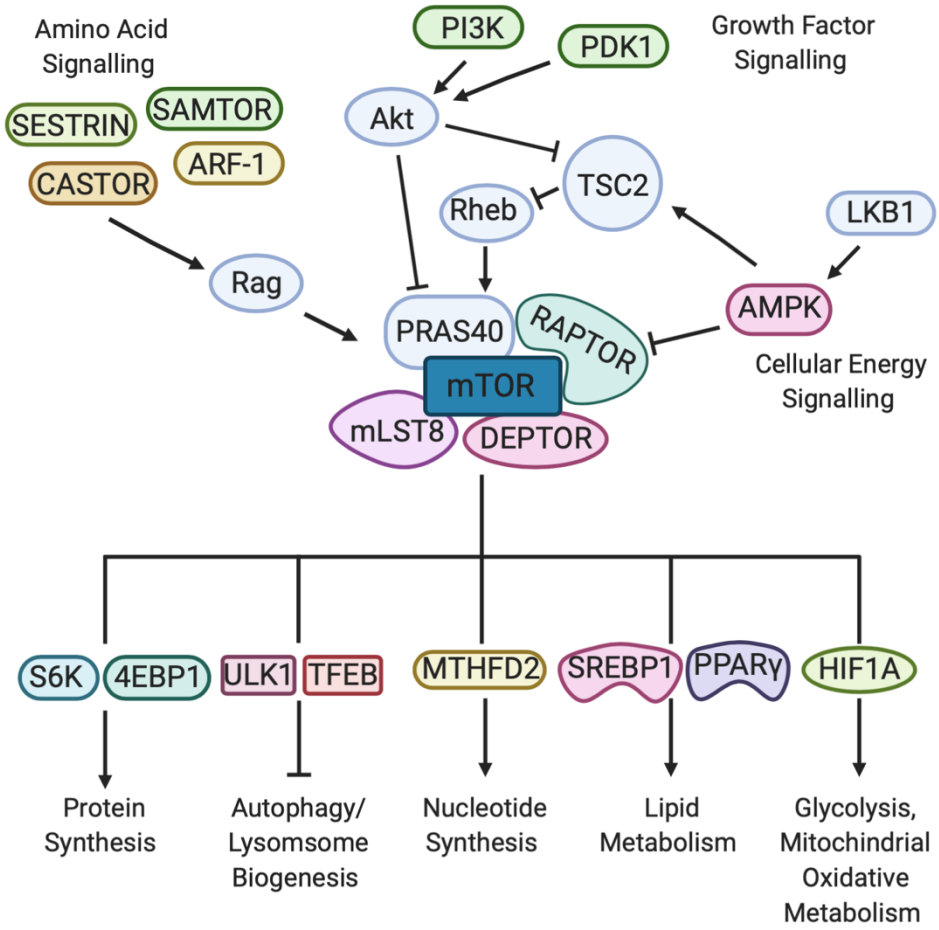

Figure 4.1 mTORC1 Signalling Network

mTORC1 regulates key cellular metabolism and growth signalling networks downstream of growth factor signalling, amino acid signalling and cellular energy sensing.

mTORC1 promotes cellular growth and proliferation through promoting multiple biosynthetic and metabolic pathways (Figure 4.1). Activation of mTORC1 promotes protein synthesis through two main effectors p70S6 Kinase 1 (S6K1) and eIF4E Binding Protein (4EBP) (Figure 4.1). Phosphorylation of S6K1 at hydrophobic motif site, Thr389, enables a subsequent activating phosphorylation by PDK1[437,438]. S6K has a number of downstream targets which it phosphorylates and activates including, ribosomal protein S6 (S6) a component of the 40S ribosome[439], the translation initiation factor eIF4B[440], eukaryotic elongation factor 2 (eEF2) kinase involved in translation elongation[441] and programmed cell death 4 (PDCD4) a regulator of eIF4A helicase[442]. Thus, S6K promotes translation at multiple steps. 4E-BP1 inhibits translation through sequestering eIF4E, phosphorylated by mTORC1 at two sites (Thr37 and Thr46) , followed by two further phosphorylation events (Ser65 and Thr70) which leads to eIF4E release from 4E-BP1 and subsequent formation of the eIF4 complex initiation of translation[443,444].

De novo lipid synthesis is also under the control of mTORC1 signalling through activating the SREBP transcription factors which are master regulators of lipid metabolism and control the expression of metabolic genes involved in FA and cholesterol synthesis[248,445] (Figure 4.1). mTORC1-mediated control of SREBP activity is modulated through two mechanisms, firstly though a S6K mediated mechanism which leads to an increase in processed SREBP1[446], and secondly through phosphorylation of the phosphatidic acid phosphatase lipin1 , which prevents it's nuclear translocation and inhibition of SREBP dependent transcription[447]. Although the precise mechanism is not yet fully understood, mTORC1 is also able to promote FA synthesis through up-regulating the expression of the nuclear receptor PPARγ, a master regulator of adipogenesis[448].

The mTORC1-S6K signalling axis is also involved in the promotion of nucleotide synthesis, S6K phosphorylates and activates carbamolyl-phosphate synthase 2, (CAS) the rate-limiting enzyme for *de novo* synthesis of pyrimidines[449]. mTORC1 also modulates nucleotide biosynthesis through the activation of the transcription factor ATF4 which drives the expression of the enzyme methylenetetrahydrofolate dehydrogenase 2 (MTHFD2), involved in purine synthesis[450] (Figure 4.1).

Glucose metabolism is also modulated by mTORC1 signalling. Active mTORC1 drives a switch from oxidative phosphorylation towards glycolysis through the upregulation of HIF1α, a key transcription factor modulating the expression of numerous genes involved in glycolysis[446] (Figure 4.1).

In addition to promoting multiple anabolic pathways, mTORC1 is an inhibitor of cellular catabolic programmes, primarily through regulating autophagy (Figure 4.1). mTORC1 directly inhibits autophagy though an inhibitory phosphorylation of the autophagy initiating kinase ULK-1[451], and indirectly through the phosphorylation of the master regulator of lysosome biogenesis TFEB which prevents its nuclear localisation and thus lysomal genes[452].

We hypothesised that the optimal method for determining the myriad of signalling cascades both regulating and regulated by mTOR, downstream of DGAT1 modulation, would be through the use of quantitative SILAC-based phospho-proteomics on human melanoma cell lines. Phosphorylation is a wide-spread post-translational modification critical in the regulation of almost all cellular signalling processes, and as outlined above, is critical in regulating signalling through mTOR. Using a titanium bead enrichment based phospho-proteomic approach, previously described[354], allows for an unbiased system-wide analysis of the signalling cascades downstream of DGAT1 modulation. The use of Stable Isotope Labelling in Cell Culture (SILAC) methods, allows for the multiplexing of samples and the ratio of intensities

of the peptides by heavy v light amino acids can be used to establish the relative quantities of the respective proteins or phosphorylation events[453].

4.2 Aims

- To identify the mechanism by which DGAT1 modulates mTOR signalling changes through carrying out phospho-proteomic analysis of human melanoma cells, following short term inhibition of DGAT1 .

- Investigate the impact of DGAT1 modulation through inhibition, knockdown or over-expression on human melanoma cell line growth and proliferation.

4.3 Results

Having uncovered DGAT1/Dgat1a as a proto-oncogene in our zebrafish models of melanoma, we next assessed the impact of DGAT1 antagonism in human melanoma cell lines, with high protein levels of DGAT1 (DGAT1 ^{High}) (Figure 3.2D) and cell lines with known amplification of DGAT1 (DGAT1^{Amp}). Inhibition of DGAT1, using four different selective inhibitors, in all four DGAT1^{High} cell lines led to a reduction in cell number after a period of 96 h, as determined by crystal violet staining (Figure 4.2A). In agreement with the observed reduction in cell number, we observed reduced cell cycle progression in all four DGAT1^{High} cell lines upon 24 h DGAT1 inhibition (Figure 4.2B). Additionally, a reduction in cell number was also observed in DGAT1^{AMP} cell lines upon pharmacological antagonism with two different DGAT1 inhibitors (Figure 4.2C). Indicating that the enzymatic activity of DGAT1 is important in melanoma cell growth and proliferation.

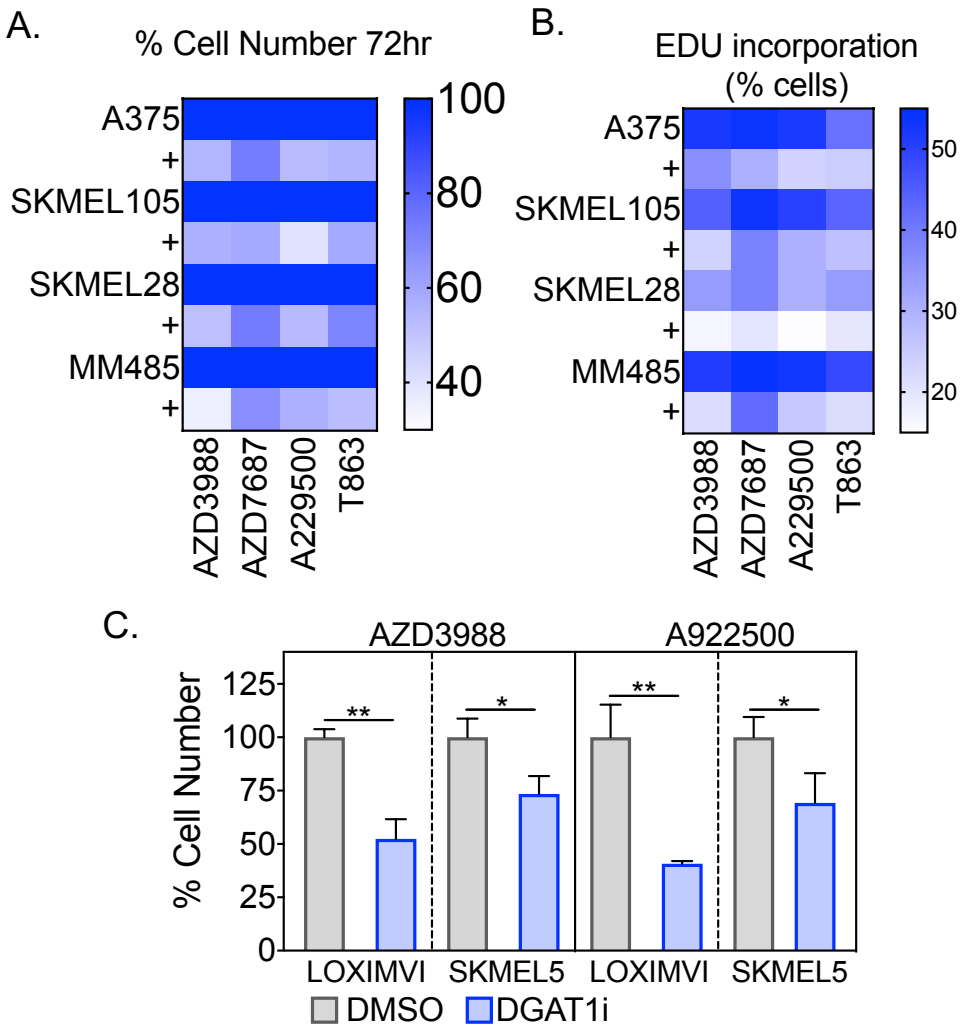

Figure 4.2 DGAT1 inhibition decreases melanoma cell proliferation

(A) Heatmap of relative cell number of indicated DGAT1^{High} cell lines stained with crystal violet following 72 h treatment with/without indicated DGAT1 inhibitor (Mean, n>3). (B) Quantification of the percentage of cells in S-phase using EdU incorporation following 24 h treatment of indicated DGAT1^{High} cell lines with/without indicated DGAT1 inhibitor in indicated cell lines (Mean, n>3). (C) Bar graph of relative cell number of indicated DGAT1^{Amp} cell lines stained with crystal violet following 72 h treatment with/without indicated DGAT1 inhibitor (Mean, n>3) (unpaired two-sided t-test).

Having uncovered alterations in key oncogenic signalling networks such as mTOR signalling and alterations in lipid metabolism in our zebrafish melanoma models overexpressing Dgat1a, we wanted to further dissect which of these signalling changes were directly dependent on DGAT1. In order to do this, we used the A375 melanoma cell line model, which we found to have high levels of DGAT1 expression ($DGAT1^{High}$) (Figure 3.1D) and investigated the initial signalling changes that occur following DGAT1 inhibition. We performed unbiased quantitative mass-spectrometry (MS)-based phospho-proteomics. A375 cells were first labelled using Stable Isotope Labelling in Cell Culture (SILAC) methods, creating two populations of cells, one labelled with natural variants of the amino acids second one with heavy variants of the amino acids and SILAC incorporation was confirmed (data not shown) (Figure 4.3A). We analysed phosphorylated peptides from SILAC-labelled $DGAT1^{high}$ A375 melanoma cells following 4h treatment with the DGAT1 inhibitor A922500, and a strong correlation was found between the 3 individual repeats (Figure 4.3B). Phospho-sites with a SILAC ratio of greater than 1.5 were considered up-regulated whilst those with a ratio less than 0.75 were considered down-regulated. Analysis of the enriched phospho-peptides post-4h DGAT1 inhibition revealed P70S6K and PDK3/4 as key kinases responsible for the enriched phospho-sites (Figure 4.3C). Further analysis of the significantly enriched up or down- phospho-sites again highlighted P70S6K as a key hub protein downstream of DGAT1 inhibition, along with both mTOR and CDK1 (Figure 4.3D). This is in agreement with the GSEA analysis of our zebrafish melanoma models overexpressing Dgat1a.

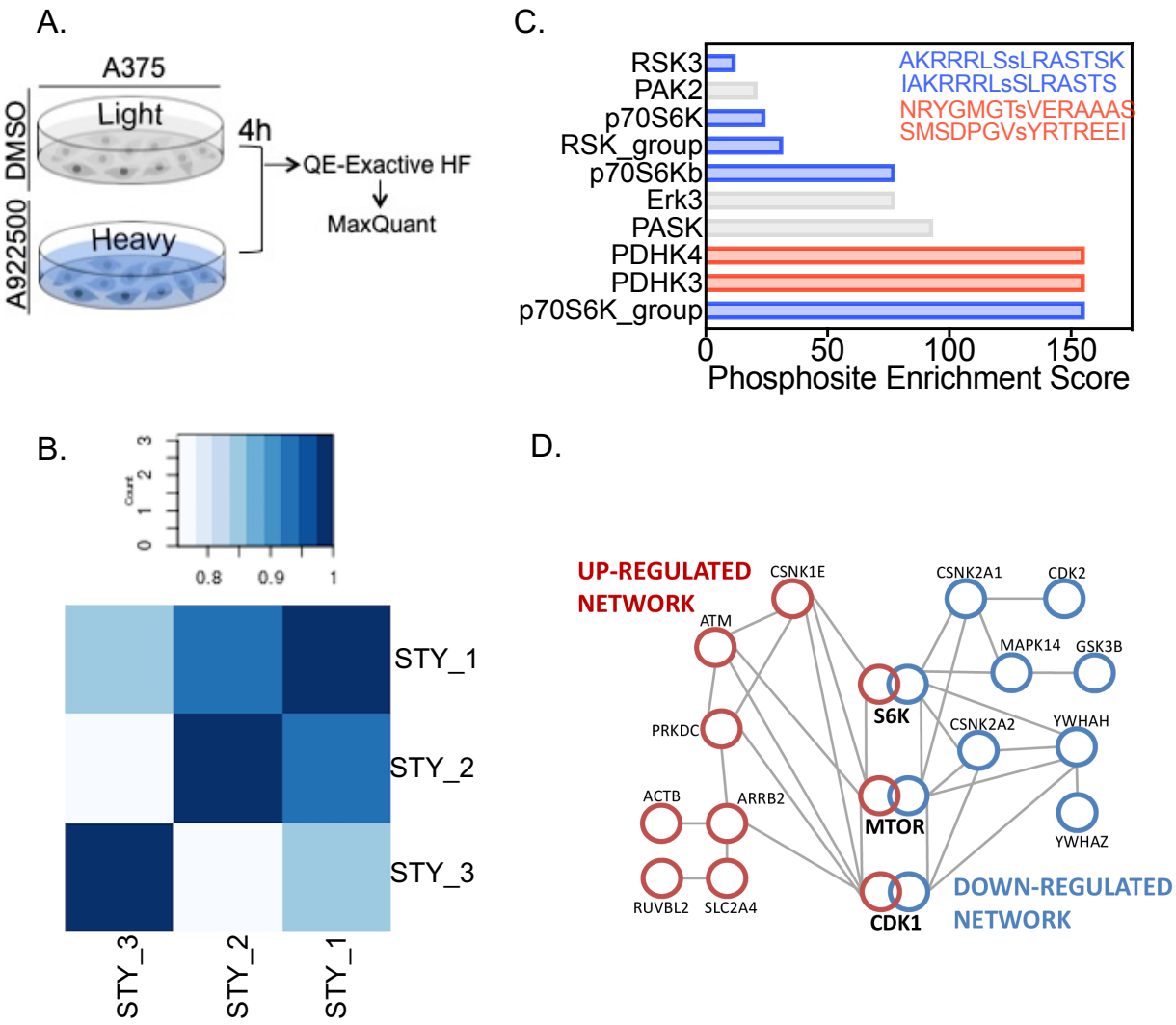

Figure 4.3 Phospho-proteomic analysis reveals changes in mTOR singling upon DGAT1 inhibition

(A) Phospho-proteomics workflow diagram. (B) Pearson correlation between phospho-proteome samples following treatment of A375 cells with/without A922500 for 4 h (n=3). (C) Bar graph depicting the enriched phosphorylated sites (WebGestalt) of up- (59) and down-regulated (96) phosphorylated proteins in A375 cells after treatment with A922500 for 4 h. (D) Network map depicting protein hub analysis of both up- and down-regulated phosphorylated protein sites in A375 cells following treatment with A922500 for 4 h (right) (n=3) (Enrichr).

To confirm the alterations observed in S6 kinase (S6K) and mTOR signalling observed in our phospho-proteomic analysis post-DGAT1 inhibition, we used western blotting to detect phosphorylation of the downstream S6K/mTOR targets ribosomal S6 (S6) and Eukaryotic Translation Elongation Factor 2 (eEF2). A panel of DGAT1^{High} melanoma cell lines (A375, SKMEL105, MM485, SKMEL28) and two melanoma cell lines with known DGAT1 amplification (DGAT1^{AMP}) (LOXIMVI, SKMEL5), were treated with three different DGAT1 inhibitors (A922500, T863, AZD3988) for a period of 2-8 h. In both DGAT1^{High} and DGAT1^{AMP} cell lines treatment with a DGAT1 inhibitor led to a decrease in phospho-S6 levels and an increase in phospho-eEF2 levels, indicating that DGAT1 inhibition leads to a decrease in mTOR-S6K signalling (Figure 4.4A-C). Although the timing of the alerted levels of phospho-S6 or phospho-eEF2 post DGAT1 inhibition varied with each drug and across the cell lines, the occurrence of both decreased phospho-S6 levels and increase in the level of phospho-eEF2 was consistent (Figure 4.4C). Interestingly, treatment of the panel of DGAT1^{High} cell lines with the DGAT2 inhibitor PF-06424439 over the same time course did not lead to alterations in the levels of phospho-S6 (Figure 4.4D), indicating that the observed alterations in S6K signalling were DGAT1 specific.

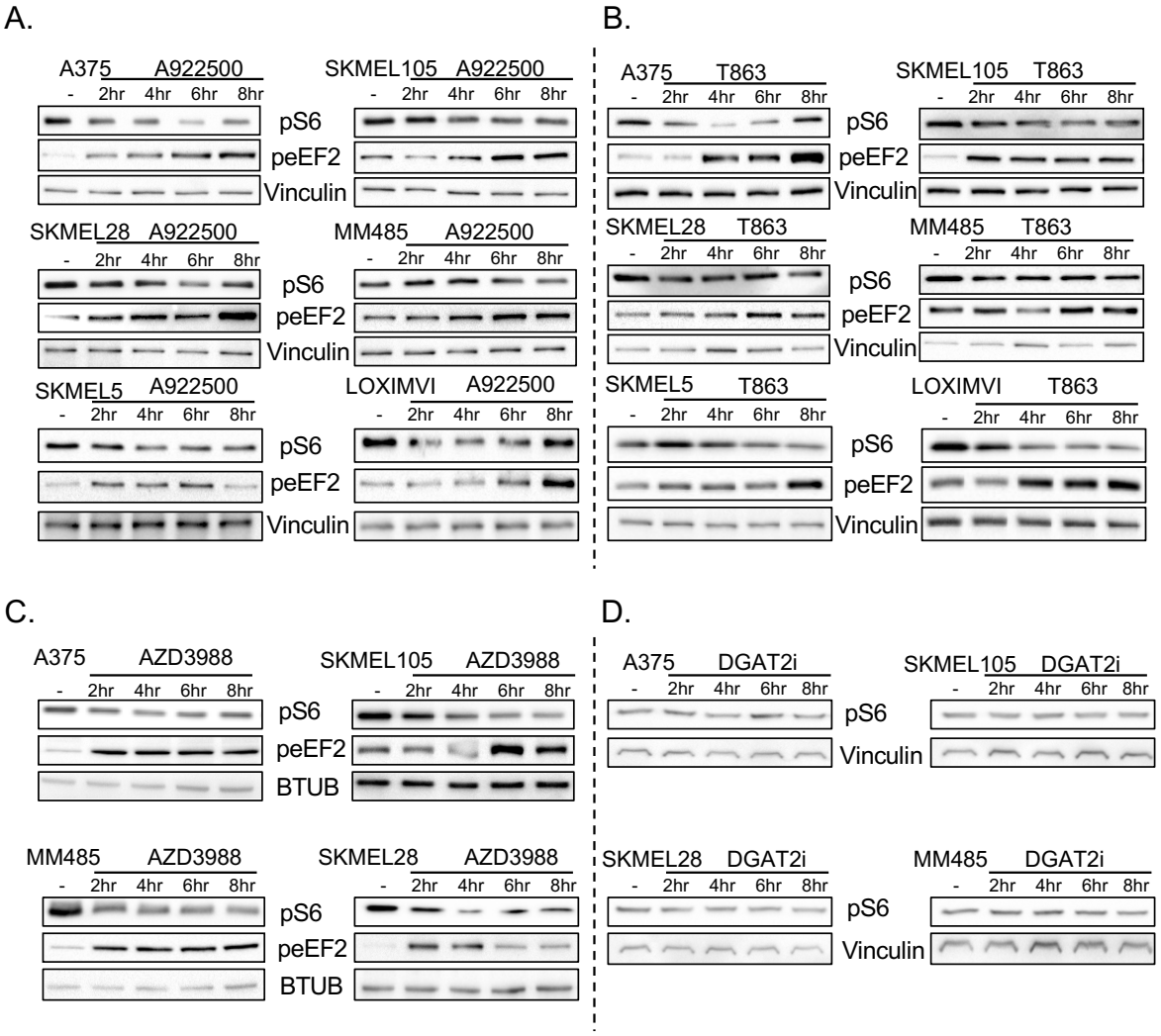

Figure 4.4 DGAT1 inhibition decreases S6K signalling

(A) Protein expression of phospho-S6 and phospho-eEF2 in indicated cell lines following treatment with/without the DGAT1 inhibitor A922500 for 2-8 h. (B) Protein expression of phospho-S6 and phospho-eEF2 in indicated cell lines following treatment with/without the DGAT1 inhibitor T863 for 2-8 h. (C) Protein expression of phospho-S6 and phospho-eEF2 in indicated cell lines following treatment with/without the DGAT1 inhibitor AZD3988 for 2-8 h. (D) Protein expression of phospho-S6 in indicated cell lines following treatment with/without the DGAT2 inhibitor PF-06424439 for 2-8 h.

Using the same approach, we looked to confirm the observed alterations in PDK3/4 activity, examining both the total protein levels of PDK4 and phosphorylation levels of the PDK4 target pDHe1a. Treatment of the panel of DGAT1^{High} with the DGAT1 inhibitor A922500 did not lead to any consistent changes to either total PDK4 or phospho-pDHe1a levels (Figure 4.5). Moreover, PDK3/4 was not highlighted in our protein hub analysis (Figure 4.3D).

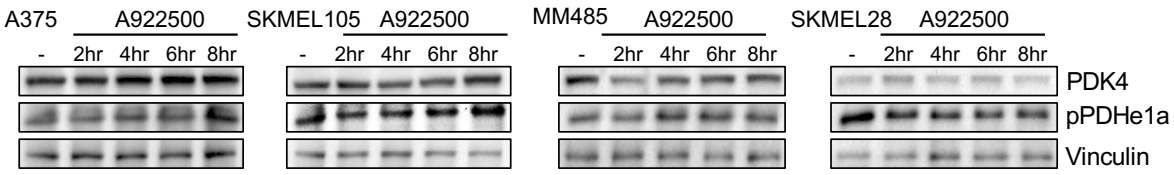

Figure 4.5 DGAT1 inhibition does not impact on PDK3/4 activity in melanoma cells
Protein expression of phospho-PDHe1a and PDK4 in indicated cell lines following treatment with/without the DGAT1 inhibitor A922500 for 2-8 h.

We next investigated the possible mechanism upstream of mTOR that may be behind the inhibition of S6K signalling upon short term DGAT1 antagonism. We found increased activation of AMPK after inhibition of DGAT1 for 2 and 4 h, in agreement with a decrease in S6K signalling at the same timepoints, indicated by reduced phosphorylation of S6 (Figure 4.6). Pharmacological inhibition of AMPK, using Compound C, rescued the decrease in phosphorylated S6 upon DGAT1 inhibition (Figure 4.6). Indicating that short term inhibition of DGAT1 leads to energetic stress in melanoma cells and activation of AMPK and that AMPK is a key modulator of the mTOR-S6K signalling axis downstream of DGAT1.

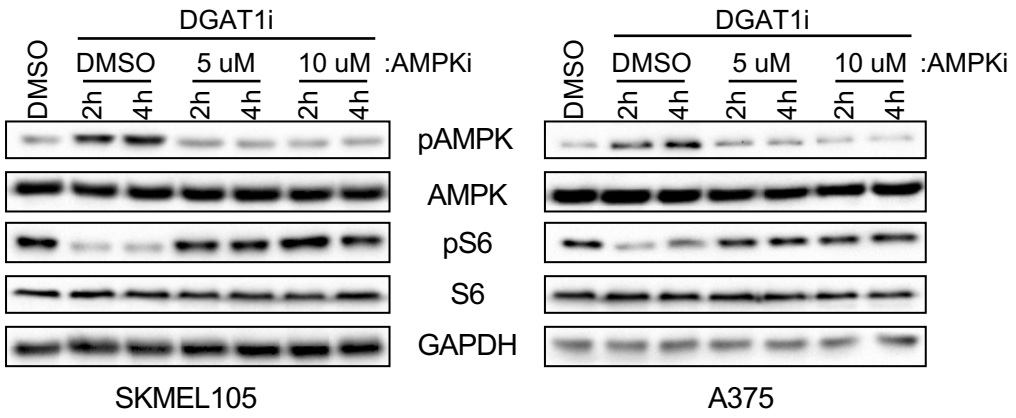

Figure 4.6 AMPK modulates S6K activity downstream of DGAT1 inhibition

Protein expression of phospho-AMPK, AMPK, phospho-S6 and S6 in indicated cell lines following treatment with/without the DGAT1 inhibitor A922500 and with/without the AMPK inhibitor Compound C for 2-4 h.

Given the effect of DGAT1 inhibition on mTOR signalling and melanoma cell growth, we next assessed whether knockdown of DGAT1 using siRNA oligos would replicate the impact on melanoma cell proliferation as pharmacological inhibition of DGAT1. Using time-lapse microscopy, in three DGAT1^{High} melanoma cell lines we observed a reduction in melanoma cell growth over a period of ~90h upon knockdown of DGAT1 with either an individual DGAT1 targeting oligo, or a pool of oligos (Figure 4.7A). The reduction in melanoma cell growth upon DGAT1 knockdown was accompanied by both an decrease in the levels of phospho-S6 and an increase in the levels of phospho-eEF2, as determine by western blotting (Figure 4.7A). The reduction in melanoma cell proliferation upon DGAT1 knockdown was further confirmed using an EdU assay, demonstrating that DGAT1 knockdown leads to a reduction of the number of cells in S-phase after 72h (Figure 4.7B). Thus, DGAT1 knockdown leads to decrease in melanoma cell proliferation and growth, which is likely due to reduced mTOR signalling through S6K.

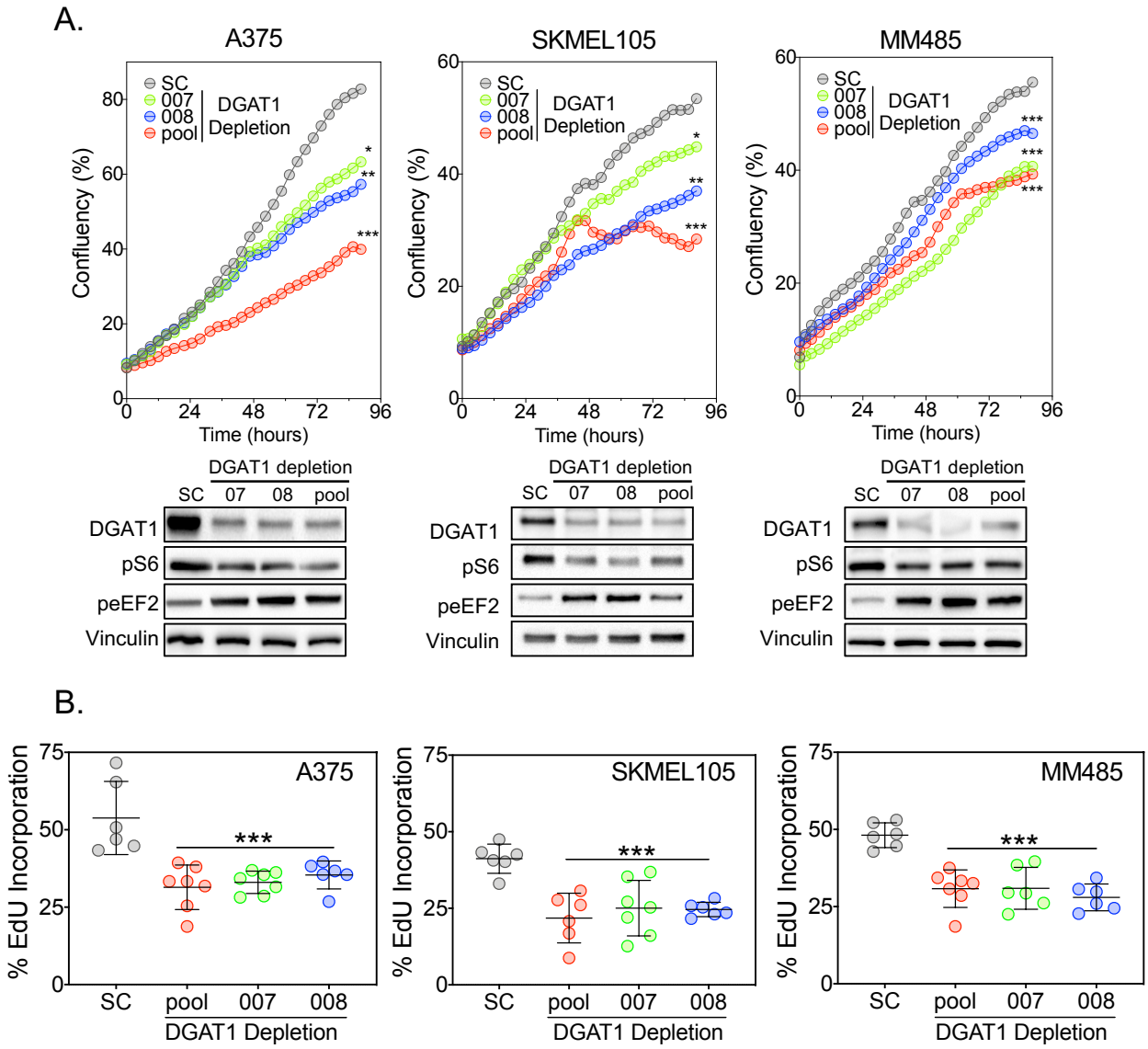

Figure 4.7 Knockdown of DGAT1 decrease melanoma cell proliferation

(A) Confluency curves of indicated cell lines transfected with indicated siRNAs targeting DGAT1 (007, 008, pool) or scrambled control (SC), determined by time-lapse microscopy using an incucyte zoom system (Mean, n=3) (upper) (one-way Anova). Protein expression of DGAT1, phospho-S6 and phospho-eEF2 in indicated cell lines transfected with indicated siRNAs targeting DGAT1 (007, 008, pool) or scrambled control (SC) (lower). (B) Quantification of the percentage of cells in S-phase using EdU incorporation following transfection of indicated cell lines with indicated siRNAs targeting DGAT1 (007, 008, pool) or scrambled control (SC) (lower) (unpaired two-sided t-test).

Contrastingly, the knockdown of DGAT2 using both individual siRNA oligos and a pool of oligos targeting DGAT2 did not lead to a reduction in melanoma cell growth over a period of 72 h, or cause a reduction in phospho-S6 level, in A375 melanoma cells (Figure 4.8A). Furthermore, pharmacological antagonism of DGAT2 in our DGAT1^{High} melanoma cell line panel, did not reduce cell-cycle progression after a period of 24 h (Figure 4.8B), again, highlighting the specificity of DGAT1 in modulating melanoma cell growth and proliferation.

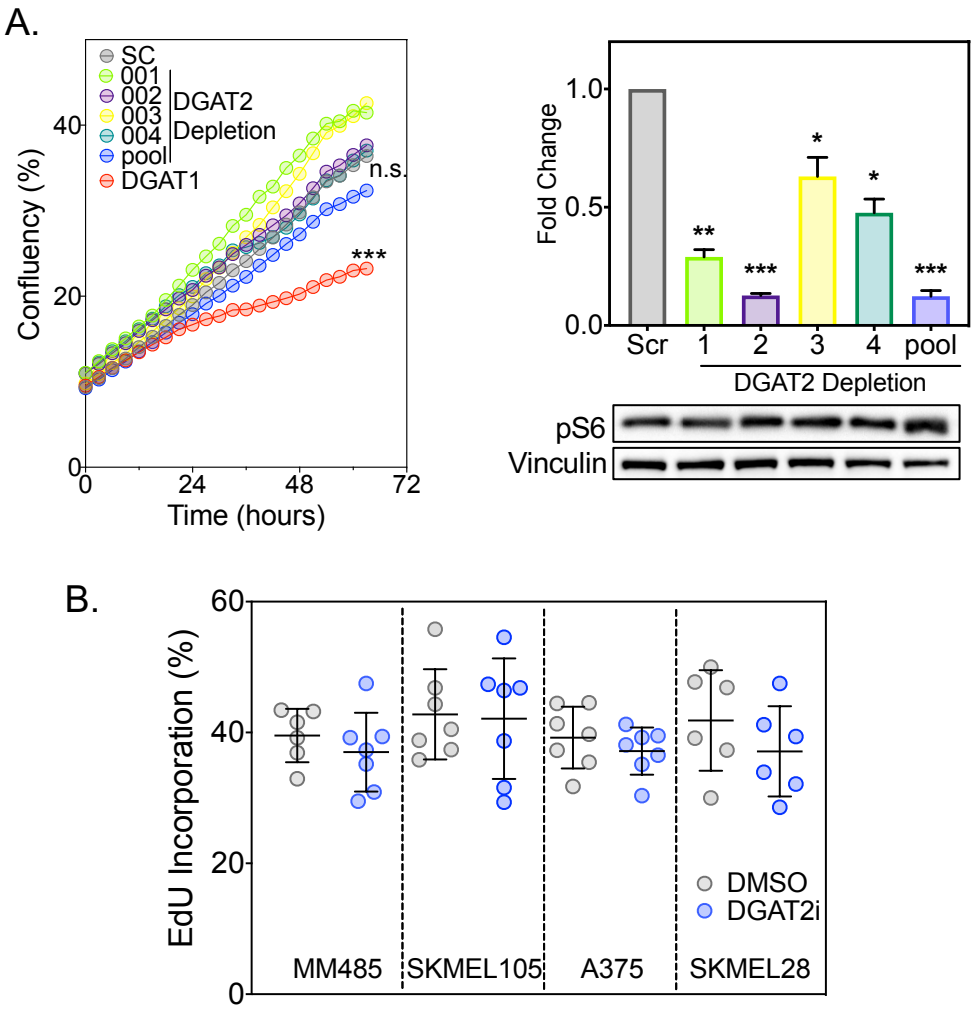

Figure 4.8 DGAT2 suppression does not impact upon melanoma cell proliferation

(A) Confluency curves of A375 cells transfected with indicated siRNAs targeting DGAT2 (001, 002, 003, 004, pool) or scrambled control (SC), determined by time-lapse microscopy using an incucyte zoom system (Mean, n=3) (left) (one-way Anova). RTqPCR analysis of the gene expression of DGAT2 in A375 cells cells transfected with indicated siRNAs targeting DGAT2 (001, 002, 003, 004, pool) or scrambled control (SC) (Mean, n=3) (right upper) (unpaired two-sided t-test).. Protein expression of phospsho-S6 in A375 cells cells transfected with indicated siRNAs targeting DGAT2 (001, 002, 003, 004, pool) or scrambled control (SC) (Mean, n=3) (right lower). (B) Quantification of the percentage of cells in S-phase using EdU incorporation in indicated cell lines following treatment with/without the DGAT2 inhibitor PF-06424439 for 24 h. (unpaired two-sided t-test).

We further investigated the impact of DGAT1 modulation on human melanoma cell growth by overexpressing DGAT1 using a lentiviral over-expression vector. We selected a human melanoma cell line that expressed lower levels of DGAT1 ($DGAT1^{Low}$) (888MEL) and following lentiviral overexpression of DGAT1 we carried out clonal selection to create four DGAT1 overexpressing clones. The DGAT1 over-expression clones displayed an increased growth rate and an increase in levels of phospho-S6, in DGAT-Clone 3 (DGAT-C3) this was matched with increased cell cycle progression, when compared to the 888MEL parental cell line (Figure 4.9A-B). In order to directly assess the link between DGAT1, S6K and melanoma cell growth and proliferation, we took the DGAT1 overexpressing clone 3 cells and the parental 888MEL cells and treated them with two different S6K inhibitors. Pharmacological antagonism of S6K in the DGAT-C3 cells significantly negated the increased proliferation rate observed due to over-expression of DGAT1, reducing the DGAT-C3 melanoma cells proliferation rate comparable to the 888MEL parental control (Figure 4.9C). Inhibition of S6K in the parental 888MEL did not significantly affect cell proliferation (Figure 4.9C). The inhibition of S6K activity was confirmed by the observation of reduced levels of phospho-S6 in both 888MEL and DGAT-C3 melanoma cells (Figure 4.9C). To further corroborate the link between DGAT1, S6K and melanoma cell growth, we overexpressed either HA-tagged constitutively active mutant $S6K^{454}$ or GFP in $DGAT1^{High}$ melanoma cells in which DGAT1 had been knocked down or inhibited. Over-expression of S6K partially rescued the growth, proliferation and phospho-S6 levels in the DGAT1 supressed melanoma cells. Together, we can conclude that DGAT1 promotes melanoma cell proliferation through stimulating S6K activity.

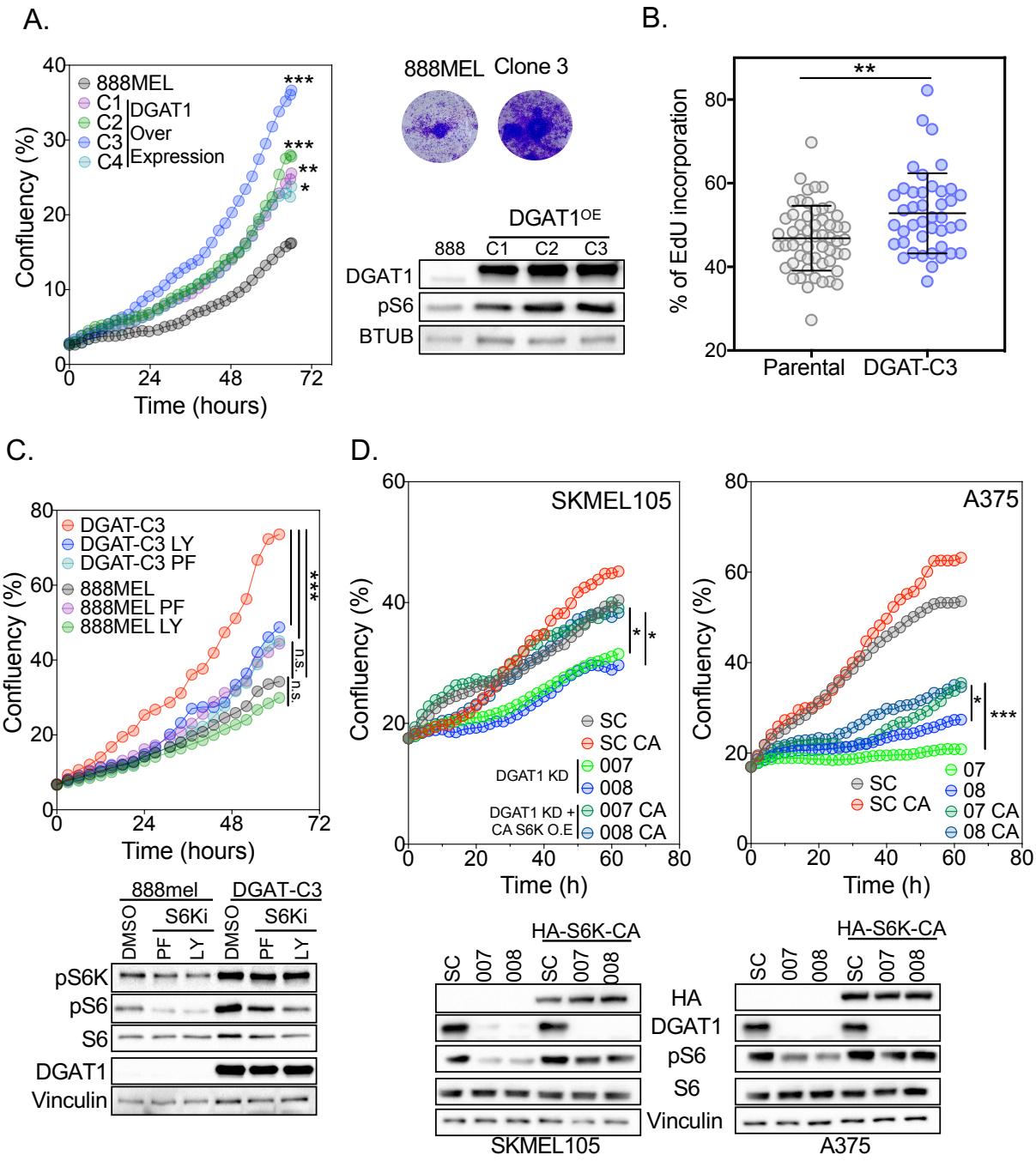
A.
888MEL
C1
C2
C3
C4
DGAT1 Over Expression
Confluency (%)
Time (hours)
888MEL Clone 3
DGAT1OE
888
C1
C2
C3
DGAT1
pS6
BTUB
B.
% of EdU incorporation
Parental
DGAT-C3
C.
DGAT-C3
DGAT-C3 LY
DGAT-C3 PF
888MEL
888MEL PF
888MEL LY
n.s.
Confluency (%)
Time (hours)
888mel
DGAT-C3
DMSO
S6Ki
PF
LY
pS6K
pS6
S6
DGAT1
Vinculin
D.
SKMEL105
A375
Confluency (%)
Time (h)
SC
SC CA
DGAT1 KD
007
008
DGAT1 KD + CA S6K O.E
007 CA
008 CA
HA-S6K-CA
HA
DGAT1
pS6
S6
Vinculin
SKMEL105
A375

Figure 4.9 DGAT1 modulation impacts melanoma cell proliferation in an S6K dependent manner

(A) Confluency curves of parental 888MEL cells and 888mel cells following lentiviral transduction with a DGAT1 over-expression vector and clonal selection, determined by time-lapse microscopy using an incucyte zoom system (Mean, n=3) (left) (one-way Anova). Crystal violet staining of parental 888MEL cells and DGAT1 over-expressing 888MEL cells (clone 3) after 72h growth (upper right). Protein expression of DGAT1 and phospho-S6 in parental 888MEL cells and DGAT1 over-expressing clones following lentiviral transduction with a DGAT1 over-expression vector (lower right). (B) Quantification of the percentage of 888MEL parental cells or Clone 3 DGAT1 over-expressing cells in S-phase following Edu incorporation (Mean ± SD, n>40) (unpaired two-sided t-test). (C) Confluency curves of 888MEL and clone 3 cells following treatment with/without 1uM LY2584702 or 10uM PF-4708671 determined by time-lapse microscopy using an incucyte zoom system (Mean ± SD, n=3) (one-way Anova) (upper). Protein expression of phospho-P70S6K, P70S6K, phospho-S6, S6, phospho-eEF2 and DGAT1 in indicated cell lines following treatment with/without 1uM LY2584702 or 10uM PF-4708671 for 72 h (lower). (D) Confluency curves of indicated cell lines following both over-expression of constitutively active (CA) S6 kinase or GFP and transfection with a DGAT1 targeting siRNA or scrambled control (SC), (Mean, n=3) (one-way Anova) (upper). Protein expression in indicated cell lines cells of HA-tag, DGAT1, phospho-S6 and S6 following both over expression of either GFP or constitutively active S6-kinase and transfection with a DGAT1 targeting siRNA (007,008) or scrambled control (SC) (lower).

Cancer cells are capable of sustaining cell growth despite transient or limited nutrient availability in the tumour microenvironment, arising from poor vascularization, thus we investigated the role of DGAT1 in allowing cancer cells to tolerate nutrient and oxygen deprivation in culture. First, we found that DGAT1 inhibition greatly impaired proliferation of $DGAT1^{High}$ melanoma cells when external lipid sources were restricted (Figure 4.10A). The greatest reduction in cell number post DGAT1 inhibition was observed at the lowest levels of serum (Figure 4.10A). Second, we explored the importance of DGAT1 under hypoxic conditions. Again, we found that DGAT1 inhibition had a profound effect on melanoma cell number under low oxygen conditions, which was further exacerbated by limiting serum (Figure 4.10B). The largest reduction in cell number after DGAT1 antagonism was observed at the lowest level of serum under hypoxic conditions (Figure 4.10B). Additionally, relative to growth of control cells, transient DGAT1 overexpression augmented melanoma cell growth to a greater extent under hypoxic conditions (Figure 4.10C). Taken together, up-regulation of DGAT1 confers a growth advantage to melanoma cells, which is even more profound under stress conditions likely to be encountered in the tumour microenvironment.

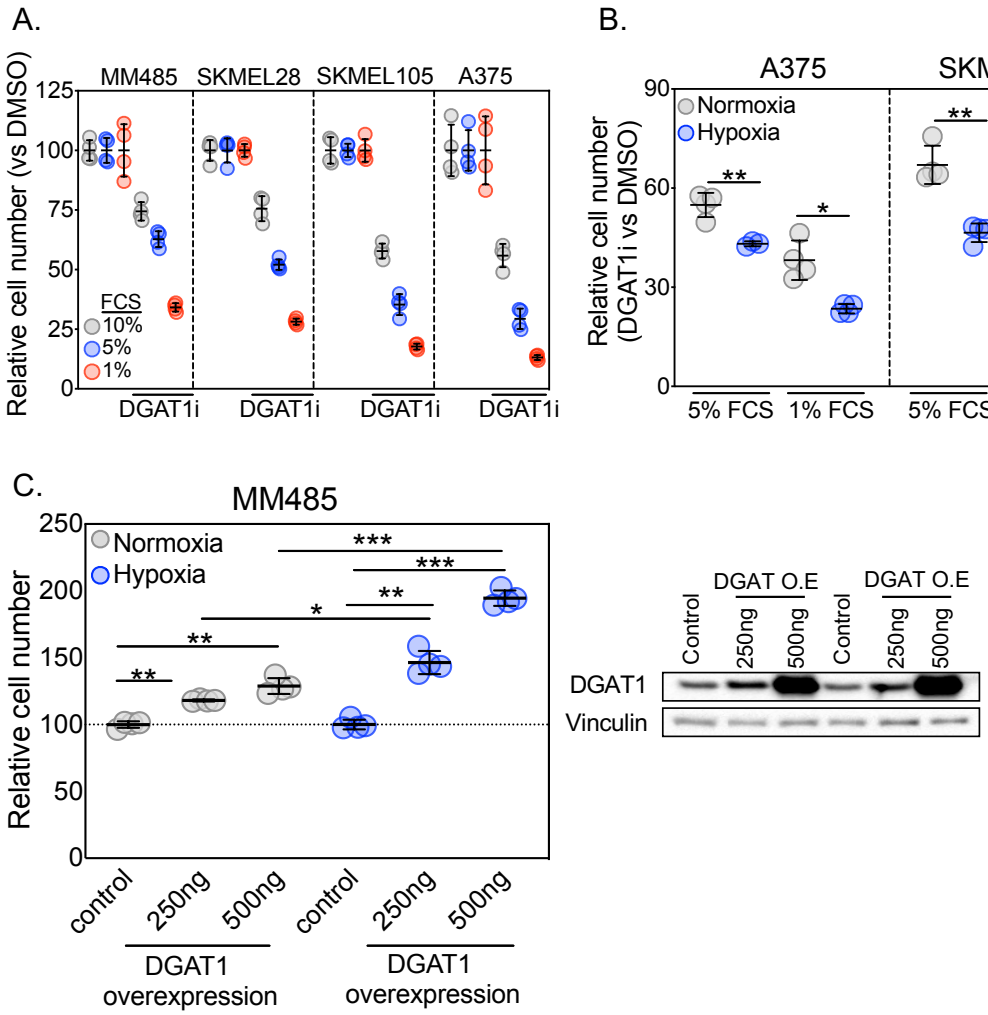

Figure 4.10 The impact of DGAT1 modulation on melanoma cell growth is enhanced under condition of stress

(A) Graph showing relative cell number determined by crystal violet following 72 h DGAT1 inhibitor treatment (A922500) of indicated cell lines grown in varying concentrations of foetal calf serum (FCS) (Mean, n>3). (B) Graph of relative cell number of indicated cell lines determined by crystal violet following 48 h DGAT1 inhibitor treatment (A922500) under normoxic or hypoxic conditions (1% O2) with cells grown in varying concentrations of foetal calf serum (FCS) (relative to DMSO control for each condition) (Mean, n>3) (unpaired two-sided t-test). (C) Relative cell number determined by crystal violet following transfection of MM485 cells with DGAT1 overexpression vector or an empty vector control under normoxic or hypoxic conditions for 48 h. (1 % O2) (upper) (Mean, n>3) (one-way Anova). Corresponding protein expression of DGAT1 (lower).

4.4 Discussion

In this part of the study, we investigated the impact of DGAT1 modulation on human melanoma cell line growth and proliferation and further elucidated the signalling networks modulated by DGAT1 in order to gain further insight into the mechanism underlying the oncogenic nature of DGAT1. DGAT1 has previously been mooted as a therapeutic target for the treatment of obesity and diabetes and as such, selective chemical inhibitors of DGAT1 have been developed[455–458]. The antagonism of DGAT1 using either the four selective chemical inhibitors or two individual siRNA oligos led to a decrease in DGAT1^{High} and DGAT1^{Amp} melanoma cell line growth and proliferation in both BRAF^{mut} and NRAS^{mut} backgrounds. The use of multiple cell lines and selective DGAT1 inhibitors increases the confidence that not only is DGAT1 highly important for melanoma cell growth but that the observed effect is specific to inhibition of DGAT1 and not due to off-target effects This is in agreement with DGAT1 modulation in zebrafish melanoma models accelerating both mutant NRAS and BRAF driven melanoma development. Moreover, the over-expression of DGAT1 in a DGAT1^{low} melanoma cell line increased cell growth and proliferation. The observation that the overexpression of DGAT1 increased the cellular proliferation and growth in four separate clones also points to the specificity of the effect. A rescue experiment could be performed to add evidence towards the specificity of the observed reduction in proliferation, in which alongside siRNA knockdown, an siRNA resistant form of DGAT1 could be transiently overexpressed to determine whether overexpression of DGAT1 is able to rescue the decrease in proliferation. Additionally, knockdown of DGAT1 in the DGAT1 over-expressing cells would provide further proof demonstrating that the observed increase in melanoma cell proliferation upon DGAT1 inhibition is a specific effect of DGAT1.

We also observed that under conditions of nutrient stress and hypoxia, the suppression of cell growth upon DGAT1 inhibition was enhanced and that the growth advantage conferred by DGAT1 overexpression in human melanoma cell lines was greatest under these conditions. Supporting these observations, LD have been shown

to be induced upon both nutrient stress and hypoxia, downstream of autophagy, highlighting their importance under conditions of cellular stress[294,295,299,300]. LD prevent lipotoxicity, provide efficient transfer of FA to the mitochondria for FAO and manage redox homeostasis, as such modulation of DGAT1 and thus LD would impact cell growth under conditions of cellular stress [295,298,300,304].

The observed decrease in melanoma cell proliferation upon DGAT1 antagonism, is in agreement with prostate cancer and glioblastoma cell line models, in which DGAT1 antagonism using shRNA, siRNA or small molecule inhibition led to a reduction in cellular proliferation and growth[340,341,391]. Furthermore, inhibition of the putative lipid metabolic oncogenes/drivers FASN (which catalyses the rate limiting step in FA synthesis), and FATP1 (the FA transporter) leads to a reduction in melanoma cell proliferation and growth in both *in vitro* and *in vivo* models[256–258,266], highlighting the importance of lipid metabolism in melanoma.

Intriguingly, the reduction in melanoma cell proliferation observed upon DGAT1 inhibition occurred after only 24h, therefore, in order to investigate the signalling changes occurring behind this halt in proliferation, we used a global and unbiased SILAC-based phospho-proteomic approach. We found phosphosites regulated by S6K to be enriched in the DGAT1^{High} human melanoma cell line A375 after 4h of DGAT1 inhibition. Protein hub analysis of the differentially phosphorylated proteins after 4h DGAT1 inhibition revealed mTOR, S6K and CDK1 as the key protein hub regulating signalling downstream of DGAT1. This is in agreement with the role of mTORC1 as a critical regulator of S6K[437,438]. This finding was confirmed in a panel of DGAT1^{High} and DGAT1^{Amp} melanoma cell lines, in which the altered phosphorylation of the downstream S6K targets S6 and eEF2 was observed using four different DGAT1 inhibitors. Alterations in S6K signalling downstream of DGAT1 modulation was also observed over longer time frames; knockdown of DGAT1 in DGAT1^{High} melanoma cell decreased levels of phospho-S6 whereas stable over-expression of DGAT1 in DGAT1^{Low} melanoma cells increased levels of phospho-S6, indicating a role for S6K in

melanoma cell growth and proliferation downstream of DGAT1. Alterations in mTOR signalling upon DGAT1 overexpression were also observed in the RNA-seq data in our zebrafish model of melanoma (Chapter 3), both highlighting mTOR as a key signalling node downstream of DGAT1 and demonstrating the ability of zebrafish to model aspects of human melanoma.

mTOR signalling is a key regulator of cell growth and proliferation and has been reported to have a significant impact on tumour progression across multiple cancer types including melanoma. Upregulation of downstream effectors such as S6K, 4E-BP1 and eIF4E has been observed in breast, ovarian , colon, prostate and renal cancers and is associated with worse patient outcome[459–463]. The ectopic overexpression of eIF4E is able to transform cells *in vivo*[464], an effect we observed with DGAT1 overexpression in our LoF P53 model of melanoma in zebrafish (Chapter 3). mTOR signalling is frequently activated in melanoma through alterations in upstream signalling pathways such as loss of the tumour suppressor PTEN[113,119], amplification of AKT[36,465], mutations in PIK3CA[129]. The most common mutations in melanoma $BRAF^{V600E}$ and $NRAS^{Q61R/L}$ can also activate mTOR signalling downstream of hyperactivated MAPK signalling[466,467]. As observed in other tumours types, mTOR signalling activation is associated with a worse patient outcome in melanoma[468]. Conversely, inhibition of either mTOR directly, or inhibition of S6K as single agents or in combination therapies has been shown to decrease melanoma cell growth[469–473], inhibition of mTOR has also shown to inhibit melanogenesis[474]. Taken together, it appears that the ability of DGAT1 to modulate mTOR signalling, with overexpression of DGAT1 leading to increased mTOR activation, may play a key role in the growth advantage conferred by DGAT1 in melanoma cells.

We were able to demonstrate that short term DGAT1 inhibition led to a decrease in signalling through the mTOR/S6K signalling axis, using phospho-proteomic analysis, and able to uncover in part how DGAT1 was able to modulate this rapid change in signalling upstream of mTOR. We found the mechanism behind the decrease in

mTOR/S6K signaling observed after short term DGAT1 inhibition is the phosphorylation and activation of AMPK, which can inhibit mTOR signalling through both Raptor[436] and TSC2[435] (Figure 4.1). The activation of AMPK has been observed post DGAT1 inhibition in prostate cancer, although this was after siRNA knockdown over a much longer time period[475]. Antagonism of DGAT1 has been shown to lead to mitochondrial oxidative stress in normal cells and cancer cells, oxidative stress leads to the activation of AMPK and could be reason for the decrease in mTOR signalling we observed after DGAT1 inhibition[295,476]. However, in the studies, the antagonism of DGAT1 was again for a much longer time period and the induction of oxidative stress after only 4h DGAT1 inhibition is perhaps unlikely. The reasons behind the energetic stress and activation of AMPK we observed upon short term DGAT1 inhibition require further investigation. Moreover, there are further mechanisms by which energetic stress induced by DGAT1 may lead to inhibition of mTOR in an AMPK independent manner such as disassociation of the TTT-RUVBL complex[477] or TCS2 regulation by REDD1, which also require further exploration. A further possible mechanism leading to the inhibition of mTOR signalling is the induction of ER stress due to DGAT1 inhibition. DGAT1 is resident in the ER and it is here where lipid droplets are formed. Inhibition of DGAT1 may lead to an accumulation of toxic FA leading to ER stress, a phenomena that has been observed upon inhibition of both DGAT1 and DGAT2 in adipocytes[288]. A toxic build-up of FA in the ER could lead to an alteration in ER membrane lipids which has been shown to directly activate the unfolded-protein response (UPR)[478], which can lead to mTOR inhibition[479,480]. Changes in the levels of key signalling lipid species may also be driving the decrease in mTOR signalling post DGAT1 inhibition, given the role of DGAT1 in TAG synthesis. However, an increase in the levels of both DAG and PA would be expected after DGAT1 inhibition and both of these lipid species are known activators of mTOR signalling through activating PKC[481], and binding directly to the FKBP12-rapamycin-binding domain of mTOR respectively[482]. As such, the potential signalling lipid species that may cause inhibition of mTOR signalling downstream of DGAT1 are not clear.

Demonstrating the key role of S6K in DGAT1 modulated melanoma cell growth, inhibition of S6K in melanoma cells stably over-expressing DGAT1 reduced cell growth to levels observed in the parental $DGAT1^{Low}$ cells. Additionally, over-expression S6K partially rescued cell growth following DGAT1 depletion. However, this was only a partial rescue and highlights that, further to modulating S6K signalling, increased DGAT1 expression may play other tumour promoting roles in melanoma such as preventing lipotoxicity, maintaining redox homeostasis, and aiding in efficient FAO[81,298,300,476]. Highlighting which of these roles increased expression of DGAT1 plays in melanoma will be the focus of the next chapters in this study.

In conclusion, taken together this data demonstrates that DGAT1 is able to promote melanoma cell growth and proliferation through driving increased signalling through the mTOR/S6K signalling axis. The growth advantage conferred by increased DGAT1 expression is greatest under conditions likely to be found in the tumour microenvironment such as hypoxia and nutrient stress.

Chapter 5 – DGAT1 is essential for lipid droplet formation and acts as a caretaker of mitochondrial health

5.1 Introduction

The reprogramming of cellular metabolism and specifically lipid metabolism is now beginning to be appreciated as a critical aspect of cellular transformation and tumour progression. As we have identified DGAT1 as a bone fide lipid metabolic melanoma oncogene driving melanoma initiation and progression, in part through driving mTOR/S6K signalling, we wanted to further investigate its direct role in lipid metabolism in melanoma cells.

DGAT1 catalyses the final committing step in TAG synthesis and thus LD formation, we hypothesised that DGAT1 driven LD formation may play a significant role in the pro-tumorigenic effects of DGAT1. Altered FA storage in the form of LD is a key hallmark in the altered lipid metabolic phenotype of cancer cells; in melanoma increased LD are associated with both overall survival and metastatic survival and correlate with stemness[320–322]. The tumour promoting roles of LD have been demonstrated across a number of cancer types and impact upon numerous cancer hallmarks[275]. A crucial role of LD in cancer cells is managing stress such as nutrient stress, hypoxia, oxidative stress and lipotoxic stress[294–296,299,300,305]. LD balance lipid homeostasis through storing free fatty acids (FFA), DAGs, CEs and ceramides into neutral lipids, thus preventing a build-up of toxic FA upon increased lipid uptake, under hypoxic conditions or the release of FA through increased autophagy upon nutrient stress[283–285,300]. LD are able to manage redox homeostasis, preventing the build-up of ROS and selectively sequester PUFA, which are highly vulnerable to peroxidation and amplify ROS[290,305,483]. LD also act as specialised sites for the

synthesis of eicosanoid lipid species; in melanoma the eicosanoids play a key role both promoting cellar proliferation and in immune evasion[312,313,315].

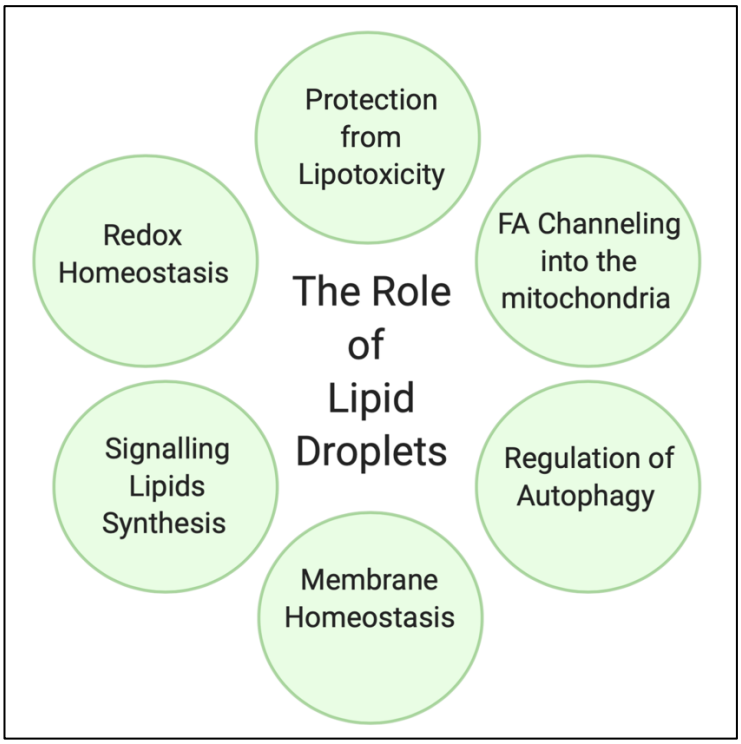

Figure 5.1 The Role of Lipid Droplets

Lipid droplets play multiple protective role in cancer cells under stress. Figure made in Biorender.

LD are found associated with a number of other organelles such as the ER, lysosomes, the nucleus and, perhaps the most important for regulation of cellular energetics, the mitochondria. The relationship between LD and mitochondria is a complex one, it appears that the transfer of FA can occur in both directions, channelling from LD to the mitochondria for FAO, and from the mitochondria to LD supporting LD expansion[484]. This flux of FA between mitochondria and LD is determined by cellular conditions. The channelling of FA into the mitochondria has been shown to be crucial for cells under starvation conditions, in which FA are channelled into the mitochondria to fuel FAO and enable cell survival[298]. This was perhaps most elegantly demonstrated in mouse embryonic fibroblasts, which under starvation conditions

channelled FA, liberated from LD by the cytosolic lipase ATGL, into the mitochondria in a carnitine palmitoyltransferase-1A (CPT-1A) dependent manner[298]. Additionally, the efficient transfer of liberated FA into the mitochondria is dependent on a the close proximity of tubulated mitochondria and LD[298], with the relocation of LD facilitating mitochondrial-LD interactions dependent on activation of the energy sensor AMPK[297]. This critical link between LD and mitochondria to efficiently transfer FA to the mitochondria for FAO has also been demonstrated in cancer cells under both nutrient stress and upon reoxygenation after hypoxia[290,296,301]. Although seemingly antagonistic to the role of FAO by mitochondria, studies in adipose tissue and cells have also demonstrated that recruitment of mitochondria to LD, in a Perilipin5 (PLIN5) dependent manner, led to an increase in LD mass[484,485]. The mechanism by which mitochondria support LD mass is thought to be through providing ATP for TAG synthesis[484,485]. As LD have been demonstrated to play a key role in multiple cancer hallmarks and cellular energetics, investigating whether DGAT1 is critical for LD biogenesis would provide further clues into the mechanisms by which DGAT1 acts as a melanoma oncogene.

Despite being composed of common building blocks such as FA and cholesterol, it is estimated that the number of molecular lipid species is between 10,000 to 1 million[486,487], the LIPID MAPS database currently has annotated 43,000 biologically relevant lipids[488]. In agreement with their vast diversity, different lipid species are known to be involved in numerous cellular functions, underpinned by their biophysical properties. Increased membrane synthesis is critical for highly proliferative cancer cells, the major structural lipids are the glycerophospholipids: phosphatidylcholine (PC), phosphatidylethanolamine (PE), phosphatidylserine (PS) and phosphatidylinositol (PI). Membrane fluidity is determined by two further classes of lipids: cholesterol and sphingolipids. In addition to their role in biological membranes, hydrolysis of glycerophospholipids and sphingolipids produces an array of signalling lipids. The sphingolipid ceramide plays a key role in the regulation of apoptosis, ceramide can cause the downregulation of FLICE inhibitory protein which is an known inhibitor of caspase 8[489,490]. Ceramide is also able to modulate apoptosis

through downregulation of another apoptosis inhibitor Survivin[491,492], induction of mitochondrial outer membrane permeabilization[493,494] and regulation of TRAIL and CD95 clustering[495,496]. As well as its role in apoptosis, ceramides also regulate cell cycle, increased ceramide leads to an increase in the CDK inhibitor p21 causing a G1 arrest[497,498]. Another sphingolipid, sphingosine-1-phosphate (S1P), is also a potent pleiotropic lipid mediator which is exported and acts on a number of cellular processes through its receptors (S1PR1-5)[499]. Each of the five S1PR receptors play specific roles. SP1R1 is able to activate numerous signalling pathways such as the MAPK pathway , the PI3K pathway, RAC signalling and STAT3 signalling[499,500]. As such S1P- S1PR1 signalling is able to promote cell growth and survival , cell motility and invasion, angiogenesis and immune cell trafficking[500–502]. S1PR3 activation has been shown to promote tumorigenesis and reduce survival in breast cancer patients[503]. PI also play a role in PI3K signalling, upon activation by cell surface receptors, PI3K catalyses the formation of phosphatidylinositol-3,4,5-trisphosphate ($PI(3,4,5)P_3$), another pleiotropic lipid mediator which is capable of activating a number of proteins involved in a broad range of cellular functions[504]. $PI(3,4,5)P_3$ is able to modulate the activity of over 40 proteins through their pleckstrin homology (PH) domains, causing membrane localisation. Perhaps the most well-known target of $PI(3,4,5)P_3$ is Akt and it is through Akt that it controls cell growth, survival, motility and apoptosis[504–507]. Hydrolysis of PC by endothelial lipases leads to the production of Lysophosphatidylcholine (LPC), which like S1P signals through G-protein coupled receptors[508,509]. LPC activates a plethora of signalling pathways involved predominantly in the inflammatory response, increasing the release of proinflammatory cytokines such as interleukin-1 beta (IL-1β), IL-6, tumour necrosis factor alpha (TNF-α) and interferon gamma (IFNγ) from both immune cells and adipocytes[510,511]. LPC is also involved in stabilising the polarisation of macrophages to the pro-inflammatory M1 phenotype[512].

Focusing on DGAT1 related pathways, almost all the major intermediates of TAG synthesis and breakdown are biologically active signalling lipids. DAG are key regulators of protein kinase C (PKC) and activate PKC in conjunction with PS and

calcium ions[513]. Analysis of different DAG species has also highlighted that polyunsaturated species are better activators of PKC than monounsaturated species[514]. DAG accumulation has been linked with insulin resistance, this is thought to be through the activation of PKC and subsequent phosphorylation and inhibition of the insulin receptor[515–518]. MAG has also been shown to play a role in insulin signalling, stimulating insulin secretion in pancreatic beta cells though activation of Mammalian Unc13-1[519]. MAG can also directly regulate lipid metabolism through binding and activating the transcription factors PPARα and γ[520]. The most widely studied lipid intermediate of TAG synthesis involved in cell signalling is lysophosphatidic acid (LPA), especially in the context of cancer cell signalling. LPA, through binding to well-characterised receptors (LPAR1-3), regulates cancer cell proliferation, invasion and metastasis[521]. The regulation of cancer cell invasion and metastasis is thought to be through multiple mechanisms including, activating the expression of matrix metalloproteinases[522,523], activation of Rac1 signalling modulating cytoskeletal rearrangements[524] and through modulation of focal adhesion formation[525].

It is not just different lipid species that can impact on cell signalling and metabolism but also alterations in FA saturation can dramatically alter the biological properties of lipids and, as such, their impact on cell signalling and metabolism and critically its impact in cancer cells. Studies have demonstrated that the increase in *de novo* lipid synthesis observed in cancer cells leads to an increase FA saturation in membrane lipids, which may have a role in protecting cancer cells from oxidative stress as saturated FA are less susceptible to peroxidation[526]. Lipidomic analysis of human breast tissue revealed that increased levels of saturation in membrane lipids was associated with cancer progression and worse patient survival[527]. Despite this, accumulation of saturated FA species (SFA) has been shown to be toxic in non-adipose tissue[528,529]. The key enzyme in modulating lipid desaturation is Stearoyl-CoA desaturase (SCD), catalysing the formation of mono-unsaturated FA. Inhibition of SCD in cancer cells leads to ER stress, cell cycle inhibition and cell death, underlining the importance of regulating the levels of SFA[530–533]. Cancer cells can also

overcome SFA induced toxicity by increasing the uptake of unsaturated FA, this becomes particularly important during hypoxia which constrains the activity of SCD[303,534]. However, increased levels of PUFA can led to cells becoming more susceptible to oxidative stress as PUFA are highly prone to peroxidation which can lead to cell death[305,306,535]. Studies in breast cancer revealed than one mechanism by which cancer cells shield PUFA from oxidative stress is through sequestering them in LD[290], a phenomena also observed in drosophila[483].

All of this together points to the importance of lipid signalling in modulating a number of cancer hallmarks such as proliferation, resistance to cell death, metastasis, angiogenesis and altered cellular metabolism. As such, the global profiling of changes in the levels of lipid species using ultra/high performance liquid chromatography upon DGAT1 modulation will shed light into why DGAT1 amplification and up-regulation is beneficial for melanoma cells and provide further clues into the role of DGAT1 in melanoma metabolism and it role as a lipid metabolic oncogene.

5.2 Aims

- To identify whether DGAT1 is essential in LD formation in melanoma cells.

- Investigate the impact of DGAT1 modulation on the global cellular lipidome using ultra/high performance liquid chromatography.

- Analyse global lipid changes to assess the impact of DGAT1 modulation upon melanoma cell lipid metabolism.

5.3 Results

As DGAT1 catalyses the final and committing step in in TAG synthesis, which can be assembled to form LD, we assessed the role of DGAT1 in LD formation in melanoma cells. A time course from 2-72 h in four DGAT1^{High} melanoma cell lines revealed that inhibition of DGAT1 led to a decrease in observed LD beginning between 12-24 h and continuing up until 72 h, as determined by staining with the neutral lipid dye BODIPY™ 493/503 (Figure 5.2 A-D). Different basal levels of LD were observed in the four cell lines, with A375 cell having the highest number of LD per cell (Figure 5.2 A-D); however, the time frame for the observed reduction in LD numbers post DGAT1 inhibition was the same.

A.

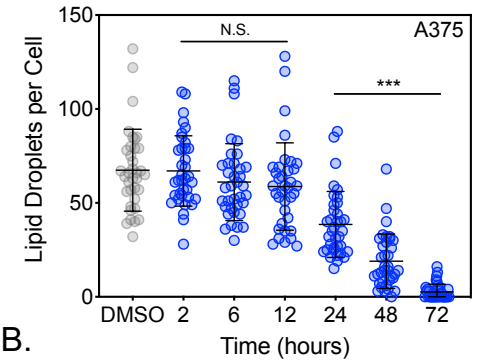
A375
N.S.
***
Lipid Droplets per Cell
150
100
50
0
DMSO 2 6 12 24 48 72
Time (hours)

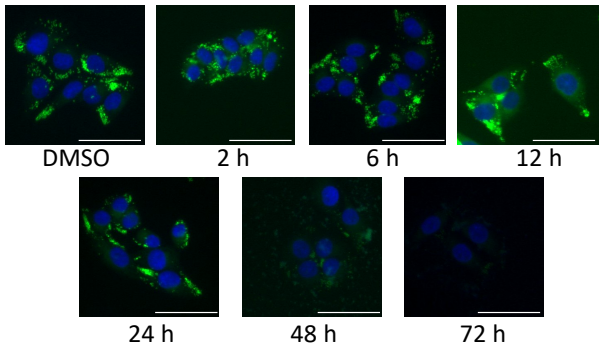
DMSO
2 h
6 h
12 h
24 h
48 h
72 h

B.

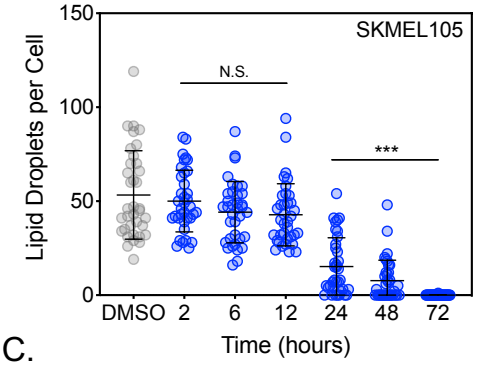
SKMEL105
N.S.
***
Lipid Droplets per Cell
150
100
50
0
DMSO 2 6 12 24 48 72
Time (hours)

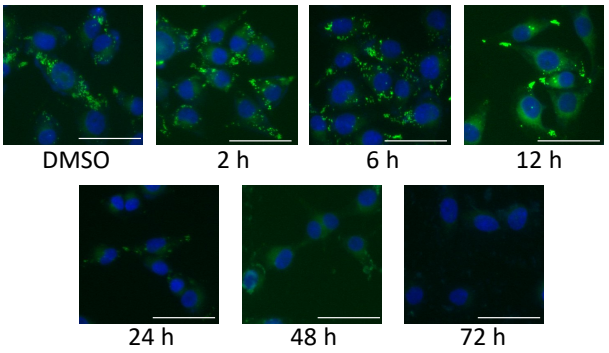
DMSO
2 h
6 h
12 h
24 h
48 h
72 h

C.

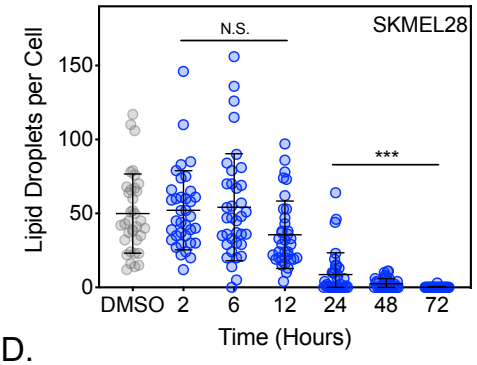
SKMEL28
N.S.
***
Lipid Droplets per Cell
150
100
50
0
DMSO 2 6 12 24 48 72
Time (Hours)

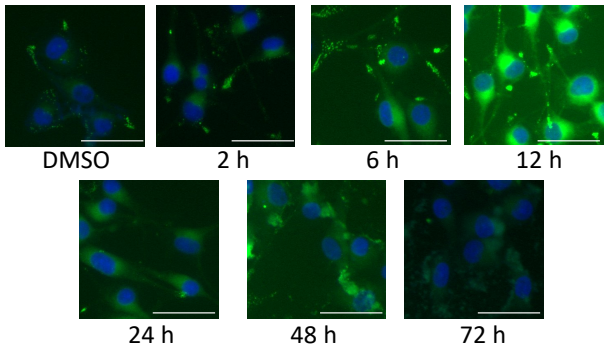
DMSO
2 h
6 h
12 h
24 h
48 h
72 h

D.

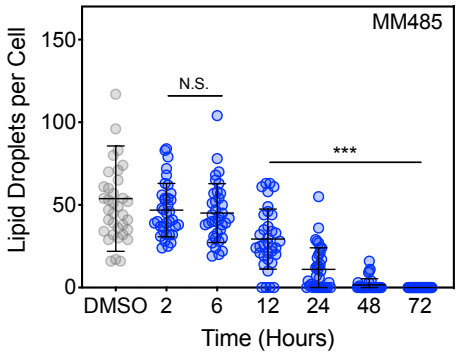
MM485
N.S.
***
Lipid Droplets per Cell
150
100
50
0
DMSO 2 6 12 24 48 72
Time (Hours)

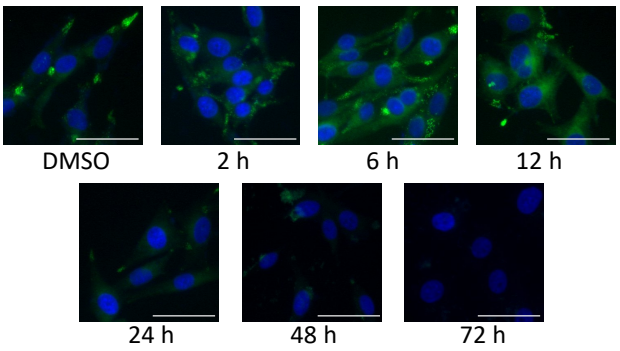
DMSO
2 h
6 h
12 h
24 h
48 h
72 h

Figure 5.2 DGAT1 is essential for lipid droplets in melanoma cells.

(A-D) Quantification of the number of lipid droplets per cell following BODIPY staining. Indicated cell lines were treated with/without AZD3988 for 2-72 h (Mean ± SD, n>30) (one-way Anova) (Left). Representative images of lipid droplets following BODIPY staining in indicated cell lines treated with/without AZD3988 for 2-72 h (scale bar 50 µm) (right).

Knockdown of DGAT1 using both a pool and two individual DGAT1 targeting oligos also led to a decrease in the number of LD per cell in A375 and SKMEL105 DGAT1^{High} melanoma cell after a period of 72 h (Figure 5.3 A-B). Staining with a second neutral lipid dye, HCS LipidTOX™, also confirmed a decrease in the number of LD per cell after inhibition of DGAT1 for 24 h (Figure 5.3 C). Knockdown of DGAT2 with a pool or individual DGAT2 targeting oligos did not lead to a decrease in the number of lipid droplets per cell in A375 melanoma cells after 72 h, as determined by BODIPY™ 493/503 staining. This demonstrates the importance of DGAT1, but not DGAT2, in the formation and maintenance of LD in human melanoma cell lines.

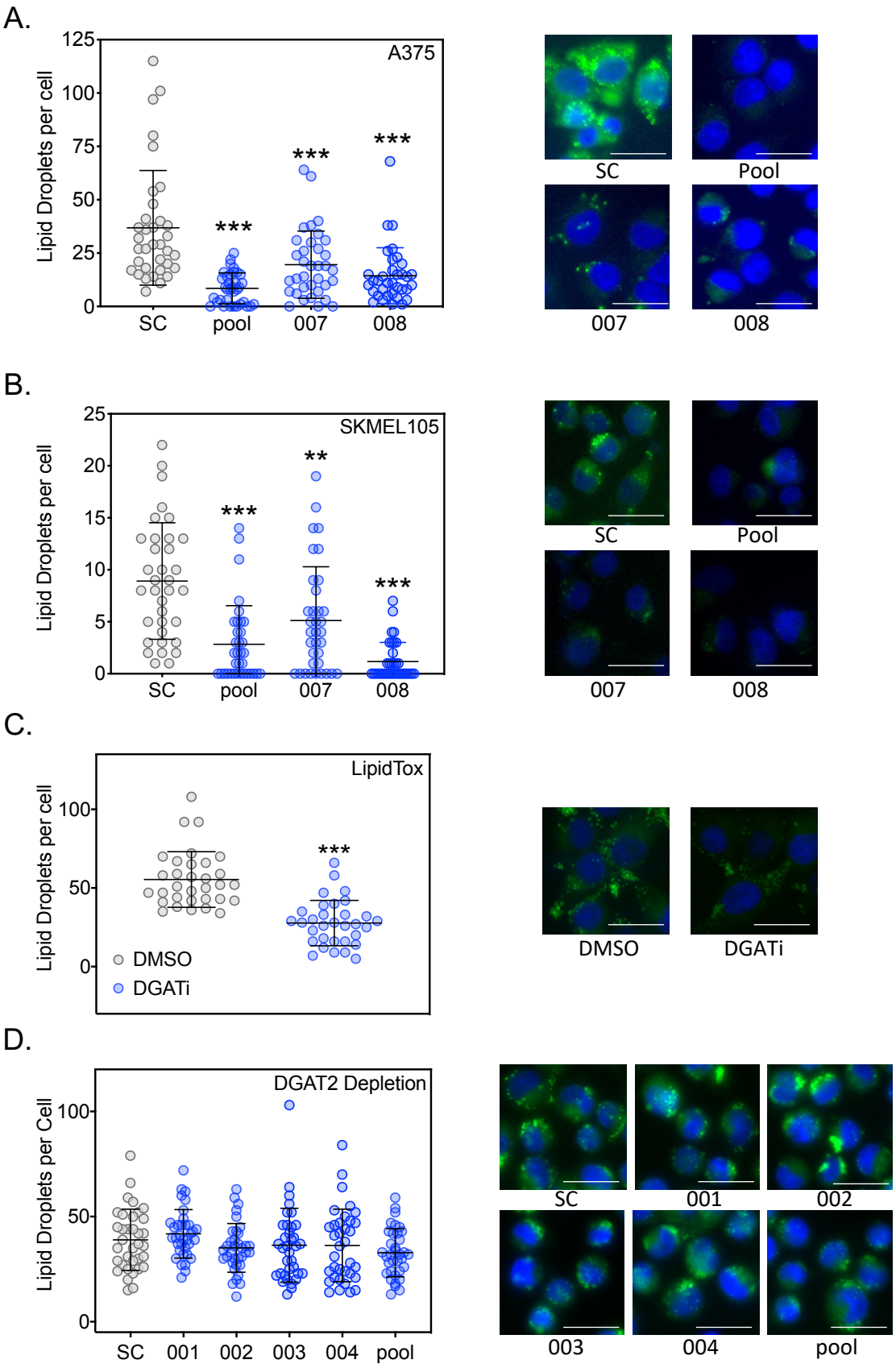
A.
A375
Lipid Droplets per cell
125
100
75
50
25
0
***
***
***
SC
pool
007
008
SC
Pool
007
008
B.
SKMEL105
Lipid Droplets per cell
25
20
15
10
5
0
***
**
***
SC
pool
007
008
SC
Pool
007
008
C.
LipidTox
Lipid Droplets per cell
100
50
0
***
DMSO
DGATi
DMSO
DGATi
D.
DGAT2 Depletion
Lipid Droplets per Cell
100
50
0
SC
001
002
003
004
pool
SC
001
002
003
004
pool

Figure 5.3 DGAT1 but not DGAT2 is essential for lipid droplets in melanoma cells.
(A) Quantification of the number of lipid droplets per cell following BODIPY staining. A375 were transfected with either individual or a pool of DGAT1 targeting oligos (007,008, pool) or a scrambled control (SC) for 48 h (Mean ± SD, n>30) (one-way Anova) (Left). Representative images of lipid droplets following BODIPY staining in A375 cells transfected with either individual or a pool of DGAT1 targeting oligos (007,008, pool) or a scrambled control (SC) for 48 h (scale bar 50 μm) (right). (B) as for (A) but SKMEL105 cells. (C) Quantification of the number of lipid droplets per cell following LIPIDTOX staining. A375 cells were treated with/without A922500 for 24 h (Mean ± SD, n>30) (t-test) (Left). Representative images of lipid droplets following BODIPY staining in indicated cell lines treated with/without A922500 for 24 h (scale bar 50 μm) (right). (D) Quantification of the number of lipid droplets per cell following BODIPY staining. A375 were transfected with either individual or a pool of DGAT2 targeting oligos (001,002,003,004, pool) or a scrambled control (SC) for 48 h (Mean ± SD, n>30) (one-way Anova) (Left). Representative images of lipid droplets following BODIPY staining in A375 cells transfected with either individual or a pool of DGAT2 targeting oligos (001,002,003,004, pool) or a scrambled control (SC) for 48 h(scale bar 50 μm) (right).

The capacity of DGAT1 to store DAG and FA in LD has potential implications in both cell growth signalling and ATP production, as DAG, FA and their derivatives are both fuel molecules and allosteric regulators of metabolic enzymes and kinases. Therefore, we addressed the direct effects of DGAT1 on melanoma lipid metabolism using an unbiased approach, performing Ultra-High- Performance Liquid Chromatography-Mass-Spectrometry (UHPLC-MS) to identify and contrast lipid species. We selected two DGAT1^{High} melanoma cell lines and chose two time points (24 & 72 h) based on when we observed changes in LD number (Figure 5.2 A-B), as we believed this would allow for the greatest insight into lipid metabolic changes downstream of DGAT1. As anticipated, in the SKMEL105 cells we observed a significant reduction of multiple TAG species at both 24 and 72 h, with the greatest reduction observed at 72 h (Figure 5.4 A-C). We also observed significant increase in a number of different lipid species, including Lysophosphatidylcholines (LPC) and Lysophosphatidylethanolamine (LPE), both key components of biological membranes and important lipid signalling molecules (Figure 5.4 A-C). The most striking change upon DGAT1 inhibition was the observed increase in several acyl carnitine (AcCa) species, key determinants of the rate of FAO (Figure 5.3 A-C). Some similar observations were made upon DGAT1 inhibition in A375 melanoma cells, the largest increases were observed in several AcCa species and increases in multiple LPC species detected (Figure 5.4 D-F). Surprisingly, despite the observed decrease in the number of LD we did not observe a decrease in TAG species in the A375 melanoma cells upon either 24 or 72 h DGAT1 inhibition, this may be due to compensation from other enzymes able to carry out the same reaction, such as DGAT2 (Figure 5.4 D-F).

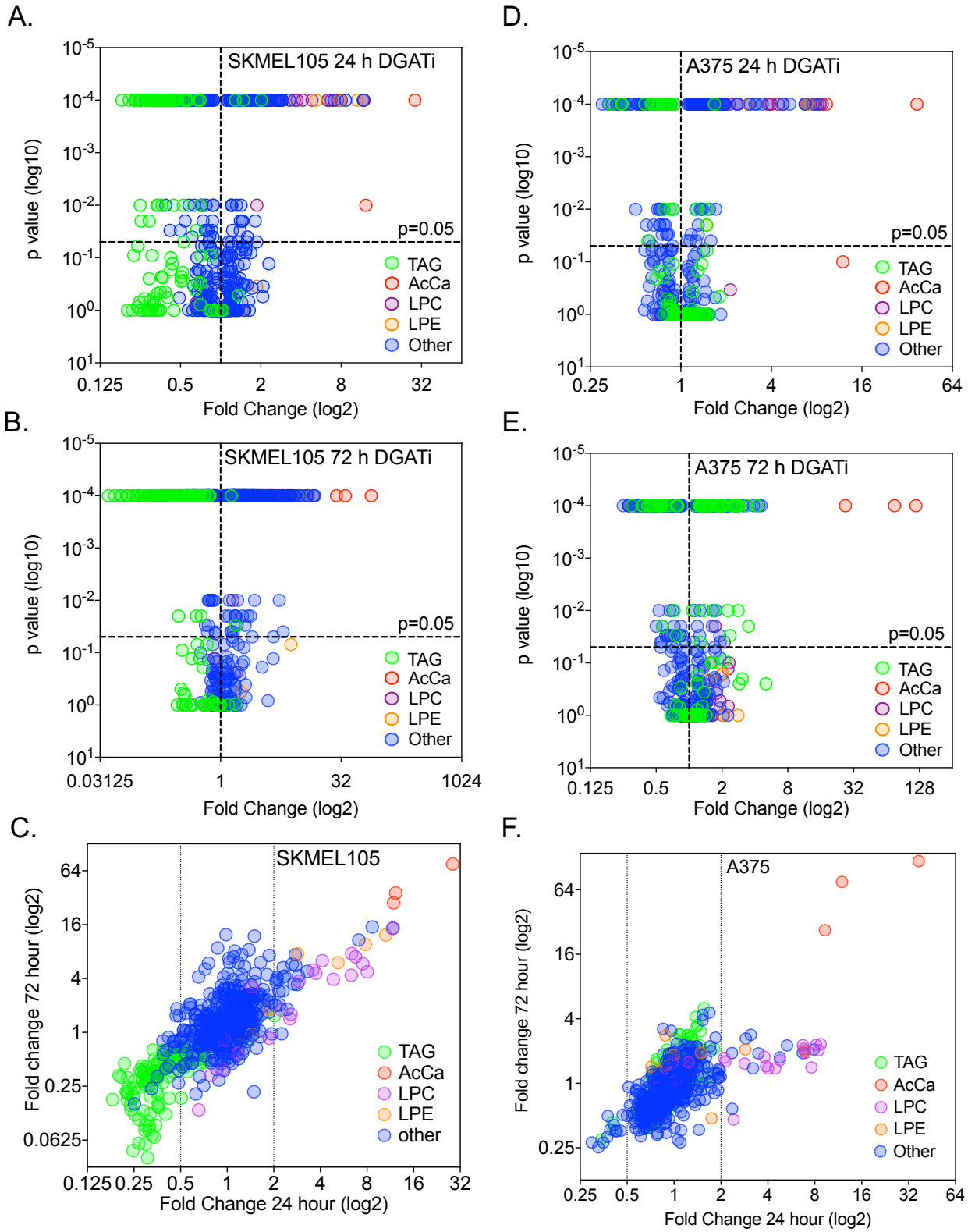
A.
SKMEL105 24 h DGATi
p value (log10)
Fold Change (log2)
p=0.05
TAG
AcCa
LPC
LPE
Other
B.
SKMEL105 72 h DGATi
C.
SKMEL105
Fold change 72 hour (log2)
Fold Change 24 hour (log2)
other
D.
A375 24 h DGATi
E.
A375 72 h DGATi
F.
A375

Figure 5.4 DGAT1 inhibition increases levels of acyl carnitines in melanoma cells

(A) UHPLC-lipidomic analysis of SKMEL105 cells following treatment with/without A922500 for 24 h (showing lipid species that were annotated using MS/MS). Fold-change calculated relative to DMSO treated control and plotted against adjusted *p*-value (t-test, Turkey's HDR, Benjamini-Hochburg). TAG (triacyclglycerides), LPC (lysophosphatidycholine), AcCa (acyl carnitine), LPE (lysophosphatidylethanolamine). (B) as for (A) but treatment with/without A922500 for 72 h. (C) as for (A) and (B) but fold-change at 24 h plotted v fold-change at 72 h. (D) as for (A) but in A375 cells. (E) as for (B) but in A375 cells. (F) as for (C) but in A375 cells.

We also investigated both LD formation and lipid metabolic changes using UHPLC-MS in the DGAT1 over-expressing cells we created (clone 3), comparing them to the DGAT1^{Low} parental cells (888MEL). Using BODIPY to stain LD, we observed a dramatic increase in the number of LD upon stable DGAT1 overexpression in the clone 3 cells when compared to the parental control cells (Figure 5.5 A). The UHPLC-MS revealed significant increases in multiple TAG species upon DGAT1 over-expression (Figure 5.5 A), in contrast to the decrease in multiple TAG species observed upon DGAT1 inhibition in the SKMEL105 cells (Figure 5.3 A-C). Again, contrasting the observed lipid species changes upon DGAT1 inhibition, overexpression of DGAT1 led to a profound increase in TAG species accompanied by a decrease in multiple AcCa species (Figure 5.5 A). Additionally, we carried out UHPLC-MS on the tumours generated in our *in vivo* zebrafish models of melanoma, contrasting lipid species extracted from NRAS^{mut} Dgat1a over-expressing or NRAS^{mut} EGFP-expressing zebrafish tumors. As detected in our DGAT1 overexpressing human melanoma cell line model, this analysis revealed increases in multiple TAG species and decreases in multiple AcCa species upon Dgat1a overexpression (Figure 5.5 B). However, after correcting the analysis for multiple testing the changes were not statistically significant, despite the clear trend. This lack of statistical significance does not mean that DGAT1 does not play a key role in TAG synthesis and thus LD formation in these tumours, as there are several experimental limitations when carrying out UHPLC_MS on complex whole tumour samples that may be behind the lack of statistical significance. First, EGFP-expressing tumors also express high levels of Dgat1a and have numerous LD. Second, whole tumour analysis also means that lipids originating from associated stromal cells will be included with lipids derived from tumour cells in analysis. Both issues mean that lipidome differences between Dgat1-over-expressing and EGFP-expressing tumors are likely to be reduced in magnitude.

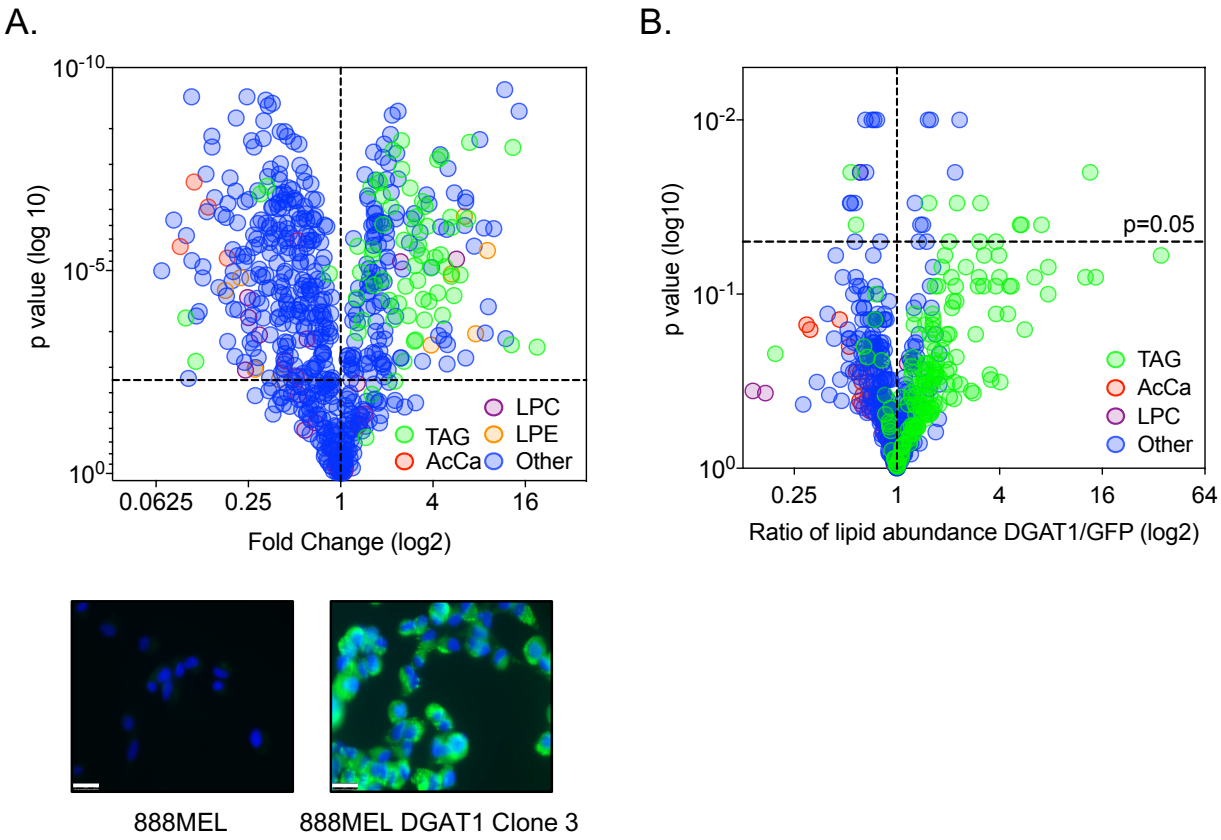

Figure 5.5 DGAT1 over-expression decreases levels of acyl carnitines in melanoma cells

(A) UHPLC-lipidomic analysis of 888MEL parental and Clone 3 DGAT1 over-expressing cells (showing lipid species that were annotated using MS/MS). Fold-change is calculated relative to the 888MEL parental cells. (upper) (t-test, Turkey's HDR, Benjamini-Hochburg). Representative images of 888MEL and Clone 3 cells stained with BODIPY (scale bar 50 µm)(Lower). (B) Lipidomic profiling using UHPLC-MS of $NRAS^{G12D}$-positive EGFP-expressing (n=6) and NRASG12D-positive Dgat1a-over-expressing (n=6) tumors showing the ratio of lipid species (annotated by MS/MS) and plotted against *p*-value (t-test, Turkey's HDR, Benjamini-Hochburg). TAG (triacyclglycerides), LPC (lysophosphatidycholine), AcCa (acyl carnitine).

Combining the DGAT1 inhibition and DGAT1 overexpression lipidomic data highlighted the lipid species with the largest changes upon DGAT1 modulation and provided clarity on whether lipid species were negatively or positively regulated by DGAT1. Comparing the fold changes of lipid species after 72 h DGAT1 inhibition and DGAT1 overexpression demonstrated that AcCa species were the most altered lipid species negatively regulated by DGAT1. Whereas as anticipated, multiple TAG species were found to have the largest fold changes of lipid species positively regulated by DGAT1 (Figure 5.6 A). Looking specifically at alterations in TAG species in both the 72 h DGAT1 inhibitor treated SKMEL105 cells and the $NRAS^{mut}$ Dgat1a overexpressing tumours highlighted a possible substrate specificity of DGAT1 (Figure 5.6 B-C). The largest fold changes upon DGAT1 modulation were found in TAG species with longer poly-unsaturated FA (PUFA) chains (Figure 5.6 B-C), this has possible implications for lipid toxicity as PUFA are particularly sensitive to oxygen-centred radicals which leads to the generation of toxic lipid peroxides[305,306,535].

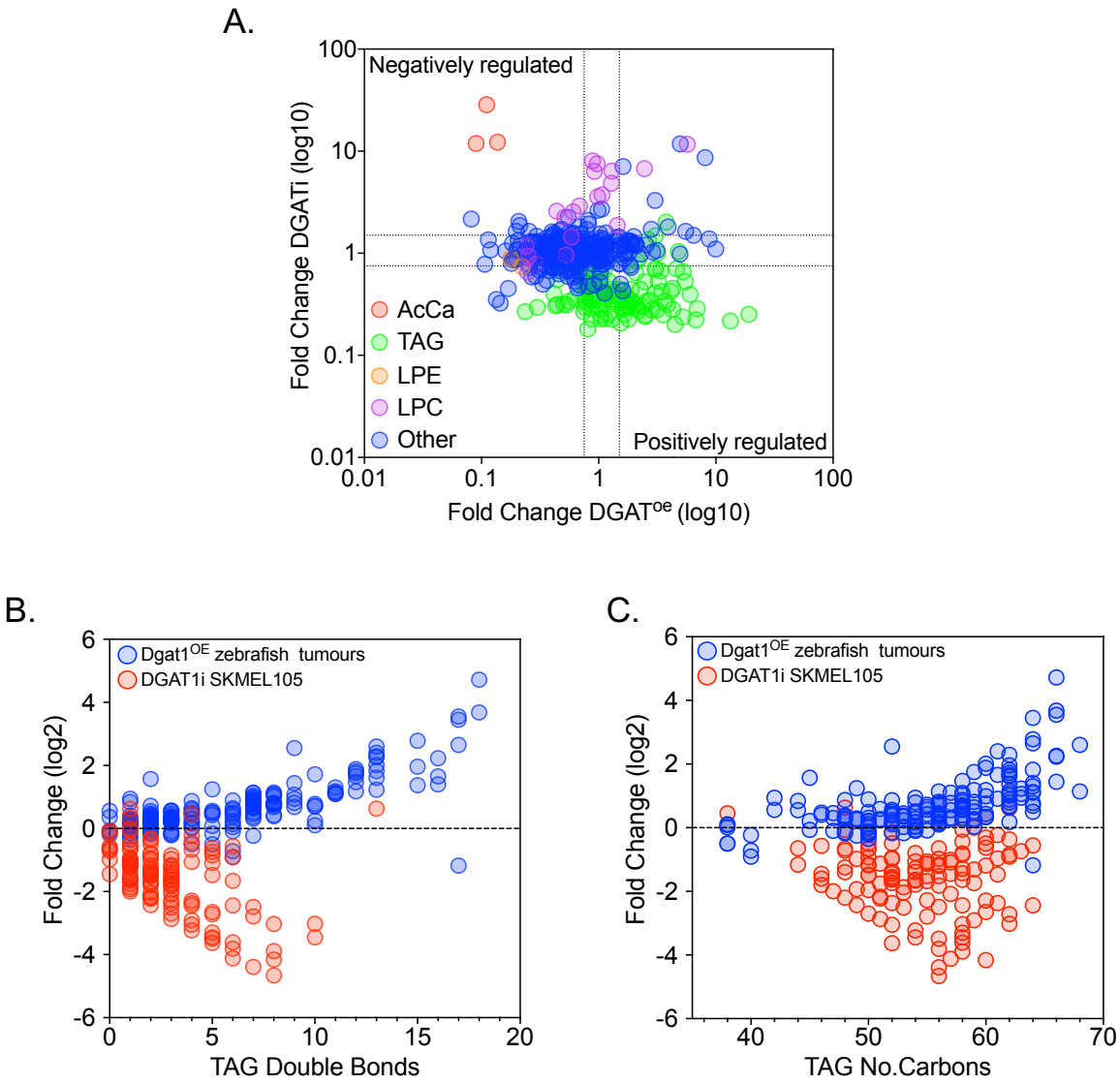

Figure 5.6 DGAT1 shows substrates specificity towards longer poly-unsaturated FA chains

(A) UHPLC-lipidomic analysis, lipid species fold changes in SKMEL105 following 72h A922500 plotted versus lipid species fold changes observed in clone 3 cells relative to 888MEL parental cells. TAG (triacyclglycerides), LPC (lysophosphatidycholine), AcCa (acyl carnitine), LPE (lysophosphatidylethanolamine). (B) UHPLC- lipidomic analysis of SKMEL105 cells following treatment with A922500 for 72 h and $NRAS^{G12D}$-positive Dgat1a-over-expressing (n=6) tumors showing the number of carbon-carbon double bonds in TAG species compared to the fold increase. Fold increase calculated as per figure 5.4B and figure 5.5B respectively. (C) as for (B) but showing the number of carbons in TAG species.

The significant impact of DGAT1 modulation on the levels of AcCa species indicated that DGAT1 may play a key role in modulating the rate of FAO. AcCa, are the products of an esterification reaction linking L-carnitine to FA (typically long chain), the resultant AcCa are transported into the mitochondria and processed into acetyl-CoA through FAO. Excess FAO can lead to an overloading of the mitochondria and subsequently mitochondrial dysfunction. Therefore, in order to assess the direct impact of DGAT1 modulation on mitochondrial respiration and health we used the Seahorse Analyzer, which is able to determine the basal respiration rate, spare respiratory capacity and rate of ATP production in the mitochondria. Upon 48 h DGAT1 inhibition we observed evidence of impaired ATP production and a reduction in both basal respiration and spare respiratory capacity, despite the increased levels of AcCa (Figure 5.7 A-B). The impaired ATP production observed following DGAT1 inhibition was confirmed through the detection of increased levels of phosphorylated AMPK and RAPTOR (Figure 5.7 C). Interrogating further the mitochondrial dysfunction observed upon DGAT1 inhibition, we used JC-1 to look at mitochondrial membrane potential, the probe forms red J-aggregates in healthy mitochondria which are lost when mitochondrial membrane potential is lost. Inhibition or knockdown of DGAT1 led to a loss of mitochondrial membrane potential after 48 h in both A375 and SKMEL105 melanoma cells, as determined by flow cytometry analysis using JC-1 (Figure 5.7 D). This was confirmed through western blotting for the markers of loss of mitochondrial membrane potential; a decrease in the levels of cleaved PINK1 and an increase in total levels of the mitophagy factor PARKIN was observed after DGAT1 inhibition (Figure 5.7 E). Additionally, blocking the synthesis of AcCa through using the carnitine palmitoyl transferase inhibitor Etoximir was able to partially rescue mitochondrial membrane potential and cellular proliferation, after inhibition of DGAT1 (Figure 5.7 F-G).

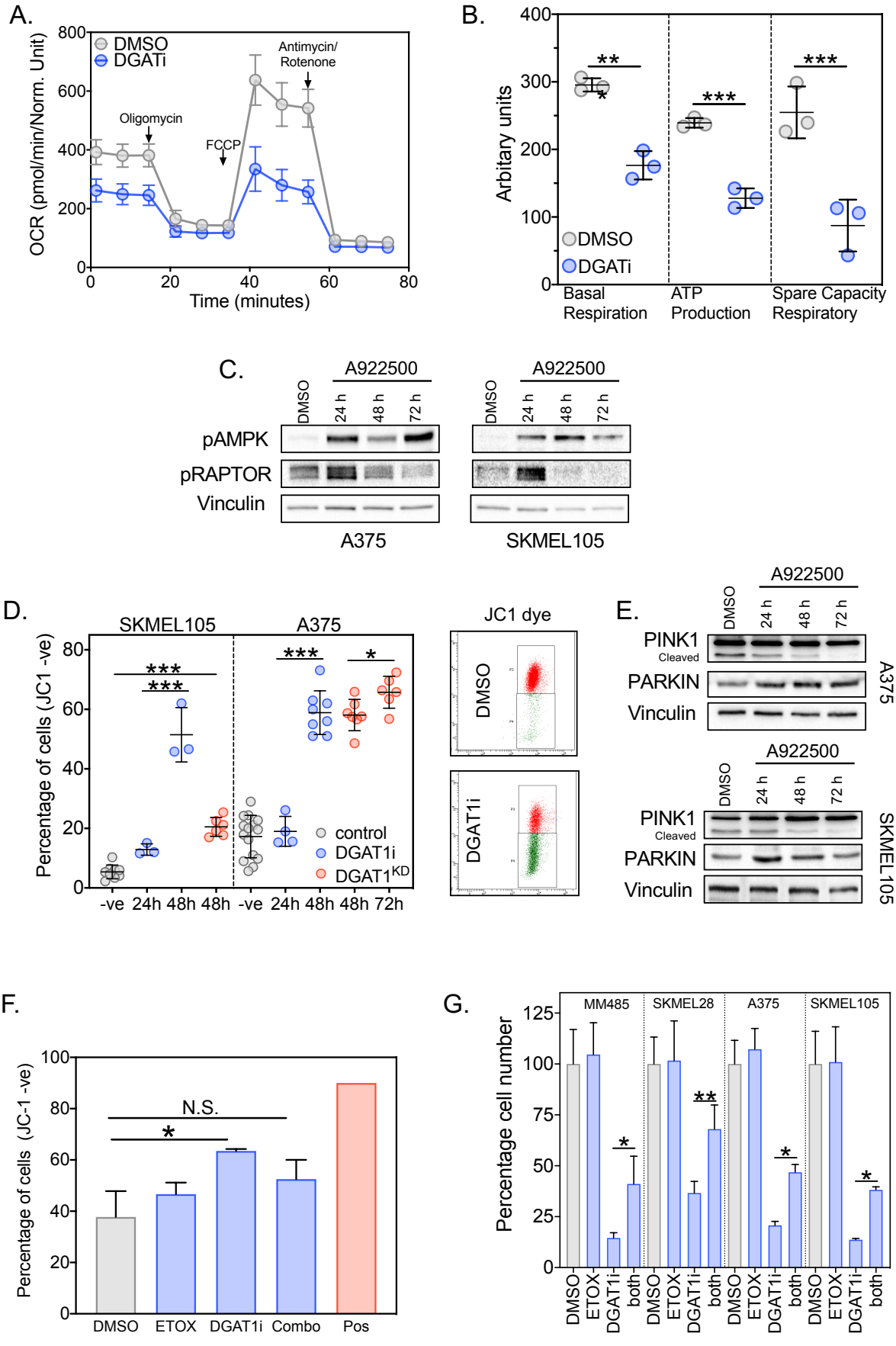
A.
OCR (pmol/min/Norm. Unit)
DMSO
DGATi
Oligomycin
FCCP
Antimycin/
Rotenone
Time (minutes)
B.
Arbitary units
DMSO
DGATi
Basal
Respiration
ATP
Production
Spare Capacity
Respiratory
C.
A922500
DMSO
24 h
48 h
72 h
pAMPK
pRAPTOR
Vinculin
A375
SKMEL105
D.
SKMEL105
A375
Percentage of cells (JC1 -ve)
control
DGAT1i
DGAT1KD
-ve 24h 48h 48h -ve 24h 48h 48h 72h
JC1 dye
DMSO
DGAT1i
E.
A922500
PINK1
Cleaved
PARKIN
Vinculin
A375
SKMEL105
F.
Percentage of cells (JC-1 -ve)
N.S.
DMSO
ETOX
DGAT1i
Combo
Pos
G.
Percentage cell number
MM485
SKMEL28
A375
SKMEL105
DMSO
ETOX
DGAT1i-
both

Figure 5.7 DGAT1 is caretaker of mitochondrial health

(A) Oxygen consumption rate in A375 cells following treatment with/without A922500 for 48 h. Oligomycin, FCCP, as well as rotenone and antimycin A were sequentially added as indicated. (B) as for (A) Basal respiration, ATP production and spare respiratory capacity were calculated (Mean ± SD, n=3) (unpaired two way t-test). (C) Protein expression of phospho-AMPK and phospho-RAPTOR in indicated cell lines following treatment with/without A922500 for 24-72 h. (D) Indicated cell lines were stained with JC-1 dye following treatment with/without A922500 for 24-48 h or following transfection with DGAT1 targeting siRNA for 48-72 h. The percentage of cells that lost red J- aggregates was calculated by using 1uM CCP as a positive control for loss of mitochondrial membrane potential and comparing this to untreated cells to create two populations of cells in the flow cytometry analysis (left) (Mean ± SD, n>3). (E) Protein expression of PINK1 and PARKIN in indicated cell lines following treatment with/without A922500 for 24-48 h (right). (F) A375 cells were stained with JC-1 dye following treatment with/without A922500 for 48 h and with/without Etoximir for 4 h. The percentage of cells that lost red J-aggregates was calculated by using 1uM CCP as a positive control for loss of mitochondrial membrane potential and comparing this to untreated cells to create two populations of cells in the flow cytometry analysis (Mean± SD, n>3) (one-way Anova). (G) Relative cell number as determined by crystal violet staining, indicted cell lines were treated with/without A922500 for 48h and with/without etoximir for 24 h (Mean± SD, n=3) (one-way Anova).

We can conclude that DGAT1 plays a critical role in TAG synthesis and thus LD biosynthesis and maintenance in melanoma. The maintenance and synthesis of LD may be linked to the ability of DGAT1 to maintain mitochondrial function through regulating the availability of FA for FAO.

5.4 Discussion

The final step in LD biogenesis is the conversion of DAG to TAG, catalysed by the DGAT enzymes. Here, we revealed that DGAT1 is essential for LD biosynthesis in melanoma cells. Both pharmacological antagonism and knockdown of DGAT1 led to a decrease in LD numbers over time in a number of DGAT1^{High} melanoma cell lines. This result was further validated through the use of a second neutral lipid dye, LipidTox. Additionally, stable lentiviral overexpression of DGAT1 in a DGAT1^{Low} melanoma cell line led to a dramatic increase in LD. These results are in agreement with studies in prostate cancer and glioblastoma cell lines. Pharmacological inhibition of DGAT1 in both LNCaP and PC-3 prostate cancer cell lines and siRNA knockdown of DGAT1 in LNCaP cells resulted in a decrease in lipid droplet numbers per cell, as determined by the neutral lipid stains Bodipy and Oil-red-O[340,475]. In glioblastoma cell lines antagonism of DGAT1 led through either pharmacological inhibition or shRNA knockdown led to a decrease in the number of LD both *in vitro* and *in vivo*[476]. However, in adipocytes and liver cells, studies have shown that inhibition of both DGAT1 and DGAT2 is required to significantly reduce LD numbers, this may be due to the increased expression levels of DGAT2 compared to DGAT1 in untransformed cell types[476,536]. Additionally, in a cell line model of renal cell carcinoma, antagonism of both DGAT1 and DGAT2 simultaneously led to a decrease in the number of LD, although the impact of inhibition of DGAT1 or DGAT2 alone on LD number was not assessed[304]. The expression of both DGAT1 and DGAT2 could be assessed in our melanoma cell line panel to address this hypothesis through the use of RTqPCR. In contrast to DGAT1, siRNA knockdown of DGAT2 did not significantly affect LD numbers in melanoma cells. This is also in agreement with studies in glioblastoma in

which antagonism of DGAT2 through chemical inhibition or shRNA knockdown did not significantly impact LD numbers[476]. Our data and other studies highlight a dependence on DGAT1 in transformed cells for LD formation, modulation of DGAT1 activity alone impacts upon LD levels.

In agreement with the critical role of DGAT1 in LD formation in melanoma cells, UHPLC-MS identified significant changes in multiple TAG species upon modulation of DGAT1. Inhibition of DGAT1 in DGAT1^{High} SKMEL105 melanoma cells led to a significant decrease in multiple species of TAG at both 24 and 72 h. This is in contrast to the increases in multiple TAG species in both our DGAT1 overexpression models, the DGAT1 overexpressing clone 3 888MEL cells and the *in vivo* oncogenic NRAS driven DGAT1 overexpression zebrafish melanoma model (although the changes in TAG species in our zebrafish melanoma model did not reach statistical significance). This data indicated that DGAT1 is the predominant enzyme controlling TAG synthesis in melanoma cells. This dependence on DGAT1 for TAG synthesis is also observed in glioblastoma cell line models and in starved mouse embryonic fibroblast, with global lipidomic analysis revealing a decrease in multiple TAG species upon DGAT1 inhibition[295,476].

Intriguingly, in the A375 melanoma cell line model we did not observe a significant decrease in TAG species upon 24 or 72 h DGAT1 inhibition, which is at odds with the decrease in lipid droplets we observed in this cell line model upon DGAT1 inhibition. This may be due to compensation from enzymes able to catalyses the same reaction such as DGAT2[323], this could be investigated through inhibiting both DGAT1 and DGAT2 simultaneously followed by analysis of TAG species levels. To determine whether this result is an outlier, further UHPLC-MS analysis could be carried out in another DGAT1^{High} cell line after DGAT1 inhibition, however, as we observed contrasting changes in our DGAT1 inhibition and DGAT1 overexpression models, we have confidence that DGAT1 does play a critical role in TAG synthesis in melanoma.

No significant changes in the levels of DAG species were detected in our UHPLC-MS analysis, which may be due to limitations of the technique. Alternatively, this may be due to alternate metabolization of DAG by either its degradation by lipases, its re-its conversion to PC by CDP-choline:1,2-diacylglycerol choline phosphotransferases (CPTs), or its phosphorylation by diacylglycerol kinases (DGKs)[537]. As a key regulators and activators of PKC a build-up of DAG would lead to hyper-activation of PKC and subsequent activation of mTOR signalling[538–540]. Thus, the observation of no build-up of DAG species is in agreement with the decrease in mTOR signalling we observe in chapter 4 upon DGAT1 inhibition. However, a more targeted lipidomic approach directly assessing DAG species would provide deeper insight into the role of DAG signalling upon DGAT1 modulation.

The discovery that DGAT1 is the key enzyme governing both TAG synthesis and LD formation opens up further questions into mechanisms behind the oncogenic nature of DGAT1. As previously discussed, LD play a wide range of roles in the modulation of numerous hallmarks of cancer[275]. However, our UHPLC-MS analysis highlighted that multiple AcCa species were found to have the largest changes upon DGAT1 modulation. Inhibition of DGAT1 led to a dramatic increase in the levels of multiple AcCa species in two DGAT1^{High} melanoma cell lines. Contrastingly, overexpression of DGAT1 in a DGAT1^{Low} melanoma led to a significant decrease in AcCa levels, an effect also observed in our NRAS driven Dgat1a overexpressing zebrafish model of melanoma, although these changes did not reach significance. The production of AcCa is catalysed by CPT1 linking L-carnitine and typically long-chain fatty acids (LCFA), AcCa is then shuttled into the mitochondria for FAO. It appears that DGAT1 inhibition shifts lipid homeostasis; typically, once imported into a cell, LCFA can go down one of two routes following activation, (1) through forming LCFA-CoA , esterification into TAG for storage or (2) conversion into AcCa and subsequent FAO in the mitochondria[541]. Inhibition of DGAT1 prevents the esterification of LCFA-CoA into TAG and thus, in order to prevent a build-up of toxic FFA, it appears that melanoma cells shift their lipid metabolism to increase the conversion of LCFA-CoA into AcCa. In agreement with a role for DGAT1 in the storage of LCFA, TAG species

containing the greatest number of carbons were the most affected upon DGAT1 modulation. An increase in AcCa upon DGAT1 antagonism through either pharmacological inhibition or knockdown through shRNA is also observed in starved mouse embryonic fibroblasts and glioblastoma cell lines, indicating that this is not just a melanoma specific effect[295,476]. However, a build-up of acylcarnitine has previously been suggested to be lipotoxic and disrupts mitochondrial homeostasis[542,543]. Indeed, upon 48 h DGAT1 inhibition we observe a decrease in mitochondrial function and loss of mitochondrial membrane potential, leading to energetic stress and AMPK activation. The loss of mitochondrial membrane potential can be partially rescued through prevention of AcCa build-up through the use of the CPT1 inhibitor Etomoxir, indicating that it is the build-up of AcCa causing the mitochondrial dysfunction observed upon DGAT1 inhibition. To determine whether the increase in AcCa species does lead to rampant FAO prior to mitochondrial dysfunction, a time course of DGAT1 inhibition could be carried out and FAO measured directly, which is possible using the Seahorse analyser.

The disruption of mitochondrial homeostasis through an increased flux of FA leading to increased AcCa production and aberrant FAO has major implications in cell REDOX. Mitochondria play an important role in the production of ROS modulating REDOX-dependent cellular processes; however, disruption of mitochondrial homeostasis can lead to aberrant ROS production which is toxic to cells. This may be of even greater importance in the context of DGAT1 inhibition, as LD have been shown to play a key role in sequestering PUFA which are highly vulnerable to peroxidation. Lipid peroxides are a highly toxic ROS species which can lead to cellular death through a mechanism known as ferroptosis[305,306,535]. Inhibition of DGAT1 in our DGAT1^{High} melanoma cell line model led to a significant decrease in the TAG species with a high number of double bonds. This is in contrast to our zebrafish melanoma model in which a significant increase in TAG species with a high number of double bonds was observed. This is in agreement with a model in which DGAT1 is critical for the sequestration of PUFA in LD to protect them from peroxidation[290,483]. The impact of

DGAT1 modulation on both ROS production and protection from ROS will be investigated further in the following chapter.

From this data we can conclude that DGAT1 is the critical enzyme for TAG synthesis and LD biogenesis in melanoma and sequesters FFA, preventing a build-up of toxic AcCa which is toxic to the mitochondria. DGAT1 appears to selectively sequester PUFA into LD protecting them from peroxidation and subsequent lipotoxicity. Thus, part of the oncogenic mechanism of DGAT1 may be in allowing melanoma cell to safely sequester FA preventing lipotoxicity and mitochondrial dysfunction due to aberrant FAO.

Chapter 6 - DGAT1 promotes survival of melanoma cells in the presence of ROS

6.1 Introduction

Our work in chapter 5 identified that DGAT1 is critical in maintaining mitochondrial function and health in melanoma cells. Inhibition of DGAT1 led to a crash in mitochondrial respiratory capacity and loss of mitochondrial membrane potential, due to a toxic build-up of AcCa. Mitochondria are central to maintaining cellular REDOX-dependent processes which influence signalling, proliferation, differentiation, metabolism and apoptosis[544]. In mammalian cells, evidence points towards mitochondria being key generators of ROS that drive redox sensitive cellular processes and are themselves sensitive to ROS flux which alters mitochondrial function[545–547]. In cancer cells ROS has been shown to play a dynamic role in cancer initiation and progression, with cancer cells typically having higher levels of ROS than untransformed cells[544,548]. However, increased ROS comes at a cost; as ROS levels become too high they can cause apoptosis, ferroptosis and necroptosis, thus cancer cells need to tightly regulate ROS using antioxidant mechanisms[549–551]. By playing a critical role in mitochondrial function in melanoma cells, DGAT1 may be crucial in maintaining ROS at pro-tumorigenic levels and preventing ROS induced cell death.

Increased ROS levels in cancer cells usually occurs in the early stages of transformation alongside oncogene activation, this is thought to be due to ROS induced genetic instability. ROS can cause DNA damage through causing DNA adducts, base modification and gene mutation. ROS catalyses the oxidation of guanosine to 8-hydoxy-2'-deoxyadenosine which can lead from a G:C to T:A point mutation[552]. Studies have demonstrated that the ROS agent H_2O_2 can cause an activating mutation in the human oncogene HRAS[553] and inactivating mutations in the tumour suppressor p53 gene[554]. In addition to mutation of DNA, ROS is also able to affect the expression of genes through altering DNA methylation[555]. In

hepatocellular carcinoma, H_2O_2 has been shown to cause the downregulation of E-cadherin, which is associated with metastasis and worse patient outcome[556,557]. A similar effect is also observed in colorectal cancer in which H_2O_2 causes methylation of the RUNX3 protomer and subsequent downregulation of this tumour suppressor, an effect which can be reversed through the addition of ROS scavenging agents[558].

Increased ROS generation is observed downstream of several oncogenes such as *Cmyc*, *Kras* and *BRCA1*[559–562] and ROS has been shown to be essential in *Kras* mediated tumorigenesis through regulation of MAPK signalling[563]. ROS generated downstream of oncogenes play a wide role in cancer development and progression. They are also able to modulate signalling proteins controlling pathways involved in tumour cell proliferation. ROS has been shown to activate the two main pathways implicated in cancer cell proliferation, MAPK and PI3K. In ovarian cancer ROS were shown to activate MAPK signalling through causing the degradation of MAPK phosphatase 3 (MKP3), a negative regulator of ERK1/2[564]. The PI3K pathway is also activated by ROS in a similar manner with ROS inactivating the phosphatases phosphatase and tensin homolog (PTEN) and protein tyrosine phosphatase 1B (PTP1B), leading to constitutive PI3K signalling[565,566].

In addition to promoting cellular proliferation, ROS also plays a key role in promoting cancer cell motility and metastasis through promotion of decreased cell adhesion, anchorage-independent survival and intravasation. Mechanisms behind ROS driven metastasis include driving increased expression of matrix metalloproteinases (MMPs) which promotes invasion[567,568], suppression of anoikis driven apoptosis upon cellular detachment from the ECM[569,570] and increasing Rac1 activity which promotes both cell migration and intravasation[571,572].

A further key tumour promoting role of ROS is augmenting angiogenesis, facilitating the supply of oxygen and nutrient supply to the centre of a tumour. In the centre of

a tumour, the hypoxic and nutrient starved conditions can cause oxidative stress; it is the ROS produced that leads to an increase in vascular epithelial growth factor (VEGF) expression driven through the transcription factor HIF-1 α[573,574]. The use of ROS scavengers or suppression of endogenous ROS leads to a decrease in VEGF expression and attenuation of angiogenesis, highlighting the key role of ROS in this process[575–577].

Discoveries linking ROS increases in cancer cells to the modulation of numerous cancer hallmarks and promoting tumour initiation and progression have led to the development of treatment strategies designed to reduce the levels of ROS in cancer cells. In a mouse model of lymphoma, treatment with the ROS scavengers N-acetyl cysteine (NAC) and vitamin C was shown to inhibit tumorigenesis[578]. Similar results using ROS scavenging compounds have been achieved in pre-clinical models of prostate, oral, breast and gastrointestinal cancer[579–582]. However, in contrast to these results, treatment with either NAC or vitamin E in a mouse model of lung cancer accelerated tumour progression[583] and in a melanoma mouse model NAC treatment increased metastasis[584]. Several large scale clinical trials have now demonstrated that dietary supplementation with antioxidants has no benefit in cancer prevention or progression and in some cases even increased cancer incidence[585–588]. It is possible that these results may be due to lack of specificity in scavenging pro-tumorigenic ROS in cancer cells or even to lowering ROS levels below a toxic threshold which enables cancer cells to survive and grow.

The opposite therapeutic approach is to increase cellular ROS levels in order to overwhelm the cellular anti-ROS response and cause ROS-induced cell death in cancer cells. Despite the pro-tumorigenic effects of increased ROS in cancer cells, this increase in ROS may come at a cost, leaving cancer cells balancing right on the edge of ROS induced cell death and acutely sensitive to ROS inducing agents. The accumulation of ROS in cancer cells must be tightly regulated in order to maintain REDOX balance; this is carried out by an antioxidant system under the control of the

transcription factor nuclear factor erythroid 2–related factor 2 (NRF2). Under oxidative stress, NRF2 dissociates from the cytoplasmic protein Kelch-like ECH-associated protein 1 (KEAP1) which, under normal conditions, would target NRF2 to the proteosome, thus stabilising NRF2 and allowing it to translocate to the nucleus[589,590]. NRF2 can then activate a myriad of anti-oxidant enzymes including the Superoxide dismutase (SOD) family of enzymes which are located in various cellular compartments and convert O_2^- to H_2O_2 and peroxiredoxins (PRXs), glutathione peroxidases (GPXs), and catalase (CAT) which reduce H_2O_2 into water (H_2O)[591–593]. NRF2 is also able to regulate metabolic pathways such as the pentose phosphate pathway to increase NADPH production, a critical co-factor and reducing agent in the antioxidant defence system[594]. Upregulation and activation of antioxidant mechanisms are often observed in cancer. Upregulation of NRF2 or mutation of NRF2 or KEAP1 leading to NRF2 activation is observed in multiple cancer types including melanoma[595–599]. Furthermore, NRF2 signalling has been shown to be critical for tumour initiation and progression, with knockdown of NRF2 leading to ROS induced cancer cell death[600,601].

A number of widely used chemotherapeutic agents including cisplatin, carboplatin doxorubicin and procarbazine function by increasing ROS and cause irreversible oxidative damage which forms the basis for their anti-tumour effect[602,603]. More recently biologics such as Retuximab, a monoclonal antibody against CD20, were shown to increase ROS production in lymphoma cells and cause cell death[604]. More targeted approaches include interfering with glutathione ROS scavenging system by either conjugating with glutathione or inhibiting glutathione synthesis, or through inhibition of the therodoxin antioxidant system. Both approaches lead to increased oxidative stress and cancer cell death[605–607]. Targeted approaches also led to the development of inhibitors of key ROS metabolism enzymes such as SODs, HMOX and catalase, which are currently in development and have been shown to have antitumorigenic properties[608–611].

The increasing understanding of the complexity of both the pro-tumorigenic and antitumorigenic roles of ROS in cancer is revealing new insights into oncogenic mechanisms and providing new therapeutic opportunities. An understanding of the role of DGAT1 in modulating mitochondrial function and health and thus it's impact upon melanoma cell REDOX balance will both aid in understanding why the amplification and upregulation of DGAT1 is selected for in melanoma cells and illuminate whether DGAT1 inhibition could become a part of melanoma therapy.

6.2 Aims

- Investigate the impact of long term DGAT1 inhibition upon signalling and metabolism in melanoma cells through using global proteome analysis.

- To identify whether modulation of DGAT1 impacts directly upon ROS species levels in melanoma cells.

- Investigate the impact of DGAT1 modulation of melanoma cell survival.

6.3 Results

In the previous chapter, our lipidomic analysis uncovered changes in lipid species critical for mitochondrial FAO and a decrease in mitochondrial respiratory capacity upon long term DGAT1 inhibition. In order to investigate the impact these changes in levels of lipid species and decreased mitochondrial function had on melanoma cell signalling and metabolism, we performed unbiased MS-based whole proteome analysis in SILAC-labelled DGAT1^{High} A375 cells. Analysis of peptides from SILAC-labelled DGAT1^{High} A375 melanoma cells following 72h treatment with the DGAT1 inhibitor A922500 revealed a strong correlation between the three individual repeats (Figure 6.1A). Peptides with a SILAC ratio of greater than 1.5 were considered up-regulated whilst those with a ratio less than 0.75 were considered down-regulated (Figure 6.1B). Analysis of the differentially expressed, up-regulated proteins upon DGAT1 inhibition revealed three key areas of altered signalling in melanoma cells. Firstly, we observed an enrichment of proteins involved in FAO (Figure 6.1B), consistent with the increase in AcCa species observed in two DGAT1^{High} melanoma cell lines upon long term inhibition of DGAT1. Secondly, enrichment of PPAR signalling indicates alterations in lipid metabolism upon DGAT1 inhibition (Figure 6.1B), which may be due to an increase in available lipid regulators of PPAR activity. Finally, the most striking enrichment is an increase in NRF2 activity and oxidative stress (Figure 6.1B). Increased NRF2 activity is a well-established response to ROS production and acts to dampen cellular damage due to ROS. Using RTqPCR we confirmed the increase in a number of genes involved in both FAO, NRF2 and ROS signalling upon pharmacological inhibition of DGAT1 in both A375 and SKMEl105 melanoma cells (Figure 6.1C). The NRF2 target gene HMOX1 and mediator of NRFR2 signalling, SESN2, were the most up-regulated genes after DGAT1 inhibition in both melanoma cell lines (Figure 6.1C).

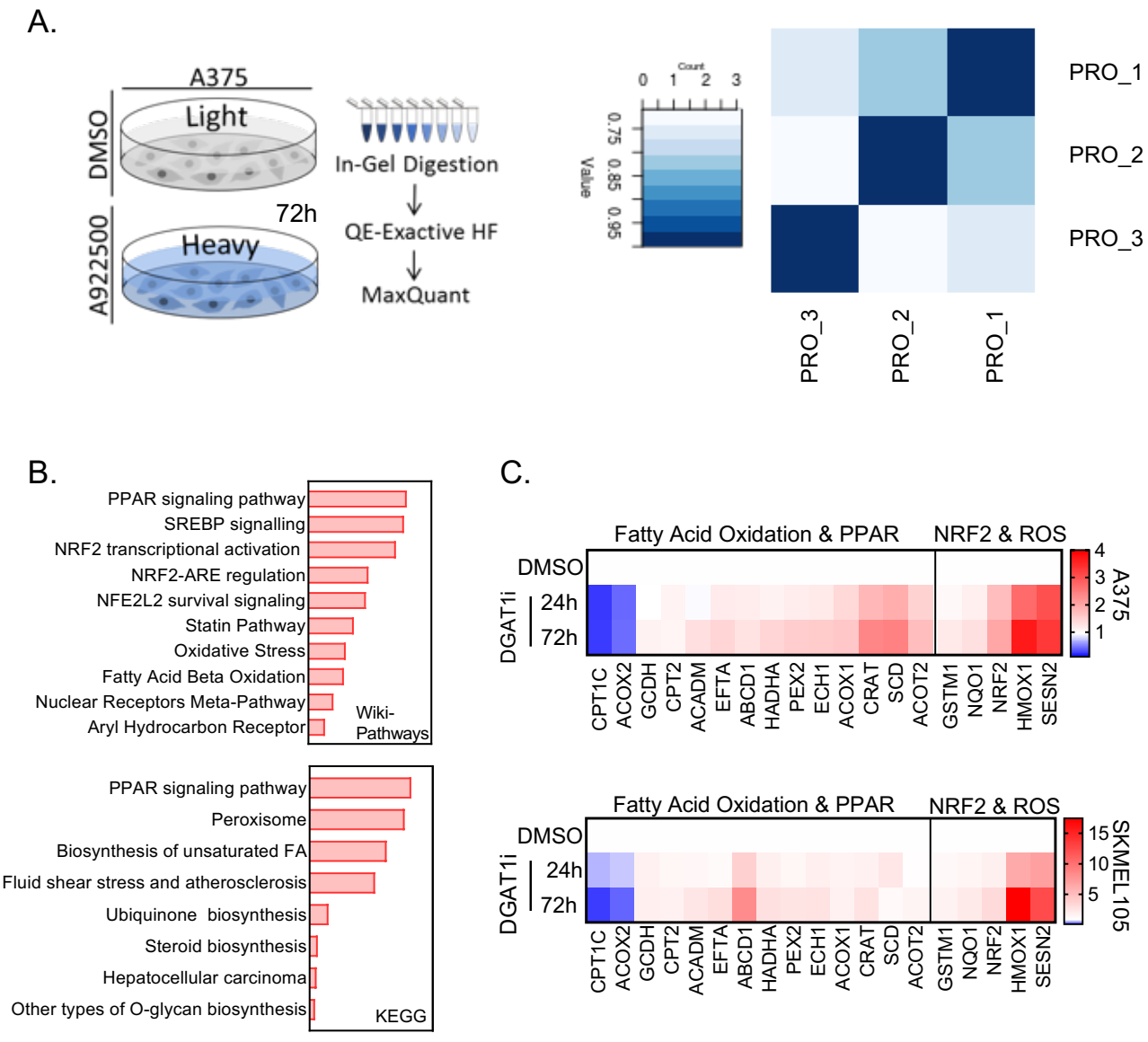

Figure 6.1 DGAT1 inhibition increases FAO and ROS signalling

(A) SILAC-based total proteome analysis by mass spectrometry (Left). . (c) Pearson correlation between total proteome samples following treatment of A375 cells with/without A922500 for 72 h (n=3)(Right).(B) Gene Ontology of up-regulated proteins (114) ranked by combined score (wikipathways) or log adjusted P values (metascape). (C) RT-qPCR analysis of indicated genes in A375 and SKMEL105 cells following 24-72 h treatment A922500, Fold-change calculated relative to DMSO treated control (Mean, n=3).

We next assessed ROS levels directly in melanoma cells using cell permeable fluorogenic probes which, when oxidised, result in detectable alterations in fluorescence. Using Dihydroethidium (DHE) to measure ROS levels, we observed an increase in ROS upon DGAT1 inhibition in a panel of four DGAT1^{High} melanoma cell lines (Figure 6.2A). Significant increases in ROS were observed at 24 h post DGAT1 inhibition and continued to increase up to 72 h (Figure 6.2A). The increase in cellular ROS observed upon 48 h and 72 h DGAT1 inhibition was confirmed using both a second DGAT1 inhibitor (AZD3988) and a second fluorogenic probe for ROS detection, 2',7'-dichlorodihydrofluorescein diacetate (H2DCFDA) (Figure 6.2B-C). Knockdown of DGAT1 also lead to an increase in ROS levels in two DGAT1^{High} melanoma cell lines, as determined by DHE (Figure 6.2D). Activation of AMPK through activating phosphorylation was also observed upon DGAT1 knockdown at 48 and 72 h, indicating that energetic stress was also occurring concurrently with production of ROS (Figure 6.2D). In addition to measuring cellular ROS levels, we were also able to specifically measure the levels of mitochondrial ROS using the fluorogenic probe mitosox that is specifically targeted to the mitochondria and when oxidised by superoxide produces red fluorescence. Pharmacological inhibition of DGAT1 in two melanoma cell lines for 48 h led to an increase in mitochondrial superoxide production, as determined using flow cytometry (Figure 6.2E).

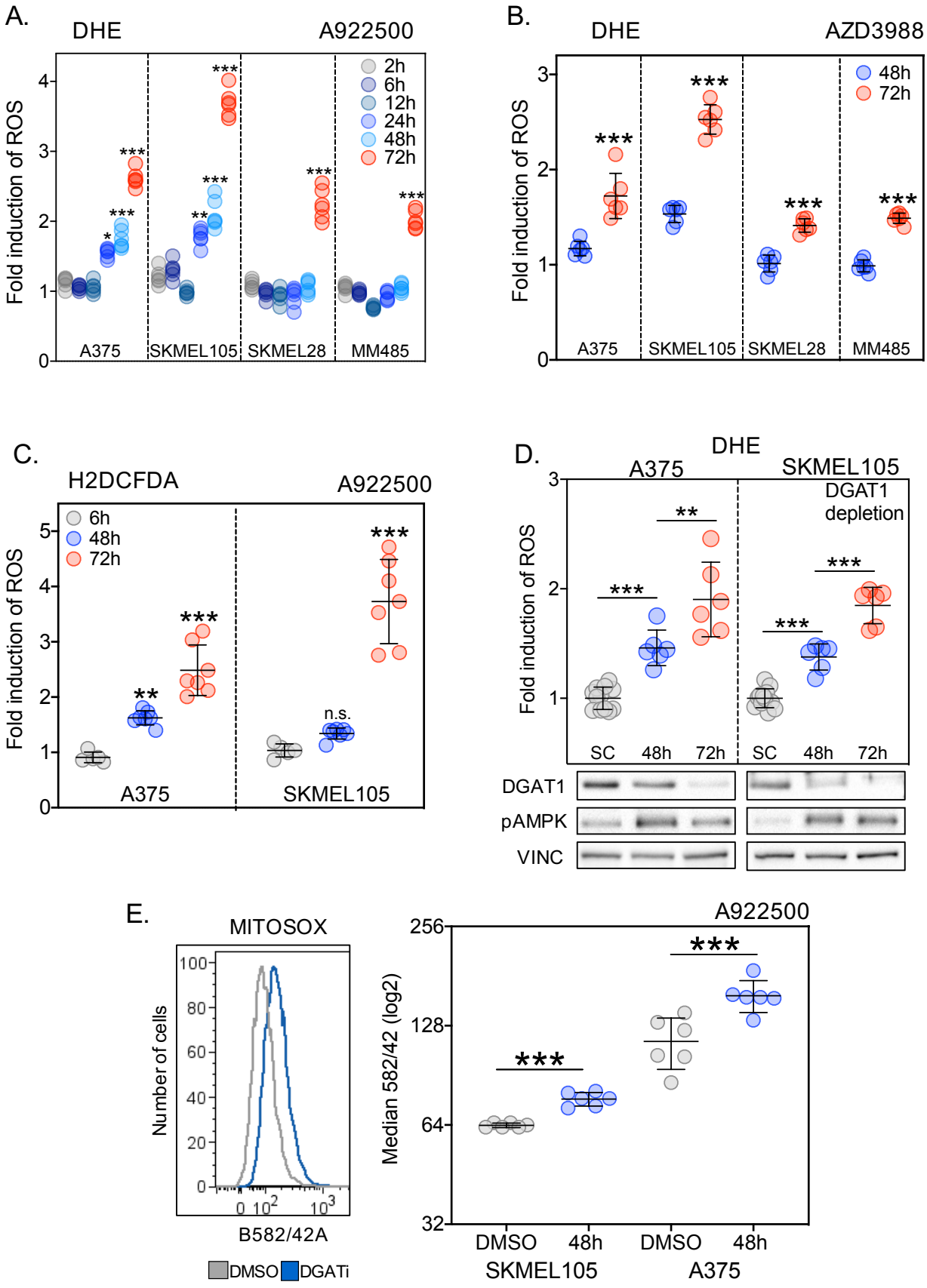
A.
DHE
A922500
Fold induction of ROS
2h
6h
12h
24h
48h
72h
A375
SKMEL105
SKMEL28
MM485
B.
DHE
AZD3988
48h
72h
C.
H2DCFDA
A922500
6h
48h
72h
n.s.
D.
DHE
A375
SKMEL105
DGAT1
depletion
SC
48h
72h
DGAT1
pAMPK
VINC
E.
MITOSOX
Number of cells
B582/42A
DMSO
DGATi
A922500
Median 582/42 (log2)
DMSO
48h
SKMEL105
A375

Figure 6.2 DGAT1 suppression increases cellular ROS levels

(A) Quantification of ROS levels using dihydroethidium fluorescence (ex 480nm, em 570nm) following treatment of indicated cell lines with A922500 for 2-72 h. Fluorescence was normalised to relative cell number using crystal violet staining. Fold-change calculated relative to DMSO treated control (Mean, n>4). (B) as for (A) indicated cell lines were but treated with AZD3988 for 24 and 72 h. (C) Quantification of ROS levels using H2DCFDA (ex 480nm, em 535nm) in indicated cell lines following treatment with/without A922500 for 48-72 h. Fluorescence was normalised to relative cell number using crystal violet staining. Fold-change calculated relative to DMSO treated control (Mean, n>4). (D) Quantification of ROS levels using dihydroethidium fluorescence (ex 480nm, em 570nm) in indicated cell lines following transfection with either DGAT1 targeting siRNA or a scrambled control for 48-72 h. Fold- change calculated relative to scrambled control (Mean± SD, n=3)(Upper). Corresponding protein expression of DGAT1 and phospho-AMPK (Lower). (E) Indicated cell lines were stained with mitosox dye following treatment with A922500 for 48 h. Median fluorescence was determined using flow cytometry (Mean± SD, n=6) (two-way Anova used in all figure sections).

Next, we assessed the impact of increased ROS production induced by long term DGAT1 inhibition on melanoma cell survival. In parallel to increased ROS production, we observed increased protein expression of the ROS response markers superoxide dismutase 1 and 2 (SOD1/2) and induction of apoptotic cell death, as determined by cleavage of caspase 3, upon 48- and 72-hour inhibition of DGAT1 in a panel of DGAT1^{High} melanoma cell lines (Figure 6.3A). The induction of apoptotic cell death was also observed, using a fluorescent readout of cleaved caspase activity and time-lapse microscopy, upon siRNA knockdown of DGAT1 using two individual siRNA oligos and a pool of DGAT1 targeting oligos (Figure 6.3B). Moreover, addition of the ROS scavenging compounds Ebselen and Tempol was able to partially rescue the induction of apoptosis from DGAT1 inhibition in two DGAT1^{High} cell lines, indicating that the increase ROS production, induced by DGAT1 antagonism, was in part driving apoptosis in melanoma cells (Figure 6.3C).

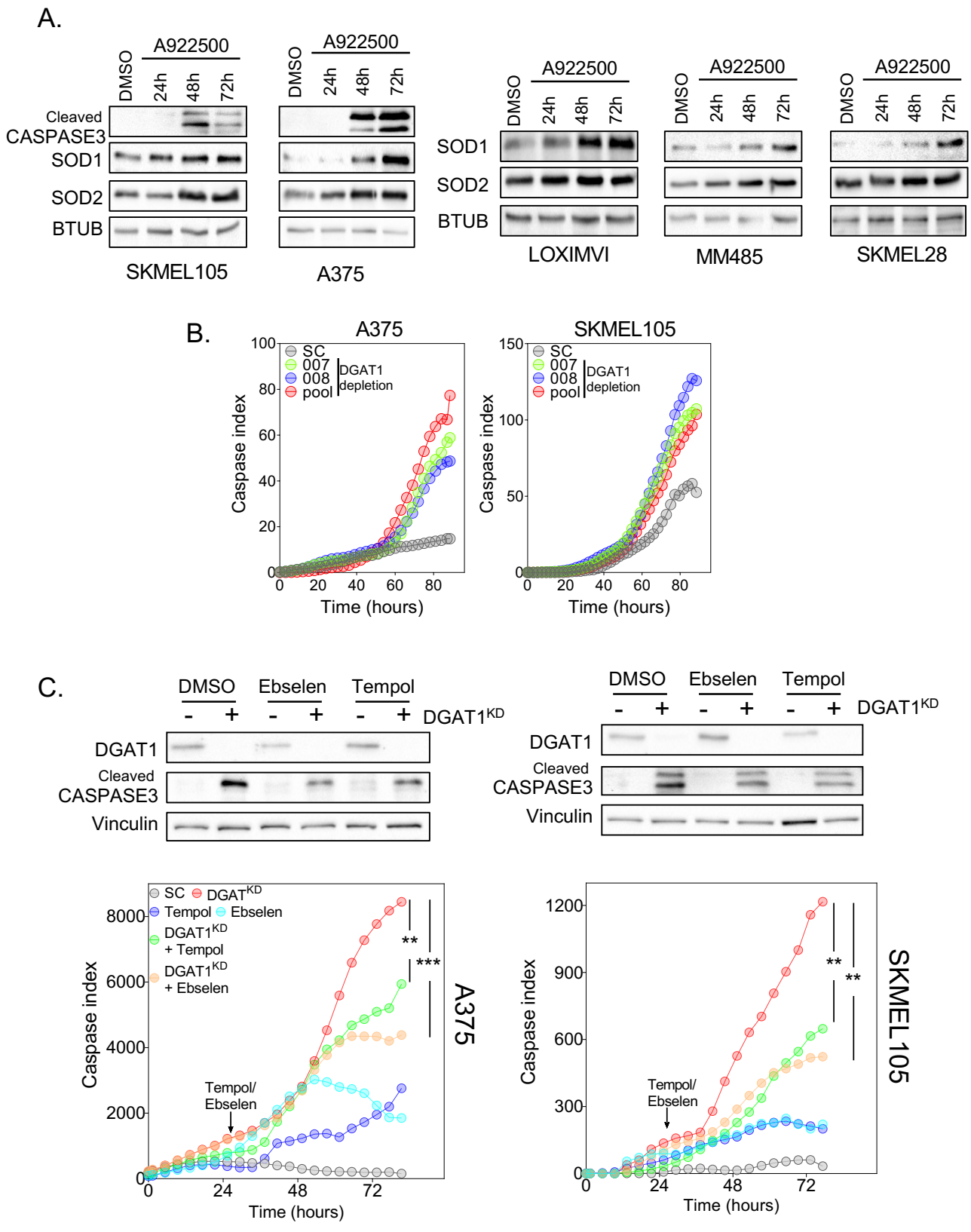
A.
A922500
DMSO
24h
48h
72h
Cleaved CASPASE3
SOD1
SOD2
BTUB
SKMEL105
A375
LOXIMVI
MM485
SKMEL28
B.
A375
SKMEL105
SC
007
008
pool
DGAT1 depletion
Caspase index
Time (hours)
C.
DMSO
Ebselen
Tempol
DGAT1KD
DGAT1
Cleaved CASPASE3
Vinculin
SC
DGATKD
Tempol
Ebselen
DGAT1KD + Tempol
DGAT1KD + Ebselen
Tempol/ Ebselen
**
***
A375
SKMEL105

Figure 6.3 ROS induced by DGAT1 suppression leads to melanoma cell apoptosis

(A) Protein expression of SOD1, SOD2 and cleaved caspase3 in indicated melanoma cell lines treated with A922500 for 24, 48, or 72 h. (B) Cleaved caspase index in indicated cell lines following transfection with either a DGAT1 targeting siRNA (007,008, pool) or a scrambled control determined by time-lapse microscopy using an incucyte zoom system (Mean, n=3). (C) Cleaved caspase index in indicated cell lines following transfection with either a DGAT1 targeting siRNA or a scrambled control determined by time-lapse microscopy using an incucyte zoom system. At 24h cells were treated with/without Ebselen or Tempol (Lower)(Mean, n=3) (one-way Anova). Corresponding protein expression of DGAT1 and cleaved caspse3 in indicated cell lines (Upper).

Conversely, stable lentiviral over-expression of DGAT1 in $DGAT1^{Low}$ 888MEL melanoma cells led to an increased resistance to the ROS inducing agents paraquat and menadione (Figure 6.4A). Western blotting for cleaved caspase revealed that lentiviral over-expression of DGAT1 resulted in decreased apoptosis of melanoma cells upon treatment with the ROS inducing agent paraquat (Figure 6.4B). We also observed that stable lentiviral over-expression of DGAT1 led to an increased number of surviving melanoma cells under conditions of nutrient stress (limited FCS) and hypoxia (1% O_2) (Figure 6.4C), further underpinning a protective role for DGAT1 in melanoma cells under conditions of stress. Western blotting indicated that the increased survival advantage observed upon DGAT1 overexpression was due to less apoptosis occurring under stress conditions, when compared to the parental $DGAT1^{Low}$ melanoma cells (Figure 6.4C). Alongside the decreased levels of caspase activity, we also observed lower protein expression of the response marker SOD2, indicating that overexpression of DGAT1 reduces the production of ROS in melanoma cells induced under stress conditions (Figure 6.4C).

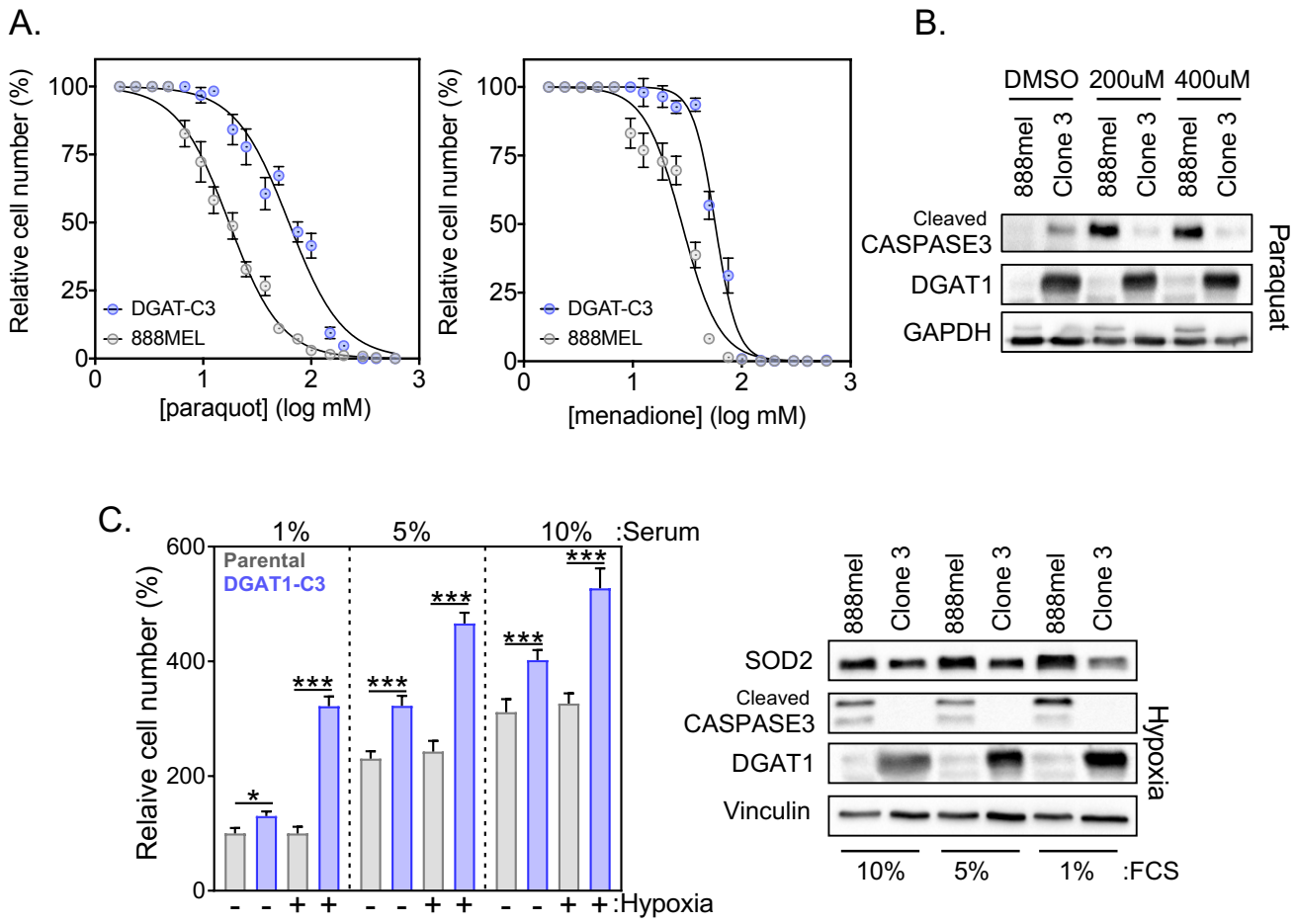

Figure 6.4 Over-expression of DGAT1 increases melanoma cell resistance to ROS inducing agents

(A) Drug-dose response in 888mel or clone 3 DGAT1 over-expressing cells measuring relative cell number as defined by crystal violet staining after 72hr treatment of indicated ROS inducers (Mean ± SD, n=3). (B) Protein expression of cleaved caspase3 and DGAT1 in 888MEL and Clone 3 cells following treatment with indicated concentrations of Paraquat for 72 h (lower). (C) Relative cell number of indicated cell lines stained with crystal violet following 48h culture in indicated FCS serum levels under hypoxic conditions (1% O2) (Mean ± SEM, n>3) (one-way Anova) (Left). Protein expression of SOD2, cleaved caspase 3, DGAT1 in indicated cell lines following 48h culture in indicated FCS serum levels under hypoxic conditions (1% O2) (Right).

In order to explore the specificity of the role of DGAT1 in ROS production and survival in melanoma cells, we inhibited and knocked down DGAT2, which is able to catalyse the same reaction. In contrast to antagonism of DGAT1, pharmacological inhibition of DGAT2 did not lead to an increase in ROS production and knockdown of DGAT2 using siRNA oligos did not lead to apoptosis in $DGAT1^{High}$ melanoma cells (Figure 6.5 A-B). This is in agreement with our data demonstrating that DGAT1 but not DGAT2 is an oncogene in melanoma and indicates that the role of DGAT1 in modulating ROS production and sensitivity to ROS may be part of its oncogenic mechanism.

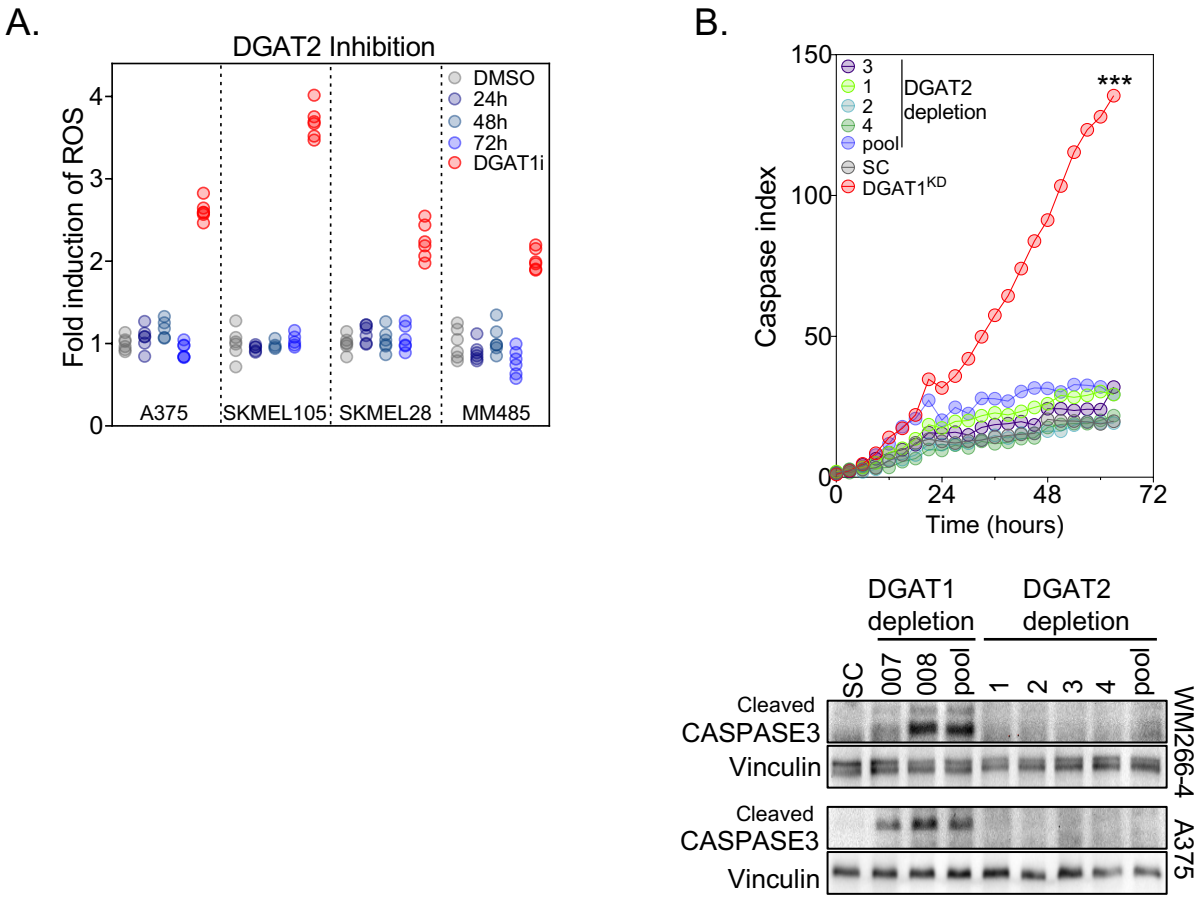

Figure 6.5 DGAT2 suppression does generate ROS or cause melanoma cell apoptosis

(A) Quantification of ROS levels using dihydroethidium fluorescence (ex 480nm, em 570nm) in indicated cell lines following treatment with 50uM DGAT2i for 24-72 h or the DGAT1 inhibitor A922500 for 72 h. Fold-change calculated relative to DMSO treated control (Mean, n>3). (B) Cleaved caspase index in A375 cells following transfection with either a DGAT2 targeting siRNA (001,002,003,004, pool), DGAT1 targeting siRNA or a scrambled control determined by time-lapse microscopy using an incucyte zoom system (Mean, n=3) (one-way Anova) (Upper). Protein expression of cleaved caspase3 in indicated cell lines following transfection with either a DGAT2 targeting siRNA (001,002,003,004, pool), DGAT1 targeting siRNA (007,008, pool) or a scrambled control (Lower).

Our data, in agreement with other studies, indicated that DGAT1 plays a role in the sequestration of PUFA in LD. In sequestering PUFA in LD, DGAT1 plays a role in protecting them from oxygen centred ROS which can act upon PUFA to form cytotoxic lipid peroxide species. Therefore, we next assessed the impact of DGAT1 modulation specifically on the generation of lipid peroxides. C11-BODIPY is a fluorescent neutral lipid probe which, when oxidation occurs, shifts in fluorescence emission peak from ~590 nm to ~510 nm. Inhibition of DGAT1 for 24 or 72 h resulted in an increase in lipid peroxidation in two DGAT1^{High} melanoma cell lines, with significantly more oxidised C11-BODIPY present at 72 h, as determined by flow cytometry (Figure 6.6A). Using mitochondrial targeted C11-BODIPY, we observed an increase in lipid peroxidation upon DGAT1 inhibition specifically in the mitochondria (Figure 6.6B), an expected outcome of aberrant FAO. Moreover, knockdown of DGAT1 using siRNA oligos led to an increase in protein attachment of 4-Hydroxynonenal (4HNE) in melanoma cell lines, a by-product of increase lipid peroxidation (Figure 6.6C). Contrastingly, transient DGAT1 over-expression led to a reduction in protein attachment of 4-Hydroxynonenal (4HNE) in both melanoma cell lines and also in in zebrafish tumors over- expressing Dgat1a (Figure 6.6C-D).

In order to assess the impact of lipid peroxide driven ferroptosis in the reduction in melanoma cell survival that we observed upon antagonism of DGAT1, we used ferrostatin-1 (Ferro-1), a potent inhibitor of ferroptosis. Addition of Ferro-1 partially rescued the reduction in cell number observed upon DGAT1 inhibition, an effect also observed with the ROS scavenging agents Tempol and Ebselen (Figure 6.6E). However, unlike Ebselen or Tempol, the addition of Ferro-1 did not rescue induction of apoptosis driven by DGAT1 inhibition, this is expected as ferroptosis is an apoptosis-independent form of cell death (Figure 6.6E). Combining Ferro-1 with either Tempol or Ebselen led to the greatest rescue of the reduction in cell number upon DGAT1 inhibition and surprisingly also led to an increased rescue of apoptosis driven by DGAT1 inhibition when compared to the use of Tempol and Ebselen alone (Figure 6.6E). This data indicates that DGAT1 acts to supress lipid peroxidation in both cell lines and tumours and that the reduction in melanoma cell number upon DGAT1 inhibition is, in part, due to lipid peroxide driven ferroptosis.

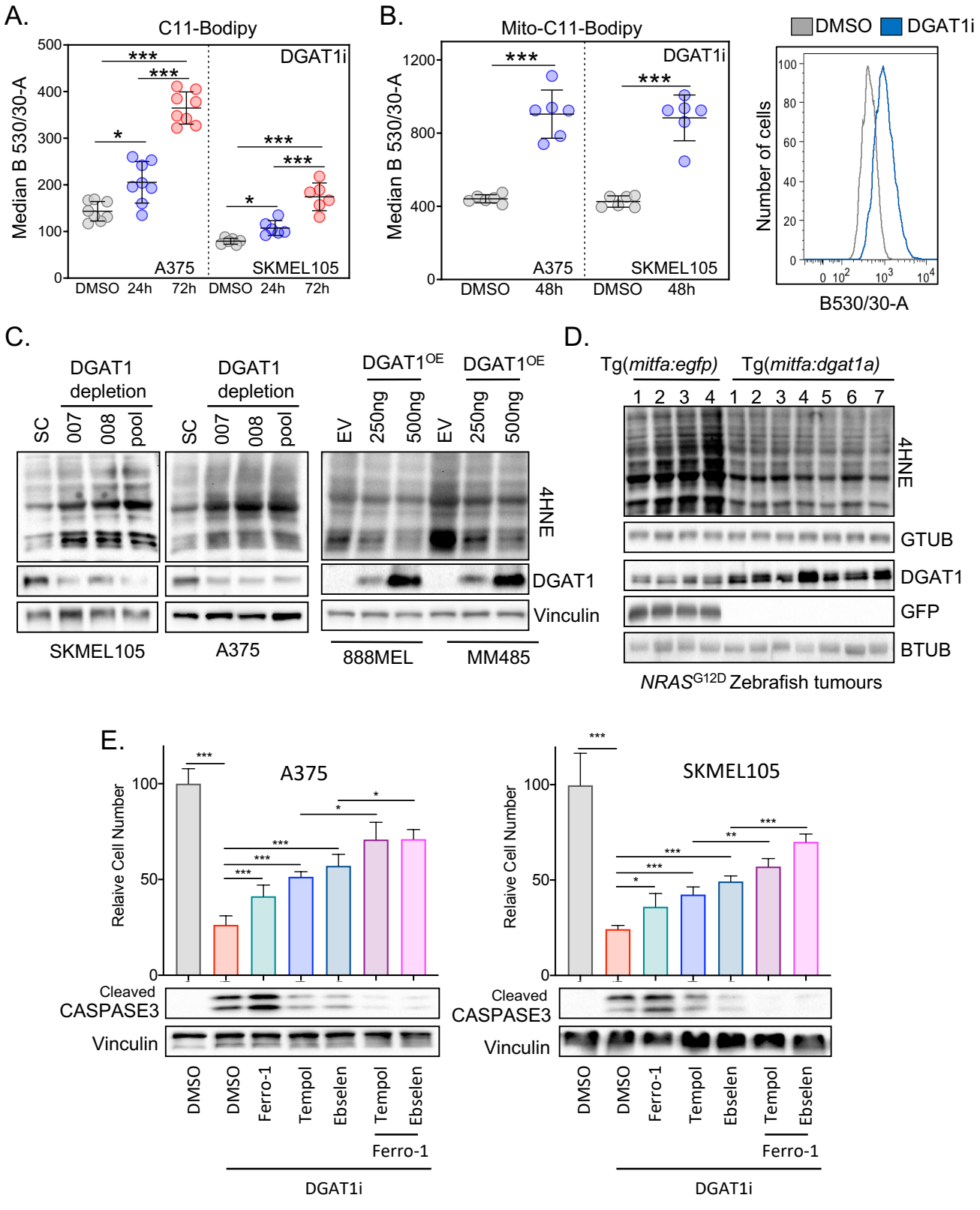
A.
C11-Bodipy
DGAT1i
Median B 530/30-A
A375
SKMEL105
DMSO 24h 72h DMSO 24h 72h
B.
Mito-C11-Bodipy
DGAT1i
Median B 530/30-A
A375
SKMEL105
DMSO 48h DMSO 48h
DMSO
DGAT1i
Number of cells
B530/30-A
C.
DGAT1 depletion
DGAT1 depletion
DGAT1OE
DGAT1OE
SC
007
008
pool
SC
007
008
pool
EV
250ng
500ng
EV
250ng
500ng
4HNE
DGAT1
Vinculin
SKMEL105
A375
888MEL
MM485
D.
Tg(mitfa:egfp)
Tg(mitfa:dgat1a)
1 2 3 4 1 2 3 4 5 6 7
4HNE
GTUB
DGAT1
GFP
BTUB
NRASG12D Zebrafish tumours
E.
A375
SKMEL105
Relaive Cell Number
Cleaved CASPASE3
Vinculin
DMSO
DMSO
Ferro-1
Tempol
Ebselen
Tempol
Ebselen
Ferro-1
DGAT1i

Figure 6.6 DGAT1 negatively regulates lipid peroxide generation and ferroptosis

(A) Indicated cell lines stained with C11-Bodipy following treatment with A922500 for 24-72 h. Median fluorescence was determined using flow cytometry (Median± SD, n>6) (two-way Anova). (B) Indicated cell lines stained with Mito C11-Bodipy following treatment with A922500 for 24-72 h. Median fluorescence was determined using flow cytometry (Median± SD, n>6) (two-way Anova). (C) Protein expression of DGAT1 and 4-Hydroxynonenal following transfection with either DGAT1 targeting siRNA or a scrambled control for 48 h. (Left) Protein expression of DGAT1 and 4-Hydroxynonenal following transfection with either DGAT1 over-expression vector or an empty vector control for 48 h (Right). (D) Protein expression of Dgat1, GFP and 4-Hydroxynonenal in NRASG12D-positive GFP- expressing (n=4) and NRASG12D-positive Dgat1a over-expressing (n=7) tumors. (E) Relative cell number following crystal violet staining, indicated cells were either with/without A922500, Ferrsostatin-1, Ebselen and Tempol (Upper) (one-way Anova). Corresponding protein expression of cleaved caspase-3 in indicated cell lines.

Not all cells underwent ferroptosis or apoptosis upon antagonism of DGAT1. A fraction of melanoma cells survived, indicating that not all cells produce toxic levels of ROS upon DGAT1 inhibition due to the activation of a potent anti-ROS mechanisms. Therefore, we next wanted to explore the potent anti-ROS mechanisms which were acting to counteract the induction of toxic levels of ROS and apoptosis induced upon DGAT1 suppression. Investigation into the anti-ROS response downstream of DGAT1 may lead to the identification of targets which may synergise with DGAT1 inhibition to induce melanoma cell death. Our mass spec analysis revealed enrichment of NRF2 signaling upon inhibition of DGAT1, and qPCR analysis of NRF2 target genes revealed SENS2 as a highly upregulated gene product upon DGAT1 inhibition (Figure 6.1 B-C). Therefore, we next confirmed increased protein expression of SESN2 upon DGAT1 inhibition in a panel of $DGAT1^{High}$ and $DGAT1^{AMP}$ melanoma cell lines; all cell lines responded similarly with the highest levels of SENS2 expression observed at 72 h (Figure 6.7A). Combined siRNA knockdown of SESN2 and DGAT1 inhibition led to a significant increase in both gene expression of the ROS response gene HMOX1 and increased production of ROS in melanoma cells (Figure 6.7 B-D). Moreover, combined knockdown of SESN2 and DGAT1 led to a significant decrease in melanoma cell proliferation and significant increase in melanoma cell apoptosis over 72 h when compared to DGAT1 knockdown alone (Figure 6E). An increase in melanoma cell apoptosis was also observed when combining knockdown of SESN2 with pharmacological inhibition of DGAT1 in $DGAT1^{High}$ melanoma cells (Figure 6.7F). Thus, we can conclude that SESN2 acts as a counterfoil to DGAT1, co-ordinating anti-ROS mechanisms downstream of DGAT1 inhibition, aiding in preventing ROS induced melanoma cell death.

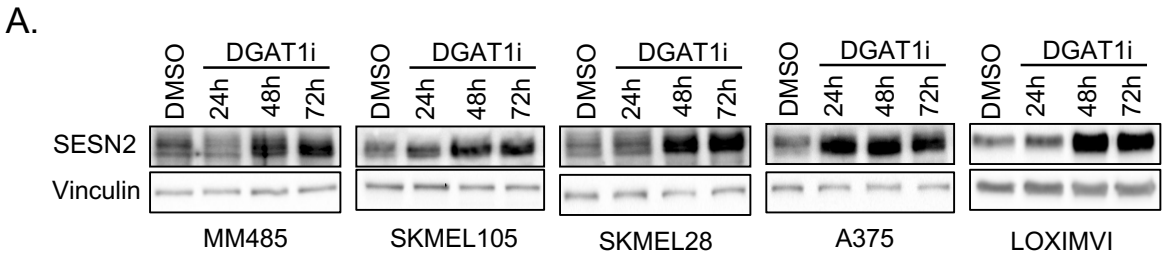
A.
DMSO
DGAT1i
24h
48h
72h
SESN2
Vinculin
MM485
SKMEL105
SKMEL28
A375
LOXIMVI

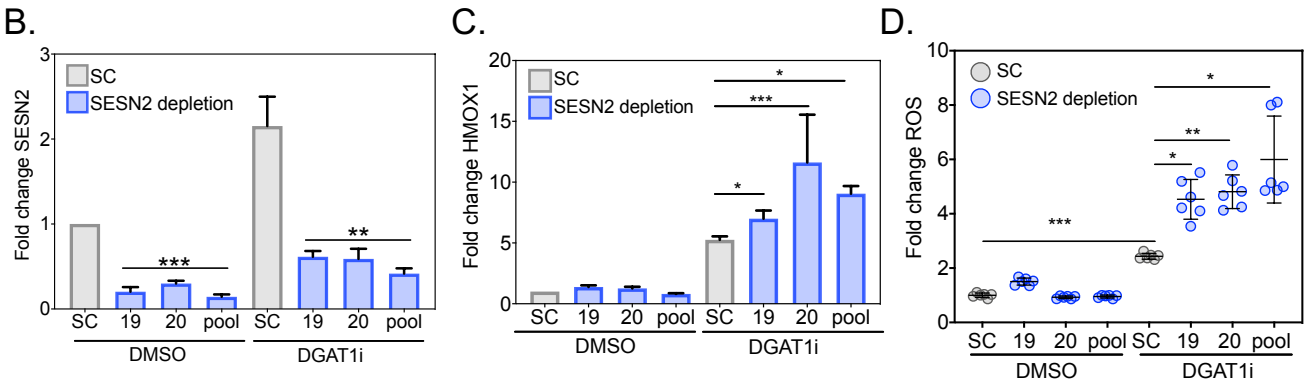
B.
Fold change SESN2
SC
SESN2 depletion
C.
Fold change HMOX1
D.
Fold change ROS
SC 19 20 pool SC 19 20 pool
DMSO
DGAT1i

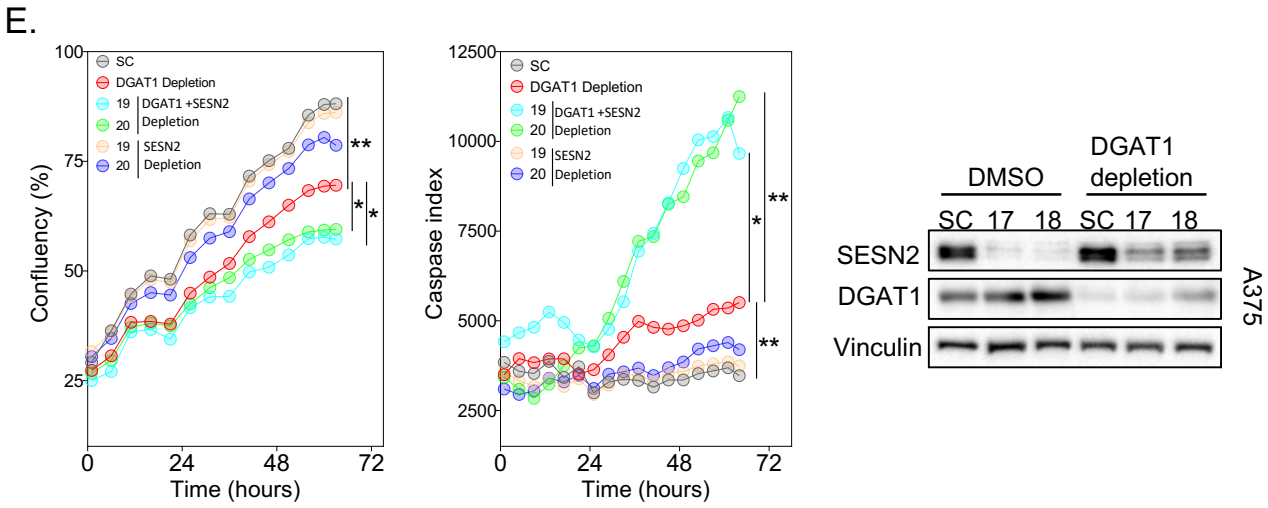
E.
Confluency (%)
SC
DGAT1 Depletion
19 20 DGAT1 +SESN2 Depletion
19 20 SESN2 Depletion
Time (hours)
Caspase index
DMSO
DGAT1 depletion
SC 17 18 SC 17 18
SESN2
DGAT1
Vinculin
A375

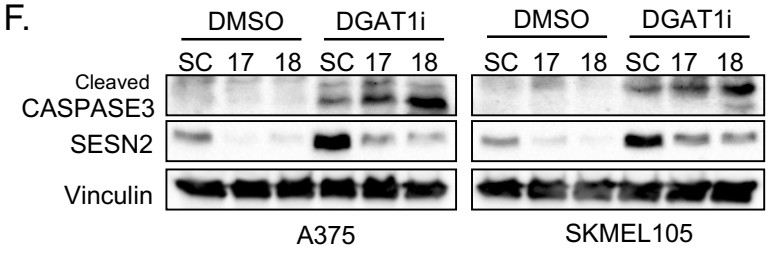
F.
DMSO
DGAT1i
SC 17 18 SC 17 18 SC 17 18 SC 17 18
Cleaved CASPASE3
SESN2
Vinculin
A375
SKMEL105

Figure 6.7 SESN2 expression is increased by DGAT1 suppression and co-ordinates cellular ROS response

(A) Protein expression of SESN2 in indicated melanoma cell lines treated with A922500 for 24, 48, or 72 h. (B) Relative SESN2 expression A375 cells transfected with SESN2 targeting siRNA (19, 20) or a scrambled control followed by treatment with A922500 for 24h. Fold-change calculated relative to DMSO treated control (Mean ± SD, n=3) (one-way Anova). (C) as for (B) but relative HMOX1 expression. (D) Quantification of ROS levels using dihydroethidium fluorescence (ex 480nm, em 570nm) following treatment of A375 cells with/without A922500 for 24 h and transfection with either a SESN2 targeting siRNA or a scrambled control. Fluorescence was normalised to relative cell number using crystal violet staining. Fold-change calculated relative to scrambled treated control (Mean± SD, n>4) (one-way Anova). (E) Confluency curves of A375 cells transfected with either SESN2 or DGAT1 targeting or scrambled siRNA (Mean, n=3) (one-way Anova) (Left). Corresponding cleaved-caspase index (Middle). Corresponding protein expression of DGAT1 and Sestrin 2 (Right). (F) Protein expression of SESN2 and Caspase 3 in indicated cell lines following transfection with SESN2 targeting siRNA or a scrambled control and treatment with/without A922500 for 24 hours.

6.4 Discussion

In this part of the study, we investigated the impact of DGAT1 modulation on human melanoma cell line survival. In agreement with our observations that long term DGAT1 inhibition leads to a build-up of AcCa species, indicative of increase FAO, unbiased MS-based whole proteome analysis of DGAT1^{High} melanoma cells also indicated that long term DGAT1 inhibition led to an increase in FAO. Gene-set enrichment analysis of up-regulated proteins demonstrated that long term DGAT1 inhibition in DGAT^{High} melanoma cells caused lipid metabolic reprogramming, with enrichment of PPAR signalling, SBREP signalling and FAO signalling observed. Increases in gene products involved in FAO and lipid metabolic reprogramming upon DGAT1 inhibition were confirmed in two DGAT1^{High} melanoma cell lines using RTqPCR, indicating that, as with the increases in AcCa species observed, this is not just a cell line specific effect. The alterations observed may be due to an excess of FFA in melanoma cells upon DGAT1 inhibition which are known to modulate PPAR and SREBP-1 activity[612–614], direct measurements of FFA using available colorimetric or fluorometric assay kits would confirm this hypothesis.

Strikingly, gene-set enrichment analysis also highlighted that DGAT1 inhibition led to enrichment of proteins involved in the cellular anti-ROS response modulated by NRF2, activated when ROS levels become toxic in order to remove ROS species and help cells survive. Increased expression of NRF2 target genes involved in ROS scavenging and breakdown, such as SOD1/2 and HMOX-1, at both the mRNA level and protein level were confirmed by our MS-based whole proteome analysis. Direct measurement of ROS levels using multiple cell permeable fluorogenic probes indicated that, in agreement with an activation of an anti-ROS response, pharmacological inhibition or siRNA knockdown of DGAT1 leads to an increase in cellular ROS and specifically increases mitochondrial ROS species. Again, this was demonstrated in multiple DGAT1^{High} melanoma cell lines with both oncogenic BRAF and NRAS mutations and using two DGAT1 inhibitors. Increased ROS levels have been shown to lead to cancer cell death by overwhelming the anti-oxidant response and

tipping the balance from the tumour promoting roles of ROS towards tumour inhibitory roles[549,550]. Inhibition of DGAT1 lead to apoptosis in DGAT1^{High} melanoma cells from 48 h. Addition of the ROS scavenging agents Ebselen[615] and Tempol[616] partially rescued apoptotic cell death upon DGAT1 knockdown in two DGAT1^{High} melanoma cells, confirming that the apoptosis observed in melanoma cells is ROS induced. Concurrent to the observed increases in cellular and mitochondrial ROS, we also observed increased lipid peroxidation upon DGAT1 inhibition both generally, and specifically in the mitochondria. Lipid peroxides are generated when PUFA react with oxygen-centred radicals and are highly toxic ROS species and can induce a none apoptotic form of cell death termed ferroptosis[306,535]. Using ferrostatin-1 an inhibitor of ferroptotic cell death[617] we demonstrated that the reduction in melanoma cell number observed upon long term DGAT1 inhibition is, in part, due to a build-up of lipid peroxides and ferroptosis. Interestingly, the use of ferrostatin-1 in combination with either tempol or Ebselen led to the greatest rescue of melanoma cell apoptosis upon DGAT1 inhibition, despite treatment with ferrostatin-1 alone in combination with DGAT1 inhibition having no impact upon melanoma cell apoptosis. The mechanism behind this is not clear, it may be that lipid peroxides, as well as inducing ferroptosis, have impacts on mitochondrial health that ROS scavengers cannot stop. Thus, as well as ferroptosis, lipid peroxides may contribute to apoptosis, but only when other ROS species that may have larger impacts upon mitochondrial health and apoptosis induction are at lower levels. Further insight into the links between ROS, mitochondrial health, ferroptosis and apoptosis could be gleaned through carrying out further combination studies using the different inhibitors, investigating the impact upon ROS and lipid peroxide levels using the fluorescent dyes we have already used , and investigating mitochondrial health using the seahorse analyser. In agreement with our data, a study in glioblastoma cells also observed increases in ROS levels and induction of apoptosis upon DGAT1 inhibition, which was partially rescued through the addition of a ROS scavenging agent[391].

It appears, in part, that the oncogenic role of DGAT1 is maintaining cellular REDOX homeostasis through the sequestration of FFA into LD, to prevent mitochondrial overloading and ROS production, and through preferentially sequestering PUFA into LD, protecting them from oxygen-centred radicals and lipid peroxidation. In agreement with this, over-expression of DGAT1 in a DGAT1^{Low} melanoma cell line led to increased resistance to ROS induced cell death. Additionally, under conditions of cellular stress known to lead to increased ROS production, such as nutrient stress and hypoxia, stable over-expression DGAT1 led to lower levels of activation of anti-ROS pathways, as shown by decreased levels of SOD1, and a reduction in melanoma cell death compared to parental controls. Moreover, in line with a role in sequestering PUFA to prevent the production of toxic lipid peroxides, transient overexpression of DGAT1 led to a decrease in increased protein attachment of 4-Hydroxynonenal (4HNE), a by-product of lipid peroxidation, both *in vitro* and *in vivo,* in our oncogenic NRAS driven zebrafish model of melanoma. Therefore, both *in vitro* and *in vivo* DGAT1 plays a key role in preventing a build-up of toxic lipid peroxides. This is in agreement with a study in breast cancer which demonstrated that DGAT1 was critical in sequestering PUFA in LD to prevent lipid peroxide formation[290], as was also demonstrated in drosophila[483].

In order to further prove our hypothesis, that it is a flux of FFA into the mitochondria and aberrant FAO that is behind the increases in ROS observed, and to further investigate the mechanism behind this, there are several experiments that could be carried out in addition to the direct measurement of FA. Firstly, as in the previous chapter where we used the CPT1 inhibitor etomoxir[618] to demonstrate that increased import of FA into the mitochondria was the reason that DGAT1 inhibition led to a loss of mitochondrial membrane potential, a similar experiment could be carried out, this time investigating the impact of CPT1 inhibition on ROS production and mitochondrial ROS production. The specific role of mitochondrial ROS in melanoma cell apoptosis upon DGAT1 inhibition could also be investigated through the use of the mitochondrial specific ROS scavenger Mitotempo[619], and experiments similar to those we undertook using the ROS scavengers tempol and Ebselen. Further evidence

for the role of DGAT1 in sequestering PUFA and preventing the formation of lipid peroxides could be achieved through experiments feeding PUFA, such as arachidonic acid[620], to both DGAT1^{Low} 888MEL melanoma cells and clone 3 DGAT1 over-expressing cells and exposing them to conditions that would induce cellular stress and ROS such as nutrient starvation or hypoxia. Cells could also be treated with ROS inducing agents such as paraquat and menadione, followed by assessment of both lipid peroxidation and melanoma cell survival. We would anticipate that the over-expression of DGAT1 would facilitate the sequestration of PUFA and protect them from peroxidation by oxygen centred radicals and therefore increase melanoma cell survival under conditions of cellular stress and PUFA excess. The same experiments could also be carried out with knockdown or inhibition of DGAT1, and would be expected to decrease melanoma cell survival under cellular stress and PUFA excess.

In contrast to DGAT1, pharmacological inhibition or knockdown of DGAT2 did not lead to increased ROS production or melanoma cell apoptosis. Again, this highlights that although DGAT2 is able to catalyse the same reaction synthesising TAG[325], DGAT1 plays a specific role in melanoma cells in modulating both LD formation and cellular REDOX. This may be due to a number of factors such as, expression level, cellular location or a substrate preference of LCFA and PUFA. Although further work would need to be carried out to confirm these hypotheses.

The pharmacological inhibition or siRNA knockdown of DGAT1 only led to melanoma cell death in a proportion of melanoma cells. Our proteomic analysis indicated that inhibition of DGAT1 led to activation of anti-ROS mechanisms, which may be preventing a toxic build-up of ROS in surviving melanoma cells. We found SESN2 to be highly up regulated at both the mRNA and protein level upon DGAT1 inhibition in a panel of DGAT1^{High} melanoma cell lines. SESN2 expression is increased upon oxidative stress in a NRF2-dependent manner, through an ARE site present in the promoter of SESN2[621]. The role of SENS2 in the cellular antioxidant pathway is thought to be two-fold. Firstly, SENS2 is able to breakdown ROS itself through an N-

terminal subdomain with an oxidoreductase motif which is able to reduce alkylhydroperoxide radicals[622]. Secondly, and considered the primary role of SESN2, is modulating the expression of other key ROS scavenging enzymes, through activation and stabilisation of NRF2. SESN2 does this by interacting with KEAP1, a negative regulator of NRF2, and the autophagic factor p62, leading to autophagic degradation of KEAP1 and activation of NRF2, which can then activate the expression of key enzymes involved in ROS breakdown[623]. Our data is in agreement with the known roles of SENS2 in the cellular anti-ROS response, knockdown of SENS2 in combination with DGAT1 inhibition leads to a significant increase in both ROS levels. Perhaps surprisingly, gene expression levels of HMOX-1 were significantly increased upon SESN2 knockdown. This may be due to other ROS induced mechanisms able to modulate NRF2 activity and a consequence of the increase in ROS levels observed upon combined antagonism of SENS2 and DGAT1. Other NRF2 targets could also be investigated such as NQO1, SOD1/2 and catalase at both the gene and protein expression level to further confirm this hypothesis. Concurrent with increased in ROS levels observed upon combined antagonism of SESN2 and DGAT1, when compared with DGAT1 antagonism alone, an increase in melanoma cell apoptosis is also observed. SESN2 appears to act as a counterfoil to DGAT1, ameliorating the effects of DGAT1 inhibition on melanoma cell proliferation and survival through anti-ROS mechanism.

Interestingly, SESN2 is also a regulator of mTOR signalling, inhibiting mTOR activation through two mechanisms. Firstly, through direct interaction with GATOR2, liberating GATOR1 from GATOR2 mediated inhibition, making it free to inactivate mTOR[624]. Secondly, through interacting with AMPK, promoting activating phosphorylation, and thus AMPK mediated mTOR inhibition[625]. Therefore, SENS2 could also be playing a role in the inhibition of mTOR-S6K signalling we see after antagonism of DGAT1. However, we would need to carry out further work looking at mTOR signalling downstream of combined SESN2 and DGAT1 antagonism over a time course, such as phospho-S6 and phospho-eEF2 and interaction between SESN2 and GATOR or AMPK, through co-immunoprecipitation. It is likely that if SESN2 is playing a role in the

inhibition of mTOR-S6K signalling downstream of DGAT1, it is through a different mechanism to oxidative stress induced expression increases. We do not see increase in cellular ROS levels in a timeframe that fits with the rapid inhibition of mTOR-S6K signalling we observed after DGAT1 inhibition.

Our data potentially highlights DGAT1 inhibition as a novel therapy for use in melanoma, as inhibition of DGAT1 causes ROS induced apoptosis and ferroptosis in melanoma cells. DGAT1 inhibition or shRNA knockdown has already been shown to reduce tumour growth in glioblastoma mouse xenograft models[476]. To further explore the therapeutic potential of DGAT1 inhibition, mouse xenograft models using DGAT1^{High} melanoma cells should be used to investigate the impact of DGAT1 inhibition in melanoma in an *in vivo* setting. Patient derived xenograft models with known DGAT1 amplifications and increases in DGAT1 expression level could also be used to investigate the therapeutic benefit of DGAT1 inhibition in melanoma but would only come after confirmation of a therapeutic benefit in xenograft models. Our data demonstrated that a proportion of melanoma cells survive DGAT1 inhibition, through the activation of the cellular anti-ROS response. We demonstrated that inhibition of part of the cellular anti-ROS response, through knockdown of SESN2, synergised with DGAT1 inhibition to increase both ROS levels and melanoma cell death. Inhibitors of SENS2 have not yet been developed, however inhibitors of other key anti-ROS enzymes such as SODs, HMOX and catalase are currently in development and may synergise with DGAT1 inhibition in melanoma [608–611]. Both *in vitro* experiments similar to that carried out in this study and *in vivo* mouse xenograft studies would enable the assessment of combination therapies targeting both DGAT1 and the enzymes critical in the cellular antioxidant response.

Overall, this section of the study demonstrated that DGAT1 plays a key role in modulating cellular REDOX, by both maintaining mitochondrial function and sequestering PUFA in LD, both of which prevent a toxic build-up of ROS. Therefore, amplification of DGAT1 in melanoma cells is advantageous in the high ROS conditions

often observed in cancer cells. Our results also indicted that DGAT1 inhibition may provide a therapeutic benefit in the treatment of melanoma, however as outlined above, more work needs to be done to explore this hypothesis.

Chapter 7- General Discussion

Despite the development and success of both targeted and immune based therapies, if diagnosed with late-stage melanoma, only 50% of patients survive for more than one year. Moreover, multiple resistance mechanisms exist to both targeted therapies, in the form of BRAF and MEK inhibitors, and immunotherapies, such as anti-PD1 and anti-CTLA4. These therapies focus predominantly on targeting only a few cancer hallmarks including sustained proliferation, resistance to cell death and evasion of the immune system. One further cancer hallmark that is perhaps therapeutically untapped is dysregulated cellular energetics, specifically the role of dysregulated lipid metabolism. The key role of dysregulated lipid metabolism is becoming increasing clear and encompasses more than just increased FA uptake and lipid synthesis. Here, we have uncovered the amplification and up-regulation of a novel and bone fide oncogene DGAT1, which allows for the increased storage of FA in cancer cells, promoting melanoma development and growth.

Using cross-species oncogenomic analysis encompassing RAS and BRAF driven zebrafish melanoma models and using the TGCA SKCM data set, we identified DGAT1 as amplified and upregulated in melanoma. High levels of DGAT1 expression were also associated with a worse melanoma patient survival. *DGAT1* is located on human chromosome 8 and is co-amplified along with other putative oncogenes *GDF6, MYC* and *ASAP1;* both *GDF6 and MYC* have been previously shown to play a role in promoting melanoma tumour initiation and growth using *in vivo* models. However, we only found *DGAT1*/dgat1a and *GDF6/*gdf6b to be amplified in a mutant BRAF driven zebrafish melanoma model and, of these four putative oncogenes, only high DGAT1 expression to be predictive of melanoma survival. Thus, we identified DGAT1 as having all the genetic hallmarks of a melanoma oncogene. Using the lineage restricted miniCoopR system we demonstrated that DGAT1 is indeed a *bona fide* melanoma oncogene, as the melanocyte specific over-expression of DGAT1/Dgat1a accelerated both mutant BRAF and mutant NRAS driven zebrafish melanoma and

strikingly, induced melanoma formation in zebrafish melanocytes only lacking in functional p53.

The cross-species oncogenomic approach we took comparing zebrafish and human melanoma to identify DGAT1 has been used to identify other putative tumour promoting genetic alterations such as *GDF6*[390] and *SETB1*[343] in melanoma and novel oncogenic genetic alterations and novel oncogenic events in both rhabdomyosarcoma and T-cell acute lymphoblastic leukaemia[399,400]. Underpinning the use of cross-species oncogenomic approaches using zebrafish and human genomic data is the high degree of conservation between zebrafish and human genes involved in tumorigenesis[365,366]. Moreover, the miniCoopR system we used to investigate the oncogenic potential of DGAT1 has also been used to establish other oncogenic modifiers in melanoma such as *SETDB1*[343], *GDF6*[390], *LPL*[267] and *FATP1*[266]. It is not only zebrafish that have been used in powerful cross-species oncogenomic approaches, but also genetically defined mouse tumour models have been used to identify oncogenic genetic events. *NED9* was identified as a metastasis gene in melanoma[626] and *YAP1* and *DLC1* were identified to drive tumorigenesis in hepatocellular carcinoma[627,628]. The development of high resolution genomic sequencing has led to a wealth of genomic data across many cancer types, with the challenge now to identify driver events amongst a vast number of genetic alterations, which in melanoma is more than 10 per Mb[59]. Here, in identifying DGAT1 as novel metabolic oncogene in melanoma, we have confirmed the power of cross-species genomic approaches to sift through and identify conserved genetic events, with relevance to human disease. This is an approach that has been taken to highlight other putative driver events in tumour development, as outlined above, and will continue to be a key method used to identify oncogenic events in tumours.

Our identification of DGAT1 as a lipid metabolic oncogene in melanoma adds to a growing weight of evidence for the importance of lipid metabolism in melanoma development and progression. Genetic alterations and altered expression profiles

have been identified in melanoma encompassing FA synthesis, catabolism and uptake, enrichment of genes involved in both FA uptake and catabolism has been shown to be predictive of a worse patient outcome in melanoma[247]. Moreover, genes involved in FA uptake such as the FABP family, FATP family, CD36 and LPL have also been shown to be important in multiple aspects of melanoma progression such as proliferation, invasion and metastasis[261–267]. Increased lipid synthesis is also observed in melanoma[251,252], constitutive MAPK signalling drives an increase in FASN expression, which is associated with metastasis and is associated with worse patient outcome[253–255]. Furthermore, alterations in FAO through the upregulation of CPT2, important for translocation of FA into the mitochondria, has also been demonstrated to be important for metastasis; metastatic cells have been shown to be more reliant on FAO[261,271]. Although important for melanoma progression, none of these lipid metabolic genes have been shown to be truly oncogenic and induce melanoma formation in the absence of either oncogenic NRAS or BRAF as we have shown for DGAT1/Dgat1a. This indicates that the storage of FA is perhaps central to the altered lipid metabolic phenotype in melanoma cells. We find *DGAT1* to be amplified and up-regulated in both BRAF and NRAS mutant melanoma and increased FA uptake has been observed in both mutant RAS driven and mutant BRAF driven melanoma. Thus, the altered lipid metabolic phenotype in melanoma appears to be independent of the oncogenic driver mutation. Further investigation into the interplay between FA synthesis, uptake, catabolism and storage and their role in the stages of melanoma progression from development through to metastasis, using models like our zebrafish model in Chapter 3, would shed new light onto the dependency of melanoma cells on lipid metabolism and perhaps provide new therapeutic opportunities. Moreover, this understanding would allow the identification of lipid metabolic gene signatures, predictive of melanoma dependency on lipid metabolism, and allow for selection of patients that would gain the most benefit.

In addition to melanoma, we found *DGAT1* to be amplified in a large number of cancer types; 6 % of all cancer patients in the TGCA dataset and 15 % of cell lines in the cancer cell line encyclopaedia. Yet, this data doesn't account for up-regulation of

DGAT1 mRNA through transcriptional mechanisms. In melanoma, high DGAT1 mRNA levels are found in 16 % of samples, compared to 7 % with amplification of DGAT1 (TGCA SKCM dataset). Therefore, just investigating amplification of DGAT1 in multiple cancer types is possibly an underestimation of the frequency of tumours that may be dependent on DGAT1. This is in agreement with studies that demonstrate an up-regulation of DGAT1 expression in prostate cancer cell lines and glioblastoma models when compared to untransformed tissue[340,476]. Furthermore, abundant LD have been observed across numerous cancer types[275,629], which is consistent with amplified and up-regulated DGAT1. Future work should investigate whether DGAT1 is an oncogene in more cancer types using *in vivo* genetic models in mice. Ovarian cancer and invasive breast cancer were found to have the highest frequency of *DGAT1* amplification and have been shown to have altered lipid metabolism including both LD and increases in FA uptake linked with disease progression[290,630–634]. Our work has not only identified DGAT1 as a lipid metabolic oncogene in melanoma but also as a potential oncogene across a number of different cancer types.

Continuing our cross-species approach using zebrafish models and integrating multiple omics platforms including transcriptomics, proteomics, phospho-proteomics and lipidomics, combined with cellular assays assessing behaviour, signalling and stress, we identified the mechanisms by which DGAT1 promotes melanoma development and progression. Firstly, DGAT1 stimulates melanoma cell proliferation through driving mTOR-S6K signalling. Using transcriptomic analysis of DGAT1/Dgat1a over-expressing zebrafish tumours and DGAT1^{High} melanoma patients we found an enrichment of mTOR signalling, when assessing over lapping significantly enriched gene sets. Modulation of mTOR signalling by DGAT1 was confirmed in melanoma cell lines through phospho-proteomic analysis after DGAT1 inhibition which again found an enrichment of mTOR signalling and additionally the downstream regulator of mTOR signalling S6K, this finding was confirmed in a panel of DGAT1^{High} melanoma cell lines. Overexpression of S6K was able to partially rescue the growth inhibitory effects of DGAT1 antagonism, conversely inhibition of S6K

reduced the growth promoting effect of over-expression of DGAT1. It is not immediately clear the precise mechanism by which the enzymatic activity of DGAT1 impacts upon mTOR-S6K signalling. mTOR is a signalling hub integrating multiple cellular metabolic and growth signals, playing a key role in the regulation of cellular proliferation and growth and plays a role in lipid metabolism[411–413]. One such factor, maybe be changes in lipid species such as phosphatidic acid which is essential for mTOR activity[635], DAG which act as co-activators of PKC, which then inhibit mTOR signalling[636], or arachidonic acids which have also been shown to play a role in activating mTOR signalling[637]. Levels of these lipids could be altered by the action of DGAT1 sequestering FA and DAG into TAG species, however, changes in these species were not observed in our lipidomic analysis of melanoma cell lines or our DGAT1/Dgat1a over-expressing zebrafish melanoma model. It is an area of the study that warrants further investigation as active mTOR–S6K signaling has been shown to promote lipogenesis and LD biogenesis[638–640], suggesting an interplay between mTOR signaling and lipogenesis which is mutually re-enforcing.

In this study we did highlight one mechanism by which the enzymatic activity DGAT1 impacts upon mTOR signalling, this was through modulation of AMPK activation, which through interaction with RAPTOR is able to inhibit mTOR signalling. We found both short-term and long-term antagonism of DGAT1 led to AMPK activation. Furthermore, the suppression of S6K signalling upon short term DGAT1 inhibition was rescued by inhibiting AMPK. We hypothesise that the activation of AMPK upon DGAT1 is due to aberrant FAO, caused by a flux of FFA. Although we did not measure FAO directly, we observed an increase in AcCa species upon DGAT1 inhibition and concurrently a decrease in mitochondrial respiratory function and loss of mitochondrial membrane potential. Conversely, over-expression of DGAT1 in both a melanoma cell and zebrafish melanoma models led to a decrease in AcCa species. The timing of the observed increases in AcCa species and decreases in mitochondrial function were intimately linked with a decrease in TAG species and the number of LD in melanoma cells; in agreement with a role for LD in sequestering FFA and delivering it to mitochondria in a controlled manner. Our data demonstrated that DGAT1

promotes mitochondrial respiratory function by controlling FA flux into the mitochondria, and thereby supressing AMPK and promoting mTOR-S6K signalling. This in agreement with other studies in both glioblastoma and mouse embryonic fibroblast, which also find DGAT1 driven LD biogenesis to be critical in maintaining mitochondrial health[295,391].

The role of DGAT1 in maintaining mitochondrial health means it has a key role to pay in the maintenance of cellular REDOX-dependent processes, to which mitochondria are central. Mitochondria are both key generators of ROS and themselves highly sensitive to ROS levels[545–547]. In keeping with the timing of both decreases in LD droplet numbers and mitochondrial function, we observed significant increases in ROS species in melanoma cells, including lipid peroxides specifically in the mitochondria, upon DGAT1 antagonism. The increase in ROS levels upon DGAT1 antagonism impacted upon melanoma cell survival, causing melanoma cell death through both ferroptosis and apoptosis and can be rescued through the use of both ROS scavenging agents and an inhibitor of ferroptosis, ferrostatin-1. Conversely, over-expression of DGAT1 in melanoma cell lines led to a reduction in lipid peroxide by-products, such as 4-HNE, and increased resistance to ROS inducing agents. A decrease in lipid peroxide driven 4-HNE was also observed upon DGAT1/Dgat1a over-expression in our zebrafish melanoma model and could be linked to the increases in TAG species with high number of double bonds in our lipidomic analysis, indicating increased sequestration of PUFA. PUFA have been found to be selectively sequestered in LD in breast cancer and drosophila models[290,483]. Therefore up-regulation of DGAT1 confers a double protection from ROS induced cell death, firstly through modulating FAO driven ROS production and the sequestration of highly ROS sensitive PUFA in lipid droplets protecting them from ROS.

LD have been shown to protect cells from a variety of cellular stresses often found in the tumour microenvironment, including hypoxia and nutrient deprivation. LD formation is increased under condition of cellular stress, which is surprising due to

TAG synthesis being an ATP consuming process[294–296]. Under nutrient stress and hypoxia, LD firstly prevent lipotoxicity due to a release of FA through autophagy [295] and preventing the build-up of saturated lipid species [304]. Secondly, LD provide storage of FA which can be transferred to the mitochondria in a highly efficient manner for ATP production through FAO, enabling cell growth[297,298,301]. LD also act as a source of unsaturated FA, not just for energy production but also essential in membrane fluidity and cell survival, which is increasingly important under conditions of cellular stress that impacts upon both FA synthesis and uptake[304]. This role for LD under conditions of cellular stress is consistent with what we observed in our melanoma cell lines, in which exposure to either hypoxia or nutrient stress exacerbated the impact of DGAT1 inhibition on melanoma cell survival. Conversely, the growth advantage conferred by over-expression of DGAT1 was the greatest under conditions of cellular stress.

Our study focused on the role of DGAT1 in modulating melanoma cell proliferation, cellular metabolism and energetics and survival. However, one aspect of cancer progression that we have not focused on is metastasis. Dis-regulated lipid uptake, anabolic and catabolic processes have been shown to contribute to cancer cell motility , invasion and metastasis[641], as discussed in depth in the Introduction. Furthermore, multiple studies have now demonstrated cross-talk between cancer cells and adipocytes that drive cancer cell proliferation , invasion and metastasis[266,631,642–644]. One study has directly linked LD to metastasis and demonstrated LD are essential for acidosis induced metastasis[645]. Conversely, the induction of oxidative stress and ferroptosis, as we have observed upon DGAT1 antagonism, has been shown to reduce cancer metastatic spread[646,647]. DGAT1 may promote metastasis through two mechanisms allowing for increased uptake and safe storage of FA in LD and preventing lipotoxicity and maintaining cellular REDOX. FA derived from LD can then be used in FAO to provide ATP to meet energetic demands of metastasis. Further experiments investigating the role of DGAT1 modulation in metastasis should carried out, through the use of *in vitro* migration and invasion assays, *in vivo* assays such as zebrafish xenografts which allow the visualisation of

individual cells migrating from the tumour mass[648] and mouse models in which cells can be luciferase labelled, again, to allow for the visualisation of metastatic spreading[649].

Our data demonstrating the induction of oxidative stress upon DGAT1 inhibition, causing melanoma cell death through apoptosis and ferroptosis indicates that DGAT1 may be a therapeutic target in melanoma. DGAT1 inhibition has now been shown to reduce tumour growth in glioblastoma mouse xenograft models. The focus of future work in the importance of DGAT1 in melanoma should be its therapeutic potential. The use of mouse xenograft studies using DGAT1^{High} melanoma cell lines would allow for further investigation into the therapeutic benefits of DGAT1 inhibition in an *in vivo* setting. It would also allow investigation into any potential toxicities that may occur upon inhibition of DGAT1, although ROS induction was not observed with DGAT1 inhibition in mouse embryonic fibroblasts, indicating that there may be a level of tumour selectivity[295]. Although clinical trials using DGAT1 inhibitors to treat diabetic patients did find diarrhoea (due to blocking fat absorption through the gut) as a side effect and this would have to be managed in patients[650]. However, our data also demonstrated that a portion of melanoma cells survive DGAT1 inhibition, this is due to the activation of the anti-ROS response mediated by NRF2. This suggests that inhibition of DGAT1 would be more therapeutically beneficial as part of a combination therapy; our data highlighted a logical combination in which inhibiting part of the cellular anti-ROS response, in this case through knockdown of SESN2, synergised with DGAT1 inhibition caused a significant increase in melanoma cell death. There are currently no inhibitors of SESN2, however inhibitors of other key anti-ROS enzymes such as HMOX1 and SOD1 are available and SOD1 inhibitors have previously been tested in clinical trials on solid cancers[608–611,651]. Another possible rational therapy combination would be the use of Erastin, a compound known to induce ferroptosis in cancer cells *in vitro* and *in vivo*[652], alongside DGAT1 inhibition to further enhance ferroptosis driven by DGAT1 inhibition. Further combinations with DGAT1 inhibition could include the use of S6K inhibitors[473], which have been used

successfully to treat melanoma *in vivo,* or the use of BRAF+MEK inhibitors which are the current standard of care[158,165,166].

Although, not addressed in this study, the inhibition of DGAT1 in melanoma may also impact on the tumour immune microenvironment, and be of therapeutic benefit in combination with immune-checkpoint blockade therapies[189,191,192]. A study has recently shown that high levels of mitochondrial lipid metabolism in melanoma is associated with increased interferon signalling, higher levels of antigen presentation and response to immunotherapy. Furthermore, lipid peroxide adducts are found to be highly immunogenic and drive adaptive immune response in fatty liver disease[653]. Immunomodulatory lipids such as COX2 and arachidonic acid are found enriched in LD, and LD are the major site of synthesis of the immunomodulatory lipids PGE_2[654,655]. It has also been shown that the polarisation of tumour associated macrophages (TAM) towards a protumour immunosuppressive phenotype is dependent on LD control of LCFA metabolism[317]. We found in melanoma cells that upregulation of DGAT1 supressed both lipid peroxidation and FAO substrate production. As such, upregulation of DGAT1 in melanoma cells is likely to be immunosuppressive, whereas inhibition of DGAT1 might drive anti-tumour immune responses and synergise with current immunotherapies.

Overall, our data shows that increased DGAT1 expression through either transcriptional mechanisms or gene amplification is a beneficial adaptation of melanoma cells. High levels of DGAT1 permit the safe accumulation of FA into LD, these FA can be used as an energy source, for lipogenesis and acts as signalling molecules. The storage of FA in LD also protects from mitochondrial dysfunction, oxidative stress, lipotoxicity and prevents suppression of growth signaling through mTOR (Figure 7.1).

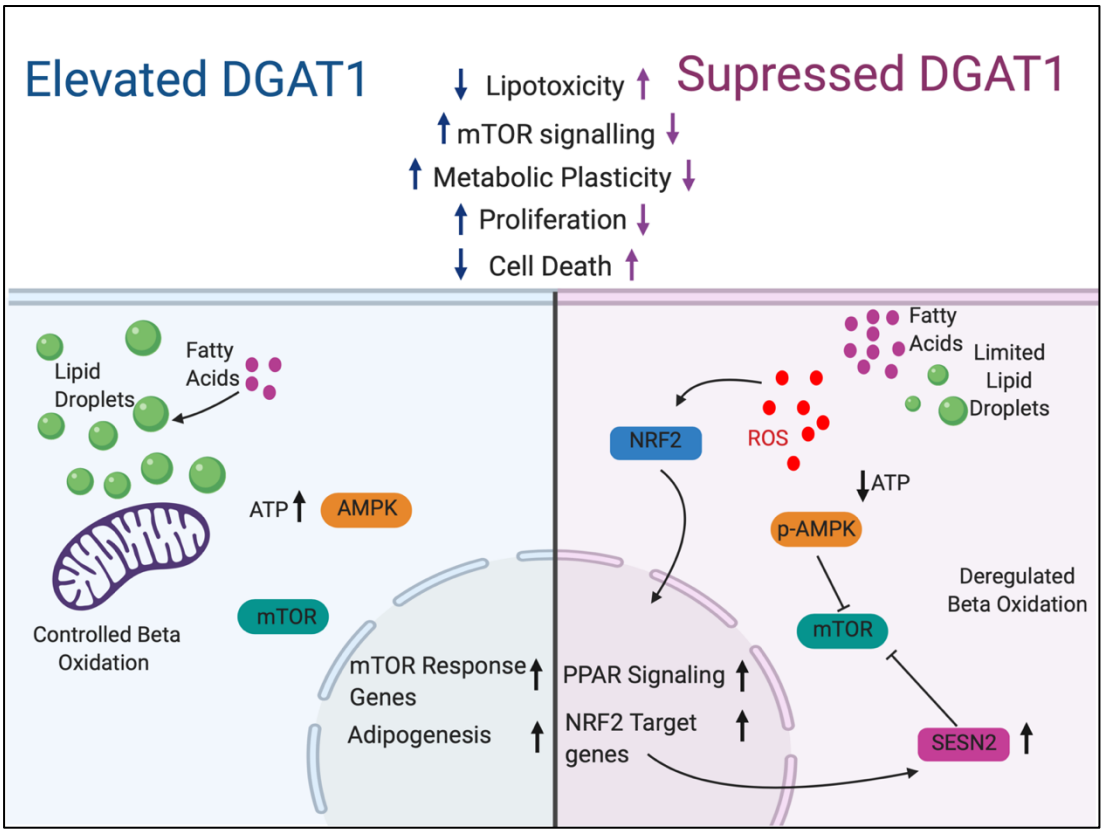

Figure 7.1 The Role of DGAT1 in melanoma

Figure made in Biorender.

References

1. Melanoma skin cancer statistics | Cancer Research UK. Available at: https://www.cancerresearchuk.org/health-professional/cancer-statistics/statistics-by-cancer-type/melanoma-skin-cancer. (Accessed: 18th February 2020)

2. Lin, J. Y. & Fisher, D. E. Melanocyte biology and skin pigmentation. *Nature* **445**, 843–850 (2007).

3. Kobayashi, N. *et al.* Supranuclear Melanin Caps Reduce Ultraviolet Induced DNA Photoproducts in Human Epidermis. *J. Invest. Dermatol.* **110**, 806–810 (1998).

4. Costin, G.-E. & Hearing, V. J. Human skin pigmentation: melanocytes modulate skin color in response to stress. *FASEB J.* **21**, 976–994 (2007).

5. Herrling, T., Jung, K. & Fuchs, J. The role of melanin as protector against free radicals in skin and its role as free radical indicator in hair. *Spectrochim. Acta Part A Mol. Biomol. Spectrosc.* **69**, 1429–1435 (2008).

6. Yaar, M. & Park, H. Y. Melanocytes: A window into the nervous system. *Journal of Investigative Dermatology* **132**, 835–845 (2012).

7. Dupin, E. & Le Douarin, N. M. Development of melanocyte precursors from the vertebrate neural crest. *Oncogene* **22**, 3016–3023 (2003).

8. Uong, A. & Zon, L. I. Melanocytes in development and cancer. *J. Cell. Physiol.* **222**, 38–41 (2010).

9. Pennello, G., Devesa, S. & Gail, M. Association of surface ultraviolet B radiation levels with melanoma and nonmelanoma skin cancer in United States blacks. *Cancer Epidemiol. Biomarkers Prev.* **9**, 291–297 (2000).

10. Gandini, S. *et al.* Meta-analysis of risk factors for cutaneous melanoma: II. Sun exposure. *Eur. J. Cancer* **41**, 45–60 (2005).

11. Elwood, J. M. & Jopson, J. Melanoma and sun exposure: An overview of published studies. *Int. J. Cancer* **73**, 198–203 (1997).

12. Green, A. *et al.* The association of use of sunbeds with cutaneous malignant melanoma and other skin cancers: A systematic review. *Int. J. Cancer* **120**, 1116–1122 (2006).

13. Goldstein, A. M., Struewing, J. P., Chidambaram, A., Fraser, M. C. & Tucker, M. A. Genotype-phenotype relationships in U.S. melanoma-prone families with CDKN2A and CDK4 mutations. *J. Natl. Cancer Inst.* **92**, 1006–10 (2000).

14. Tsao, H. & Niendorf, K. Genetic testing in hereditary melanoma. *J. Am. Acad. Dermatol.* **51**, 803–808 (2004).

15. Yokoyama, S. *et al.* A novel recurrent mutation in MITF predisposes to

familial and sporadic melanoma. *Nature* **480**, 99–103 (2011).

16. Dessinioti, C., Antoniou, C., Katsambas, A. & Stratigos, A. J. Melanocortin 1 Receptor Variants: Functional Role and Pigmentary Associations. *Photochem. Photobiol.* **87**, 978–987 (2011).

17. Gandini, S. *et al.* Meta-analysis of risk factors for cutaneous melanoma: I. Common and atypical naevi. *Eur. J. Cancer* **41**, 28–44 (2005).

18. Grob, J. J. *et al.* Count of benign melanocytic nevi as a major indicator of risk for nonfamilial nodular and superficial spreading melanoma. *Cancer* **66**, 387–395 (1990).

19. Watt, A. J., Kotsis, S. V. & Chung, K. C. Risk of Melanoma Arising in Large Congenital Melanocytic Nevi: A Systematic Review. *Plast. Reconstr. Surg.* **113**, 1968–1974 (2004).

20. Clark, W. H. *et al.* Model predicting survival in stage I melanoma based on tumor progression. *J. Natl. Cancer Inst.* **81**, 1893–1904 (1989).

21. Miller, A. J. & Mihm, M. C. Melanoma. *N. Engl. J. Med.* **355**, 51–65 (2006).

22. Davies, H. *et al.* Mutations of the BRAF gene in human cancer. *Nature* **417**, 949–954 (2002).

23. Pollock, P. M. *et al.* High frequency of BRAF mutations in nevi. *Nat. Genet.* **33**, 19–20 (2003).

24. Poynter, J. N. *et al.* BRAF and NRAS mutations in melanoma and melanocytic nevi. *Melanoma Res.* **16**, 267–273 (2006).

25. Michaloglou, C. *et al.* BRAFE600-associated senescence-like cell cycle arrest of human naevi. *Nature* **436**, 720–724 (2005).

26. Gray-Schopfer, V. C. *et al.* Cellular senescence in naevi and immortalisation in melanoma: A role for p16? *Br. J. Cancer* **95**, 496–505 (2006).

27. Weatherhead, S. C., Haniffa, M. & Lawrence, C. M. Melanomas arising from naevi and de novo melanomas ? does origin matter? *Br. J. Dermatol.* **156**, 72–76 (2007).

28. Bhatt, K. V. *et al.* Adhesion control of cyclin D1 and p27Kip1 levels is deregulated in melanoma cells through BRAF-MEK-ERK signaling. *Oncogene* **24**, 3459–3471 (2005).

29. Flores, J. F. *et al.* Loss of the p16INK4a and p15INK4b genes, as well as neighboring 9p21 markers, in sporadic melanoma. *Cancer Res.* **56**, 5023–32 (1996).

30. Sini, M. C. *et al.* Molecular alterations at chromosome 9p21 in melanocytic naevi and melanoma. *Br. J. Dermatol.* **158**, 243–250 (2008).

31. Guldberg, P. *et al.* Disruption of the MMAC1/PTEN gene by deletion or mutation is a frequent event in malignant melanoma. *Cancer Res.* **57**, 3660–

3663 (1997).

32. Stahl, J. M. *et al.* Loss of PTEN promotes tumor development in malignant melanoma. *Cancer Res.* **63**, 2881–2890 (2003).

33. Garraway, L. A. *et al.* Integrative genomic analyses identify MITF as a lineage survival oncogene amplified in malignant melanoma. *Nature* **436**, 117–122 (2005).

34. Danen, E. H. J. *et al.* E-cadherin expression in human melanoma. *Melanoma Res.* **6**, 127–131 (1996).

35. Haass, N. K., Smalley, K. S. M., Li, L. & Herlyn, M. Adhesion, migration and communication in melanocytes and melanoma. *Pigment Cell Res.* **18**, 150–159 (2005).

36. Stahl, J. M. *et al.* Deregulated Akt3 Activity Promotes Development of Malignant Melanoma. *Cancer Res.* **64**, (2004).

37. Huntington, J. T. *et al.* Overexpression of collagenase 1 (MMP-1) is mediated by the ERK pathway in invasive melanoma cells. Role of BRAF mutation and fibroblast growth factor signaling. *J. Biol. Chem.* **279**, 33168–33176 (2004).

38. Tas, F. Metastatic behavior in melanoma: Timing, pattern, survival, and influencing factors. *J. Oncol.* **2012**, (2012).

39. Hanahan, D. & Weinberg, R. A. Hallmarks of cancer: The next generation. *Cell* **144**, 646–674 (2011).

40. Duesberg, P. H. & Vogt, P. K. Differences between the ribonucleic acids of transforming and nontransforming avian tumor viruses. *Proc. Natl. Acad. Sci. U. S. A.* **67**, 1673–1680 (1970).

41. Stehelin, D., Varmus, H. E., Bishop, J. M. & Vogt, P. K. DNA related to the transforming gene(s) of avian sarcoma viruses is present in normal avian DNA. *Nature* **260**, 170–173 (1976).

42. Duesberg, P. H., Bister, K. & Vogt, P. K. The RNA of avian acute leukemia virus MC29. *Proc. Natl. Acad. Sci. U. S. A.* **74**, 4320–4324 (1977).

43. Bister, K. & Duesberg, P. H. Structure and specific sequences of avian erythroblastosis virus RNA: Evidence for multiple classes of transforming genes among avian tumor viruses. *Proc. Natl. Acad. Sci. U. S. A.* **76**, 5023–5027 (1979).

44. Vogt, P. K. Retroviral oncogenes: A historical primer. *Nature Reviews Cancer* **12**, 639–648 (2012).

45. Shih, T. Y., Weeks, M. O., Young, H. A. & Scolnick, E. M. Identification of a sarcoma virus-coded phosphoprotein in nonproducer cells transformed by Kirsten or Harvey murine sarcoma virus. *Virology* **96**, 64–79 (1979).

46. Hager, G. L. *et al.* Molecular cloning of the Harvey sarcoma virus closed circular DNA intermediates: initial structural and biological characterization.

J. Virol. **31**, 795–809 (1979).

47. Tsuchida, N. & Uesugi, S. Structure and functions of the Kirsten murine sarcoma virus genome: molecular cloning of biologically active Kirsten murine sarcoma virus DNA. *J. Virol.* **38**, 720–7 (1981).

48. Shih, C., Padhy, L. C., Murray, M. & Weinberg, R. A. Transforming genes of carcinomas and neuroblastomas introduced into mouse fibroblasts. *Nature* **290**, 261–264 (1981).

49. Der, C. J., Krontiris, T. G. & Cooper, G. M. Transforming genes of human bladder and lung carcinoma cell lines are homologous to the ras genes of Harvey and Kristen sarcoma viruses. *Proc. Natl. Acad. Sci. U. S. A.* **79**, 3637–3640 (1982).

50. Parada, L. F., Tabin, C. J., Shih, C. & Weinberg, R. A. Human EJ bladder carcinoma oncogene is homologue of Harvey sarcoma virus ras gene. *Nature* **297**, 474–478 (1982).

51. Hall, A., Marshall, C. J., Spurr, N. K. & Weiss, R. A. Identification of transforming gene in two human sarcoma cell lines as a new member of the ras gene family located on chromosome 1. *Nature* **303**, 396–400 (1983).

52. Bailey, M. H. *et al.* Comprehensive Characterization of Cancer Driver Genes and Mutations. *Cell* **173**, 371-385.e18 (2018).

53. Sherr, C. J. Principles of Tumor Suppression. *Cell* **116**, 235–246 (2004).

54. Prior, I. A., Lewis, P. D. & Mattos, C. A comprehensive survey of ras mutations in cancer. *Cancer Research* **72**, 2457–2467 (2012).

55. Garnett, M. J. & Marais, R. Guilty as charged: B-RAF is a human oncogene. *Cancer Cell* **6**, 313–319 (2004).

56. Adams, J. M., Gerondakis, S., Webb, E., Corcoran, L. M. & Cory, S. Cellular myc oncogene is altered by chromosome translocation to an immunoglobulin locus in murine plasmacytomas and is rearranged similarly in human Burkitt lymphomas. *Proc. Natl. Acad. Sci. U. S. A.* **80**, 1982–1986 (1983).

57. Tomlins, S. A. *et al.* Recurrent fusion of TMPRSS2 and ETS transcription factor genes in prostate cancer. *Science (80-.).* **310**, 644–648 (2005).

58. Ota, K. *et al.* Induction of PD-L1 expression by the EML4-ALK oncoprotein and down stream signaling pathways in non-small cell lung cancer. *Clin. Cancer Res.* **21**, 4014–4021 (2015).

59. Mar, V. J. *et al.* BRAF/NRAS wild-type melanomas have a high mutation load correlating with histologic and molecular signatures of UV damage. *Clin. Cancer Res.* **19**, 4589–4598 (2013).

60. Cohen, C. *et al.* Mitogen-actived Protein Kinase Activation Is an Early Event in Melanoma Progression. *Clin. Cancer Res.* **8**, (2002).

61. Goldsmith, Z. G. & Dhanasekaran, D. N. G Protein regulation of MAPK

networks. *Oncogene* **26**, 3122–3142 (2007).

62. Wellbrock, C., Karasarides, M. & Marais, R. The RAF proteins take centre stage. *Nat. Rev. Mol. Cell Biol.* **5**, 875–885 (2004).

63. Hillig, R. C. *et al.* Discovery of potent SOS1 inhibitors that block RAS activation via disruption of the RAS–SOS1 interaction. *Proc. Natl. Acad. Sci. U. S. A.* **116**, 2551–2560 (2019).

64. Simanshu, D. K., Nissley, D. V. & McCormick, F. RAS Proteins and Their Regulators in Human Disease. *Cell* **170**, 17–33 (2017).

65. Dhillon, A. S., Hagan, S., Rath, O. & Kolch, W. MAP kinase signalling pathways in cancer. *Oncogene* **26**, 3279–3290 (2007).

66. Cargnello, M. & Roux, P. P. Activation and Function of the MAPKs and Their Substrates, the MAPK-Activated Protein Kinases. *Microbiol. Mol. Biol. Rev.* **75**, 50–83 (2011).

67. Hemmings, B. A. & Restuccia, D. F. PI3K-PKB/Akt pathway. *Cold Spring Harb. Perspect. Biol.* **4**, a011189 (2012).

68. Porta, C., Paglino, C. & Mosca, A. Targeting PI3K/Akt/mTOR signaling in cancer. *Frontiers in Oncology* **4 APR**, (2014).

69. Hemmings, B. A. & Restuccia, D. F. PI3K-PKB/Akt pathway. *Cold Spring Harb. Perspect. Biol.* **4**, (2012).

70. Chen, C. Y., Chen, J., He, L. & Stiles, B. L. PTEN: Tumor suppressor and metabolic regulator. *Frontiers in Endocrinology* **9**, 338 (2018).

71. Leo, M. S. & Sivamani, R. K. Phytochemical modulation of the Akt/mTOR pathway and its potential use in cutaneous disease. *Archives of Dermatological Research* **306**, 861–871 (2014).

72. Saxton, R. A. & Sabatini, D. M. mTOR Signaling in Growth, Metabolism, and Disease. *Cell* **168**, 960–976 (2017).

73. Albino, A. P., Strange, R. Le, Oliff, A. I., Furth, M. E. & Old, L. J. Transforming ras genes from human melanoma: A manifestation of tumour heterogeneity? *Nature* **308**, 69–72 (1984).

74. Sanchez-Vega, F. *et al.* Oncogenic Signaling Pathways in The Cancer Genome Atlas. *Cell* **173**, 321-337.e10 (2018).

75. Akbani, R. *et al.* Genomic Classification of Cutaneous Melanoma. *Cell* **161**, 1681–1696 (2015).

76. Scheffzek, K. *et al.* The Ras-RasGAP complex: Structural basis for GTPase activation and its loss in oncogenic ras mutants. *Science (80-.).* **277**, 333–338 (1997).

77. Demunter, A., Stas, M., Degreef, H., De Wolf-Peeters, C. & Van Den Oord, J. J. Analysis of N- and K-ras mutations in the distinctive tumor progression

phases of melanoma. *J. Invest. Dermatol.* **117**, 1483–1489 (2001).

78. Omholt, K. *et al.* Screening of N-ras codon 61 mutations in paired primary and metastatic cutaneous melanomas: Mutations occur early and persist throughout tumor progression. *Clin. Cancer Res.* **8**, 3468–3474 (2002).

79. Vu, H. L. & Aplin, A. E. Targeting mutant NRAS signaling pathways in melanoma. *Pharmacological Research* **107**, 111–116 (2016).

80. Raybaud, F. *et al.* Detection of a low frequency of activated ras genes in human melanomas using a tumorigenicity assay. *Cancer Res.* **48**, 950–3 (1988).

81. Ackermann, J. *et al.* Metastasizing Melanoma Formation Caused by Expression of Activated N-RasQ61K on an INK4a-Deficient Background. *Cancer Res.* **65**, (2005).

82. Burd, C. E. *et al.* Mutation-specific RAS oncogenicity explains NRAS codon 61 selection in melanoma. *Cancer Discov.* **4**, 1418–1429 (2014).

83. Kwong, L. N. *et al.* Oncogenic NRAS signaling differentially regulates survival and proliferation in melanoma. *Nat. Med.* **18**, 1503–1510 (2012).

84. Dovey, M., White, R. M. & Zon, L. I. Oncogenic NRAS cooperates with p53 loss to generate melanoma in zebrafish. *Zebrafish* **6**, 397–404 (2009).

85. Whitwam, T. *et al.* Differential oncogenic potential of activated RAS isoforms in melanocytes. *Oncogene* **26**, 4563–4570 (2007).

86. Platz, A., Egyhazi, S., Ringborg, U. & Hansson, J. Human cutaneous melanoma; a review of NRAS and BRAF mutation frequencies in relation to histogenetic subclass and body site. *Molecular Oncology* **1**, 395–405 (2008).

87. Van der Lubbe, J. L., Rosdorff, H. J., Bos, J. L. & Van der Eb, A. J. Activation of N-ras induced by ultraviolet irradiation in vitro. *Oncogene Res.* **3**, 9–20 (1988).

88. Tormanen, V. T. & Pfeifer, G. P. Mapping of UV photoproducts within ras proto-oncogenes in UV-irradiated cells: Correlation with mutations in human skin cancer. *Oncogene* **7**, 1729–1736 (1992).

89. Pierceall, W. E., Kripke, M. L. & Ananthaswamy, H. N. N-ras mutation in ultraviolet radiation-induced murine skin cancers. *Cancer Res.* **52**, 3946–51 (1992).

90. Husain, Z., Pathak, M. A., Flotte, T. & Wick, M. M. Role of ultraviolet radiation in the induction of melanocytic tumors in hairless mice following 7,12-dimethylbenz(a)anthracene application and ultraviolet irradiation. *Cancer Res.* **51**, 4964–70 (1991).

91. Rapp, U. R. *et al.* Structure and biological activity of v-raf, a unique oncogene transduced by a retrovirus. *Proc. Natl. Acad. Sci. U. S. A.* **80**, 4218–4222 (1983).

92. Jansen, H. W., Rückert, B., Lurz, R. & Bister, K. Two unrelated cell-derived sequences in the genome of avian leukemia and carcinoma inducing retrovirus MH2. *EMBO J.* **2**, 1969–1975 (1983).

93. Jansen, H. W. *et al.* Homologous cell-derived oncogenes in avian carcinoma virus MH2 and murine sarcoma virus 3611. *Nature* **307**, 281–284 (1984).

94. Marais, R. & Marshall, C. J. Control of the ERK MAP kinase cascade by Ras and Raf. *Cancer Surv.* **27**, 101–25 (1996).

95. Wan, P. T. C. *et al.* Mechanism of activation of the RAF-ERK signaling pathway by oncogenic mutations of B-RAF. *Cell* **116**, 855–867 (2004).

96. Wellbrock, C. *et al.* V599EB-RAF is an Oncogene in Melanocytes. *Cancer Res.* **64**, 2338–2342 (2004).

97. Patton, E. E. *et al.* BRAF mutations are sufficient to promote nevi formation and cooperate with p53 in the genesis of melanoma. *Curr. Biol.* **15**, 249–254 (2005).

98. Yazdi, A. S. *et al.* Mutations of the BRAF Gene in Benign and Malignant Melanocytic Lesions. *J. Invest. Dermatol.* **121**, 1160–1162 (2003).

99. Dankort, D. *et al.* BrafV600E cooperates with Pten loss to induce metastatic melanoma. *Nat. Genet.* **41**, 544–552 (2009).

100. Goel, V. K. *et al.* Melanocytic nevus-like hyperplasia and melanoma in transgenic BRAFV600E mice. *Oncogene* **28**, 2289–2298 (2009).

101. Viros, A. *et al.* Ultraviolet radiation accelerates BRAF-driven melanomagenesis by targeting TP53. *Nature* **511**, 478–482 (2014).

102. Dhomen, N. *et al.* Oncogenic Braf Induces Melanocyte Senescence and Melanoma in Mice. *Cancer Cell* **15**, 294–303 (2009).

103. Cichowski, K. & Jacks, T. NF1 tumor suppressor gene function: Narrowing the GAP. *Cell* **104**, 593–604 (2001).

104. Krauthammer, M. *et al.* Exome sequencing identifies recurrent mutations in NF1 and RASopathy genes in sun-exposed melanomas. *Nat. Genet.* **47**, 996–1002 (2015).

105. Bernards, A. & Settleman, J. GAPs in growth factor signalling. *Growth Factors* **23**, 143–149 (2005).

106. Nissan, M. H. *et al.* Loss of NF1 in cutaneous melanoma is associated with RAS activation and MEK dependence. *Cancer Res.* **74**, 2340–2350 (2014).

107. Maertens, O. *et al.* Elucidating distinct roles for NF1 in melanomagenesis. *Cancer Discov.* **3**, 339–349 (2013).

108. Lionarons, D. A. *et al.* RAC1P29S Induces a Mesenchymal Phenotypic Switch via Serum Response Factor to Promote Melanoma Development and Therapy Resistance. *Cancer Cell* **36**, 68-83.e9 (2019).

109. Dumaz, N. *et al.* Driver KIT mutations in melanoma cluster in four hotspots. *Melanoma Res.* **25**, 88–90 (2015).

110. Liang, R., Wallace, A. R., Schadendorf, D. & Rubin, B. P. The phosphatidyl inositol 3-kinase pathway is central to the pathogenesis of Kit-activated melanoma. *Pigment Cell Melanoma Res.* **24**, 714–723 (2011).

111. Beadling, C. *et al.* KIT gene mutations and copy number in melanoma subtypes. *Clin. Cancer Res.* **14**, 6821–6828 (2008).

112. Smalley, K. S. M. *et al.* Identification of a novel subgroup of melanomas with KIT/cyclin-dependent kinase-4 overexpression. *Cancer Res.* **68**, 5743–5752 (2008).

113. Hodis, E. *et al.* A landscape of driver mutations in melanoma. *Cell* **150**, 251–263 (2012).

114. Dahl, C. *et al.* KIT Is a frequent target for epigenetic silencing in cutaneous melanoma. *J. Invest. Dermatol.* **135**, 516–524 (2015).

115. Petti, C. *et al.* Coexpression of NRASQ61R and BRAFV600E in Human Melanoma Cells Activates Senescence and Increases Susceptibility to Cell-Mediated Cytotoxicity. *Cancer Res.* **66**, 6503–6511 (2006).

116. Neiswender, J. V. *et al.* KIT suppresses BRAFV600E-mutant melanoma by attenuating oncogenic RAS/MAPK signaling. *Cancer Res.* **77**, 5820–5830 (2017).

117. Davies, M. A. The role of the PI3K-AKT pathway in melanoma. *Cancer Journal* **18**, 142–147 (2012).

118. Aguissa-Touré, A. H. & Li, G. Genetic alterations of PTEN in human melanoma. *Cellular and Molecular Life Sciences* **69**, 1475–1491 (2012).

119. Zhou, X. P. *et al.* Epigenetic PTEN silencing in malignant melanomas without PTEN mutation. *Am. J. Pathol.* **157**, 1123–1128 (2000).

120. Gupta, A., Anjomani-Virmouni, S., Koundouros, N. & Poulogiannis, G. *PARK2* loss promotes cancer progression via redox-mediated inactivation of PTEN. *Mol. Cell. Oncol.* **4**, e1329692 (2017).

121. Fenton, T. R. *et al.* Resistance to EGF receptor inhibitors in glioblastoma mediated by phosphorylation of the PTEN tumor suppressor at tyrosine 240. *Proc. Natl. Acad. Sci. U. S. A.* **109**, 14164–14169 (2012).

122. Covey, T. M., Edes, K. & Fitzpatrick, F. A. Akt activation by arachidonic acid metabolism occurs via oxidation and inactivation of PTEN tumor suppressor. *Oncogene* **26**, 5784–5792 (2007).

123. Wang, X. *et al.* NEDD4-1 Is a Proto-Oncogenic Ubiquitin Ligase for PTEN. *Cell* **128**, 129–139 (2007).

124. Chang, H., Cai, Z. & Roberts, T. M. The mechanisms underlying PTEN loss in human tumors suggest potential therapeutic opportunities. *Biomolecules* **9**,

713 (2019).

125. Koundouros, N. & Poulogiannis, G. Phosphoinositide 3-Kinase/Akt signaling and redox metabolism in cancer. *Frontiers in Oncology* **8**, 160 (2018).

126. Curtin, J. A. *et al.* Distinct Sets of Genetic Alterations in Melanoma. *N. Engl. J. Med.* **353**, 2135–2147 (2005).

127. Davies, M. A. *et al.* Integrated molecular and clinical analysis of AKT activation in metastatic melanoma. *Clin. Cancer Res.* **15**, 7538–7546 (2009).

128. You, M. J. *et al.* Genetic analysis of Pten and Ink4a/Arf interactions in the suppression of tumorigenesis in mice. *Proc. Natl. Acad. Sci. U. S. A.* **99**, 1455–1460 (2002).

129. Omholt, K., Krockel, D., Ringborg, U. & Hansson, J. Mutations of PIK3CA are rare in cutaneous melanoma. *Melanoma Res.* **16**, 197–200 (2006).

130. Sheppard, K. E. & McArthur, G. A. The cell-cycle regulator CDK4: An emerging therapeutic target in melanoma. *Clin. Cancer Res.* **19**, 5320–5328 (2013).

131. Reed, J. A. *et al.* Loss of Expression of the p16/Cyclin-dependent Kinase Inhibitor 2 Tumor Suppressor Gene in Melanocytic Lesions Correlates with Invasive Stage of Tumor Progression. *Cancer Res.* **55**, 2713–2718 (1995).

132. Krimpenfort, P., Quon, K. C., Mooi, W. J., Loonstra, A. & Berns, A. Loss of p16Ink4a confers susceptibility to metastatic melanoma in mice. *Nature* **413**, 83–86 (2001).

133. Vízkeleti, L. *et al.* The role of CCND1 alterations during the progression of cutaneous malignant melanoma. *Tumour Biol.* **33**, 2189–2199 (2012).

134. Sauter, E. R. *et al.* Cyclin D1 is a candidate oncogene in cutaneous melanoma. *Cancer Res.* **62**, 3200–6 (2002).

135. Utikal, J. *et al.* Numerical abnormalities of the Cyclin D1 gene locus on chromosome 11q13 in non-melanoma skin cancer. *Cancer Lett.* **219**, 197–204 (2005).

136. González-Ruiz, L. *et al.* An update on the implications of cyclin D1 in melanomas. *Pigment Cell Melanoma Res.* pcmr.12874 (2020). doi:10.1111/pcmr.12874

137. Garraway, L. A. *et al.* Integrative genomic analyses identify MITF as a lineage survival oncogene amplified in malignant melanoma. *Nature* **436**, 117–122 (2005).

138. Wellbrock, C. & Arozarena, I. Microphthalmia-associated transcription factor in melanoma development and MAP-kinase pathway targeted therapy. *Pigment Cell Melanoma Res.* **28**, 390–406 (2015).

139. Levy, C., Khaled, M. & Fisher, D. E. MITF: master regulator of melanocyte development and melanoma oncogene. *Trends Mol. Med.* **12**, 406–414 (2006).

140. Carreira, S. *et al.* Mitf regulation of Dia1 controls melanoma proliferation and invasiveness. *Genes Dev.* **20**, 3426–3439 (2006).

141. Hoek, K. S. & Goding, C. R. Cancer stem cells versus phenotype-switching in melanoma. *Pigment Cell and Melanoma Research* **23**, 746–759 (2010).

142. Ugurel, S. *et al.* Microphthalmia-associated transcription factor gene amplification in metastatic melanoma is a prognostic marker for patient survival, but not a predictive marker for chemosensitivity and chemotherapy response. *Clin. Cancer Res.* **13**, 6344–6350 (2007).

143. Wellbrock, C. *et al.* Oncogenic BRAF regulates melanoma proliferation through the lineage specific factor MITF. *PLoS One* **3**, e2734 (2008).

144. Du, J. *et al.* Critical role of CDK2 for melanoma growth linked to its melanocyte-specific transcriptional regulation by MITF. *Cancer Cell* **6**, 565–576 (2004).

145. McGill, G. G. *et al.* Bcl2 regulation by the melanocyte master regulator Mitf modulates lineage survival and melanoma cell viability. *Cell* **109**, 707–718 (2002).

146. Haq, R. *et al.* Oncogenic BRAF regulates oxidative metabolism via PGC1α and MITF. *Cancer Cell* **23**, 302–315 (2013).

147. Nakai, N. *et al.* Therapeutic RNA interference of malignant melanoma by electrotransfer of small interfering RNA targeting Mitf. *Gene Ther.* **14**, 357–365 (2007).

148. Feige, E. *et al.* Hypoxia-induced transcriptional repression of the melanoma-associated oncogene MITF. *Proc. Natl. Acad. Sci. U. S. A.* **108**, (2011).

149. Nikolaev, S. I. *et al.* Exome sequencing identifies recurrent somatic MAP2K1 and MAP2K2 mutations in melanoma. *Nat. Genet.* **44**, 133–139 (2012).

150. Stark, M. S. *et al.* Frequent somatic mutations in MAP3K5 and MAP3K9 in metastatic melanoma identified by exome sequencing. *Nat. Genet.* **44**, 165–169 (2012).

151. Berger, M. F. *et al.* Melanoma genome sequencing reveals frequent PREX2 mutations. *Nature* **485**, 502–506 (2012).

152. Prickett, T. D. *et al.* Analysis of the tyrosine kinome in melanoma reveals recurrent mutations in ERBB4. *Nat. Genet.* **41**, 1127–1132 (2009).

153. Avril, M. F. *et al.* Fotemustine compared with dacarbazine in patients with disseminated malignant melanoma: A phase III study. *J. Clin. Oncol.* **22**, 1118–1125 (2004).

154. Chapman, P. B. *et al.* Phase III multicenter randomized trial of the Dartmouth regimen versus dacarbazine in patients with metastatic melanoma. *J. Clin. Oncol.* **17**, 2745–2751 (1999).

155. Kim, C. *et al.* Long-Term Survival in Patients with Metastatic Melanoma

Treated with DTIC or Temozolomide. *Oncologist* **15**, 765–771 (2010).

156. Chapman, P. B. *et al.* Improved Survival with Vemurafenib in Melanoma with BRAF V600E Mutation. *N. Engl. J. Med.* **364**, 2507–2516 (2011).

157. Menzies, A. M., Long, G. V. & Murali, R. Dabrafenib and its potential for the treatment of metastatic melanoma. *Drug Design, Development and Therapy* **6**, 391–405 (2012).

158. Dummer, R. *et al.* Overall survival in patients with BRAF-mutant melanoma receiving encorafenib plus binimetinib versus vemurafenib or encorafenib (COLUMBUS): a multicentre, open-label, randomised, phase 3 trial. *Lancet Oncol.* **19**, 1315–1327 (2018).

159. Heidorn, S. J. *et al.* Kinase-Dead BRAF and Oncogenic RAS Cooperate to Drive Tumor Progression through CRAF. *Cell* **140**, 209–221 (2010).

160. Hatzivassiliou, G. *et al.* RAF inhibitors prime wild-type RAF to activate the MAPK pathway and enhance growth. *Nature* **464**, 431–435 (2010).

161. Hauschild, A. *et al.* Dabrafenib in BRAF-mutated metastatic melanoma: A multicentre, open-label, phase 3 randomised controlled trial. *Lancet* **380**, 358–365 (2012).

162. Salama, A. K. S. & Flaherty, K. T. BRAF in melanoma: Current strategies and future directions. *Clinical Cancer Research* **19**, 4326–4334 (2013).

163. Kakadia, S. *et al.* Mechanisms of resistance to BRAF and MEK inhibitors and clinical update of us food and drug administration-approved targeted therapy in advanced melanoma. *OncoTargets and Therapy* **11**, 7095–7107 (2018).

164. Flaherty, K. T. *et al.* Improved survival with MEK inhibition in BRAF-mutated melanoma. *N. Engl. J. Med.* **367**, 107–114 (2012).

165. Long, G. V *et al.* Dabrafenib and trametinib versus dabrafenib and placebo for Val600 BRAF-mutant melanoma: a multicentre, double-blind, phase 3 randomised controlled trial. *Lancet* **386**, 444–451 (2015).

166. Larkin, J. *et al.* Combined Vemurafenib and Cobimetinib in *BRAF* -Mutated Melanoma. *N. Engl. J. Med.* **371**, 1867–1876 (2014).

167. Girotti, M. R. *et al.* Inhibiting EGF Receptor or SRC Family Kinase Signaling Overcomes BRAF Inhibitor Resistance in Melanoma. *Cancer Discov.* **3**, 158–167 (2013).

168. Müller, J. *et al.* Low MITF/AXL ratio predicts early resistance to multiple targeted drugs in melanoma. *Nat. Commun.* **5**, 5712 (2014).

169. Nazarian, R. *et al.* Melanomas acquire resistance to B-RAF(V600E) inhibition by RTK or N-RAS upregulation. *Nature* **468**, 973–977 (2010).

170. Trunzer, K. *et al.* Pharmacodynamic Effects and Mechanisms of Resistance to Vemurafenib in Patients With Metastatic Melanoma. *J. Clin. Oncol.* **31**, 1767–

1774 (2013).

171. Wagle, N. *et al.* Dissecting therapeutic resistance to RAF inhibition in melanoma by tumor genomic profiling. *J. Clin. Oncol.* **29**, 3085–96 (2011).

172. Van Allen, E. M. *et al.* The genetic landscape of clinical resistance to RAF inhibition in metastatic melanoma. *Cancer Discov.* **4**, 94–109 (2014).

173. Marusiak, A. A. *et al.* Mixed lineage kinases activate MEK independently of RAF to mediate resistance to RAF inhibitors. *Nat. Commun.* **5**, 663–672 (2014).

174. Shi, H. *et al.* Melanoma whole-exome sequencing identifies V600EB-RAF amplification-mediated acquired B-RAF inhibitor resistance. *Nat. Commun.* **3**, 724 (2012).

175. Poulikakos, P. I. *et al.* RAF inhibitor resistance is mediated by dimerization of aberrantly spliced BRAF(V600E). *Nature* **480**, 387–390 (2011).

176. Whittaker, S. R. *et al.* A Genome-Scale RNA Interference Screen Implicates NF1 Loss in Resistance to RAF Inhibition. *Cancer Discov.* **3**, (2013).

177. Shi, H. *et al.* A Novel AKT1 Mutant Amplifies an Adaptive Melanoma Response to BRAF Inhibition. *Cancer Discov.* **4**, (2014).

178. Paraiso, K. H. T. *et al.* PTEN Loss Confers BRAF Inhibitor Resistance to Melanoma Cells through the Suppression of BIM Expression. *Cancer Res.* **71**, (2011).

179. Smith, M. P. *et al.* Inhibiting Drivers of Non-mutational Drug Tolerance Is a Salvage Strategy for Targeted Melanoma Therapy. *Cancer Cell* **29**, 270–284 (2016).

180. Smith, M. P. *et al.* Effect of SMURF2 targeting on susceptibility to MEK inhibitors in melanoma. *J. Natl. Cancer Inst.* **105**, 33–46 (2013).

181. Haq, R. *et al.* BCL2A1 is a lineage-specific antiapoptotic melanoma oncogene that confers resistance to BRAF inhibition. *Proc. Natl. Acad. Sci.* **110**, 4321–4326 (2013).

182. Hirata, E. *et al.* Intravital imaging reveals how BRAF inhibition generates drug-tolerant microenvironments with high integrin β1/FAK signaling. *Cancer Cell* **27**, 574–88 (2015).

183. Wang, T. *et al.* BRAF Inhibition Stimulates Melanoma-Associated Macrophages to Drive Tumor Growth. *Clin. Cancer Res.* **21**, 1652–1664 (2015).

184. Smith, M. P. *et al.* The Immune Microenvironment Confers Resistance to MAPK Pathway Inhibitors through Macrophage-Derived TNF. *Cancer Discov.* **4**, 1214–1229 (2014).

185. Pardoll, D. M. The blockade of immune checkpoints in cancer immunotherapy. *Nature Reviews Cancer* **12**, 252–264 (2012).

186. Hodi, F. S. *et al.* Improved survival with ipilimumab in patients with metastatic melanoma. *N. Engl. J. Med.* **363**, 711–723 (2010).

187. Prieto, P. A. *et al.* CTLA-4 blockade with ipilimumab: Long-term follow-up of 177 patients with metastatic melanoma. *Clin. Cancer Res.* **18**, 2039–2047 (2012).

188. Robert, C. *et al.* Ipilimumab plus Dacarbazine for Previously Untreated Metastatic Melanoma. *N. Engl. J. Med.* **364**, 2517–2526 (2011).

189. Schadendorf, D. *et al.* Pooled Analysis of Long-Term Survival Data From Phase II and Phase III Trials of Ipilimumab in Unresectable or Metastatic Melanoma. *J. Clin. Oncol.* **33**, 1889–1894 (2015).

190. Topalian, S. L. *et al.* Survival, durable tumor remission, and long-term safety in patients with advanced melanoma receiving nivolumab. *J. Clin. Oncol.* **32**, 1020–1030 (2014).

191. Ribas, A. *et al.* Pembrolizumab versus investigator-choice chemotherapy for ipilimumab-refractory melanoma (KEYNOTE-002): A randomised, controlled, phase 2 trial. *Lancet Oncol.* **16**, 908–918 (2015).

192. Weber, J. S. *et al.* Nivolumab versus chemotherapy in patients with advanced melanoma who progressed after anti-CTLA-4 treatment (CheckMate 037): A randomised, controlled, open-label, phase 3 trial. *Lancet Oncol.* **16**, 375–384 (2015).

193. Robert, C. *et al.* Nivolumab in previously untreated melanoma without BRAF mutation. *N. Engl. J. Med.* **372**, 320–330 (2015).

194. Larkin, J. *et al.* Combined nivolumab and ipilimumab or monotherapy in untreated Melanoma. *N. Engl. J. Med.* **373**, 23–34 (2015).

195. Robert, C. *et al.* Pembrolizumab versus Ipilimumab in Advanced Melanoma. *N. Engl. J. Med.* **372**, 2521–2532 (2015).

196. Wolchok, J. D. *et al.* Overall Survival with Combined Nivolumab and Ipilimumab in Advanced Melanoma. *N. Engl. J. Med.* **377**, 1345–1356 (2017).

197. Weber, J. S., Kähler, K. C. & Hauschild, A. Management of immune-related adverse events and kinetics of response with ipilimumab. *Journal of Clinical Oncology* **30**, 2691–2697 (2012).

198. Imbert, C. *et al.* Resistance of melanoma to immune checkpoint inhibitors is overcome by targeting the sphingosine kinase-1. *Nat. Commun.* **11**, 1–14 (2020).

199. Chew, G. L. *et al.* DUX4 Suppresses MHC Class I to Promote Cancer Immune Evasion and Resistance to Checkpoint Blockade. *Dev. Cell* **50**, 658-671.e7 (2019).

200. Sade-Feldman, M. *et al.* Resistance to checkpoint blockade therapy through inactivation of antigen presentation. *Nat. Commun.* **8**, 1–11 (2017).

201. Zaretsky, J. M. *et al.* Mutations Associated with Acquired Resistance to PD-1 Blockade in Melanoma. *N. Engl. J. Med.* **375**, 819–829 (2016).

202. Peng, W. *et al.* Loss of PTEN promotes resistance to T cell–mediated immunotherapy. *Cancer Discov.* **6**, 202–216 (2016).

203. Trujillo, J. A. *et al.* Secondary resistance to immunotherapy associated with β-catenin pathway activation or PTEN loss in metastatic melanoma. *J. Immunother. Cancer* **7**, 295 (2019).

204. Luke, J. J., Bao, R., Sweis, R. F., Spranger, S. & Gajewski, T. F. WNT/b-catenin pathway activation correlates with immune exclusion across human cancers. *Clin. Cancer Res.* **25**, 3074–3083 (2019).

205. Benci, J. L. *et al.* Tumor Interferon Signaling Regulates a Multigenic Resistance Program to Immune Checkpoint Blockade. *Cell* **167**, 1540-1554.e12 (2016).

206. De Berardinis, R. J. & Chandel, N. S. Fundamentals of cancer metabolism. *Science Advances* **2**, (2016).

207. Fischer, G. M. *et al.* Metabolic strategies of melanoma cells: Mechanisms, interactions with the tumor microenvironment, and therapeutic implications. *Pigment Cell and Melanoma Research* **31**, 11–30 (2018).

208. Warburg, O. & Minami, S. Versuche an Überlebendem Carcinom-gewebe. *Klin. Wochenschr.* **2**, 776–777 (1923).

209. Weinhouse, S., Warburg, O., Burk, D. & Schade, A. L. On respiratory impairment in cancer cells. *Science (80-.).* **124**, 267–272 (1956).

210. Locasale, J. W. & Cantley, L. C. Metabolic flux and the regulation of mammalian cell growth. *Cell Metabolism* **14**, 443–451 (2011).

211. Science, O. W.- & 1956, undefined. On the origin of cancer cells. *JSTOR*

212. Scott, D. A. *et al.* Comparative metabolic flux profiling of melanoma cell lines: Beyond the Warburg effect. *J. Biol. Chem.* **286**, 42626–42634 (2011).

213. Vazquez, F. *et al.* PGC1α Expression Defines a Subset of Human Melanoma Tumors with Increased Mitochondrial Capacity and Resistance to Oxidative Stress. *Cancer Cell* **23**, 287–301 (2013).

214. Ran, F. A. *et al.* Genome engineering using the CRISPR-Cas9 system. *Nat. Protoc.* **8**, 2281–308 (2013).

215. Hall, A. *et al.* Dysfunctional oxidative phosphorylation makes malignant melanoma cells addicted to glycolysis driven by the V600EBRAF oncogene. *Oncotarget* **4**, 584–599 (2013).

216. Kluza, J. *et al.* Inactivation of the HIF-1α/PDK3 signaling axis drives melanoma toward mitochondrial oxidative metabolism and potentiates the therapeutic activity of pro-oxidants. *Cancer Res.* **72**, 5035–5047 (2012).

217. Parmenter, T. J. *et al.* Response of BRAF-mutant melanoma to BRAF inhibition is mediated by a network of transcriptional regulators of glycolysis. *Cancer Discov.* **4**, 423–433 (2014).

218. Kaplon, J. *et al.* A key role for mitochondrial gatekeeper pyruvate dehydrogenase in oncogene-induced senescence. *Nature* **498**, 109–112 (2013).

219. Zundel, W. *et al.* Loss of PTEN facilitates HIF-1-mediated gene expression. *Genes Dev.* **14**, 391 (2000).

220. Chen, C., Pore, N., Behrooz, A., Ismail-Beigi, F. & Maity, A. Regulation of glut1 mRNA by hypoxia-inducible factor-1: Interaction between H-ras and hypoxia. *J. Biol. Chem.* **276**, 9519–9525 (2001).

221. Hayashi, M. *et al.* Induction of glucose transporter 1 expression through hypoxia-inducible factor 1α under hypoxic conditions in trophoblast-derived cells. *J. Endocrinol.* **183**, 145–154 (2004).

222. Guppy, M. The hypoxic core: A possible answer to the cancer paradox. *Biochem. Biophys. Res. Commun.* **299**, 676–680 (2002).

223. Eales, K. L., Hollinshead, K. E. R. & Tennant, D. A. Hypoxia and metabolic adaptation of cancer cells. *Oncogenesis* **5**, e190–e190 (2016).

224. Shestov, A. A. *et al.* Quantitative determinants of aerobic glycolysis identify flux through the enzyme GAPDH as a limiting step. *Elife* **3**, 1–18 (2014).

225. Slavov, N., Budnik, B. A., Schwab, D., Airoldi, E. M. & van Oudenaarden, A. Constant Growth Rate Can Be Supported by Decreasing Energy Flux and Increasing Aerobic Glycolysis. *Cell Rep.* **7**, 705–714 (2014).

226. Chang, C. H. *et al.* Metabolic Competition in the Tumor Microenvironment Is a Driver of Cancer Progression. *Cell* **162**, 1229–1241 (2015).

227. Payen, V. L., Porporato, P. E., Baselet, B. & Sonveaux, P. Metabolic changes associated with tumor metastasis, part 1: Tumor pH, glycolysis and the pentose phosphate pathway. *Cellular and Molecular Life Sciences* **73**, 1333–1348 (2016).

228. Vahle, A. K. *et al.* Extracellular matrix composition and interstitial pH modulate NHE1-mediated melanoma cell motility. *Int. J. Oncol.* **44**, 78–90 (2014).

229. Végran, F., Boidot, R., Michiels, C., Sonveaux, P. & Feron, O. Lactate influx through the endothelial cell monocarboxylate transporter MCT1 supports an NF-kB/IL-8 pathway that drives tumor angiogenesis. *Cancer Res.* **71**, 2550–2560 (2011).

230. Xiaojun, X., Hansen, A. Zur, Coy, J. F. & Löchelt, M. Transketolase-like protein 1 (TKTL1) Is required for rap and full viability of human tumor cells. *Int. J. Cancer* **124**, 1330–1337 (2009).

231. Cai, T. *et al.* Glucose-6-phosphate dehydrogenase and NADPH oxidase 4 control STAT3 activity in melanoma cells through a pathway involving reactive oxygen species, c-SRC and SHP2. *Am. J. Cancer Res.* **5**, 1610–1620 (2015).

232. Pinho, S. S. & Reis, C. A. Glycosylation in cancer: Mechanisms and clinical implications. *Nature Reviews Cancer* **15**, 540–555 (2015).

233. Tang, L. *et al.* N-Glycosylation in progression of skin cancer. *Medical Oncology* **36**, 1–10 (2019).

234. Newman, A. C. & Maddocks, O. D. K. One-carbon metabolism in cancer. *British Journal of Cancer* **116**, 1499–1504 (2017).

235. Locasale, J. W. *et al.* Phosphoglycerate dehydrogenase diverts glycolytic flux and contributes to oncogenesis. *Nat. Genet.* **43**, 869–874 (2011).

236. Gopal, Y. N. V. *et al.* Inhibition of mTORC1/2 overcomes resistance to MAPK pathway inhibitors mediated by PGC1α and oxidative phosphorylation in melanoma. *Cancer Res.* **74**, 7037–7047 (2014).

237. Zhang, G. *et al.* Targeting mitochondrial biogenesis to overcome drug resistance to MAPK inhibitors. *J. Clin. Invest.* **126**, 1834–1856 (2016).

238. Birsoy, K. *et al.* An Essential Role of the Mitochondrial Electron Transport Chain in Cell Proliferation Is to Enable Aspartate Synthesis. *Cell* **162**, 540–551 (2015).

239. Ratnikov, B. *et al.* Glutamate and asparagine cataplerosis underlie glutamine addiction in melanoma. *Oncotarget* **6**, 7379–7389 (2015).

240. Bauer, D. E., Hatzivassiliou, G., Zhao, F., Andreadis, C. & Thompson, C. B. ATP citrate lyase is an important component of cell growth and transformation. *Oncogene* **24**, 6314–6322 (2005).

241. Ratnikov, B. I., Scott, D. A., Osterman, A. L., Smith, J. W. & Ronai, Z. A. Metabolic rewiring in melanoma. *Oncogene* **36**, 147–157 (2017).

242. Filipp, F. V., Scott, D. A., Ronai, Z. A., Osterman, A. L. & Smith, J. W. Reverse TCA cycle flux through isocitrate dehydrogenases 1 and 2 is required for lipogenesis in hypoxic melanoma cells. *Pigment Cell Melanoma Res.* **25**, 375–383 (2012).

243. Wang, Q. *et al.* Targeting glutamine transport to suppress melanoma cell growth. *Int. J. Cancer* **135**, 1060–1071 (2014).

244. Pavlova, N. N. & Thompson, C. B. The Emerging Hallmarks of Cancer Metabolism. *Cell Metabolism* **23**, 27–47 (2016).

245. Cheng, C., Geng, F., Cheng, X. & Guo, D. Lipid metabolism reprogramming and its potential targets in cancer. *Cancer communications (London, England)* **38**, 27 (2018).

246. Santos, C. R. & Schulze, A. Lipid metabolism in cancer. *FEBS J.* **279**, 2610–

2623 (2012).

247. Nath, A. & Chan, C. Genetic alterations in fatty acid transport and metabolism genes are associated with metastatic progression and poor prognosis of human cancers. *Sci. Rep.* **6**, 1–13 (2016).

248. Eberlé, D., Hegarty, B., Bossard, P., Ferré, P. & Foufelle, F. SREBP transcription factors: Master regulators of lipid homeostasis. *Biochimie* **86**, 839–848 (2004).

249. Kim, J. B. *et al.* Nutritional and insulin regulation of fatty acid synthetase and leptin gene expression through ADD1/SREBP1. *J. Clin. Invest.* **101**, 1–9 (1998).

250. Menendez, J. A. & Lupu, R. Fatty acid synthase and the lipogenic phenotype in cancer pathogenesis. *Nature Reviews Cancer* **7**, 763–777 (2007).

251. Talebi, A. *et al.* Sustained SREBP-1-dependent lipogenesis as a key mediator of resistance to BRAF-targeted therapy. *Nat. Commun.* **9**, 1–11 (2018).

252. Ricoult, S. J. H., Yecies, J. L., Ben-Sahra, I. & Manning, B. D. Oncogenic PI3K and K-Ras stimulate de novo lipid synthesis through mTORC1 and SREBP. *Oncogene* **35**, 1250–1260 (2016).

253. Saab, J., Santos-Zabala, M. L., Loda, M., Stack, E. C. & Hollmann, T. J. Fatty acid synthase and acetyl-CoA carboxylase are expressed in nodal metastatic melanoma but not in benign intracapsular nodal nevi. *Am. J. Dermatopathol.* **40**, 259–264 (2018).

254. Innocenzi, D. *et al.* Fatty acid synthase expression in melanoma. *J. Cutan. Pathol.* **30**, 23–28 (2003).

255. Kapur, P., Rakheja, D., Roy, L. C. & Hoang, M. P. Fatty acid synthase expression in cutaneous melanocytic neoplasms. *Mod. Pathol.* **18**, 1107–1112 (2005).

256. Zecchin, K. G. *et al.* Inhibition of fatty acid synthase in melanoma cells activates the intrinsic pathway of apoptosis. *Lab. Investig.* **91**, 232–240 (2011).

257. Wu, J. *et al.* Iciartin, a novel FASN inhibitor, exerts anti-melanoma activities through IGF-1R/STAT3 signaling. *Oncotarget* **7**, 51251–51269 (2016).

258. Seguin, F. *et al.* The fatty acid synthase inhibitor orlistat reduces experimental metastases and angiogenesis in B16-F10 melanomas. *Br. J. Cancer* **107**, 977–987 (2012).

259. Guo, W. *et al.* ATP-Citrate Lyase Epigenetically Potentiates Oxidative Phosphorylation to Promote Melanoma Growth and Adaptive Resistance to MAPK Inhibition. *Clin. Cancer Res.* **26**, 2725–2739 (2020).

260. Jones, S. F. & Infante, J. R. Molecular pathways: Fatty acid synthase. *Clin. Cancer Res.* **21**, 5434–5438 (2015).

261. Sumantran, V. N., Mishra, P. & Sudhakar, N. Microarray analysis of

differentially expressed genes regulating lipid metabolism during melanoma progression. *Indian J. Biochem. Biophys.* **52**, 125–131 (2015).

262. Slipicevic, A. *et al.* The fatty acid binding protein 7 (FABP7) is involved in proliferation and invasion of melanoma cells. *BMC Cancer* **8**, 276 (2008).

263. Goto, Y. *et al.* Aberrant fatty acid-binding protein-7 gene expression in cutaneous malignant melanoma. *J. Invest. Dermatol.* **130**, 221–9 (2010).

264. Goto, Y. *et al.* A new melanoma antigen fatty acid-binding protein 7, involved in proliferation and invasion, is a potential target for immunotherapy and molecular target therapy. *Cancer Res.* **66**, 4443–4449 (2006).

265. Pascual, G. *et al.* Targeting metastasis-initiating cells through the fatty acid receptor CD36. *Nature* **541**, 41–45 (2017).

266. Zhang, M. *et al.* Adipocyte-derived lipids mediate melanoma progression via FATP proteins. *Cancer Discov.* **8**, 1006–1025 (2018).

267. Henderson, F. *et al.* Enhanced fatty acid scavenging and glycerophospholipid metabolism accompany melanocyte neoplasia progression in Zebrafish. *Cancer Res.* **79**, 2136–2151 (2019).

268. Ma, Y. *et al.* Fatty acid oxidation: An emerging facet of metabolic transformation in cancer. *Cancer Lett.* **435**, 92–100 (2018).

269. Carracedo, A., Cantley, L. C. & Pandolfi, P. P. Cancer metabolism: Fatty acid oxidation in the limelight. *Nat. Rev. Cancer* **13**, 227–232 (2013).

270. Houten, S. M. & Wanders, R. J. A. A general introduction to the biochemistry of mitochondrial fatty acid β-oxidation. *Journal of Inherited Metabolic Disease* **33**, 469–477 (2010).

271. Rodrigues, M. F. *et al.* Enhanced OXPHOS, glutaminolysis and β-oxidation constitute the metastatic phenotype of melanoma cells. *Biochem. J.* **473**, 703–715 (2016).

272. Lazar, I. *et al.* Adipocyte Exosomes Promote Melanoma Aggressiveness through Fatty Acid Oxidation: A Novel Mechanism Linking Obesity and Cancer. *Cancer Res.* **76**, 4051–4057 (2016).

273. MH, A., RC, H. & G, F. Lipid-secreting Mammary Carcinoma. Report of a Case Associated With Paget's Disease of the Nipple. *Cancer* **16**, (1963).

274. Wright, D. H. Lipid content of malignant lymphomas. *J. Clin. Pathol.* **21**, 643–649 (1968).

275. Cruz, A. L. S., Barreto, E. de A., Fazolini, N. P. B., Viola, J. P. B. & Bozza, P. T. Lipid droplets: platforms with multiple functions in cancer hallmarks. *Cell Death and Disease* **11**, 1–16 (2020).

276. Cases, S. *et al.* Identification of a gene encoding an acyl CoA:diacylglycerol acyltransferase, a key enzyme in triacylglycerol synthesis. *Proc. Natl. Acad. Sci. U. S. A.* **95**, 13018–13023 (1998).

277. Cases, S. *et al.* Cloning of DGAT2, a Second Mammalian Diacylglycerol Acyltransferase, and Related Family Members. *J. Biol. Chem.* **276**, 38870–38876 (2001).

278. Chang, T. Y., Li, B. L., Chang, C. C. Y. & Urano, Y. Acyl-coenzyme A:cholesterol acyltransferases. *American Journal of Physiology - Endocrinology and Metabolism* **297**, E1 (2009).

279. Walther, T. C., Chung, J. & Farese, R. V. Lipid droplet biogenesis. *Annual Review of Cell and Developmental Biology* **33**, 491–510 (2017).

280. Jackson, C. L. Lipid droplet biogenesis. *Current Opinion in Cell Biology* **59**, 88–96 (2019).

281. Olzmann, J. A. & Carvalho, P. Dynamics and functions of lipid droplets. *Nature Reviews Molecular Cell Biology* **20**, 137–155 (2019).

282. Zechner, R., Madeo, F. & Kratky, D. Cytosolic lipolysis and lipophagy: Two sides of the same coin. *Nature Reviews Molecular Cell Biology* **18**, 671–684 (2017).

283. Singh, R. *et al.* Autophagy regulates lipid metabolism. *Nature* **458**, 1131–1135 (2009).

284. Listenberger, L. L. *et al.* Triglyceride accumulation protects against fatty acid-induced lipotoxicity. *Proc. Natl. Acad. Sci. U. S. A.* **100**, 3077–3082 (2003).

285. Senkal, C. E. *et al.* Ceramide Is Metabolized to Acylceramide and Stored in Lipid Droplets. *Cell Metab.* **25**, 686–697 (2017).

286. Koliwad, S. K. *et al.* DGAT1-dependent triacylglycerol storage by macrophages protects mice from diet-induced insulin resistance and inflammation. *J. Clin. Invest.* **120**, 756–767 (2010).

287. Liu, L. *et al.* DGAT1 expression increases heart triglyceride content but ameliorates lipotoxicity. *J. Biol. Chem.* **284**, 36312–36323 (2009).

288. Chitraju, C. *et al.* Triglyceride Synthesis by DGAT1 Protects Adipocytes from Lipid-Induced ER Stress during Lipolysis. *Cell Metab.* **26**, 407-418.e3 (2017).

289. Jarc, E., Eichmann, T. O., Zimmermann, R. & Petan, T. Lipidomic data on lipid droplet triglyceride remodelling associated with protection of breast cancer cells from lipotoxic stress. *Data Br.* **18**, 234–240 (2018).

290. Jarc, E. *et al.* Lipid droplets induced by secreted phospholipase A2 and unsaturated fatty acids protect breast cancer cells from nutrient and lipotoxic stress. *Biochim. Biophys. Acta - Mol. Cell Biol. Lipids* **1863**, 247–265 (2018).

291. Przybytkowski, E. *et al.* Upregulation of cellular triacylglycerol - Free fatty acid cycling by oleate is associated with long-term serum-free survival of human breast cancer cells. *Biochem. Cell Biol.* **85**, 301–310 (2007).

292. Hardy, S. *et al.* Saturated fatty acid-induced apoptosis in MDA-MB-231 breast

cancer cells. A role for cardiolipin. *J. Biol. Chem.* **278**, 31861–70 (2003).

293. Hardy, S., Langelier, Y. & Prentki, M. Oleate Activates Phosphatidylinositol 3-Kinase and Promotes Proliferation and Reduces Apoptosis of MDA-MB-231 Breast Cancer Cells, Whereas Palmitate Has Opposite Effects1. *Cancer Res.* **60**, (2000).

294. Guštin, E., Jarc, E., Kump, A. & Petan, T. Lipid droplet formation in hela cervical cancer cells depends on cell density and the concentration of exogenous unsaturated fatty acids. *Acta Chim. Slov.* **64**, 549–554 (2017).

295. Nguyen, T. B. *et al.* DGAT1-Dependent Lipid Droplet Biogenesis Protects Mitochondrial Function during Starvation-Induced Autophagy. *Dev. Cell* **42**, 9-21.e5 (2017).

296. Cabodevilla, A. G. *et al.* Cell survival during complete nutrient deprivation depends on lipid droplet-fueled β-oxidation of fatty acids. *J. Biol. Chem.* **288**, 27777–27788 (2013).

297. Herms, A. *et al.* AMPK activation promotes lipid droplet dispersion on detyrosinated microtubules to increase mitochondrial fatty acid oxidation. *Nat. Commun.* **6**, 1–14 (2015).

298. Rambold, A. S., Cohen, S. & Lippincott-Schwartz, J. Fatty acid trafficking in starved cells: Regulation by lipid droplet lipolysis, autophagy, and mitochondrial fusion dynamics. *Dev. Cell* **32**, 678–692 (2015).

299. Koizume, S. & Miyagi, Y. Lipid droplets: A key cellular organelle associated with cancer cell survival under normoxia and hypoxia. *International Journal of Molecular Sciences* **17**, (2016).

300. Bensaad, K. *et al.* Fatty acid uptake and lipid storage induced by HIF-1α contribute to cell growth and survival after hypoxia-reoxygenation. *Cell Rep.* **9**, 349–365 (2014).

301. Schlaepfer, I. R. *et al.* Hypoxia induces triglycerides accumulation in prostate cancer cells and extracellular vesicles supporting growth and invasiveness following reoxygenation. *Oncotarget* **6**, 22836–22856 (2015).

302. Zoula, S. *et al.* Pimonidazole binding in C6 rat brain glioma: Relation with lipid droplet detection. *Br. J. Cancer* **88**, 1439–1444 (2003).

303. Kamphorst, J. J. *et al.* Hypoxic and Ras-transformed cells support growth by scavenging unsaturated fatty acids from lysophospholipids. *Proc. Natl. Acad. Sci. U. S. A.* **110**, 8882–8887 (2013).

304. Ackerman, D. *et al.* Triglycerides Promote Lipid Homeostasis during Hypoxic Stress by Balancing Fatty Acid Saturation. *Cell Rep.* **24**, 2596-2605.e5 (2018).

305. Barrera, G., Balaram, P., Fang, B., Fujimoto, N. & Hansen, O. Oxidative Stress and Lipid Peroxidation Products in Cancer Progression and Therapy. *Int. Sch. Res. Netw. ISRN Oncol.* **2012**, (2012).

306. Gaschler, M. M. & Stockwell, B. R. Lipid peroxidation in cell death. *Biochemical and Biophysical Research Communications* **482**, 419–425 (2017).

307. Cruz, A. L. S. *et al.* Cell Cycle Progression Regulates Biogenesis and Cellular Localization of Lipid Droplets. *Mol. Cell. Biol.* **39**, (2019).

308. Patel, D. *et al.* A late G1 lipid checkpoint that is dysregulated in clear cell renal carcinoma cells. *J. Biol. Chem.* **292**, 936–944 (2017).

309. Qi, W. *et al.* FOXO3 growth inhibition of colonic cells is dependent on intraepithelial lipid droplet density. *J. Biol. Chem.* **288**, 16274–16281 (2013).

310. Yu, W., Cassara, J. & Weller, P. F. Phosphatidylinositide 3-kinase localizes to cytoplasmic lipid bodies in human polymorphonuclear leukocytes and other myeloid-derived cells. *Blood* **95**, 1078–1085 (2000).

311. Yu, W. *et al.* Co-compartmentalization of MAP kinases and cytosolic phospholipase A2 at cytoplasmic arachidonate-rich lipid bodies. *Am. J. Pathol.* **152**, 759–769 (1998).

312. Gomes, R. N., Costa, S. F. da & Colquhoun, A. Eicosanoids and cancer. *Clinics* **73**, (2018).

313. Kim, S. H. *et al.* Microsomal PGE2 synthase-1 regulates melanoma cell survival and associates with melanoma disease progression. *Pigment Cell Melanoma Res.* **29**, 297–308 (2016).

314. Accioly, M. T. *et al.* Lipid bodies are reservoirs of cyclooxygenase-2 and sites of prostaglandin-E2 synthesis in colon cancer cells. *Cancer Res.* **68**, 1732–1740 (2008).

315. Kim, S. H. *et al.* The COX2 effector microsomal PGE2 synthase 1 is a regulator of immunosuppression in cutaneous melanoma. *Clin. Cancer Res.* **25**, 1650–1663 (2019).

316. Veglia, F. *et al.* Lipid bodies containing oxidatively truncated lipids block antigen cross-presentation by dendritic cells in cancer. *Nat. Commun.* **8**, 1–16 (2017).

317. Wu, H. *et al.* Lipid droplet-dependent fatty acid metabolism controls the immune suppressive phenotype of tumor-associated macrophages. *EMBO Mol. Med.* **11**, (2019).

318. Wu, H. *et al.* Oleate but not stearate induces the regulatory phenotype of myeloid suppressor cells. *Sci. Rep.* **7**, 1–14 (2017).

319. Zhang, Y. *et al.* Fatty acid-binding protein E-FABP restricts tumor growth by promoting IFN-b responses in tumor-associated macrophages. *Cancer Res.* **74**, 2986–2998 (2014).

320. Fujimoto, M. *et al.* Adipophilin expression in cutaneous malignant melanoma. *J. Cutan. Pathol.* **44**, 228–236 (2017).

321. Fujimoto, M. *et al.* Adipophilin expression in cutaneous malignant melanoma

is associated with high proliferation and poor clinical prognosis. *Lab. Investig.* **100**, 727–737 (2020).

322. Giampietri, C. *et al.* Lipid storage and autophagy in melanoma cancer cells. *Int. J. Mol. Sci.* **18**, (2017).

323. Yen, C. L. E., Stone, S. J., Koliwad, S., Harris, C. & Farese, R. V. DGAT enzymes and triacylglycerol biosynthesis. *Journal of Lipid Research* **49**, 2283–2301 (2008).

324. Hung, Y. H., Carreiro, A. L. & Buhman, K. K. Dgat1 and Dgat2 regulate enterocyte triacylglycerol distribution and alter proteins associated with cytoplasmic lipid droplets in response to dietary fat. *Biochim. Biophys. Acta - Mol. Cell Biol. Lipids* **1862**, 600–614 (2017).

325. Bhatt-Wessel, B., Jordan, T. W., Miller, J. H. & Peng, L. Role of DGAT enzymes in triacylglycerol metabolism. *Archives of Biochemistry and Biophysics* **655**, 1–11 (2018).

326. Stone, S. J. *et al.* The endoplasmic reticulum enzyme DGAT2 is found in mitochondria-associated membranes and has a mitochondrial targeting signal that promotes its association with mitochondria. *J. Biol. Chem.* **284**, 5352–5361 (2009).

327. McFie, P. J., Banman, S. L. & Stone, S. J. Diacylglycerol acyltransferase-2 contains a c-terminal sequence that interacts with lipid droplets. *Biochim. Biophys. Acta - Mol. Cell Biol. Lipids* **1863**, 1068–1081 (2018).

328. Stone, S. J. *et al.* Lipopenia and Skin Barrier Abnormalities in DGAT2-deficient Mice. *J. Biol. Chem.* **279**, 11767–11776 (2004).

329. Smith, S. J. *et al.* Obesity resistance and multiple mechanisms of triglyceride synthesis in mice lacking Dgat. *Nat. Genet.* **25**, 87–90 (2000).

330. Chen, H. C. *et al.* Increased insulin and leptin sensitivity in mice lacking acyl CoA:diacylglycerol acyltransferase 1. *J. Clin. Invest.* **109**, 1049–1055 (2002).

331. Chen, H. C., Ladha, Z., Smith, S. J. & Farese, R. V. Analysis of energy expenditure at different ambient temperatures in mice lacking DGAT1. *Am. J. Physiol. - Endocrinol. Metab.* **284**, (2003).

332. Buhman, K. K. *et al.* DGAT1 is not essential for intestinal triacylglycerol absorption or chylomicron synthesis. *J. Biol. Chem.* **277**, 25474–25479 (2002).

333. Tsuda, N. *et al.* Intestine-Targeted DGAT1 Inhibition Improves Obesity and Insulin Resistance without Skin Aberrations in Mice. *PLoS One* **9**, e112027 (2014).

334. Cao, J. *et al.* Targeting acyl-CoA:Diacylglycerol Acyltransferase 1 (DGAT1) with small molecule inhibitors for the treatment of metabolic diseases. *J. Biol. Chem.* **286**, 41838–41851 (2011).

335. Lee, B., Fast, A. M., Zhu, J., Cheng, J. X. & Buhman, K. K. Intestine-specific

expression of acyl CoA:diacylglycerol acyltransferase 1 reverses resistance to diet-induced hepatic steatosis and obesity in Dgat1 -/- mice. *J. Lipid Res.* **51**, 1770–1780 (2010).

336. Chen, H. C. Enhancing energy and glucose metabolism by disrupting triglyceride synthesis: Lessons from mice lacking DGAT1. *Nutrition and Metabolism* **3**, 10 (2006).

337. Chen, H. C. *et al.* Role of adipocyte-derived factors in enhancing insulin signaling in skeletal muscle and white adipose tissue of mice lacking acyl CoA: diacylglycerol acyltransferase 1. *Diabetes* **53**, 1445–1451 (2004).

338. Chen, H. C., Stone, S. J., Zhou, P., Buhman, K. K. & Farese, R. V. Dissociation of obesity and impaired glucose disposal in mice overexpressing acyl coenzyme A: Diacylglycerol acyltransferase 1 in white adipose tissue. *Diabetes* **51**, 3189–3195 (2002).

339. Liu, L. *et al.* Cardiomyocyte-specific loss of diacylglycerol acyltransferase 1 (DGAT1) reproduces the abnormalities in lipids found in severe heart failure. *J. Biol. Chem.* **289**, 29881–29891 (2014).

340. Nardi, F. *et al.* DGAT1 Inhibitor Suppresses Prostate Tumor Growth and Migration by Regulating Intracellular Lipids and Non-Centrosomal MTOC Protein GM130. *Sci. Rep.* **9**, 1–14 (2019).

341. Mitra, R., Le, T. T., Gorjala, P. & Goodman, O. B. Positive regulation of prostate cancer cell growth by lipid droplet forming and processing enzymes DGAT1 and ABHD5. *BMC Cancer* **17**, 631 (2017).

342. Casar, B. *et al.* RAS at the Golgi antagonizes malignant transformation through PTPRκ-mediated inhibition of ERK activation. *Nat. Commun.* **9**, 1–17 (2018).

343. Ceol, C. J. *et al.* The histone methyltransferase SETDB1 is recurrently amplified in melanoma and accelerates its onset. *Nature* **471**, 513–518 (2011).

344. Gao, J. *et al.* Integrative analysis of complex cancer genomics and clinical profiles using the cBioPortal. *Sci. Signal.* **6**, (2013).

345. Mermel, C. H. *et al.* GISTIC2.0 facilitates sensitive and confident localization of the targets of focal somatic copy-number alteration in human cancers. *Genome Biol.* **12**, (2011).

346. Chen, E. Y. *et al.* Enrichr: Interactive and collaborative HTML5 gene list enrichment analysis tool. *BMC Bioinformatics* **14**, 128 (2013).

347. Zhou, Y. *et al.* Metascape provides a biologist-oriented resource for the analysis of systems-level datasets. *Nat. Commun.* **10**, 1–10 (2019).

348. Anaya, J. OncoLnc: Linking TCGA survival data to mRNAs, miRNAs, and lncRNAs. *PeerJ Comput. Sci.* **2016**, e67 (2016).

349. Rhodes, D. R. *et al.* ONCOMINE: A Cancer Microarray Database and Integrated Data-Mining Platform. *Neoplasia* **6**, 1–6 (2004).

350. Bolger, A. M., Lohse, M. & Usadel, B. Trimmomatic: A flexible trimmer for Illumina sequence data. *Bioinformatics* **30**, 2114–2120 (2014).

351. Dobin, A. *et al.* STAR: Ultrafast universal RNA-seq aligner. *Bioinformatics* **29**, 15–21 (2013).

352. Liao, Y., Smyth, G. K. & Shi, W. FeatureCounts: An efficient general purpose program for assigning sequence reads to genomic features. *Bioinformatics* **30**, 923–930 (2014).

353. Love, M. I., Huber, W. & Anders, S. Moderated estimation of fold change and dispersion for RNA-seq data with DESeq2. *Genome Biol.* **15**, 550 (2014).

354. Jersie-Christensen, R. R., Sultan, A. & Olsen, J. V. Simple and reproducible sample preparation for single- shot phosphoproteomics with high sensitivity. in *Methods in Molecular Biology* **1355**, 251–260 (Humana Press Inc., 2016).

355. Francavilla, C. *et al.* Multilayered proteomics reveals molecular switches dictating ligand-dependent EGFR trafficking. *Nat. Struct. Mol. Biol.* **23**, 608–618 (2016).

356. Cox, J. *et al.* Andromeda: A peptide search engine integrated into the MaxQuant environment. *J. Proteome Res.* **10**, 1794–1805 (2011).

357. Olsen, J. V. *et al.* Global, In Vivo, and Site-Specific Phosphorylation Dynamics in Signaling Networks. *Cell* **127**, 635–648 (2006).

358. Zhang, B., Kirov, S. & Snoddy, J. WebGestalt: An integrated system for exploring gene sets in various biological contexts. *Nucleic Acids Res.* **33**, (2005).

359. Chambers, M. C. *et al.* A cross-platform toolkit for mass spectrometry and proteomics. *Nature Biotechnology* **30**, 918–920 (2012).

360. Libiseller, G. *et al.* IPO: A tool for automated optimization of XCMS parameters. *BMC Bioinformatics* **16**, (2015).

361. Smith, C. A., Want, E. J., O'Maille, G., Abagyan, R. & Siuzdak, G. XCMS: Processing mass spectrometry data for metabolite profiling using nonlinear peak alignment, matching, and identification. *Anal. Chem.* **78**, 779–787 (2006).

362. Parsons, H. M., Ludwig, C., Günther, U. L. & Viant, M. R. Improved classification accuracy in 1- and 2-dimensional NMR metabolomics data using the variance stabilising generalised logarithm transformation. *BMC Bioinformatics* **8**, 234 (2007).

363. Sumner, L. W. *et al.* Proposed minimum reporting standards for chemical analysis: Chemical Analysis Working Group (CAWG) Metabolomics Standards Initiative (MSI). *Metabolomics* **3**, 211–221 (2007).

364. Spence, R., Gerlach, G., Lawrence, C. & Smith, C. The behaviour and ecology of the zebrafish, Danio rerio. *Biological Reviews* **83**, 13–34 (2008).

365. Howe, K. *et al.* The zebrafish reference genome sequence and its relationship to the human genome. *Nature* **496**, 498–503 (2013).

366. Carneiro, M. C., De Castro, I. P. & Ferreira, M. G. Telomeres in aging and disease: Lessons from zebrafish. *DMM Disease Models and Mechanisms* **9**, 737–748 (2016).

367. Pliss, G. B., Zabezhinski, M. A., Petrov, A. S. & Khudoley, V. V. Peculiarities of N-nitramines carcinogenic action. *Arch. Geschwulstforsch.* **52**, 629–34 (1982).

368. Beckwith, L. G., Moore, J. L., Tsao-Wu, G. S., Harshbarger, J. C. & Cheng, K. C. Ethylnitrosourea induces neoplasia in zebrafish (Danio rerio). *Lab. Investig.* **80**, 379–385 (2000).

369. Spitsbergen, J. M. *et al.* Neoplasia in zebrafish (Danio rerio) treated with N-methyl-N'-nitro-N-nitrosoguanidine by three exposure routes at different developmental stages. *Toxicol. Pathol.* **28**, 716–725 (2000).

370. Langenau, D. M. *et al.* Myc-induced T cell leukemia in transgenic zebrafish. *Science (80-.).* **299**, 887–890 (2003).

371. Hong, W. Y. *et al.* Targeted expression of human MYCN selectively causes pancreatic neuroendocrine tumors in transgenic zebrafish. *Cancer Res.* **64**, 7256–7262 (2004).

372. Berghmans, S. *et al.* tp53 mutant zebrafish develop malignant peripheral nerve sheath tumors. *Proc. Natl. Acad. Sci. U. S. A.* **102**, 407–412 (2005).

373. Hwang, W. Y. *et al.* Efficient genome editing in zebrafish using a CRISPR-Cas system. *Nat. Biotechnol.* **31**, 227–229 (2013).

374. Ablain, J., Durand, E. M., Yang, S., Zhou, Y. & Zon, L. I. A CRISPR/Cas9 vector system for tissue-specific gene disruption in zebrafish. *Dev. Cell* **32**, 756–764 (2015).

375. J, A. *et al.* Human tumor genomics and zebrafish modeling identify SPRED1 loss as a driver of mucosal melanoma. *Science* **362**, (2018).

376. White, R. M. *et al.* Transparent Adult Zebrafish as a Tool for In Vivo Transplantation Analysis. *Cell Stem Cell* **2**, 183–189 (2008).

377. Moore, J. C. *et al.* Single-cell imaging of normal and malignant cell engraftment into optically clear prkdc-null scid zebrafish. *J. Exp. Med.* **213**, 2575–2589 (2016).

378. Haldi, M., Ton, C., Seng, W. L. & McGrath, P. Human melanoma cells transplanted into zebrafish proliferate, migrate, produce melanin, form masses and stimulate angiogenesis in zebrafish. *Angiogenesis* **9**, 139–151 (2006).

379. Chapman, A. *et al.* Heterogeneous tumor subpopulations cooperate to drive

invasion. *Cell Rep.* **8**, 688–695 (2014).

380. Traver, D. *et al.* Effects of lethal irradiation in zebrafish and rescue by hematopoietic cell transplantation. *Blood* **104**, 1298–1305 (2004).

381. Venkatesan, A. M. *et al.* Ligand-activated BMP signaling inhibits cell differentiation and death to promote melanoma. *J. Clin. Invest.* **128**, 294–308 (2018).

382. Travnickova, J. *et al.* Zebrafish MITF-low melanoma subtype models reveal transcriptional subclusters and MITF-independent residual disease. *Cancer Res.* **79**, 5769–5784 (2019).

383. Michailidou, C. *et al.* Dissecting the roles of Raf- and PI3K-signalling pathways in melanoma formation and progression in a zebrafish model. *DMM Dis. Model. Mech.* **2**, 399–411 (2009).

384. Mouti, M. A., Dee, C., Coupland, S. E. & Hurlstone, A. F. L. Minimal contribution of ERK1/2-MAPK signalling towards the maintenance of oncogenic GNAQQ209P-driven uveal melanomas in zebrafish. *Oncotarget* **7**, 39654–39670 (2016).

385. Kaufman, C. K. *et al.* A zebrafish melanoma model reveals emergence of neural crest identity during melanoma initiation. *Science (80-.).* **351**, (2016).

386. Wang, J. & Li, Y. CD36 tango in cancer: Signaling pathways and functions. *Theranostics* **9**, 4893–4908 (2019).

387. Liang, Y. *et al.* CD36 plays a critical role in proliferation, migration and tamoxifen-inhibited growth of ER-positive breast cancer cells. *Oncogenesis* **7**, 1–14 (2018).

388. Silverstein, R. L. & Febbraio, M. CD36, a scavenger receptor involved in immunity, metabolism, angiogenesis, and behavior. *Science Signaling* **2**, re3 (2009).

389. Bastã-An, B. C., Leboit, E., Hamm, H., Brã, E.-B. & Pinkel, D. *Chromosomal Gains and Losses in Primary Cutaneous Melanomas Detected by Comparative Genomic Hybridization1*. *CANCER RESEARCH* **58**, (1998).

390. Venkatesan, A. M. *et al.* Ligand-activated BMP signaling inhibits cell differentiation and death to promote melanoma. *J. Clin. Invest.* **128**, 294–308 (2018).

391. Cheng, X. *et al.* Targeting DGAT1 Ameliorates Glioblastoma by Increasing Fat Catabolism and Oxidative Stress. *Cell Metab.* (2020). doi:10.1016/J.CMET.2020.06.002

392. Yu, Y.-H. *et al.* Posttranscriptional Control of the Expression and Function of Diacylglycerol Acyltransferase-1 in Mouse Adipocytes. *J. Biol. Chem.* **277**, 50876–50884 (2002).

393. Zhuang, D. *et al.* C-MYC overexpression is required for continuous

suppression of oncogene-induced senescence in melanoma cells. *Oncogene* **27**, 6623–6634 (2008).

394. Kfoury, A. *et al.* AMPK promotes survival of c-Myc-positive melanoma cells by suppressing oxidative stress. *EMBO J.* **37**, (2018).

395. Müller, T. *et al.* ASAP1 promotes tumor cell motility and invasiveness, stimulates metastasis formation in vivo, and correlates with poor survival in colorectal cancer patients. *Oncogene* **29**, 2393–2403 (2010).

396. Lin, D. *et al.* ASAP1, a gene at 8q24, is associated with prostate cancer metastasis. *Cancer Res.* **68**, 4352–4359 (2008).

397. Hou, T. *et al.* Overexpression of ASAP1 is associated with poor prognosis in epithelial ovarian cancer. *Int. J. Clin. Exp. Pathol.* **7**, 280–7 (2014).

398. White, R. M. Cross-species oncogenomics using zebrafish models of cancer. *Current Opinion in Genetics and Development* **30**, 73–79 (2015).

399. Rudner, L. A. *et al.* Shared acquired genomic changes in zebrafish and human T-ALL. *Oncogene* **30**, 4289–4296 (2011).

400. Chen, E. Y. *et al.* Cross-Species Array Comparative Genomic Hybridization Identifies Novel Oncogenic Events in Zebrafish and Human Embryonal Rhabdomyosarcoma. *PLoS Genet.* **9**, e1003727 (2013).

401. Meegalla, R. L., Billheimer, J. T. & Cheng, D. Concerted elevation of acyl-coenzyme A:diacylglycerol acyltransferase (DGAT) activity through independent stimulation of mRNA expression of DGAT1 and DGAT2 by carbohydrate and insulin. *Biochem. Biophys. Res. Commun.* **298**, 317–323 (2002).

402. Ludwig, E. H. *et al.* DGAT1 promoter polymorphism associated with alterations in body mass index, high density lipoprotein levels and blood pressure in Turkish women. *Clin. Genet.* **62**, 68–73 (2002).

403. Taylor, J. S., Braasch, I., Frickey, T., Meyer, A. & Van de Peer, Y. Genome duplication, a trait shared by 22,000 species of ray-finned fish. *Genome Res.* **13**, 382–390 (2003).

404. Garraway, L. A. *et al.* Integrative genomic analyses identify MITF as a lineage survival oncogene amplified in malignant melanoma. *Nature* **436**, 117–122 (2005).

405. Müller, J. *et al.* Low MITF/AXL ratio predicts early resistance to multiple targeted drugs in melanoma. *Nat. Commun.* **5**, (2014).

406. Ennen, M. *et al.* MITF-high and MITF-low cells and a novel subpopulation expressing genes of both cell states contribute to intra- and intertumoral heterogeneity of primary melanoma. *Clin. Cancer Res.* **23**, 7097–7107 (2017).

407. Zeng, H. *et al.* Bi-allelic Loss of CDKN2A Initiates Melanoma Invasion via BRN2 Activation. *Cancer Cell* **34**, 56-68.e9 (2018).

408. Škalamera, D. *et al.* Melanoma mutations modify melanocyte dynamics in co-culture with keratinocytes or fibroblasts. *J. Cell Sci.* **132**, (2019).

409. Dankort, D. *et al.* BRAF V600E cooperates with PTEN silencing to elicit metastatic melanoma. *Nat. Genet.* **41**, 544–552 (2009).

410. Ackermann, J. *et al.* Metastasizing melanoma formation caused by expression of activated N-RasQ61K on an INK4a-deficient background. *Cancer Res.* **65**, 4005–4011 (2005).

411. Kim, J. & Guan, K. L. mTOR as a central hub of nutrient signalling and cell growth. *Nature Cell Biology* **21**, 63–71 (2019).

412. Mao, Z. & Zhang, W. Role of mTOR in glucose and lipid metabolism. *International Journal of Molecular Sciences* **19**, (2018).

413. Lamming, D. W. & Sabatini, D. M. Cell Metabolism Minireview A Central Role for mTOR in Lipid Homeostasis. (2013). doi:10.1016/j.cmet.2013.08.002

414. Yen, C. L. E., Monetti, M., Burri, B. J. & Farese, R. V. The triacylglycerol synthesis enzyme DGAT1 also catalyzes the synthesis of diacylglycerols, waxes, and retinyl esters. *J. Lipid Res.* **46**, 1502–1511 (2005).

415. Liu, G. Y. & Sabatini, D. M. mTOR at the nexus of nutrition, growth, ageing and disease. *Nature Reviews Molecular Cell Biology* **21**, 183–203 (2020).

416. Tian, T., Li, X. & Zhang, J. mTOR signaling in cancer and mtor inhibitors in solid tumor targeting therapy. *International Journal of Molecular Sciences* **20**, (2019).

417. Murugan, A. K. mTOR: Role in cancer, metastasis and drug resistance. *Seminars in Cancer Biology* **59**, 92–111 (2019).

418. Peterson, T. R. *et al.* DEPTOR Is an mTOR Inhibitor Frequently Overexpressed in Multiple Myeloma Cells and Required for Their Survival. *Cell* **137**, 873–886 (2009).

419. Kim, D. H. *et al.* GβL, a positive regulator of the rapamycin-sensitive pathway required for the nutrient-sensitive interaction between raptor and mTOR. *Mol. Cell* **11**, 895–904 (2003).

420. Kim, D. H. *et al.* mTOR interacts with raptor to form a nutrient-sensitive complex that signals to the cell growth machinery. *Cell* **110**, 163–175 (2002).

421. Wang, L., Harris, T. E., Roth, R. A. & Lawrence, J. C. PRAS40 regulates mTORC1 kinase activity by functioning as a direct inhibitor of substrate binding. *J. Biol. Chem.* **282**, 20036–20044 (2007).

422. Manning, B. D., Tee, A. R., Logsdon, M. N., Blenis, J. & Cantley, L. C. Identification of the tuberous sclerosis complex-2 tumor suppressor gene product tuberin as a target of the phosphoinositide 3-kinase/Akt pathway. *Mol. Cell* **10**, 151–162 (2002).

423. Roux, P. P., Ballif, B. A., Anjum, R., Gygi, S. P. & Blenis, J. Tumor-promoting

phorbol esters and activated Ras inactivate the tuberous sclerosis tumor suppressor complex via p90 ribosomal S6 kinase. *Proc. Natl. Acad. Sci. U. S. A.* **101**, 13489–13494 (2004).

424. Menon, S. *et al.* Spatial control of the TSC complex integrates insulin and nutrient regulation of mTORC1 at the lysosome. *Cell* **156**, 771–785 (2014).

425. Yang, H. *et al.* Mechanisms of mTORC1 activation by RHEB and inhibition by PRAS40. *Nature* **552**, 368–373 (2017).

426. Haar, E. Vander, Lee, S. il, Bandhakavi, S., Griffin, T. J. & Kim, D. H. Insulin signalling to mTOR mediated by the Akt/PKB substrate PRAS40. *Nat. Cell Biol.* **9**, 316–323 (2007).

427. Sancak, Y. *et al.* The rag GTPases bind raptor and mediate amino acid signaling to mTORC1. *Science (80-.).* **320**, 1496–1501 (2008).

428. Sancak, Y. *et al.* Ragulator-rag complex targets mTORC1 to the lysosomal surface and is necessary for its activation by amino acids. *Cell* **141**, 290–303 (2010).

429. Wang, S. *et al.* Lysosomal amino acid transporter SLC38A9 signals arginine sufficiency to mTORC1. *Science (80-.).* **347**, 188–194 (2015).

430. Wolfson, R. L. *et al.* Sestrin2 is a leucine sensor for the mTORC1 pathway. *Science (80-.).* **351**, 43–48 (2016).

431. Chantranupong, L. *et al.* The CASTOR Proteins Are Arginine Sensors for the mTORC1 Pathway. *Cell* **165**, 153–164 (2016).

432. Gu, X. *et al.* SAMTOR is an S-adenosylmethionine sensor for the mTORC1 pathway. *Science (80-.).* **358**, 813–818 (2017).

433. Hawley, S. A. *et al.* 5’-AMP activates the AMP-activated protein kinase cascade, and Ca2+/calmodulin activates the calmodulin-dependent protein kinase I cascade, via three independent mechanisms. *J. Biol. Chem.* **270**, 27186–27191 (1995).

434. Suter, M. *et al.* Dissecting the role of 5’-AMP for allosteric stimulation, activation, and deactivation of AMP-activated protein kinase. *J. Biol. Chem.* **281**, 32207–32216 (2006).

435. Inoki, K., Zhu, T. & Guan, K. L. TSC2 Mediates Cellular Energy Response to Control Cell Growth and Survival. *Cell* **115**, 577–590 (2003).

436. Gwinn, D. M. *et al.* AMPK Phosphorylation of Raptor Mediates a Metabolic Checkpoint. *Mol. Cell* **30**, 214–226 (2008).

437. Pullen, N. & Thomas, G. The modular phosphorylation and activation of p70(s6k). in *FEBS Letters* **410**, 78–82 (FEBS Lett, 1997).

438. Alessi, D., Kozlowski, M. T., Weng, Q. P., Morrice, N. & Avruch, J. 3-phosphoinositide-dependent protein kinase 1 (PDK1) phosphorylates and activates the p70 S6 kinase in vivo and in vitro. *Curr. Biol.* **8**, 69–81 (1998).

439. Kozma, S. C. *et al.* Cloning of the mitogen-activated S6 kinase from rat liver reveals an enzyme of the second messenger subfamily. *Proc. Natl. Acad. Sci. U. S. A.* **87**, 7365–7369 (1990).

440. Raught, B. *et al.* Phosphorylation of eucaryotic translation initiation factor 4B Ser422 is modulated by S6 kinases. *EMBO J.* **23**, 1761–1769 (2004).

441. Wang, X. *et al.* Regulation of elongation factor 2 kinase by p90(RSK1) and p70 S6 kinase. *EMBO J.* **20**, 4370–4379 (2001).

442. Dorrello, N. V. *et al.* S6k1- and βTRCP-mediated degradation of PDCD4 promotes protein translation and cell growth. *Science (80-.).* **314**, 467–471 (2006).

443. Gingras, A. C. *et al.* Regulation of 4E-BP1 phosphorylation: A novel two step mechanism. *Genes Dev.* **13**, 1422–1437 (1999).

444. Pause, A. *et al.* Insulin-dependent stimulation of protein synthesis by phosphorylation of a regulator of 5'-cap function. *Nature* **371**, 762–767 (1994).

445. Porstmann, T. *et al.* SREBP Activity Is Regulated by mTORC1 and Contributes to Akt-Dependent Cell Growth. *Cell Metab.* **8**, 224–236 (2008).

446. Düvel, K. *et al.* Activation of a metabolic gene regulatory network downstream of mTOR complex 1. *Mol. Cell* **39**, 171–183 (2010).

447. Peterson, T. R. *et al.* MTOR complex 1 regulates lipin 1 localization to control the srebp pathway. *Cell* **146**, 408–420 (2011).

448. Kim, J. E. & Chen, J. Regulation of peroxisome proliferator-activated receptor-γ activity by mammalian target of rapamycin and amino acids in adipogenesis. *Diabetes* **53**, 2748–2756 (2004).

449. Ben-Sahra, I., Howell, J. J., Asara, J. M. & Manning, B. D. Stimulation of de novo pyrimidine synthesis by growth signaling through mTOR and S6K1. *Science (80-.).* **339**, 1323–1328 (2013).

450. Ben-Sahra, I., Hoxhaj, G., Ricoult, S. J. H., Asara, J. M. & Manning, B. D. mTORC1 induces purine synthesis through control of the mitochondrial tetrahydrofolate cycle. *Science (80-.).* **351**, 728–733 (2016).

451. Kim, J., Kundu, M., Viollet, B. & Guan, K. L. AMPK and mTOR regulate autophagy through direct phosphorylation of Ulk1. *Nat. Cell Biol.* **13**, 132–141 (2011).

452. Martina, J. A., Chen, Y., Gucek, M. & Puertollano, R. MTORC1 functions as a transcriptional regulator of autophagy by preventing nuclear transport of TFEB. *Autophagy* **8**, 903–914 (2012).

453. Puente, L. G., Lee, R. E. C. & Megeney, L. A. Phospho-Proteomics. *Methods* **527**, 311–319 (2009).

454. Schalm, S. S. & Blenis, J. Identification of a conserved motif required for

mTOR signaling. *Curr. Biol.* **12**, 632–639 (2002).

455. Cao, J. *et al.* Targeting acyl-CoA:Diacylglycerol Acyltransferase 1 (DGAT1) with small molecule inhibitors for the treatment of metabolic diseases. *J. Biol. Chem.* **286**, 41838–41851 (2011).

456. McCoull, W. *et al.* Identification, optimisation and in vivo evaluation of oxadiazole DGAT-1 inhibitors for the treatment of obesity and diabetes. *Bioorganic Med. Chem. Lett.* **22**, 3873–3878 (2012).

457. Barlind, J. G. *et al.* Design and optimization of pyrazinecarboxamide-based inhibitors of diacylglycerol acyltransferase 1 ((DGAT1) leading to a clinical candidate dimethylpyrazinecarboxamide phenylcyclohexylacetic acid (AZD7687). *J. Med. Chem.* **55**, 10610–10629 (2012).

458. Tsuda, N. *et al.* Intestine-Targeted DGAT1 Inhibition Improves Obesity and Insulin Resistance without Skin Aberrations in Mice. *PLoS One* **9**, e112027 (2014).

459. Armengol, G. *et al.* 4E-binding protein 1: A key molecular 'funnel factor' in human cancer with clinical implications. *Cancer Research* **67**, 7551–7555 (2007).

460. Pantuck, A. J. *et al.* Prognostic relevance of the mTOR pathway in renal cell carcinoma: Implications for molecular patient selection for targeted therapy. *Cancer* **109**, 2257–2267 (2007).

461. Bjornsti, M. A. & Houghton, P. J. Lost in translation: Dysregulation of cap-dependent translation and cancer. *Cancer Cell* **5**, 519–523 (2004).

462. No, J. H. *et al.* Activation of mTOR signaling pathway associated with adverse prognostic factors of epithelial ovarian cancer. *Gynecol. Oncol.* **121**, 8–12 (2011).

463. Bärlund, M. *et al. Detecting Activation of Ribosomal Protein S6 Kinase by Complementary DNA and Tissue Microarray Analysis*.

464. Ruggero, D. *et al.* The translation factor eIF-4E promotes tumor formation and cooperates with c-Myc in lymphomagenesis. *Nat. Med.* **10**, 484–486 (2004).

465. Dhawan, P., Singh, A. B., Ellis, D. L. & Richmond, A. *Constitutive Activation of Akt/Protein Kinase B in Melanoma Leads to Up-Regulation of Nuclear Factor-B and Tumor Progression 1*.

466. Carrière, A. *et al.* Oncogenic MAPK Signaling Stimulates mTORC1 Activity by Promoting RSK-Mediated Raptor Phosphorylation. *Curr. Biol.* **18**, 1269–1277 (2008).

467. Ballif, B. A. *et al.* Quantitative phosphorylation profiling of the ERK/p90 ribosomal S6 kinase-signaling cassette and its targets, the tuberous sclerosis tumor suppressors. *Proc. Natl. Acad. Sci. U. S. A.* **102**, 667–672 (2005).

468. Pópulo, H. *et al.* mTOR pathway activation in cutaneous melanoma is associated with poorer prognosis characteristics. *Pigment Cell and Melanoma Research* **24**, 254–257 (2011).

469. Molhoek, K. R., Brautigan, D. L. & Slingluff, C. L. Synergistic inhibition of human melanoma proliferation by combination treatment with B-Raf inhibitor BAY43-9006 and mTOR inhibitor rapamycin. *J. Transl. Med.* **3**, 39 (2005).

470. Karbowniczek, M., Spittle, C. S., Morrison, T., Wu, H. & Henske, E. P. mTOR is activated in the majority of malignant melanomas. *J. Invest. Dermatol.* **128**, 980–987 (2008).

471. Silva, J. M., Bulman, C. & McMahon, M. BRAFV600E cooperates with PI3K signaling, independent of AKT, to regulate melanoma cell proliferation. *Mol. Cancer Res.* **12**, 447–463 (2014).

472. Syed, D. N. *et al.* Fisetin inhibits human melanoma cell growth through direct binding to p70S6K and mTOR: Findings from 3-D melanoma skin equivalents and computational modeling. *Biochem. Pharmacol.* **89**, 349–360 (2014).

473. Romano, G. *et al.* A preexisting rare PIK3CA e545k subpopulation confers clinical resistance to MEK plus CDK4/6 inhibition in NRAS melanoma and is dependent on S6K1 signaling. *Cancer Discov.* **8**, 556–567 (2018).

474. Ohcuchi, K., Banno, Y., Nakagawa, Y., Akao, Y. & Nozawa, Y. Negative regulation of melanogenesis by phospholipase D1 through mTOR/p70 S6 kinase 1 signaling in mouse B16 melanoma cells. *J. Cell. Physiol.* **205**, 444–451 (2005).

475. Mitra, R., Le, T. T., Gorjala, P. & Goodman, O. B. Positive regulation of prostate cancer cell growth by lipid droplet forming and processing enzymes DGAT1 and ABHD5. *BMC Cancer* **17**, 631 (2017).

476. Cheng, X. *et al.* Targeting DGAT1 Ameliorates Glioblastoma by Increasing Fat Catabolism and Oxidative Stress. *Cell Metab.* (2020). doi:10.1016/j.cmet.2020.06.002

477. Kim, S. G. *et al.* Metabolic Stress Controls mTORC1 Lysosomal Localization and Dimerization by Regulating the TTT-RUVBL1/2 Complex. *Mol. Cell* **49**, 172–185 (2013).

478. Volmer, R., Van Der Ploeg, K. & Ron, D. Membrane lipid saturation activates endoplasmic reticulum unfolded protein response transducers through their transmembrane domains. *Proc. Natl. Acad. Sci. U. S. A.* **110**, 4628–4633 (2013).

479. Appenzeller-Herzog, C. & Hall, M. N. Bidirectional crosstalk between endoplasmic reticulum stress and mTOR signaling. *Trends in Cell Biology* **22**, 274–282 (2012).

480. Qin, L., Wang, Z., Tao, L. & Wang, Y. ER stress negatively regulates AKT/TSC/mTOR pathway to enhance autophagy. *Autophagy* **239**, 239–247

(2010).

481. Huang, K. P. The mechanism of protein kinase C activation. *Trends in Neurosciences* **12**, 425–432 (1989).

482. Veverka, V. *et al.* Structural characterization of the interaction of mTOR with phosphatidic acid and a novel class of inhibitor: Compelling evidence for a central role of the FRB domain in small molecule-mediated regulation of mTOR. *Oncogene* **27**, 585–595 (2008).

483. Bailey, A. P. *et al.* Antioxidant Role for Lipid Droplets in a Stem Cell Niche of Drosophila. *Cell* **163**, 340–353 (2015).

484. Benador, I. Y. *et al.* Mitochondria Bound to Lipid Droplets Have Unique Bioenergetics, Composition, and Dynamics that Support Lipid Droplet Expansion. *Cell Metab.* **27**, 869-885.e6 (2018).

485. Benador, I. Y., Veliova, M., Liesa, M. & Shirihai, O. S. Mitochondria Bound to Lipid Droplets: Where Mitochondrial Dynamics Regulate Lipid Storage and Utilization. *Cell Metabolism* **29**, 827–835 (2019).

486. Li, L. *et al.* Mass spectrometry methodology in lipid analysis. *International Journal of Molecular Sciences* **15**, 10492–10507 (2014).

487. Lydic, T. A. & Goo, Y.-H. Lipidomics unveils the complexity of the lipidome in metabolic diseases. *Clin. Transl. Med.* **7**, 4 (2018).

488. Sud, M. *et al.* LMSD: LIPID MAPS structure database. *Nucleic Acids Res.* **35**, (2007).

489. Yoon, G. *et al.* Ceramide increases Fas-mediated apoptosis in glioblastoma cells through FLIP down-regulation. *J. Neurooncol.* **60**, 135–141 (2002).

490. Nam, S. Y., Amoscato, A. A. & Lee, Y. J. Low glucose-enhanced TRAIL cytotoxicity is mediated through the ceramide–Akt–FLIP pathway. *Oncogene* **21**, 337–346 (2002).

491. Temme, A. *et al.* Nuclear localization of Survivin renders HeLa tumor cells more sensitive to apoptosis by induction of p53 and Bax. *Cancer Lett.* **250**, 177–193 (2007).

492. Liu, X. *et al.* Targeting of survivin by nanoliposomal ceramide induces complete remission in a rat model of NK-LGL leukemia. *Blood* **116**, 4192–4201 (2010).

493. Morad, S. A. F. *et al.* Ceramide-antiestrogen nanoliposomal combinations-novel impact of hormonal therapy in hormone-insensitive breast cancer. *Mol. Cancer Ther.* **11**, 2352–2361 (2012).

494. Ganesan, V. *et al.* Ceramide and activated Bax act synergistically to permeabilize the mitochondrial outer membrane. *Apoptosis* **15**, 553–562 (2010).

495. Grassmé, H., Cremesti, A., Kolesnick, R. & Gulbins, E. Ceramide-mediated

clustering is required for CD95-DISC formation. *Oncogene* **22**, 5457–5470 (2003).

496. Miyaji, M. *et al.* Role of membrane sphingomyelin and ceramide in platform formation for Fas-mediated apoptosis. *J. Exp. Med.* **202**, 249–259 (2005).

497. Lee, J. Y., Bielawska, A. E. & Obeid, L. M. Regulation of cyclin-dependent kinase 2 activity by ceramide. *Exp. Cell Res.* **261**, 303–311 (2000).

498. Kim, W. H., Kang, K. H., Kim, M. Y. & Choi, K. H. Induction of p53-independent p21 during ceramide-induced G1 arrest in human hepatocarcinoma cells. *Biochem. Cell Biol.* **78**, 127–135 (2000).

499. Wang, P. *et al.* Roles of sphingosine-1-phosphate signaling in cancer. *Cancer Cell International* **19**, 1–12 (2019).

500. Takabe, K. & Spiegel, S. Export of sphingosine-1-phosphate and cancer progression. *Journal of Lipid Research* **55**, 1839–1846 (2014).

501. Nagahashi, M. *et al.* Sphingosine-1-phosphate produced by sphingosine kinase 1 promotes breast cancer progression by stimulating angiogenesis and lymphangiogenesis. *Cancer Res.* **72**, 726–735 (2012).

502. Weichand, B. *et al.* S1PR1 on tumor-associated macrophages promotes lymphangiogenesis and metastasis via NLRP3/IL-1ß. *J. Exp. Med.* **214**, 2695–2713 (2017).

503. Watson, C. *et al.* High expression of sphingosine 1-phosphate receptors, S1P1and S1P3, sphingosine kinase 1, and extracellular signal-regulated kinase-1/2 is associated with development of tamoxifen resistance in estrogen receptor-positive breast cancer patients. *Am. J. Pathol.* **177**, 2205–2215 (2010).

504. Riehle, R. D., Cornea, S. & Degterev, A. Role of Phosphatidylinositol 3,4,5-Trisphosphate in Cell Signaling. in *Advances in experimental medicine and biology* **991**, 105–139 (Adv Exp Med Biol, 2013).

505. Liang, J. & Slingerland, J. M. Multiple roles of the PI3K/PKB (Akt) pathway in cell cycle progression. *Cell cycle (Georgetown, Tex.)* **2**, 336–342 (2003).

506. Datta, S. R. *et al.* Akt phosphorylation of BAD couples survival signals to the cell- intrinsic death machinery. *Cell* **91**, 231–241 (1997).

507. Dibble, C. C. & Cantley, L. C. Regulation of mTORC1 by PI3K signaling. *Trends in Cell Biology* **25**, 545–555 (2015).

508. Gauster, M. *et al.* Endothelial lipase releases saturated and unsaturated fatty acids of high density lipoprotein phosphatidylcholine. *J. Lipid Res.* **46**, 1517–1525 (2005).

509. Radu, C. G., Yang, L. V., Riedinger, M., Au, M. & Witte, O. N. T cell chemotaxis to lysophosphatidylcholine through the G2A receptor. *Proc. Natl. Acad. Sci. U. S. A.* **101**, 245–250 (2004).

510. Sato, A., Kumagai, T. & Ebina, K. A Synthetic Biotinylated Peptide, BP21, Inhibits the Induction of mRNA Expression of Inflammatory Substances by Oxidized- and Lyso-Phosphatidylcholine. *Drug Dev. Res.* **75**, 246–256 (2014).

511. Huang, Y. H., Schäfer-Elinder, L., Wu, R., Claesson, H. E. & Frostegård, J. Lysophosphatidylcholine (LPC) induces proinflammatory cytokines by a platelet-activating factor (PAF) receptor-dependent mechanism. *Clin. Exp. Immunol.* **116**, 326–331 (1999).

512. Qin, X., Qiu, C. & Zhao, L. Lysophosphatidylcholine perpetuates macrophage polarization toward classically activated phenotype in inflammation. *Cell. Immunol.* **289**, 185–190 (2014).

513. Wakelam, M. J. O. Diacylglycerol - When is it an intracellular messenger? *Biochimica et Biophysica Acta - Molecular and Cell Biology of Lipids* **1436**, 117–126 (1998).

514. Marignani, P. A., Epand, R. M. & Sebaldt, R. J. Acyl chain dependence of diacylglycerol activation of protein kinase C activity in vitro. *Biochem. Biophys. Res. Commun.* **225**, 469–473 (1996).

515. Li, Y. *et al.* Protein kinase C θ inhibits insulin signaling by phosphorylating IRS1 at Ser1101. *J. Biol. Chem.* **279**, 45304–45307 (2004).

516. Turinsky, J., Bayly, B. P. & O'Sullivan, D. M. 1,2-Diacylglycerol and ceramide levels in rat liver and skeletal muscle in vivo. *Am. J. Physiol. - Endocrinol. Metab.* **261**, (1991).

517. Jornayvaz, F. R. *et al.* Hepatic insulin resistance in mice with hepatic overexpression of diacylglycerol acyltransferase 2. *Proc. Natl. Acad. Sci. U. S. A.* **108**, 5748–5752 (2011).

518. Jornayvaz, F. R. *et al.* A high-fat, ketogenic diet causes hepatic insulin resistance in mice, despite increasing energy expenditure and preventing weight gain. *Am. J. Physiol. - Endocrinol. Metab.* **299**, (2010).

519. Zhao, S. *et al.* α/β-Hydrolase domain-6 and saturated long chain monoacylglycerol regulate insulin secretion promoted by both fuel and non-fuel stimuli. *Mol. Metab.* **4**, 940–950 (2015).

520. Zhao, S. *et al.* α/β-Hydrolase Domain 6 Deletion Induces Adipose Browning and Prevents Obesity and Type 2 Diabetes. *Cell Rep.* **14**, 2872–2888 (2016).

521. Ray, U. & Roy, S. S. Aberrant lipid metabolism in cancer cells – the role of oncolipid-activated signaling. *FEBS J.* **285**, 432–443 (2018).

522. Fishman, D. A., Liu, Y., Ellerbroek, S. M. & Stack, M. S. Lysophosphatidic acid promotes matrix metalloproteinase (MMP) activation and MMP-dependent invasion in ovarian cancer cells. *Cancer Res.* **61**, 3194–3199 (2001).

523. Park, S. Y. *et al.* Lysophosphatidic acid augments human hepatocellular carcinoma cell invasion through LPA1 receptor and MMP-9 expression. *Oncogene* **30**, 1351–1359 (2011).

524. Van Leeuwen, F. N. *et al.* Rac activation by lysophosphatidic acid LPA1 receptors through the guanine nucleotide exchange factor Tiam1. *J. Biol. Chem.* **278**, 400–406 (2003).

525. Bian, D. *et al.* The G12/13-RhoA signaling pathway contributes to efficient lysophosphatidic acid-stimulated cell migration. *Oncogene* **25**, 2234–2244 (2006).

526. Rysman, E. *et al.* De novo lipogenesis protects cancer cells from free radicals and chemotherapeutics by promoting membrane lipid saturation. *Cancer Res.* **70**, 8117–8126 (2010).

527. Hilvo, M. *et al.* Novel theranostic opportunities offered by characterization of altered membrane lipid metabolism in breast cancer progression. *Cancer Res.* **71**, 3236–3245 (2011).

528. Piccolis, M. *et al.* Probing the Global Cellular Responses to Lipotoxicity Caused by Saturated Fatty Acids. *Mol. Cell* **74**, 32-44.e8 (2019).

529. Shen, Y. *et al.* Metabolic activity induces membrane phase separation in endoplasmic reticulum. *Proc. Natl. Acad. Sci. U. S. A.* **114**, 13394–13399 (2017).

530. Hess, D., Chisholm, J. W. & Igal, R. A. Inhibition of stearoylCoA desaturase activity blocks cell cycle progression and induces programmed cell death in lung cancer cells. *PLoS One* **5**, (2010).

531. Ariyama, H., Kono, N., Matsuda, S., Inoue, T. & Arai, H. Decrease in membrane phospholipid unsaturation induces unfolded protein response. *J. Biol. Chem.* **285**, 22027–22035 (2010).

532. Peck, B. *et al.* Inhibition of fatty acid desaturation is detrimental to cancer cell survival in metabolically compromised environments. *Cancer Metab.* **4**, (2016).

533. Fritz, V. *et al.* Abrogation of De novo lipogenesis by stearoyl-CoA desaturase 1 inhibition interferes with oncogenic signaling and blocks prostate cancer progression in mice. *Mol. Cancer Ther.* **9**, 1740–1754 (2010).

534. Young, R. M. *et al.* Dysregulated mTORC1 renders cells critically dependent on desaturated lipids for survival under tumor-like stress. *Genes Dev.* **27**, 1115–1131 (2013).

535. Yang, W. S. *et al.* Peroxidation of polyunsaturated fatty acids by lipoxygenases drives ferroptosis. *Proc. Natl. Acad. Sci. U. S. A.* **113**, E4966–E4975 (2016).

536. Harris, C. A. *et al.* DGAT enzymes are required for triacylglycerol synthesis and lipid droplets in adipocytes. *J. Lipid Res.* **52**, 657–667 (2011).

537. Eichmann, T. O. & Lass, A. DAG tales: The multiple faces of diacylglycerol - Stereochemistry, metabolism, and signaling. *Cellular and Molecular Life Sciences* **72**, 3931–3952 (2015).

538. Fan, Q. W. *et al.* EGFR signals to mTOR through PKC and independently of Akt in glioma. *Sci. Signal.* **2**, (2009).

539. Aeder, S. E., Martin, P. M., Soh, J. W. & Hussaini, I. M. PKC-η mediates glioblastoma cell proliferation through the Akt and mTOR signaling pathways. *Oncogene* **23**, 9062–9069 (2004).

540. Moschella, P. C., Rao, V. U., McDermott, P. J. & Kuppuswamy, D. Regulation of mTOR and S6K1 activation by the nPKC isoforms, PKCε and PKCδ, in adult cardiac muscle cells. *J. Mol. Cell. Cardiol.* **43**, 754–766 (2007).

541. Aon, M. A., Bhatt, N. & Cortassa, S. Mitochondrial and cellular mechanisms for managing lipid excess. *Front. Physiol.* **5 JUL**, (2014).

542. McCoin, C. S., Knotts, T. A. & Adams, S. H. Acylcarnitines-old actors auditioning for new roles in metabolic physiology. *Nature Reviews Endocrinology* **11**, 617–625 (2015).

543. Wajner, M. & Amaral, A. U. Mitochondrial dysfunction in fatty acid oxidation disorders: Insights from human and animal studies. *Biosci. Rep.* **36**, 281 (2016).

544. Handy, D. E. & Loscalzo, J. Redox regulation of mitochondrial function. *Antioxidants and Redox Signaling* **16**, 1323–1367 (2012).

545. Yang, H. *et al.* The role of cellular reactive oxygen species in cancer chemotherapy. *Journal of Experimental and Clinical Cancer Research* **37**, 266 (2018).

546. Liou, G. Y. & Storz, P. Reactive oxygen species in cancer. *Free Radical Research* **44**, 479–496 (2010).

547. Aggarwal, V. *et al.* Role of reactive oxygen species in cancer progression: Molecular mechanisms and recent advancements. *Biomolecules* **9**, 735 (2019).

548. Zorov, D. B., Juhaszova, M. & Sollott, S. J. Mitochondrial reactive oxygen species (ROS) and ROS-induced ROS release. *Physiological Reviews* **94**, 909–950 (2014).

549. Reczek, C. R. & Chandel, N. S. The two faces of reactive oxygen species in cancer. *Annu. Rev. Cancer Biol.* **1**, 79–98 (2017).

550. Perillo, B. *et al.* ROS in cancer therapy: the bright side of the moon. *Experimental and Molecular Medicine* **52**, 192–203 (2020).

551. Galadari, S., Rahman, A., Pallichankandy, S. & Thayyullathil, F. Reactive oxygen species and cancer paradox: To promote or to suppress? *Free Radical Biology and Medicine* **104**, 144–164 (2017).

552. Dizdaroglu, M. & Jaruga, P. Mechanisms of free radical-induced damage to DNA. *Free Radical Research* **46**, 382–419 (2012).

553. Du, M. -Q, Carmichael, P. L. & Phillips, D. H. Induction of activating mutations

in the human c-Ha-ras-1 proto-oncogene by oxygen free radicals. *Mol. Carcinog.* **11**, 170–175 (1994).

554. Hussain, S. P., Aguilar, F., Amstad, P. & Cerutti, P. Oxy-radical induced mutagenesis of hotspot codons 248 and 249 of the human p53 gene. *Oncogene* **9**, 2277–2281 (1994).

555. Toyokuni, S. Molecular mechanisms of oxidative stress-induced carcinogenesis: From epidemiology to oxygenomics. *IUBMB Life* **60**, 441–447 (2008).

556. Lim, S. O. *et al.* Epigenetic Changes Induced by Reactive Oxygen Species in Hepatocellular Carcinoma: Methylation of the E-cadherin Promoter. *Gastroenterology* **135**, (2008).

557. Endo, K., Ueda, T., Ueyama, J., Ohta, T. & Terada, T. Immunoreactive E-cadherin, alpha-catenin, beta-catenin, and gamma- catenin proteins in hepatocellular carcinoma: Relationships with tumor grade, clinicopathologic parameters, and patients' survival. *Hum. Pathol.* **31**, 558–565 (2000).

558. Kang, K. A., Zhang, R., Kim, G. Y., Bae, S. C. & Hyun, J. W. Epigenetic changes induced by oxidative stress in colorectalcancer cells: Methylation of tumor suppressor RUNX3. *Tumor Biol.* **33**, 403–412 (2012).

559. Cao, L. *et al.* Absence of full-length Brca1 sensitizes mice to oxidative stress and carcinogen-induced tumorigenesis in the esophagus and forestomach. *Carcinogenesis* **28**, 1401–1407 (2007).

560. Vafa, O. *et al.* c-Myc can induce DNA damage, increase reactive oxygen species, and mitigate p53 function: A mechanism for oncogene-induced genetic instability. *Mol. Cell* **9**, 1031–1044 (2002).

561. Maciag, A., Sithanandam, G. & Anderson, L. M. Mutant K-rasV12 increases COX-2, peroxides and DNA damage in lung cells. *Carcinogenesis* **25**, 2231–2237 (2004).

562. Tanaka, H. *et al.* E2F1 and c-Myc potentiate apoptosis through inhibition of NF-KB activity that facilitates MnSOD-mediated ROS elimination. *Mol. Cell* **9**, 1017–1029 (2002).

563. Weinberg, F. *et al.* Mitochondrial metabolism and ROS generation are essential for Kras-mediated tumorigenicity. *Proc. Natl. Acad. Sci. U. S. A.* **107**, 8788–8793 (2010).

564. Chan, D. W. *et al.* Loss of MKP3 mediated by oxidative stress enhances tumorigenicity and chemoresistance of ovarian cancer cells. *Carcinogenesis* **29**, 1742–1750 (2008).

565. Kwon, J. *et al.* Reversible oxidation and inactivation of the tumor suppressor PTEN in cells stimulated with peptide growth factors. *Proc. Natl. Acad. Sci. U. S. A.* **101**, 16419–16424 (2004).

566. Salmeen, A. *et al.* Redox regulation of protein tyrosine phosphatase 1B

involves a sulphenyl-amide intermediate. *Nature* **423**, 769–773 (2003).

567. Binker, M. G., Binker-Cosen, A. A., Richards, D., Oliver, B. & Cosen-Binker, L. I. EGF promotes invasion by PANC-1 cells through Rac1/ROS-dependent secretion and activation of MMP-2. *Biochem. Biophys. Res. Commun.* **379**, 445–450 (2009).

568. Ho, B. Y., Wu, Y. M., Chang, K. J. & Pan, T. M. Dimerumic acid inhibits sw620 cell invasion by attenuating H2O2-mediated MMP-7 expression via JNK/C-Jun and ERK/C-Fos activation in an AP-1-Dependent manner. *Int. J. Biol. Sci.* **7**, 869–880 (2011).

569. Douma, S. *et al.* Suppression of anoikis and induction of metastasis by the neurotrophic receptor TrkB. *Nature* **430**, 1034–1040 (2004).

570. Giannoni, E., Fiaschi, T., Ramponi, G. & Chiarugi, P. Redox regulation of anoikis resistance of metastatic prostate cancer cells: Key role for Src and EGFR-mediated pro-survival signals. *Oncogene* **28**, 2074–2086 (2009).

571. Moldovan, L., Irani, K., Moldovan, N. I., Finkel, T. & Goldschmidt-Clermont, P. J. The Actin Cytoskeleton Reorganization Induced by Rac1 Requires the Production of Superoxide. *Antioxidants Redox Signal.* **1**, 29–43 (1999).

572. Wetering, S. van *et al.* Reactive oxygen species mediate Rac-induced loss of cell-cell adhesion in primary human endothelial cells. *J. Cell Sci.* (2002).

573. Ramakrishnan, S., Anand, V. & Roy, S. Vascular endothelial growth factor signaling in hypoxia and inflammation. *Journal of Neuroimmune Pharmacology* **9**, 142–160 (2014).

574. Gardner, L. B. & Corn, P. G. Hypoxic regulation of mRNA expression. *Cell Cycle* **7**, 1916–1924 (2008).

575. Rabbani, Z. N. *et al.* Antiangiogenic action of redox-modulating Mn(III) meso-tetrakis(N-ethylpyridinium-2-yl)porphyrin, MnTE-2-PyP5+, via suppression of oxidative stress in a mouse model of breast tumor. *Free Radic. Biol. Med.* **47**, 992–1004 (2009).

576. Xia, C. *et al.* Reactive oxygen species regulate angiogenesis and tumor growth through vascular endothelial growth factor. *Cancer Res.* **67**, 10823–10830 (2007).

577. Liu, L. Z. *et al.* Reactive oxygen species regulate epidermal growth factor-induced vascular endothelial growth factor and hypoxia-inducible factor-1α expression through activation of AKT and P70S6K1 in human ovarian cancer cells. *Free Radic. Biol. Med.* **41**, 1521–1533 (2006).

578. Gao, P. *et al.* HIF-Dependent Antitumorigenic Effect of Antioxidants In Vivo. *Cancer Cell* **12**, 230–238 (2007).

579. Zhang, X. *et al.* Natural Antioxidant-Isoliquiritigenin Selectively Inhibits Proliferation of Prostate Cancer Cells. *Clin. Exp. Pharmacol. Physiol.* **37**, no-no (2010).

580. Lee, M. F. *et al.* N-acetylcysteine (NAC) inhibits cell growth by mediating the EGFR/Akt/HMG box-containing protein 1 (HBP1) signaling pathway in invasive oral cancer. *Oral Oncol.* **49**, 129–135 (2013).

581. Hong, S. W. *et al.* Ascorbate (vitamin C) induces cell death through the apoptosis-inducing factor in human breast cancer cells. *Oncol. Rep.* **18**, 811–815 (2007).

582. Amini, A., Masoumi-Moghaddam, S., Ehteda, A. & Morris, D. L. Bromelain and N-acetylcysteine inhibit proliferation and survival of gastrointestinal cancer cells in vitro: Significance of combination therapy. *J. Exp. Clin. Cancer Res.* **33**, (2014).

583. Sayin, V. I. *et al.* Cancer: Antioxidants accelerate lung cancer progression in mice. *Sci. Transl. Med.* **6**, (2014).

584. Gal, K. Le *et al.* Antioxidants can increase melanoma metastasis in mice. *Sci. Transl. Med.* **7**, (2015).

585. Klein, E. A. *et al.* Vitamin E and the risk of prostate cancer: The selenium and vitamin E cancer prevention trial (SELECT). *JAMA - J. Am. Med. Assoc.* **306**, 1549–1556 (2011).

586. Omenn, G. S. *et al.* Effects of a combination of beta carotene and vitamin A on lung cancer and cardiovascular disease. *N. Engl. J. Med.* **334**, 1150–1155 (1996).

587. Hercberg, S. *et al.* Antioxidant supplementation increases the risk of skin cancers in women but not in men. *J. Nutr.* **137**, 2098–2105 (2007).

588. Qiao, Y. L. *et al.* Total and cancer mortality after supplementation with vitamins and minerals: Follow-up of the linxian general population nutrition intervention trial. *J. Natl. Cancer Inst.* **101**, 507–518 (2009).

589. Itoh, K. *et al.* Keap1 represses nuclear activation of antioxidant responsive elements by Nrf2 through binding to the amino-terminal Neh2 domain. *Genes Dev.* **13**, 76–86 (1999).

590. Fourquet, S., Guerois, R., Biard, D. & Toledano, M. B. Activation of NRF2 by nitrosative agents and H2O2 involves KEAP1 disulfide formation. *J. Biol. Chem.* **285**, 8463–8471 (2010).

591. Jaramillo, M. C. & Zhang, D. D. The emerging role of the Nrf2-Keap1 signaling pathway in cancer. *Genes and Development* **27**, 2179–2191 (2013).

592. Rhee, S. G., Woo, H. A., Kil, I. S. & Bae, S. H. Peroxiredoxin functions as a peroxidase and a regulator and sensor of local peroxides. *Journal of Biological Chemistry* **287**, 4403–4410 (2012).

593. Fridovich, I. Superoxide anion radical (O2/-·), superoxide dismutases, and related matters. *Journal of Biological Chemistry* **272**, 18515–18517 (1997).

594. Wu, K. C., Cui, J. Y. & Klaassen, C. D. Beneficial role of Nrf2 in regulating

NADPH generation and consumption. *Toxicol. Sci.* **123**, 590–600 (2011).

595. Park, J. Y., Kim, Y. W. & Park, Y. K. Nrf2 expression is associated with poor outcome in osteosarcoma. *Pathology* **44**, 617–621 (2012).

596. Yoo, N. J., Kim, H. R., Kim, Y. R., An, C. H. & Lee, S. H. Somatic mutations of the KEAP1 gene in common solid cancers. *Histopathology* **60**, 943–952 (2012).

597. Shibata, T. *et al.* Cancer related mutations in NRF2 impair its recognition by Keap1-Cul3 E3 ligase and promote malignancy. *Proc. Natl. Acad. Sci. U. S. A.* **105**, 13568–13573 (2008).

598. Gañán-Gómez, I., Wei, Y., Yang, H., Boyano-Adánez, M. C. & García-Manero, G. Oncogenic functions of the transcription factor Nrf2. *Free Radical Biology and Medicine* **65**, 750–764 (2013).

599. No, J. H., Kim, Y.-B. & Song, Y. S. Targeting Nrf2 Signaling to Combat Chemoresistance. *J. Cancer Prev.* **19**, 111–117 (2014).

600. Satoh, H., Moriguchi, T., Takai, J., Ebina, M. & Yamamoto, M. Nrf2 prevents initiation but accelerates progression through the kras signaling pathway during lung carcinogenesis. *Cancer Res.* **73**, 4158–4168 (2013).

601. Denicola, G. M. *et al.* Oncogene-induced Nrf2 transcription promotes ROS detoxification and tumorigenesis. *Nature* **475**, 106–110 (2011).

602. Conklin, K. A. Chemotherapy-associated oxidative stress: Impact on chemotherapeutic effectiveness. *Integrative Cancer Therapies* **3**, 294–300 (2004).

603. Kim, S. J., Kim, H. S. & Seo, Y. R. Understanding of ROS-Inducing Strategy in Anticancer Therapy. *Oxidative Medicine and Cellular Longevity* **2019**, (2019).

604. Bellosillo, B. *et al.* Complement-mediated cell death induced by rituximab in B-cell lymphoproliferative disorders is mediated in vitro by a caspase-independent mechanism involving the generation of reactive oxygen species. *Blood* **98**, 2771–2777 (2001).

605. Dvorakova, K. *et al.* Induction of oxidative stress and apoptosis in myeloma cells by the aziridine-containing agent imexon. *Biochem. Pharmacol.* **60**, 749–758 (2000).

606. Bailey, H. H. *et al.* Phase I clinical trial of intravenous L-buthionine sulfoximine and melphalan: An attempt at modulation of glutathione. *J. Clin. Oncol.* **12**, 194–205 (1994).

607. Welsh, S. J. *et al.* The thioredoxin redox inhibitors 1-methylpropyl 2-imidazolyl disulfide and pleurotin inhibit hypoxia-induced factor 1α and vascular endothelial growth factor formation. *Mol. Cancer Ther.* **2**, 235–243 (2003).

608. Huang, P., Feng, L., Oldham, E. A., Keating, M. J. & Plunkett, W. Superoxide

dismutase as a target for the selective killing of cancer cells. *Nature* **407**, 390–395 (2000).

609. Juarez, J. C. *et al.* Copper binding by tetrathiomolybdate attenuates angiogenesis and tumor cell proliferation through the inhibition of superoxide dismutase 1. *Clin. Cancer Res.* **12**, 4974–4982 (2006).

610. Smith, P. S., Zhao, W., Spitz, D. R. & Robbins, M. E. Inhibiting catalase activity sensitizes 36B10 rat glioma cells to oxidative stress. *Free Radic. Biol. Med.* **42**, 787–797 (2007).

611. Fang, J., Sawa, T., Akaike, T., Greish, K. & Maeda, H. Enhancement of chemotherapeutic response of tumor cells by a heme oxygenase inhibitor, pegylated zinc protoporphyrin. *Int. J. Cancer* **109**, 1–8 (2004).

612. Jump, D. B. *et al.* Fatty acid regulation of hepatic gene transcription. *Journal of Nutrition* **135**, 2503–2506 (2005).

613. Shimano, H. & Sato, R. SREBP-regulated lipid metabolism: Convergent physiology-divergent pathophysiology. *Nature Reviews Endocrinology* **13**, 710–730 (2017).

614. Poulsen, L. la C., Siersbæk, M. & Mandrup, S. PPARs: Fatty acid sensors controlling metabolism. *Seminars in Cell and Developmental Biology* **23**, 631–639 (2012).

615. Azad, G. K. & Tomar, R. S. Ebselen, a promising antioxidant drug: Mechanisms of action and targets of biological pathways. *Molecular Biology Reports* **41**, 4865–4879 (2014).

616. Wilcox, C. S. Effects of tempol and redox-cycling nitroxides in models of oxidative stress. *Pharmacology and Therapeutics* **126**, 119–145 (2010).

617. Miotto, G. *et al.* Insight into the mechanism of ferroptosis inhibition by ferrostatin-1. *Redox Biol.* **28**, 101328 (2020).

618. Ratheiser, K. *et al.* Inhibition by etomoxir of carnitine palmitoyltransferase I reduces hepatic glucose production and plasma lipids in non-insulin-dependent diabetes mellitus. *Metabolism* **40**, 1185–1190 (1991).

619. Trnka, J., Blaikie, F. H., Smith, R. A. J. & Murphy, M. P. A mitochondria-targeted nitroxide is reduced to its hydroxylamine by ubiquinol in mitochondria. *Free Radic. Biol. Med.* **44**, 1406–1419 (2008).

620. Tallima, H. & El Ridi, R. Arachidonic acid: Physiological roles and potential health benefits – A review. *Journal of Advanced Research* **11**, 33–41 (2018).

621. Shin, B. Y., Jin, S. H., Cho, I. J. & Ki, S. H. Nrf2-ARE pathway regulates induction of Sestrin-2 expression. *Free Radic. Biol. Med.* **53**, 834–841 (2012).

622. Kim, H. *et al.* Janus-faced Sestrin2 controls ROS and mTOR signalling through two separate functional domains. *Nat. Commun.* **6**, 1–11 (2015).

623. Bae, S. H. *et al.* Sestrins activate Nrf2 by promoting p62-dependent

autophagic degradation of keap1 and prevent oxidative liver damage. *Cell Metab.* **17**, 73–84 (2013).

624. Parmigiani, A. *et al.* Sestrins Inhibit mTORC1 Kinase Activation through the GATOR Complex. *Cell Rep.* **9**, 1281–1291 (2014).

625. Sanli, T., Linher-Melville, K., Tsakiridis, T. & Singh, G. Sestrin2 modulates AMPK subunit expression and its response to ionizing radiation in breast cancer cells. *PLoS One* **7**, (2012).

626. Kim, M. *et al.* Comparative Oncogenomics Identifies NEDD9 as a Melanoma Metastasis Gene. *Cell* **125**, 1269–1281 (2006).

627. Zender, L. *et al.* Identification and Validation of Oncogenes in Liver Cancer Using an Integrative Oncogenomic Approach. *Cell* **125**, 1253–1267 (2006).

628. Xue, W. *et al.* DLC1 is a chromosome 8p tumor suppressor whose loss promotes hepatocellular carcinoma. *Genes Dev.* **22**, 1439–1444 (2008).

629. Petan, T., Jarc, E. & Jusović, M. Lipid droplets in cancer: Guardians of fat in a stressful world. *Molecules* **23**, 11–15 (2018).

630. Monaco, M. E. Fatty acid metabolism in breast cancer subtypes. *Oncotarget* **8**, 29487–29500 (2017).

631. Ladanyi, A. *et al.* Adipocyte-induced CD36 expression drives ovarian cancer progression and metastasis. *Oncogene* **37**, 2285–2301 (2018).

632. Balaban, S. *et al.* Adipocyte lipolysis links obesity to breast cancer growth: adipocyte-derived fatty acids drive breast cancer cell proliferation and migration. *Cancer Metab.* **5**, (2017).

633. Chen, R. R. *et al.* Targeting of lipid metabolism with a metabolic inhibitor cocktail eradicates peritoneal metastases in ovarian cancer cells. *Commun. Biol.* **2**, (2019).

634. Zhao, G., Cardenas, H. & Matei, D. Ovarian cancer—why lipids matter. *Cancers* **11**, (2019).

635. Foster, D. A. Phosphatidic acid and lipid-sensing by mTOR. *Trends in Endocrinology and Metabolism* **24**, 272–278 (2013).

636. Schmitz-Peiffer, C. & Biden, T. J. Protein kinase C function in muscle, liver, and β-cells and its therapeutic implications for type 2 diabetes. *Diabetes* **57**, 1774–1783 (2008).

637. Wen, Z. H. *et al.* Critical role of arachidonic acid-activated mTOR signaling in breast carcinogenesis and angiogenesis. *Oncogene* **32**, 160–170 (2013).

638. Guri, Y. *et al.* mTORC2 Promotes Tumorigenesis via Lipid Synthesis. *Cancer Cell* **32**, 807-823.e12 (2017).

639. Porstmann, T. *et al.* SREBP Activity Is Regulated by mTORC1 and Contributes to Akt-Dependent Cell Growth. *Cell Metab.* **8**, 224–236 (2008).

640. Lee, G. *et al.* Post-transcriptional Regulation of De Novo Lipogenesis by mTORC1-S6K1-SRPK2 Signaling. *Cell* **171**, 1545-1558.e18 (2017).

641. Luo, X. *et al.* Emerging roles of lipid metabolism in cancer metastasis. *Molecular Cancer* **16**, (2017).

642. Nieman, K. M., Romero, I. L., Van Houten, B. & Lengyel, E. Adipose tissue and adipocytes support tumorigenesis and metastasis. *Biochimica et Biophysica Acta - Molecular and Cell Biology of Lipids* **1831**, 1533–1541 (2013).

643. Wu, Q. *et al.* Cancer-associated adipocytes: Key players in breast cancer progression. *Journal of Hematology and Oncology* **12**, (2019).

644. Diedrich, J. D., Herroon, M. K., Rajagurubandara, E. & Podgorski, I. The Lipid Side of Bone Marrow Adipocytes: How Tumor Cells Adapt and Survive in Bone. *Curr. Osteoporos. Rep.* **16**, 443–457 (2018).

645. Corbet, C. *et al.* TGFβ2-induced formation of lipid droplets supports acidosis-driven EMT and the metastatic spreading of cancer cells. *Nat. Commun.* **11**, 1–15 (2020).

646. Piskounova, E. *et al.* Oxidative stress inhibits distant metastasis by human melanoma cells. *Nature* **527**, 186–191 (2015).

647. Ubellacker, J. M. *et al.* Lymph protects metastasizing melanoma cells from ferroptosis. *Nature* **585**, 113–118 (2020).

648. Chapman, A. *et al.* Heterogeneous tumor subpopulations cooperate to drive invasion. *Cell Rep.* **8**, 688–695 (2014).

649. Rowling, E. J. *et al.* Cooperative behaviour and phenotype plasticity evolve during melanoma progression. *Pigment Cell Melanoma Res.* **33**, 695–708 (2020).

650. Denison, H. *et al.* Diacylglycerol acyltransferase 1 inhibition with AZD7687 alters lipid handling and hormone secretion in the gut with intolerable side effects: A randomized clinical trial. *Diabetes, Obes. Metab.* **16**, 334–343 (2014).

651. Lowndes, S. A. *et al.* Phase I study of copper-binding agent ATN-224 in patients with advanced solid tumors. *Clin. Cancer Res.* **14**, 7526–7534 (2008).

652. Shibata, Y., Yasui, H., Higashikawa, K., Miyamoto, N. & Kuge, Y. Erastin, a ferroptosis-inducing agent, sensitized cancer cells to X-ray irradiation via glutathione starvation in vitro and in vivo. *PLoS One* **14**, e0225931 (2019).

653. Sutti, S. *et al.* Adaptive immune responses triggered by oxidative stress contribute to hepatic inflammation in NASH. *Hepatology* **59**, 886–897 (2014).

654. D'Avila, H. *et al.* Mycobacterium bovis Bacillus Calmette-Guérin Induces TLR2-Mediated Formation of Lipid Bodies: Intracellular Domains for Eicosanoid Synthesis In Vivo . *J. Immunol.* **176**, 3087–3097 (2006).

655. Kalinski, P. Regulation of Immune Responses by Prostaglandin E 2 . *J.*

Immunol. **188**, 21–28 (2012).